AD 289 290

PROCEEDINGS OF THE

BLACK HILLS

SUMMER CONFERENCE

ON TRANSPORT PHENOMENA

21 - 23 AUGUST 1962

South Dakota School of Mines
and Technology
Rapid City, South Dakota

Sponsored by
South Dakota School of Mines and Technology
Office of Naval Research
Visiting Scientists Program in Physics,
American Institute of Physics

Issued as Final Report
under Office of Naval Research Contract No. Nonr(G)-00064-62
15 October 1962

Black Hills
Summer Conference
On Transport Phenomena

(Mainly heat flow and charge flow in semiconductors at elevated temperatures)

Tuesday 21 August
Through Thursday 23 August 1962

South Dakota School of Mines
and Technology
Rapid City, South Dakota

Sponsored by

South Dakota School of Mines and Technology
Office of Naval Research
Visiting Scientists Program in Physics,
American Institute of Physics

OBJECT: To bring together theorists and experimenters, especially those from laboratories where there may be only one or the other, who are especially interested in heat and charge flow in solids.

EMPHASIS: Mainly on semiconductors at elevated temperatures, although related problems in metals and at low temperatures will be discussed. Elucidation of current problems and a discussion of possible new approaches, theoretical and experimental.

A conference to bring interested listeners together to hear distinguished invited speakers, and then to encourage everyone to talk, doubt, discuss, challenge, think and argue, diverted occasionally by a contributed paper with new results or a new technique.

PROGRAM

MONDAY, 20 August

7:00 - 9:00 P. M.	Reception for all participants and their wives at home of Mr. and Mrs. Robert G. Morris, 2620 Brook Lane.

TUESDAY, 21 August

8:00 A. M.	Registration (free) — Mineral Industries Building, Room 220 (MI 220). Northeast corner of campus
9:00	Opening remarks and welcome, Mineral Industries Building, Room 222 (MI 222).
9:15	SESSION A, MI 222. G. C DANIELSON presiding *Invited Paper A1*: M. J. LAUBITZ, National Research Council, Ottawa "*Measurement of Thermal Conductivity at High Temperatures*"
10:15	Discussion
10:45	Coffee — Late Registration, MI 220
11:00	CONTRIBUTED PAPERS
12:00	Luncheon at Faculty Club, Liberal Arts Building, Basement
1:00 P. M.	Tour of South Dakota School of Mines and Technology Museum of Geology
2:00	SESSION B. MI 222. GOTTFRIED I. MOLLER presiding. *Invited Paper B1*: E. STEIGMEIER, RCA Laboratories, Princeton "*Absolute Measurement of Thermal Conductivity*"
3:00	Discussion
3:30	Coffee, MI 220
3:45	CONTRIBUTED PAPERS
5:00	Picnic, Canyon Lake Park, Fish Fry Shelter

WEDNESDAY, 22 August

9:00 A. M.	SESSION C. MI 222. KEH C. TSAO presiding *Invited Paper C1*: R. W. POWELL, National Physical Laboratory, Teddington "*The Use of Thermal Comparator Methods for the Measurement of Thermal Conductivity*"

10:00	Discussion
10:30	Coffee, MI 220
10:45	CONTRIBUTED PAPERS
12:00	Luncheon at Faculty Club
1:00 P. M.	SESSION D, MI 222. R. DANIEL REDIN presiding
	Invited Paper D1: P. G. KLEMENS, Westinghouse Research Laboratories, Pittsburgh
	"The Theory of Electrical and Thermal Conductivity of Solids"
2:00	Discussion
2:30	Coffee, MI 220
2:45	Group picture, in front of Mineral Industries Building
3:00	Excursion through Black Hills and Custer State Park
8:00	Dinner at Buffalo Room, Mount Rushmore National Memorial

THURSDAY, 23 August

9:00 A. M.	SESSION E. MI 222. SPENCER MACY presiding
	Invited Paper E1: R. K. WILLARDSON, Bell and Howell Research Center, Pasadena
	"Mixed Conduction in Semiconductors"
10:00	Discussion
10:30	Coffee, MI 220
10:45	CONTRIBUTED PAPERS
12:00	Luncheon at Faculty Club
1:00 P. M.	SESSION F, MI 222. M. D. Blue presiding
	Invited Paper F1: W. W. SCANLON, U. S. Naval Ordnance Laboratory, Silver Spring
	"Properties of Non-Stoichiometric Compound Semiconductors"
2:00	Discussion
2:30	Closing Remarks: Summing Up
3:00	Adjournment

ATTENDANCE: Open to all. No registration fee. We would appreciate notice of your coming, however, preferably by 15 August 1962.

PROCEEDINGS: Each registered participant will receive a copy of the Conference Proceedings. Those giving papers are reminded the text of their papers is due at the Conference.

LOCATION: The South Dakota School of Mines and Technology is an engineering and science college founded in 1885. With 850 students, it offers the B.S. and M.S. degrees in engineering studies, physics, chemistry, mathematics and geology. Rapid City is located on the edge of the Black Hills of South Dakota, 23 miles from Mt. Rushmore, a few hours' drive from Devil's Tower, Custer State Park and Wind Cave. It is on the direct route to the Grand Tetons, Yellowstone Park and the Pacific Northwest.

BANQUET: Buffalo Room, Mt. Rushmore National Memorial, Wednesday 22 August just before 8 P. M. We shall be seated together and order from menu. Dinners from $1.70. Not necessary to go on excursion to join us for dinner.

EXCURSION: By chartered bus from campus Wednesday afternoon, ending up at Mt. Rushmore for dinner. Bus back to Rapid City after dinner. Fare to be announced.

RECEPTION: Monday evening 7-9 P. M. 20 August for all participants and wives at 2620 Brook Lane, home of Conference Chairman. The street is poorly marked; use map, or phone for directions.

PICNIC: Tuesday evening at 5:00 P. M. in Canyon Lake Park, Fish Fry Shelter. For all participants and their families. Start as for 2620 Brook Lane, keep on Jackson Blvd. till park. Prices to be announced.

AIRPORT PICKUP: Upon notification of arrival time, we shall pick up arriving participants at the airport.

INFORMATION: For further information concerning the Conference, hotels, air schedules and highway travel write or call the Conference chairman:

Robert G. Morris
Department of Physics
South Dakota School of Mines and Technology
Rapid City, South Dakota

Phone: Area Code 605, 343-1600, ext. 223 8 A. M. — 5 P. M. MST
Area Code 605, 342-6479 Other hours

Titles and Abstracts of Papers

Printed for information of participants only. Do not give reference to following work without permission of authors.

TUESDAY MORNING, 21 August

A1. (Invited paper, one hour) MEASUREMENT OF THERMAL CONDUCTIVITY AT HIGH TEMPERATURES. M. J. Laubitz, National Research Council, Ottawa.

A2. THERMAL CONDUCTIVITY MEASUREMENTS ON SILICON TO 1000°K.* Joel J. Martin and Robert G. Morris, South Dakota School of Mines and Technology, Rapid City.—The thermal conductivity of single-crystal silicon was measured as a function of temperature from 680°K to 1000°K by means of a series comparative method. The method of Morris and Hust was used for this experiment with modifications. The samples were 23mm in diameter and 8mm in thickness. The standards were of Armco iron and had the same dimensions as the sample. Thermocouples made of platinum and platinum-10%-rhodium wire were cemented to the sample and standards with a mixture of sodium silicate and graphite. This cement was also used to provide good thermal contacts between the sample, standards, and the gradient heater. Radiation losses were reduced by using a radiation guard sectioned to match the sample and the standards. The rate of change of both the ambient temperature and the temperature differences was less than 0.01°C/min. Subtraction of the thermocouple readings was used to find the temperature differences. The thermal conductivity of silicon was found to be 0.53 watt/cm C° at 680°K and 0.31 watt cm C° at 935°K. The low-temperature values agree with those of Morris and Hust. The high-temperature values agree with those Abeles et al. obtained from thermal diffusivity measurements. A plot of 1/K versus T (K°) indicates that 1/K is linearly dependent upon T.

* This work supported in part by the Office of Naval Research

A3. THERMAL DIFFUSIVITY MEASUREMENTS ON A FINITE DISK. Paul D. Maycock, Iowa State University, Ames.—A new technique has been developed for measuring the thermal diffusivity of finite disk-shaped samples. The radial heat flow equation was solved by the method of finite differences. An axial heater was turned on and the temperatures at three radial positions were measured as functions of time. This procedure determined the boundary conditions necessary for the solution of the heat flow equation. By assuming various values of the thermal diffusivity, we obtained the solution at the middle thermocouple. The value which gave the best agreement between the computed solution at the middle thermocouple and the experimental curve obtained at the midpoint was

considered to be the best value for the diffusivity. A FORTRAN program which calculates the diffusivity from the experimental data was developed and an IBM 704 computer was used to process the data. Data on Armco iron show that the method is capable of giving correct values for thermal diffusivity.

A4. SPECIFIC HEAT OF ZIRCONIUM BY A PULSE HEATING METHOD. A. H. Klein and G. C. Danielson, Iowa State University, Ames.—The specific heat of iodide zirconium, from 25°C to the melting temperature of 1845°C, has been determined by a pulse heating method. The α - β transformation from the hexagonal close-packed structure to the body-centered cubic structure occurred at 865°C. For α - zirconium, the specific heat increased from 0.066 cal/g–°C at 25°C to 0.082 cal/g–°C at 865°C. Over the entire temperature range, our results are about three per cent lower than those of Scott. For β–zirconium, where no previous measurements seem to have been reported above 1000°C, the errors were greater than for α–zirconium. Approximate values of the specific heat in the β– range have been determined, however, from our pulse data and from previously known information on the heat of transformation and on the temperature dependence of the resistivity.

TUESDAY AFTERNOON, 21 August

B1. (Invited paper, one hour) ABSOLUTE MEASUREMENT OF THERMAL CONDUCTIVITY. E. Steigmeier, RCA Laboratories, Princeton.

B2. THERMAL MEASUREMENTS ON FERROELECTRIC BARIUM TITANATE CERAMICS. Donald D. Glower, Sandia Corporation, Albuquerque, New Mexico.—Thermal diffusivity and thermal conductivity measurements for unpoled $Ba_{1-x}Ca_xTiO_3$ ceramics ($0 \leq x \leq 0.19$) reveal that the effect of adding calcium is to decrease the thermal diffusivity in the orthorhombic and tetragonal phase, and to leave the thermal diffusivity virtually unchanged in the cubic crystal phase. Direct measurements of the thermal conductivity were made using a variation of the split rod method. These measurements agreed within 10% of indirect measurements via the thermal diffusivity, specific heat, and density. The thermal diffusivity was measured using the variation of Angstrom's heat wave method, as developed by Sidles and Danielson.

The thermal conductivity of the barium titanate ceramic, as measured with ceramics of density 5.9 gm/cm^3, is about 20% greater than reported by Yoshida. The thermal diffusivity, measured in the temperature range $-60° \leq$ to $\leq 180°$C, shows a sharp drop at the temperatures where the crystal structure changes from orthorhombic to tetragonal and tetragonal to cubic. The greatest change is at the 0°C phase change. The addition of calcium causes the greatest effect on the thermal diffusivity at low temperature.

B3. SERIES COMPARATIVE MEASUREMENTS OF THERMAL CONDUCTIVITY WITH THERMISTORS.* William G. Delinger, Francis W. Kalkbrenner† and Robert G. Morris, South Dakota School of Mines and Technology, Rapid City.—The thermistor, or thermally sensitive resistor, is a semiconductor circuit element which is suited for the measurement of small temperature differences encountered in thermal conductivity work. It can be made small in size (0.11 cm and smaller) and has a high temperature coefficient of resistance ($\cong -5\%$/deg C at 25°C). A preliminary investigation indicates thermistors are stable enough to be used as temperature sensors—the resistance being repeatable within less than 1% as the temperature is cycled to 250°C and back to 25°C. Two thermistors (matched by the Godin technique) are placed in adjacent arms of a balanced Wheatstone bridge and the unbalance current is measured when the thermistors are at different temperatures. The unbalance current is a measure of the difference in resistance of the two. The slopes of the resistance-vs-temperature curves for the two thermistors are nearly the same; this allows one to write $\Delta T = \Delta R/(dR/dT)$. The temperature can be determined from one thermistor. Using dR/dT from a previously prepared graph, one can find ΔT very precisely.

* This work supported in part by the Office of Naval Research and by a Special Research Appropriation by the State of South Dakota.

†Present Address: Boeing Company, Seattle 24, Washington.

WEDNESDAY MORNING, 22 August

C1. (Invited paper, one hour) THE USE OF THERMAL COMPARATOR METHODS FOR THE MEASUREMENT OF THERMAL CONDUCTIVITY. R. W. Powell, National Physical Laboratory, Teddington.

C2. MICROWAVE HALL MOBILITY IN GERMANIUM. Y. Nishina and G. C. Danielson, Iowa State University, Ames.—Hall mobilities of germanium single crystals have been measured at a frequency of 9000 Mc over the temperature range 30° – 300°K. The rectangular sample was placed on the wall of a rectangular cavity which was doubly degenerate in the TE_{101} mode and in the TE_{011} mode at a single resonance microwave frequency. Measurements on n-type germanium were in quantitative agreement with the theoretical analysis by Liu, Nishina, and Good. Measurements on p-type germanium were more difficult to interpret and quantitative discrepancies between the microwave Hall mobility and the corresponding dc Hall mobility were found. The magnetic field dependence of the microwave Hall mobility in p-type germanium was in qualitative agreement with the analysis of dc measurements by Willardson, Harman, and Beer.

C3. LOW-TEMPERATURE ELECTRICAL RESISTIVITY OF RARE EARTH METALS. R. V. Colvin and S. Arajs, Edgar C. Bain Laboratory For Fundamental Research, United States Steel Corporation Research Center, Monroeville, Pennsylvania.—The discussion is mainly concerned with a means used to obtain temperatures between 4°K and 300°K. Any temperature that may be desired is first obtained by rapid heating or cooling of a copper sample chamber and then the chamber temperature is maintained by supplying an amount of heat to the chamber equal to its heat losses to a liquid gas bath. A vacuum wall and a length of thin wall stainless steel provide the necessary thermal isolation from the bath.

Although the apparatus is particularly useful in conjunction with electrical resistivity measurements, appropriate modifications make it useful for a number of other physieal measurements. Precise temperature control, continuous coverage of the entire temperature range and a temperature controller that can change the sample temperature automatically in the minimum possible time are some of the features described.

Resistivity curves of a number of the rare earth elements and of a single crystal of Cr are presented to illustrate the usefulness of such equipment. The need for good measuring instruments is stressed since studies of hysteresis effects, dependence of resistivity on time and precise studies of the detailed temperature dependence of resistivity are possible.

C4. CIRCULATING CURRENTS IN THERMOELECTRIC AND GALVANOMAGNETIC EFFECTS. Milton Green, Burroughs Corporation, Burroughs Laboratories, Paoli, Pennsylvania.—Circulating currents, which are responsible for increased specimen resistance such as is observed in the Corbino disk, are associated with field forces having non-vanishing curls. For the steady state, the hole field-forees are given by the electrostatic field E, the hole "pressure-motive-field" $E_p = -(kT/e)$ (grad lnp $+ \gamma_p$grad lnT), and the Lorentz-force $\epsilon_p = v_p \times B$. The nonvanishing curls are curl E_p= grad lnT $\times$ $E_p$and curl ϵ_p= B . grad v_p $-v_p$. grad B $-$ B div v_p. The first curl exists if grad T has a component orthogonal to grad p, and the second curl will generally exist if either or both the magnetic and the velocity fields are nonuniform. Nonuniform magnetic fields are curvilinear (nonrectangular, coordinatewise), and nonuniform velocities are the result of curvilinear flow paths and/or concentration gradients. (The last category includes junctions, inhomogeneities, and other sources and sinks of eleetron-hole pairs.) Consequently, the *circulating flow* of holes in *transverse* galvanomagnetic effects is clockwise with respect to B around real or *virtual* (apparent) hole-eurrent sources (correspondingly, counterclockwise for sinks) and conversely for electron sources (or sinks). The circulation emf of holes, $\epsilon_p = \int_c V_p \times B$. dR, is a maximum in regions where sources and sinks are absent, i.e., where div $J_p = -$ div $J_n = e(g-r) = 0$, and eorrespondingly for electrons. For transverse

flow in a diverging (or converging) magnetic flux, the circulating current about the *virtual* source (or sink) of flux is counterclockwise (correspondingly clockwise) with respect to the noncirculating component of current density.

WEDNESDAY AFTERNOON, 22 August

D1. (Invited paper, one hour) THE THEORY OF ELECTRICAL AND THERMAL CONDUCTIVITY OF SOLIDS. P. G. Klemens, Westinghouse Research Laboratories, Pittsburgh.

THURSDAY MORNING, 23 August

E1. (Invited paper, one hour) MIXED CONDUCTION IN SEMICONDUCTORS. R. K. Willardson, Bell and Howell Research Center, Pasadena.

E2. SEMICONDUCTING PROPERTIES OF $Hg_{1-x}Cd_xTe$*. M. D. Blue and P. W. Kruse, Honeywell Research Center, Hopkins, Minnesota.—$Hg_{1-x}Cd_xTe$ is a semiconductor having an energy gap approximately linearly dependent upon x, ranging from 1.45 eV for CdTe to 0.02 eV for HgTe[1].

Optical measurements including transmittance, photoconductivity, the photovoltaic effect, and the PEM effect, are being employed to determine the dependence of the optical gap upon composition, found by chemical analysis.

Hall and resistivity measurements are made between 4.2 and 295°K as functions of magnetic induction. Because of the large hole to electron mobility ratio, the conductivity and Hall coefficient are determined almost entirely by electrons above 200°K. A large dependence of Hall coefficient upon magnetic field is observed.

Electrical data for a sample containing 2 per cent CdTe have been fitted in the mixed conduction region to a band model with a thermal gap of 0.025 eV. The electrical properties of the same sample after conversion from n-type to p-type (by annealing in Hg vapor) have also been measured. Estimates of electron-hole and optical mode scattering indicate these processes may limit the mobility of electrons above room temperature.

* Work performed under Contract AF 33(616)-7901 with the Air Force Systems Command.

[1] W. D. Lawson et al., J. Phys. Chem. Solids 9, 325 (1959).

E3. DYE-SENSITIZED PHOTOCONDUCTIVITY OF ZINC-OXIDE FILMS*. L. I. Grossweiner and S. J. Dudkowski, Department of Physics, Illinois Institute of Technology, Chicago.—Adsorbed eosin dye sensitizes the surface photoconductivity of zinc oxide thin films to visible wavelengths. The essential step of the proposed mechanism is the photoexcitation of holes in the dye layer and their capture

at interstitial Zn^+, thereby enhancing the zinc-oxide conductivity by increasing the conduction electron lifetime. The process has been investigated by establishing a photoconductivity level in the zinc-oxide layer with light absorbed in its fundamental band and superimposed visible light absorbed only by the dye. The equilibrium photocurrent always varies with the one-half power of the "eosin light" intensity, indicating that the holes generated in the eosin layer decay by a fast recombination with trapped electrons. The build-up and decay of sensitized photocurrent is exponential in time, with a temperature dependence which suggests that the kinetics are controlled by the carrier motion. The available information on band energies in zinc oxide and eosin is consistent with the proposed model.

* Work supported by the U. S. Atomic Energy Commission.

E4. FIELD ELECTRON EMISSION FROM SEMICONDUCTORS. W. R. Savage, Materials Research Laboratory, Corporate Research & Engineering, Texas Instruments Incorporated, Dallas 22, Texas.—The phenomenon of high field electron emission consists of the tunneling of electrons through the deformed potential barrier at the surface. The thinned barrier results from the action of a high electrostatic field at a conductor-vacuum interface. For a semiconductor the field emission current originates from both the conduction band, j_c, and valence band, j_v. The relative magnitudes of j_c and j_v depend on the bulk properties and surface condition of the semiconductor. Stratton has recently revised the theory of field emission from semiconductors. The theory includes corrections for the difference between effective and free electron masses with detailed results obtained for spherical energy surfaces. The current arising from the conduction band is proportional to the probability for emission from the Fermi level for positive Fermi energies or the bottom of the conduction band for negative energies. Deviations from linearity in the Fowler-Nordheim graph, $\ln j_c$ versus $1/F$, arise from changes in surface potential as a function of external field. The current arising from the valence band is approximately proportional to the probability of emission from the top of the valence band and is essentially independent of temperature. Experimentally the emission parameters of Fermi energy, surface potential and electron affinity plus band gap energy may be varied by selection of cathode material, bulk doping levels and surface treatment. The essential features of the theory are qualitatively consistent with experimental results.

THURSDAY AFTERNOON, 23 August

F1. (Invited paper, one hour) PROPERTIES OF NON-STOICHIOMETRIC COMPOUND SEMICONDUCTORS. W. W. Scanlon, U. S. Naval Ordnance Laboratory, Silver Spring.

PROCEEDINGS OF THE

BLACK HILLS

SUMMER CONFERENCE

ON TRANSPORT PHENOMENA

(Mainly heat flow and charge flow in
semiconductors at elevated temperatures)

Tuesday 21 August
Through Thursday 23 August 1962

South Dakota School of Mines
and Technology
Rapid City, South Dakota

Sponsored by

South Dakota School of Mines and Technology
Office of Naval Research
Visiting Scientists Program in Physics,
American Institute of Physics

Issued as Final Report under
Office of Naval Research Contract No. Nonr(G)-00064-62
Authority NR 017-459/2-6-62

15 October 1962

Before giving reference to the
work contained in this book
interested persons are requested
to obtain permission from the
authors

CONTENTS

LIST OF PARTICIPANTS

C. H. Armitage
Allis-Chalmers
Milwaukee, Wisc.

M. D. Blue
Honeywell Research Center
500 Washington Ave. So.
Hopkins, Minn.

R. J. Colvin
U.S.S. Research Center
Monroeville, Pa.

J. H. Cope
SDSM&T

Gordon C. Danielson
Physics Dept.
Iowa State University
Ames, Iowa

William G. Delinger
SDSM&T

Kenneth W. Foster
Monsanto Res. Corp.
Miamisburg, Ohio

Donald D. Glower
Sandia Corporation
Albuquerque, N. M.

Robert Wood Green
Morningside College
Sioux City, Iowa

Leonard I. Grossweiner
Physics Dept.
Illinois Institute of Tech.
Chicago, Illinois

F. A. Hamm
3M Co.
2301 Hudson Road
St. Paul 19, Minn.

Marvin W. Heller
Physics Dept.
Colorado State University
Fort Collins, Colorado

W. A. Hixson
SDSM&T

Roy L. Hoffman
SDSM&T

R. Jaggi
IBM Research Center
Yorktown Heights, N.Y.

Horst H. Kedesdy
USASRDL
Fort Monmouth, N. J.

Wally F. Klawiter
Sioux Falls College
Sioux Falls, S. D.

Arthur Klein
Physics Dept.
Iowa State University
Ames, Iowa

P. G. Klemens
Westinghouse Research Lab.
Pittsburgh 35, Pa.

E. E. Kohnke
Oklahoma State University
Stillwater, Okla.

Ronald J. Kostelecky
Physics Dept.
Mankato State College
Mankato, Minn.

M. J. Laubitz
National Research Council
Ottawa, Canada

A. L. Lingard
SDSM&T

William Lucke
Naval Research Laboratory
Washington 25, D. C.

Spencer Macy
AC Spark Plug Co., Dept. 3229
7929 S. Howell Ave.
Milwaukee 1, Wisc.

Joel J. Martin
Physics Dept.
Iowa State University
Ames, Iowa

P. D. Maycock
Texas Instr.
Box 5474
Dallas, Texas

Robert D. McCarty
National Bureau Standards
Laboratories
Boulder, Colorado

Gottfried I. Moller
Physics Dept.
State Univ. S. Dakota
Vermillion, S. D.

Rees Morgan
SDSM&T

Robert G. Morris
SDSM&T

George F. Niederauer
SDSM&T

R. W. Powell
National Physical Laboratory
Teddington, England

R. Daniel Redin
SDSM&T

William L. Reuter
SDSM&T

David Roach
SDSM&T

William R. Savage
Texas Instruments
P.O. Box 5474
Dallas 22, Texas

Wayne Scanlon
Naval Ordnance Lab.
Silver Spring, Md.

Henn H. Soonpaa
Honeywell Res. Center
500 Washington Ave. So.
Minneapolis, Minn.

Edgar Steigmeier
RCA Labs
Princeton, N. J.

E. R. Stensaas
SDSM&T

Keh C. Tsao
SDSM&T

Robert Vest
Systems Res. Laboratories, Inc.
Dayton, Ohio

Donald A. Watson
SDSM&T

Lloyd A. White
Office of Naval Research
86 E. Randolph St.
Chicago, Illinois

R. K. Willardson
Bell and Howell Res. Center
360 Sierra Madre Villa
Pasadena, Calif.

M. G. Williqman
SDSM&T

PERSONS IN GROUP PICTURE

H. Soonpaa (holding pole), M. D. Blue, G. Moller, W. G. Delinger, E. Steigmeier, L. White, R. J. Kostelecky, D. Roach, P. Maycock, R. W. Powell, W. W. Scanlon (obscured), J. J. Martin (obscured), P. G. Klemens, R. Green, E. E. Kohnke, H. Kedesdy, D. A. Watson, W. Lucke, C. H. Armitage (obscured), W. R. Savage, R. G. Morris, R. Vest, R. D. Redin, L. I. Grossweiner, R. Jaggi, D. D. Glower, M. W. Heller, G. C. Danielson, A. Klein, R. K. Willardson, G. Niederauer (partly obscured), K. W. Foster, M. J. Laubitz. Kneeling: S. Macy, W. F. Klawiter, F. A. Hamm.

A1. (Invited paper) ON THE SERIES COMPARATOR METHODS OF MEASURING THERMAL CONDUCTIVITY

by

M. J. Laubitz
Division of Applied Physics
National Research Council
Ottawa, Canada

ABSTRACT

A method of mathematical analysis of series comparators is outlined and results of calculations for one particular comparator are presented. It is shown that when the conductivity of the unknown differs significantly from the standard, the comparator gives grossly erroneous results.

Introduction

Discrepancies in the values reported for the thermal conductivity of various substances appear to be the rule, rather than the exception, and tend to be generally accepted. Such tacit glossing over is not possible in the case of the results reported for titanium carbide, as there fairly fundamental principles are involved. A brief summary of the experimental work concerned is here given. Vasilos and Kingery (1954) measured the thermal conductivity of titanium carbide in the temperature range of 100°C to 800°C using a series comparator with dense alumina as a standard, and in the range of 500°C to 1000°C using an absolute method with an ellipsoidal specimen. The two sets of results that they obtained match reasonably well in magnitude when corrected for specimen porosity, and decrease

from 0.075 cal/cm sec °C at 0°C (extrapolated) to 0.012 cal/cm sec °C at 1000°C. Vasilos and Kingery also measured the electrical resistivity of their specimens at room temperature, and obtained values from 60 to 70 μ ohm-cm. In 1961, Taylor reported the thermal conductivity of titanium carbide obtained by an absolute method involving cylindrical heat flow. His results increased almost linearly with temperature from a value of 0.078 cal/cm sec °C at 0°C (extrapolated), through 0.096 cal/cm sec °C at 1000°C to 0.11 cal/cm sec °C at 2000°C. Taylor measured the electrical resistivity of his specimen as well; it increased from 60 μ ohm-cm at room temperature to 110 μ ohm-cm at 800°C.

When these results are compared, three disturbing features appear. Primarily, there is the obvious discrepancy in the values reported for the thermal conductivity of titanium carbide, both in magnitude and in its functional variation with temperature: the two sets of results differ by a factor of 10 at 1000°C, while at room temperature there is good agreement both in thermal and electrical conductivity. Secondarily, the results of Vasilos and Kingery for temperatures larger than 300°C are smaller than the electronic contribution to the heat conductivity alone, as computed by the Wiedemann-Franz relation from the electrical resistivity results of Taylor. Admittedly, the electrical resistivity reported by Taylor is smaller than values found elsewhere in literature (see for instance Munster and Sagel 1956) but even the higher values of electrical resistivity yield an electronic heat conductivity at 800°C that

is twice as large as the measured values of Vasilos and Kingery. And thirdly, if one subtracts the electronic heat conductivity, calculated from Taylor's resistivity values, from his measured thermal conductivity one obtains a remainder that is independent of temperature rather than one displaying the 1/T relationship expected of phonon conductivity, the alternate mode of heat transfer.

It seems unlikely that the discrepancies between Taylor's results and those of Vasilos and Kingery are due to inherent differences in the specimens: small differences in composition should have little effect on thermal conductivity, while large differences in composition should significantly affect the electrical conductivities at room temperature. Neither does the assumption of cracks and voids resolve the discrepancy, for it will not account for either set of results if the other is presumed correct. One must therefore consider the only alternative: one or the other set of experimental results, or perhaps even both, are completely wrong. The following are the possibilities: the results of Vasilos and Kingery are correct, and we must assume that the Wiedemann-Franz law is invalid in this instance; or the results of Taylor are correct, and either the Wiedemann-Franz law does not hold, or the phonon conductivity does not vary inversely with temperature, or there is another important mechanism of heat transfer in titanium carbide operating at relatively low temperatures. There is of course the third, by far the most palatable choice, that neither Taylor

nor Vasilos and Kingery is correct. This last possibility does not impose upon us any further restrictions regarding transport phenomena; however, the reputations of the authors involved are such as not to make it very probable.

The solving of this riddle is not going to be an easy matter. In this paper we propose to take the first and perhaps easiest step, by taking a critical look at the comparator instrument used by Vasilos and Kingery. We will, in fact, investigate the following problem: suppose that Taylor's results are correct, which means that there is a large difference between the conductivity of the unknown and that of the standard (Al_2O_3) in the comparator used by Vasilos and Kingery; what results would one then obtain from the comparator?

Mathematical Analysis

An exact mathematical analysis of a series comparator is fairly straightforward if the conductivity of the unknown is equal to that of the standard (Laubitz 1961 - where it is shown that comparators can give erroneous results even under this ideal condition). If one allows the conductivity of the unknown to depart significantly from that of the standard, the exact analysis, although possible in principle, becomes extremely tedious. One gets involved with two infinite series, one of a Fourier and one of a Bessel type, with each of the coefficients of either series being expressed as a weighted sum of the coefficients of the other series. Clearly some approximate approach is indicated.

The system we propose to analyze is shown in Fig. 1. It consists of three specimens, each of length 2ℓ and radius a, the two end specimens being standards of conductivity k_1, and the mid-piece being the unknown of conductivity k_2. The specimens are surrounded by a guard of inner radius b, the space between the guard and the specimens being filled with insulation of conductivity k_3. Each of the specimens has two thermocouples on it, positioned a distance λ from the specimen end-faces. The guard has four thermocouples: these ideally are maintained at temperatures equal to those of the sample by means of guard heaters. The two end thermocouples are matched directly with the end thermocouples of the specimen assembly, while the two middle thermocouples are matched to the average of the two specimen thermocouples at each standard-unknown boundary. The ratio of the conductivity of the unknown to that of the standard is calculated from the ratio of the average of the two temperature differences measured on each standard to the temperature difference on the unknown.

In the analysis we will assume that the guard is perfectly lined up with the specimens, and is at its "optimum" temperature match with the specimens, by which we mean that the temperature along r = b can be expressed by a term linear in z, plus a small term to account for the matching of the middle thermocouples; these idealized temperature distributions are shown in Fig. 1. As pointed out previously (Laubitz 1961) the Vasilos and Kingery type of comparator can have wildly varying guard temperatures

while ostensibly being matched in temperature to the specimen. The assumption of an "optimum" match gives therefore the comparator the benefit of more doubt than that to which it is reasonably entitled. The assumption of an optimum match makes the mid plane of the unknown, $z = 0$, a mirror plane, and hence one of constant temperature, assumed zero for convenience. The two end planes $z = \pm 3\ell$ are also assumed planes of constant temperature, $\pm T_o$ respectively, and the deviation of the guard temperature from linearity is assumed to be represented functionally reasonably well by a term in $\sin \frac{\pi z}{3\ell}$.

We then assume the following relatively simple solutions for the temperature distribution, which satisfy the external boundary conditions.

In the standards

$$T(r,z) = T_1 + g_1(z - \ell) + \sum_n A_n \frac{I_o(\alpha_n r)}{I_o(\alpha_n a)} \sin \alpha_n z$$

In the unknown

$$T(r,z) = g_2 \cdot z + \sum_n A_n \frac{I_o(\alpha_n r)}{I_o(\alpha_n a)} \sin \alpha_n z$$

and in the insulation surrounding the specimens

$$T(r,z) = g_3 \cdot z + D \frac{F_o(\alpha_1 r, \alpha_1 a)}{F_o(\alpha_1 b, \alpha_1 a)} \sin \alpha_1 z + \sum_n B_n \frac{F_o(\alpha_n r, \alpha_n b)}{F_o(\alpha_n a, \alpha_n b)} \sin \alpha_n z$$

where

$$T_1 = \frac{T_o}{2\frac{k_2}{k_1} + 1}$$

$$\alpha_n = \frac{n\pi}{3\ell}$$

$$g_1 = \frac{T_o - T_1}{2\ell} \quad , \quad g_2 = \frac{T_1}{\ell} \quad , \quad g_3 = \frac{T_o}{3\ell}$$

and

$$D = \frac{(3T_1 - T_o)(1 - \frac{3\lambda}{4\ell})}{3 \sin \alpha_1 \ell}$$

D expresses the temperature matching conditions for the mid-thermocouples. I_o and K_o are the associated Bessel functions of the first and second kind of order zero, and

$$F_o(x,y) = I_o(x)\, K_o(y) - I_o(y)\, K_o(x)$$

It is impossible to achieve exactly the required temperature and heat flow matches at the two internal boundaries $z = \ell\ (o \leq r \leq a)$ and $r = a\ (o \leq z < \ell)$ with such relatively simple solutions. An approximate match can be obtained, however, the specific nature of the approximation being best seen by the approach of "virtual heat sources and sinks". Briefly, this approach is as follows. If two bodies 1 and 2 with conductivity k_1 and k_2 respectively have a common boundary s with normal $\underline{n}$ pointing from body 2 to body 1, then the <u>temperature distribution</u> for the composite can be calculated by substituting k_1 for k_2 in body 2, which makes it a single-body problem, and assuming a virtual heat source or sink along the surface s of specific magnitude

$$Q_s = \frac{k_1}{k_2}(k_1 - k_2)\frac{\partial T_s}{\partial n}$$

where T_s is the surface temperature in body 1 along the boundary.

In our case, we want to substitute the conductivity of the standard for that of the unknown. The source along $z = \ell\ (o \leq r \leq a)$ is given by

$$Q_s(\ell) = \frac{k_1}{k_2}(k_1 - k_2)\left[g_1 + \sum_n A_n \cdot \alpha_n \cdot \frac{I_o(\alpha_n r)}{I_o(\alpha_n a)} \cos \alpha_n \ell\right]$$

and along r = a ($o \leq z \leq \ell$)

$$Q_s(a) = \frac{k_3}{k_2}(k_1 - k_2)\left[\frac{D \sin \alpha_1 z}{a\, F_o(\alpha_1 b, \alpha_1 a)} + \sum_n B_n \frac{F_o'(\alpha_n a, \alpha_n b)}{F_o(\alpha_n a, \alpha_n b)} \sin \alpha_n z\right]$$

where F_o' is the derivative of F_o with respect to r.

So far the treatment of the virtual sources and sinks has been rigorous. We now make what might be considered the first order approximation

$$Q_s(\ell) \sim \frac{k_1}{k_2}(k_1 - k_2)\, g_1$$

$$Q_s(a) \sim \frac{k_3}{k_2}(k_1 - k_2)\frac{D \sin \alpha_1 z}{a\, F_o(\alpha_1 b, \alpha_1 a)}$$

Under this approximation explicit formulae for A_n and B_n can readily be obtained, and the temperature distribution calculated. In physical terms, the approximation means a perfect temperature match along r = a and along z = ℓ; a perfect heat flow match along r = a ($\ell \leq z \leq 3\ell$); and an approximate heat flow match along r = a ($o \leq z \leq \ell$) and along z = ℓ ($o \leq r \leq a$). Along z = ℓ, the approximation is a good one, particularly for higher values of k_1/k_3, the ratio of the conductivity of the standard is that of the insulation. Along r = a ($o \leq z \leq \ell$) the term in D included into the calculation is of the same magnitude as the first term of the rejected infinite series; subsequent terms of the series decrease approximately as n^{-2}. For $\frac{k_2}{k_1} > 1$, the range in which we are primarily interested, the term in D and the

infinite series have the same sign; hence our approximation describes only about one half of the radial heat exchange between the unknown and the insulation. For $k_2/k_1 < 1$, the contributions to the virtual heat source $Q_s(a)$ tend to cancel for some values of k_2/k_1, and reinforce for others. Of course further terms could be included in the $Q_s(a)$ making the approximation better. This makes the calculation of the coefficients A_n and B_n more complicated, but not beyond the range of a desk calculator.

Results of calculations

The aim of the calculations is to obtain the error in the results of the comparator, conveniently given by the ratio, $\frac{k_{2(obs)}}{k_2}$, of the conductivity of the unknown that the comparator yields to its true value. This ratio was calculated for an arrangement parametrically equivalent to the Vasilos and Kingery comparator for various values of k_1/k_3, the ratio of the conductivity of the standard to that of the insulation; $\frac{k_2}{k_1}$, the ratio of the conductivity of the unknown to that of the standard; and λ/γ, the relative positioning of the thermocouples on the specimens. In the calculations, the summation was extended over twelve terms of the infinite series involved. Some of the results of the calculations are shown in Figures 2, 3, and 4.

If we assume for k_2 the values reported by Taylor for titanium carbide, and for k_1 and k_3 the conductivities of alumina and insulating brick as ued by Vasilos and Kingery, we can, by graphical interpolation of Fig. 2 and 3, obtain the desired

results: the conductivity that the comparator would yield if Taylor's results were correct. These calculated results are illustrated in Fig. 5, together with the values obtained by Taylor, and by Vasilos and Kingery. Clearly we have not resolved the magnitude of the discrepancy of the experimental results; this perhaps would have been too much to hope for. However, the calculations do indicate that the comparator would yield very large errors under the assumed circumstances, and completely distort the functional variation of the conductivity with temperature. Since the calculations were made for optimum operating conditions of the comparator, unlikely to be achieved in practice, and since the approximations employed in the calculations probably tend to underestimate the heat exchange between the unknown and its surroundings, one is forced to conclude that the results obtained by Vasilos and Kingery on the comparator do not form reliable evidence against the validity of Taylor's results. The discrepancy is now therefore reduced to the results of the two absolute methods of measurement: the ellipsoidal heat flow of Vasilos and Kingery, and the radial heat flow of Taylor.

Conclusions

A method of mathematical analysis of the series comparator was outlined, for the case where the conductivity of the unknown differs widely from that of the standard. Results of calculations were given for one particular comparator, parametrically equivalent to that employed by Vasilos and Kingery in measuring

the conductivity of titanium carbide. The calculations have shown that for large values of the ratio of the conductivity of the unknown to that of the standard the results obtained from the comparator are completely unreliable, being grossly in error both in magnitude and in their functional variation with temperature. Thus, in considering the divergent results reported for the thermal conductivity of titanium carbide by Taylor and by Vasilos and Kingery, that part of the results of the latter which was obtained from the series comparator cannot be considered as being in definite disagreement with Taylor.

REFERENCES

Laubitz, M. J. 1961. Can. J. Phys. 39, p. 1029.

Munster, A. and Sagel, K. 1956. Z. Physik 144, p. 139.

Taylor, R. E. 1961. J. Am. Ceram. Soc. 44, p. 525.

Vasilos, T. and Kingery, W. D. 1954. J. Am. Ceram. Soc. 37, p. 409.

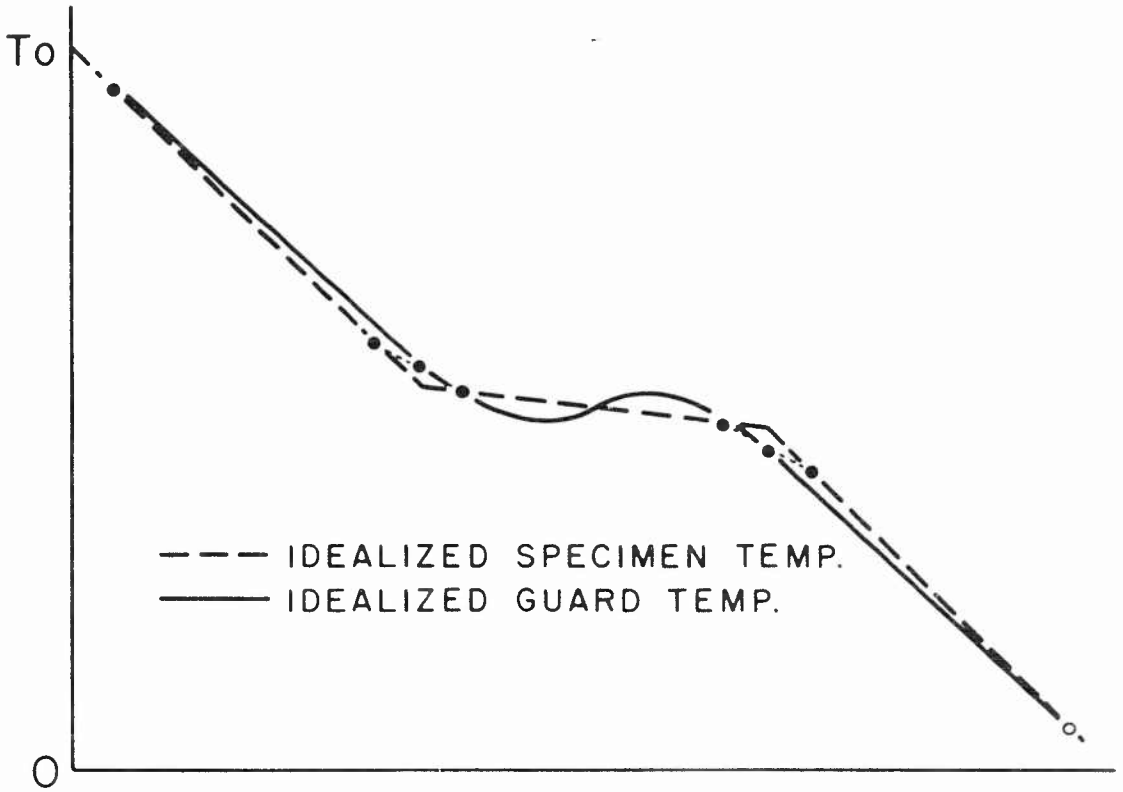

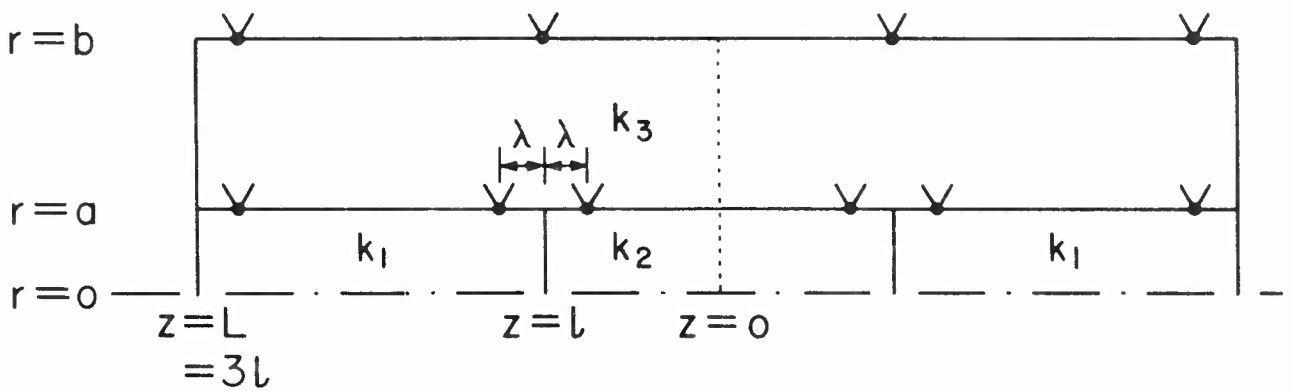

Fig. 1. Schematic representation of the system analyzed, and idealized temperatures in the system.

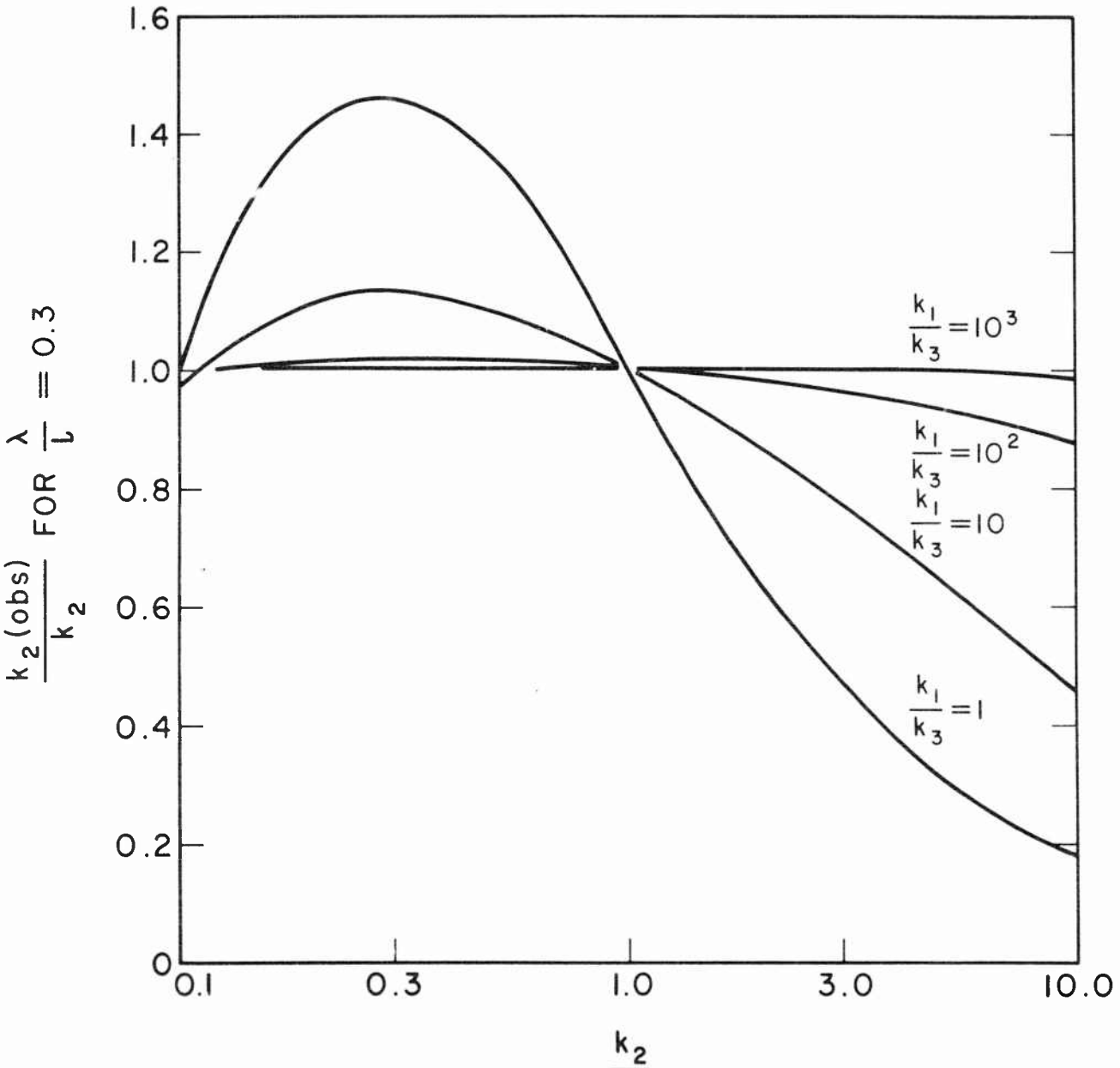

Fig. 2. Variation of $\frac{k_{2(obs)}}{k_2}$ with $\frac{k_2}{k_1}$ for $\frac{\lambda}{\ell} = 0.3$

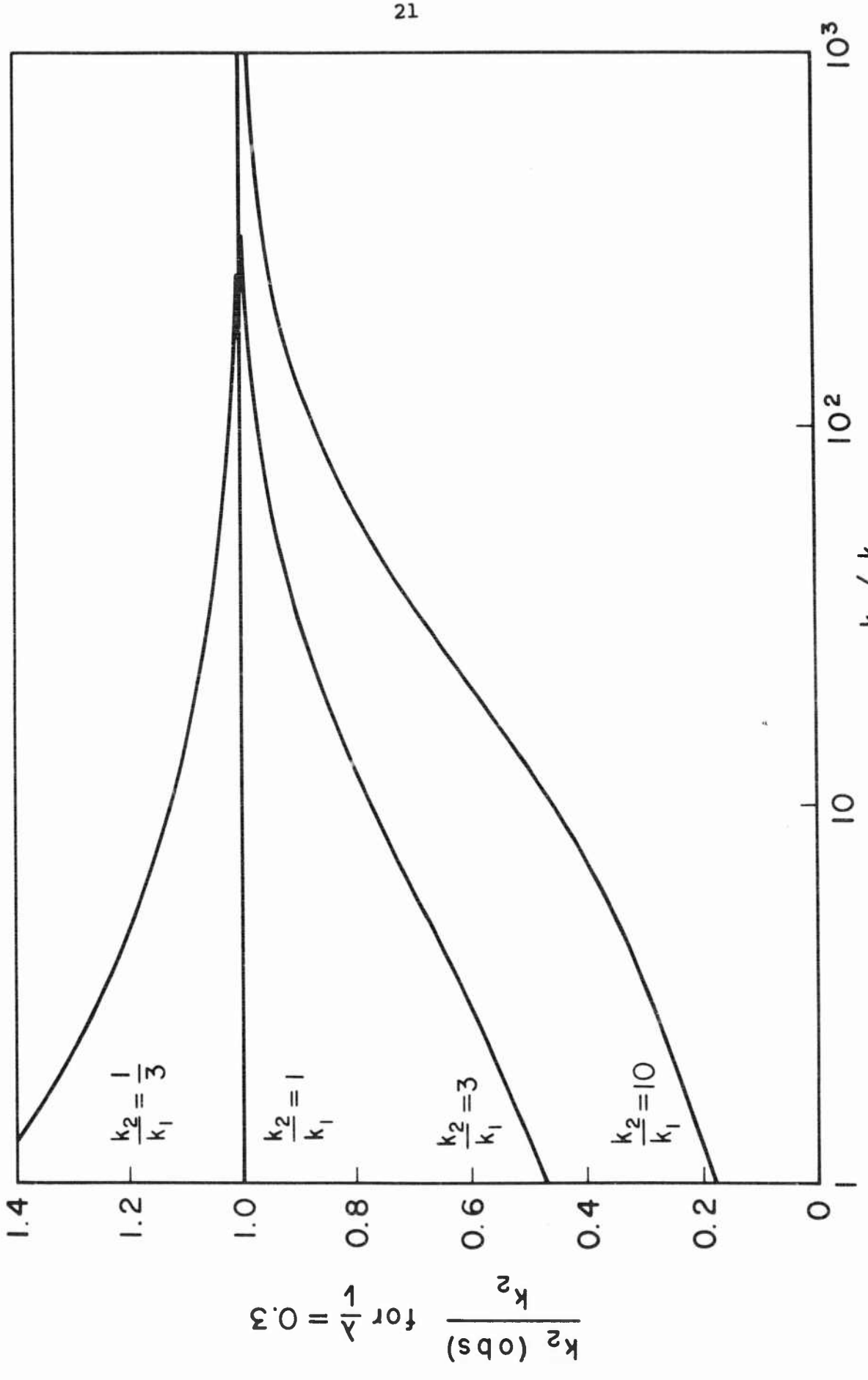

Fig. 3. Variation of $\frac{k_{2(obs)}}{k_2}$ with $\frac{k_1}{k_3}$ for $\frac{\lambda}{\ell} = 0.3$

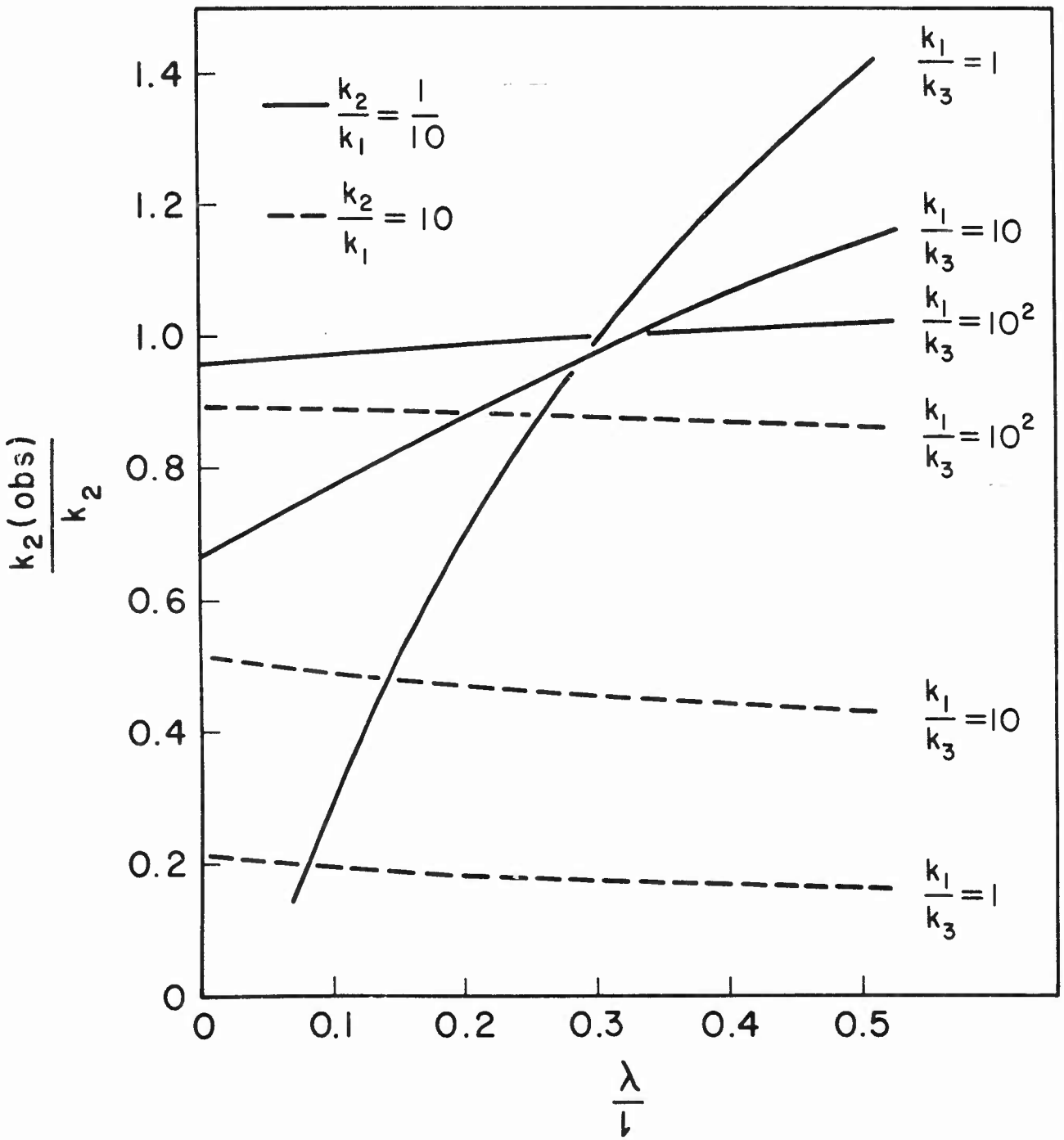

Fig. 4. Variation of $\frac{k_{2(obs)}}{k_2}$ with λ/ℓ .

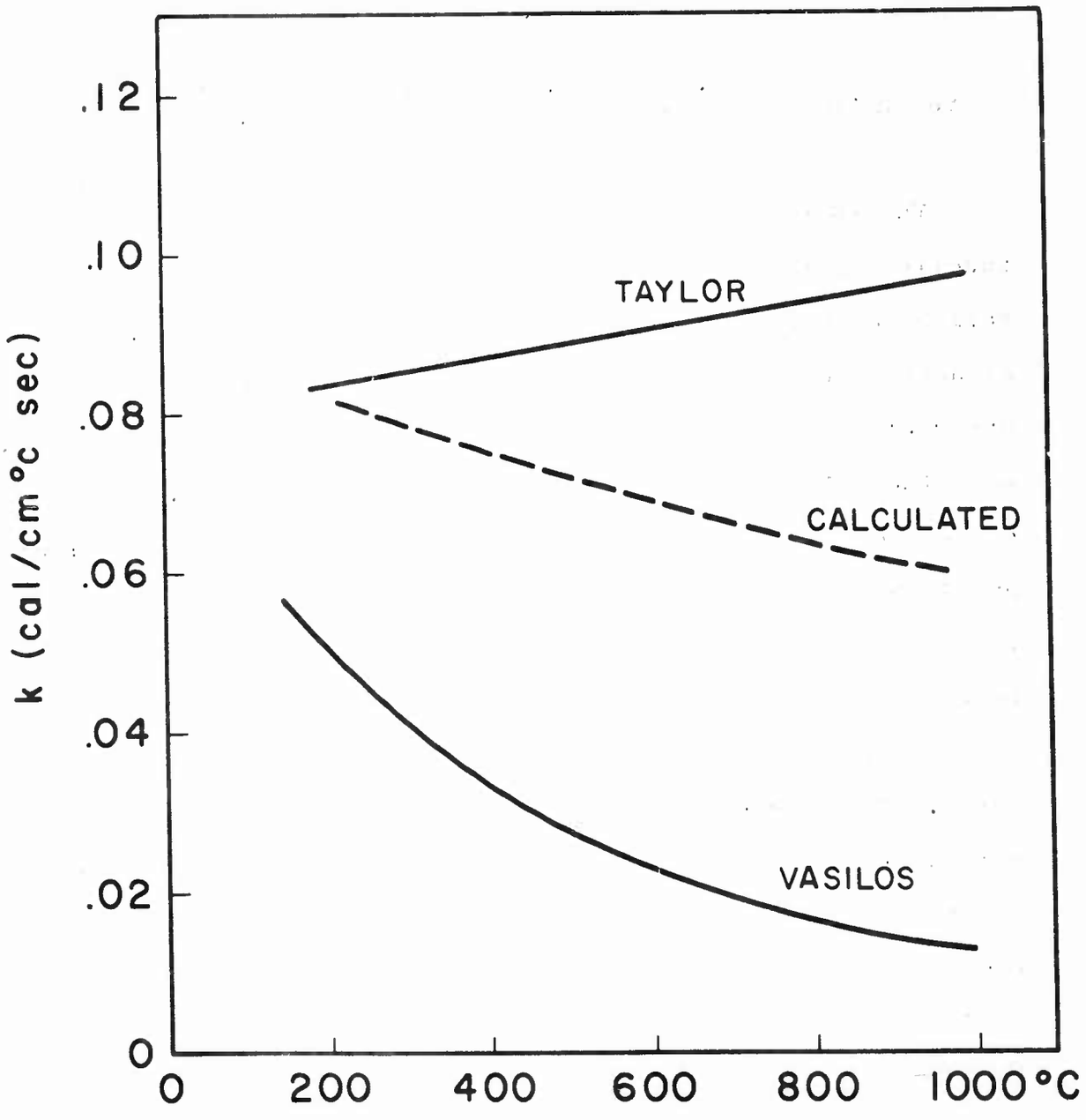

Fig. 5. Thermal conductivity of TiC, as given by Taylor and by Vasilos and Kingery. The calculated values are those that would be obtained from a Vasilos and Kingery type of comparator if Taylor's values for the conductivity of TiC were correct.

A2. THERMAL CONDUCTIVITY MEASUREMENTS ON SILICON TO 1000°K*

by

Joel J. Martin and Robert G. Morris
South Dakota School of Mines and Technology, Rapid City

The thermal conductivity of silicon was measured as a function of temperature from 680°K to 1000°K by a series comparison method similar to that of Morris and Hust (8). Two standards were used; one was placed above the sample and the other below the sample. The sample holder is shown in Fig. 1. Good thermal contacts were made at the junctions with a mixture of sodium silicate and graphite. Technical "G" Copper Cement (13) and Alundum Cement (2) were also tried in addition to the compounds previously tried by Hust (4). Technical "G" Copper Cement was no better than the sodium silicate and graphite and the Alundum Cement had no adhesive properties at these temperatures. Six thermocouples made from platinum and platinum-10% rhodium reference-grade wire were placed along the standard-sample-standard sandwich to measure the temperature drop across each element. The thermocouples were clamped to the sample holder with Transite (14) clamps. These clamps reduce the temperature drop along the thermocouple leads for a short distance away from the sandwich and, therefore, reduce radial heat losses. On early runs, the thermocouples were welded to the sandwich insuring that they will be in good thermal contact with the sandwich. However, the process was extremely time consuming

---

* This work supported in part by the Office of Naval Research.

and on later runs the thermocouples were cemented to the sandwich with the sodium silicate and graphite to speed up the measurements.

Convection losses were reduced by operating the equipment in a vacuum that was usually around $5(10)^{-5}$ mm of Hg.

Radiation losses were reduced by a self-guarding method. The guard is a cylinder of fired Lava (6) sliced to match the corresponding parts of the sandwich. The copper heat sink at the bottom of the sample holder holds that end of the guard at the same temperature as that end of the sandwich. A copper bridge performs the same function at the other end. A thermocouple was placed on the center section of the guard. The temperature at that point was usually found to be between the temperatures at the ends of the sandwich.

Three different single crystal cylindrical samples (23 mm diameter and 8 mm thickness) which were oriented with the (111) direction parallel to the cylinder axis were measured. The two n-type samples had a donor concentration of about $5(10)^{16}$ per cm^3, and the p-type sample had an acceptor concentration of about $(10)^{18}$ per cm^3. The standards were Armco magnetic ingot iron which is high purity (99.9+%) iron and is reproducible from batch to batch. Armco iron makes a good standard because its thermal conductivity has been extensively measured and it has approximately the same thermal conductivity as the silicon samples. The thermal conductivity of the standards was taken from a graph prepared from values that Powell (10) lists as most probable values.

The temperature differences are proportional to the differences in the thermocouple readings. These are measured for three or four different gradient heater currents with the ambient temperature held constant because the condition for zero heat flow in one part of the sandwich is not necessarily the same as the condition for zero heat flow in another part. The ambient temperature is taken to be the average of the readings of the two thermocouples on the sample. A plot of the temperature difference of sample versus the temperature differences of the two standards should be straight lines. Fig. 2 is a typical plot. The thermal conductivity is contained in the slope of each of these lines. It is given by

$$K_u = K_s(\Delta X_u A_s)/(m\Delta X_s A_u), \qquad (1)$$

where K_u is the thermal conductivity of the sample, K_s is the thermal conductivity of the standard, m is the slope, ΔX_u and ΔX_s are the thermocouple separations of the sample and standard, and A_u and A_s are the areas of the sample and standard respectively. The thermal conductivity is determined from Eq. 1 for both standards. Since the slopes of the lines for the two standards are different, the two standards will give different thermal conductivities for the sample if the thermocouple separation of the two standards is the same. Hornstra (3) has shown that the average of these two values will result in the correct thermal conductivity for the sample if the difference in heat flow through the top standard and the sample is the same as the difference in the heat flow between the sample and the bottom standard and if the ambient temperature remains constant.

It is believed that these conditions are experimentally fulfilled. The slopes for the two lines are determined by a curve-fitting routine on an I.B.M. 1620 computer. Data are considered usable if the temperature drop across the junctions is on the same order as the drop across the standards, if the temperature drift is less than 0.01°C per min., and if the plots of ΔV_{34} versus ΔV_{12} and ΔV_{56} are linear. This temperature drift is an improvement by a factor of five over that of Hust (5) and is good enough so that it is no longer necessary to use the comparator to measure the ΔV's directly.

Eight separate runs or mountings were made; all of the runs but the fourth and the eighth were terminated by equipment failure. These failures took the form of broken junctions, thermocouples falling off the sandwich or deteriorating, and open heater windings.

Fig. 3 shows a plot of the thermal resistivity (1/K) vs the absolute temperature. Also shown are the results of some other workers and a curve based on theory. Morris and Hust (9) give K as 0.46 watt/cm °C at 698°K; a K of 0.51 watt/cm °C would be consistent with the results of this experiment. These results agree within 10%. This is within the maximum estimated experimental error of ±2%. The results that Abeles et al. (1) obtained from thermal diffusivity measurements are bracketed by the results of this direct method. Our results are also in essential agreement with those that Shanks, Maycock, Sidles and Danielson (12) obtained from thermal diffusivity measurements.

The charge carrier contribution was calculated for 1000°K from an equation of Price (11) that includes bipolar diffusion and was found to be about 1.8% of the total thermal conductivity. A calculation based on the theory of Leibfried and Schlömann with the Grüneisen constant taken as 2 is plotted with the results. This theoretical curve falls slightly above the results of these measurements. Fig. 3 shows that K is very nearly proportional to 1/T.

REFERENCES

1. Abeles, et. al., "Thermal Conductivity of Ge-Si Alloys at High Temperatures," Phys. Rev. 125, 44 (1962).

2. Alundum Cement, Norton Company, Worcester 6, Massachusetts.

3. Hornstra, Fred Jr., "Measurement of Some Thermal and Electrical Properties of Bismuth Telluride and Indium Antimonide in a Magnetic Field," Technical Report No. 5, Contract Nonr 2964 (01), July 1, 1962 (Unpublished), Solid State Physics Project, South Dakota School of Mines and Technology, Rapid City, South Dakota, pp. 71-74.

4. Hust, Jerome G., "High-Temperature Thermal Conductivity in Bismuth Telluride and Silicon," Technial Report No. 2, Contract Nonr 2964(01), March 1, 1961 (Unpublished), Solid State Physics Project, South Dakota School of Mines and Technology, Rapid City, South Dakota

5. Ibid., pp. 72-73.

6. Lava, American Lava Corporation, Chattanooga 5, Tennessee.

7. Leibfried, Günther and Schlömann, Ernst, "Wärmeleitung in Electrisch Isolierenden Kristallen, "Nachr. Akad, Wiss. Göttingen, Math-physik. Kl. IIa, 71 (1954).

8. Morris, Robert G., and Hust, Jerome G., "Thermal Conductivity Measurements of Silicon from 30°C to 425°C," Phys. Rev. 124, 1426 (1962).

9. Ibid.

10. Powell, R. W., in Progress in International Research on Thermodynamics and Transport Properties, edited by Joseph F. Masi and Donald H. Tsai, (Academic Press, New York, 1962) p. 454.

11. Price, P. J., "Ambipolar Thermodiffusion of Electrons and Holes in Semiconductors," Phil. Mag. 46, 1252 (1955).

12. Shanks, H. R., et al., "Thermal Diffusivity of Silicon at High Temperatures," Bull. Am. Phys. Soc. Series II., 6, 174 (1961).

13. Technical "G" Copper Cement, W. V-B. Ames Company, Fremont, Ohio.

14. Transite, Johns-Manville, 22 E. 40th Street, New York 16, New York.

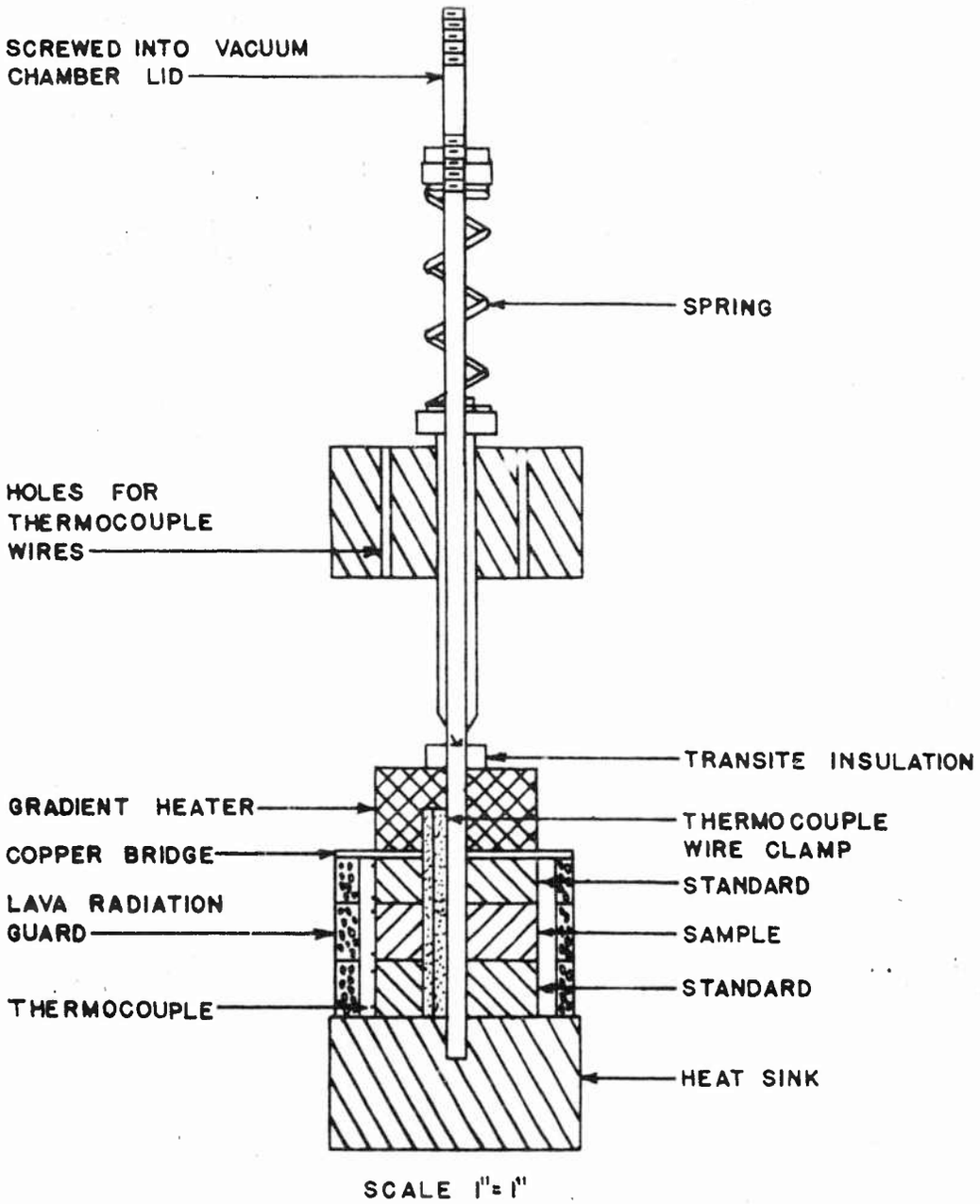

Fig. 1. Cross-section of the sample holder.

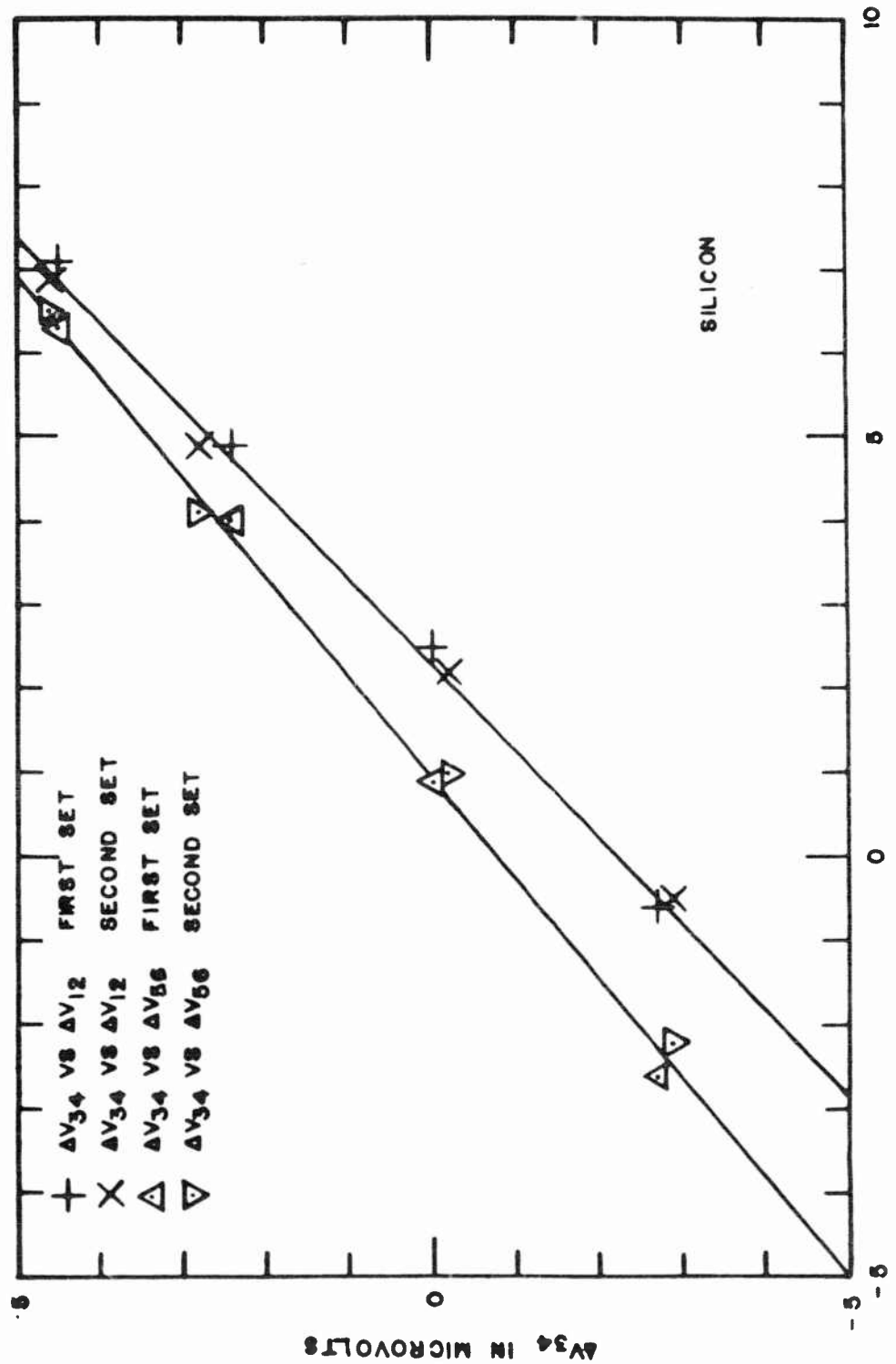

Fig. 2. Typical plot of ΔV_{34} versus ΔV_{12} and ΔV_{56}. Data taken from Run 2. $T \cong 767^{o}K$.

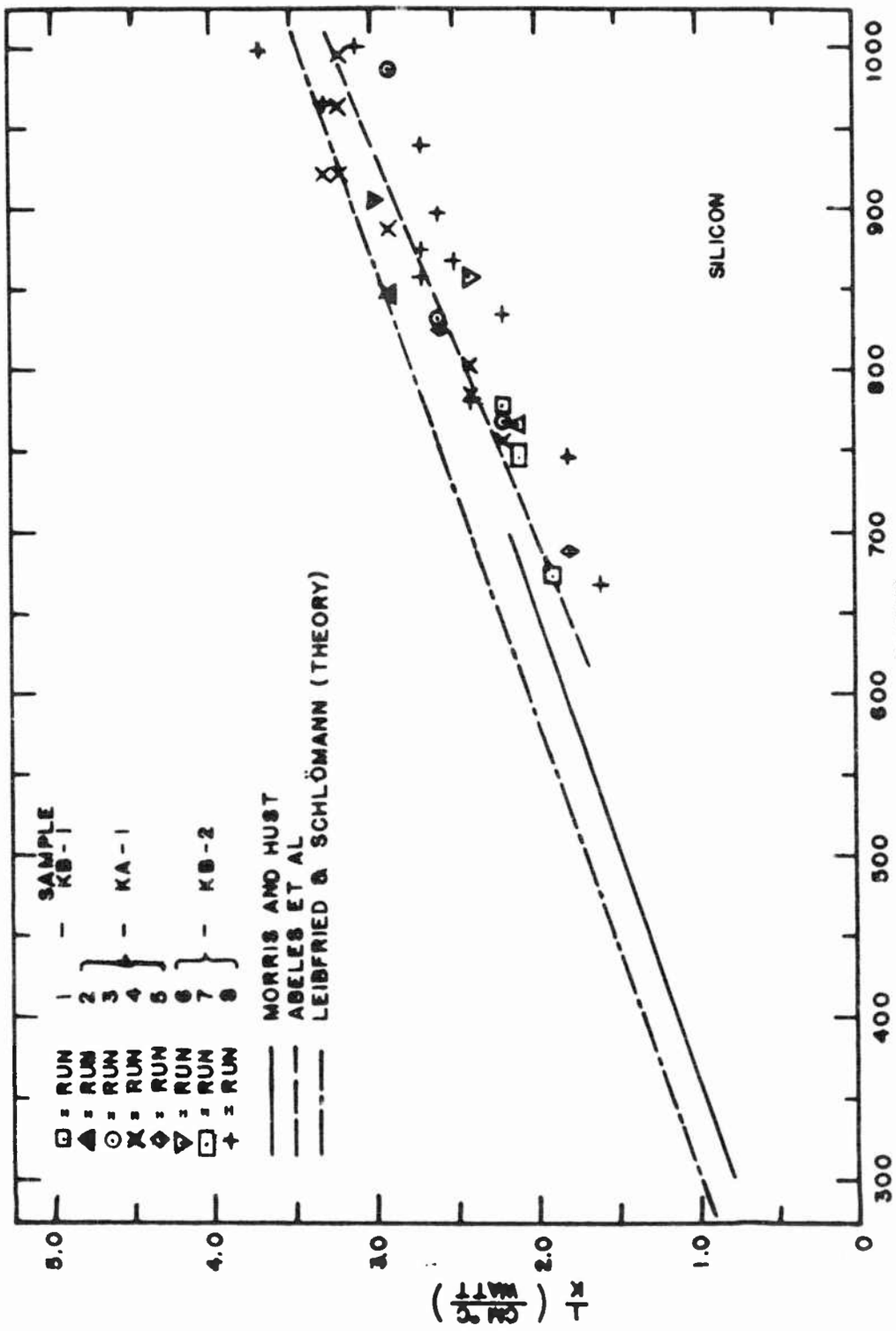

Fig. 3 Thermal resistivity of silicon as determined in this experiment. The results of other investigators and theory are shown.

A3. THERMAL DIFFUSIVITY MEASUREMENT ON A FINITE DISK*

by

Paul Dean Maycock**

Abstract:

A new technique has been developed for measuring the thermal diffusivity of finite disk-shaped samples. The radial heat flow equation was solved by the method of finite differences. An axial heater was turned on and the temperatures at three radial positions were measured as functions of time. This procedure determined the boundary conditions necessary for the solution of the heat flow equation. By assuming various values of the thermal diffusivity, we obtained the solution at the middle thermocouple. The value which gave the best agreement between the computed solution at the middle thermocouple and the experimental curve obtained at the midpoint was considered to be the best value for the diffusivity. A FORTRAN program which calculates the diffusivity from the experimental data was developed and an IBM 704 computer was used to process the data. Data on Armco iron show that the method is capable of giving correct values for thermal diffusivity.

As attendees of this conference, I'm sure you are all aware of the need for methods which make it possible to measure the thermal properties of solids at high temperatures. Historically, the measurement of the thermal conductivity (K) was the standard method for determining thermal properties of solids. Recently several investigators (1,2,3) have found it desirable to measure

---

* This research was performed at the Ames Laboratory, USAEC
Iowa State University
Ames, Iowa

**Presently at Texas Instruments Incorporated
Corporate Research & Engineering
P. O. Box 5474
Dallas 22, Texas

the thermal diffusivity (k) when the ambient temperature is greater than a few hundred degrees Centigrade. The thermal diffusivity is that property of a material which describes the temperature distribution in a material when the temperature is changing with time. The thermal conductivity (K), the thermal diffusivity (k), the specific heat (c), and the density (d) are related simply by the expression:

$$K = kcd$$

It is common in the measurement of the thermal diffusivity of a solid to choose a sample geometry which will allow a solution to the heat flow equation to be calculated from the experimental data by means of an ordinary desk calculator, thereby placing the boundary conditions such as sinusoidal heat sources and infinite lengths on the experiment (References 1-6). I would like to discuss a method where the sample is finite in the direction of heat flow and the heater has an arbitrary temperature versus time characteristic.

A typical radial geometry is shown in the first figure. A cylindrical sample and guard disks were fabricated from Armco iron with tolerances maintained to ± .001 inch. Butt welded Chromel-Alumel B&S No. 26 thermocouples were peened into the sample at preselected radii of 0.5, 1.0, and 2.0 cm.

It was necessary to guard the sample so that all heat would flow in the radial direction with no loss through the faces of the sample. Since the guard cylinders were made of the same material as the sample itself and identical to the sample in

diameter, temperature gradients perpendicular to the radial direction were practically eliminated.

The heater was a resistance type with axial symmetry. B&S No. 26 Kanthal wire was threaded into a four-hole alundum tube, which had a diameter of 0.30 cm. The resistance of the heater was 1.4 ohms. Lead-acid batteries were used as the heater power supply. Four to six volts sufficed to give a temperature rise of 1°C at the first thermocouple in less than five seconds. The heater was designed to heat the sample and guards uniformly on the axis r=0. With the sample in equilibrium with the ambient temperature, the heater was turned on and the temperature vs time records were taken at the three radii. These data were analyzed using the method of finite differences (7,8,9,10).

A brief outline of the technique is as follows:

First we note that the radial heat flow equation applies in the domain of the three thermocouples. That is, $U_t = k/r\ (U_r) + k(U_{rr})$. This can be simplified by the transformation $Z=\ln r$. The differential equation then becomes $U_t = ke^{-2z}U_{zz}$, where U_t and U_{zz} are the first partial derivative of U (temperature in arbitrary units) with respect to t and the second partial with respect to z, respectively. If we replace the partial derivatives by their finite difference expressions:

$$U_t = \frac{U\ (t+\Delta t,z)\ -\ U\ (t,z)}{\Delta t}$$

$$U_{zz} = \frac{U\ (t,z+\Delta z)\ -\ 2U\ (t,z)\ +\ U(t,z-\Delta z)}{(\Delta z)^2}$$

the resulting finite difference equation is:

$$U(t+\Delta t,z) = U(z+\Delta z,t)\left[k\Delta t e^{-2z}/(\Delta z)^2\right] + U(z,t)\left[1-2e^{2z}k\Delta t/(\Delta z)^2\right] + U(z-\Delta z,t)\left[k\Delta t e^{-2z}/(z)^2\right]$$

This gives us a linear algebraic expression which can be used to calculate the temperature distribution throughout the domain for a given set of boundary conditions and a given value of the diffusivity (k). For the sake of brevity, I shall omit the mathematical considerations as to what criterion must be met for the finite difference expression to converge to the differential equation.

In order to test the method a set of exact curves were generated using an expression given by Carslaw and Jaeger (11). These curves are shown in figure two. Here we have the temperature versus time plot for a radial sample with k=1 with an axial heater turned on at t=o sec. The heater was assumed to have a constant heat out put. The circles represent the exact solution and the crosses represent a hand calculation using the finite difference linear expression, which took approx. 100 hours. As you can see the finite difference calculation is an excellent approximation to the exact data. With this proof in hand I set out to write a FORTRAN program for the IBM 704 which would take the experimental data and calculate the diffusivity from it.

The data shown in figure three correspond to the temperature-time history at three radial points r_1, r_2, r_3 on a cylindrical sample with a heater positioned at r=0 turned on at t=0. The

position of r_2 is determined so that it is midway between r_1 and r_3 in z-space.

Using the finite difference expression, the program generates a temperature versus time curve corresponding to the center radial point r_2 for a particular value of the diffusivity (k) which is the best estimate of the thermal diffusivity for that material at the temperature of the sample. The average squared deviation (σ) between the experimental curve at the mid-point and the calculated curve for k_1 is found and stored. The computer then increases the value of k_1 by a programmed increment Δk so that $k_2 = k_1 + \Delta k$. The deviation (σ_2) is calculated and compared with the previous value (σ_1). If the deviation is less the computer continues to increase k by Δk until a minimum in the deviations is found. If the deviation for k_2 is greater than that for k_1, the computer reverses its field, decreases k by Δk, and searches for a minimum in the deviations. The value of the diffusivity (k) for which the deviations are a minimum is recorded as the thermal diffusivity for that set of data. The computer then accepts another set of data and repeats the analysis. The program is designed to handle all ranges of k, and any sample size which is large enough to determine the temperature-time curves accurately at the three radii.

The analysis of the transformed radial equation was completed using the program described above. In figure 4 the mean squared deviation (σ) for the exact data of Fig. 1 is plotted versus k for the three values of the mesh size 6, 8, and 10. The mesh size is an indication of the number of intervals the spatial domain is divided into for the finite difference

calculus. As the mesh is refined, the minimum of the curves move closer to the exact value of the diffusivity which is 0.1000 cm^2/sec. The computed value for mesh 10, k=0.1006 cm^2/sec is only 0.6% in error so that the transformed equation and its finite difference representation was considered adequate for the analysis of our experimental data. It can be seen in figure 4 that the deviation between the calculated and exact curves is less than 1.0 on a scale of 1000 units. This deviation was within the ability to measure the amplitude of the input curves used as boundary conditions for the finite difference calculation. The equipment and procedure were essentially that used by Kennedy (12). A block diagram of the equipment used to make the measurements is shown in Figure 5. The three sample thermocouples located at $r=r_1$, $r=r_2$, and $r=r_3$ were connected to bucking circuits which balanced out that part of the thermocouple output corresponding to the ambient temperature of the measurement. The heater was turned on at t=0 and the resulting temperature increases at each sample thermocouple were amplified and recorded as a function of time. The overall sensitivity of the apparatus was 50 microvolts for full scale deflection, with the time axis meaningful to ± .01 second. Full scale deflection corresponded to about 3°C so that the ambient temperature of the measurement could be assigned to each trace to a precision of 1°C or better. One-second timing pulses were used to subdivide the time axis into equal time intervals.

Room temperature (26°C.) data were taken using the method described above. The average of ten determinations for the

thermal diffusivity of Armco iron are compared with values obtained by other investigators (1,2) and Shanks (13) in Figure 6. Also, the diffusivity was calculated from Powell's (14) value of the thermal conductivity (K), Klein's (15) specific heat, c=.110 cal/deg C, and the density using the relationship k=K/cd. The agreement between the diffusivity obtained by using the radial method and by other investigators is an indication that the radial method will work.

ROOM TEMPERATURE DATA ON ARMCO IRON

INVESTIGATOR	THERMAL DIFFUSIVITY (CM^2/SEC)	METHOD
PRESENT INVESTIGATION	0.198±.005	FINITE RADIAL
ABELES	0.200±.005	MODIFIED ANGSTROM
SIDLES AND DANIELSON	0.210±.010 (EXTRAPOLATED FROM 46°C)	MODIFIED ANGSTROM
SHANKS	0.200±.005	FINITE ROD
CALCULATED FROM k=K/cd	0.200	CALCULATED

Figure 6. Armco iron data

The method should be applied to measurements at high temperatures, where a study of the adequacy of the guarding could be investigated. One could repeat the experiment with

different numbers of guard disks at a particular temperature and see if the diffusivity obtained is independent of the number of guards.

Modifications of the method could include: optical determination of the sample temperature history, different heater configurations, and modifications of the recording techniques so that the time response of the system is better. The FORTRAN program is compatable with any modification where radial heat flow is maintained.

The method offers considerable promise in the determination of the thermal properties of small samples of some semiconducting compounds at high temperatures where the thermal diffusivity is less than 0.1 cm^2/sec. It is interesting to note that this is the area where semiconductors become especially interesting for thermoelectric conversion.

REFERENCES

1. Sidles, P. H. and Danielson, G. C. Thermal diffusivity measurements at high temperatures. In Egli, P. H., ed. Thermoelectricity. pp. 270-287. New York, N.Y., John Wiley and Sons, Inc. c1960.

2. Abeles, B., Cody, G.D. and Beers, D.S. Apparatus for the measurement of the thermal diffusivity of solids at high temperatures. J. Appl. Phys. 31: 1585. 1960.

3. Becker, J.H. Several new methods to measure the thermal diffusivity of semiconductors. J. Appl. Phys. 31: 612. 1960.

4. Angstrom, A.J. Phil. Mag. 25: 130. 1863.

5. King, R.W. Phys. Rev. 6: 437. 1911.

6. Starr, C. Rev. Sci. Inst. 8: 61. 1937.

7. Milne, W.E. Numerical solution of differential equations. 1st ed. New York, N.Y., John Wiley and Sons, Inc. 1953.

8. Richtmyer, R.D. Difference methods for initial-value problems. 1st ed. New York, N.Y., Interscience Publishers, Inc. 1957.

9. Forsythe, G.E. and Wasow, W.R. Finite difference methods for partial differential equations. 1st ed. New York, N.Y., John Wiley and Sons, Inc. 1960.

10. John, F. On integration of parabolic equations by difference methods. Comm. Pure Appl. Math. 5: 111. 1952.

11. Carslaw, H.S. and Jaeger, J.C. Conduction of heat in solids. 1st ed. London, England, Oxford University Press. 1947.

12. Kennedy, W.L. An IBM 650 computer program for determining the thermal diffusivity of finite-length samples. United States Atomic Energy Commission Report. IS-137 Iowa State Univ. of Science and Technology, Ames. Inst. for Atomic Research. June, 1960.

13. Shanks, H.R., Iowa State University of Science and Technology. Room temperature diffusivity of Armco iron. (Private Communication.) 1962.

14. Powell, R.W. Proc. Phys. Soc. 51: 407. 1939.

15. Klein, A.H., Iowa State University of Science and Technology. Room temp. Specific heat of Armco iron. (Private communication.) 1962.

Figure 1. Typical radial sample configuration

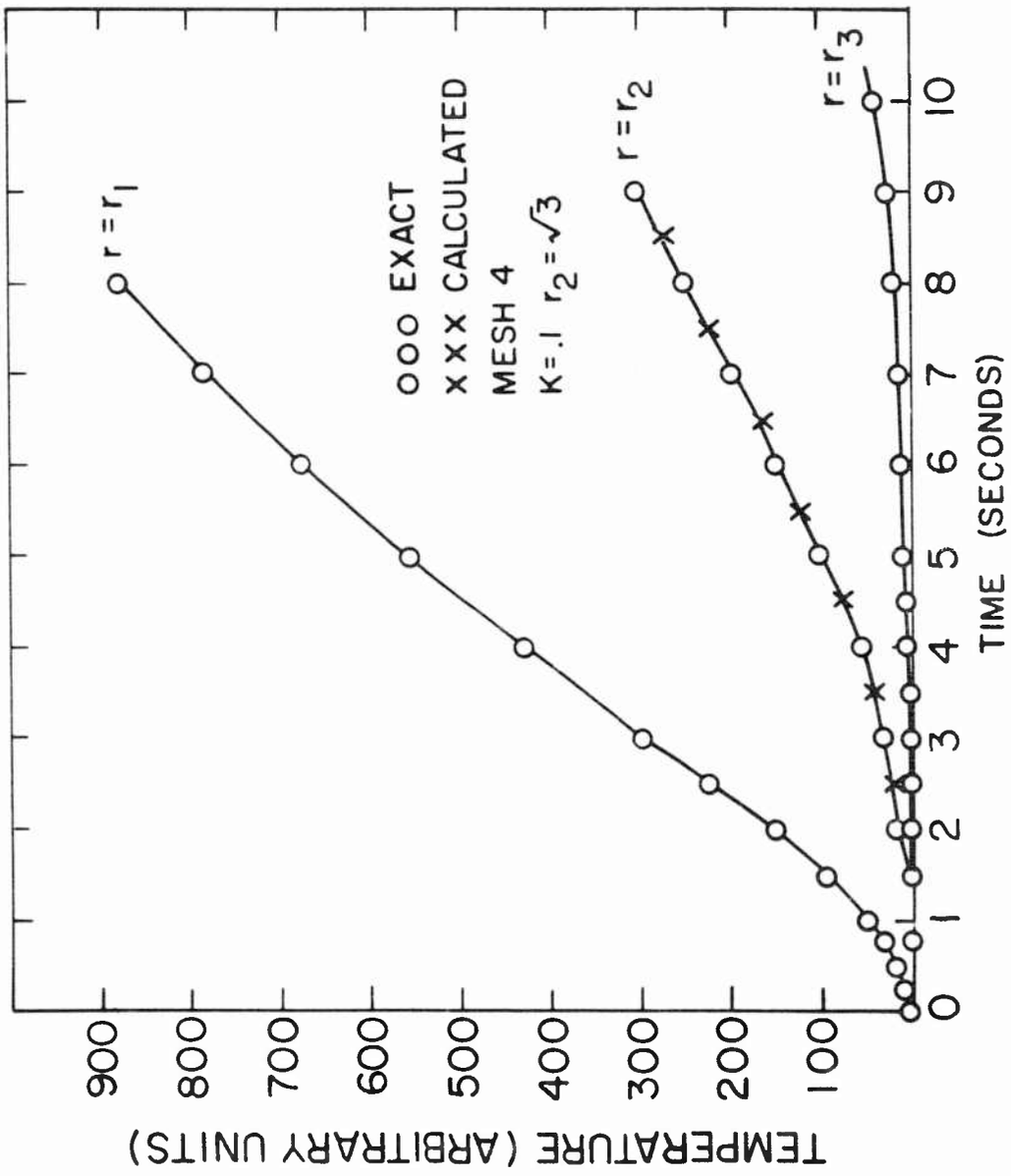

Figure 2. Exact solution to radial equation

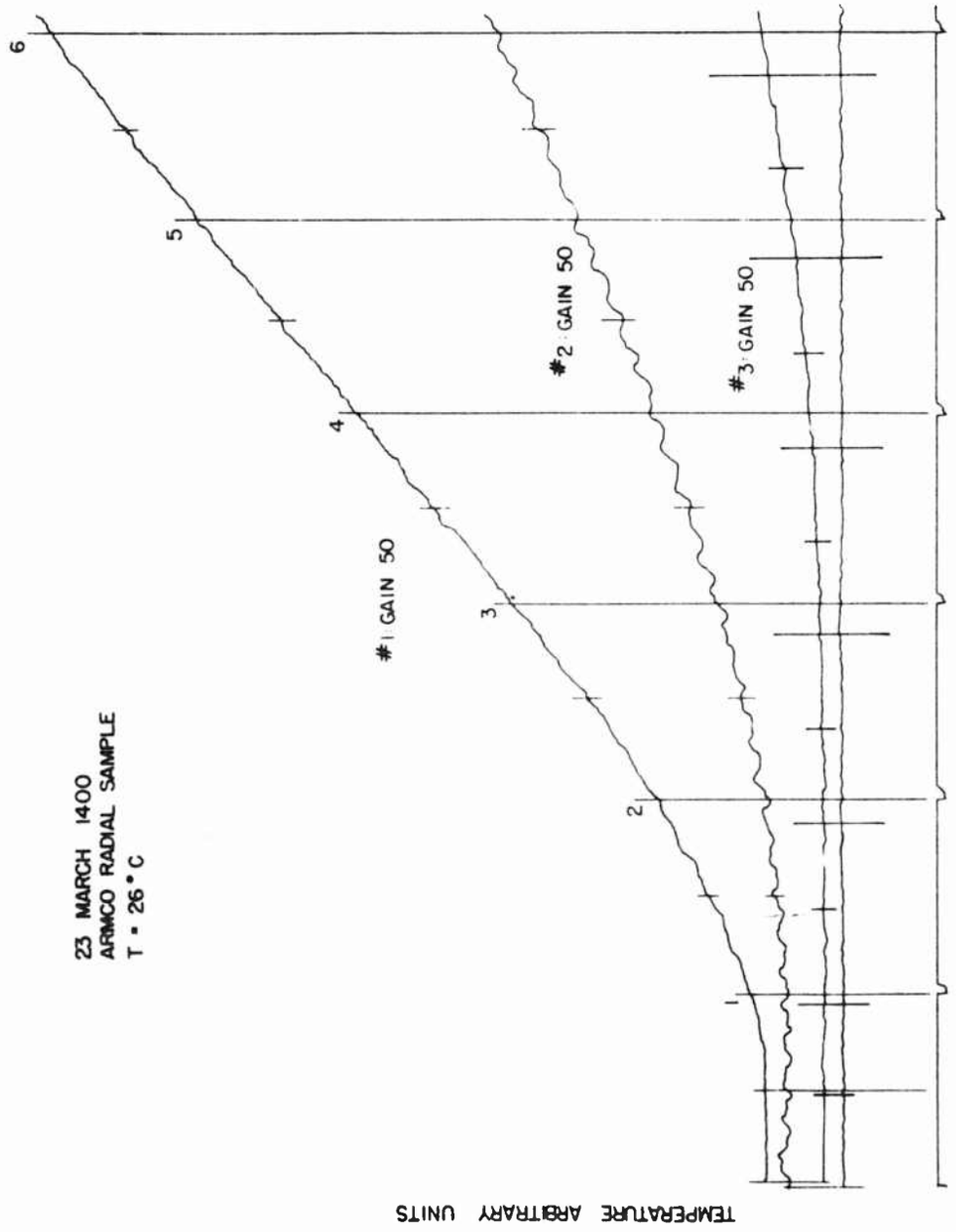

Figure 3. Experimental radial data

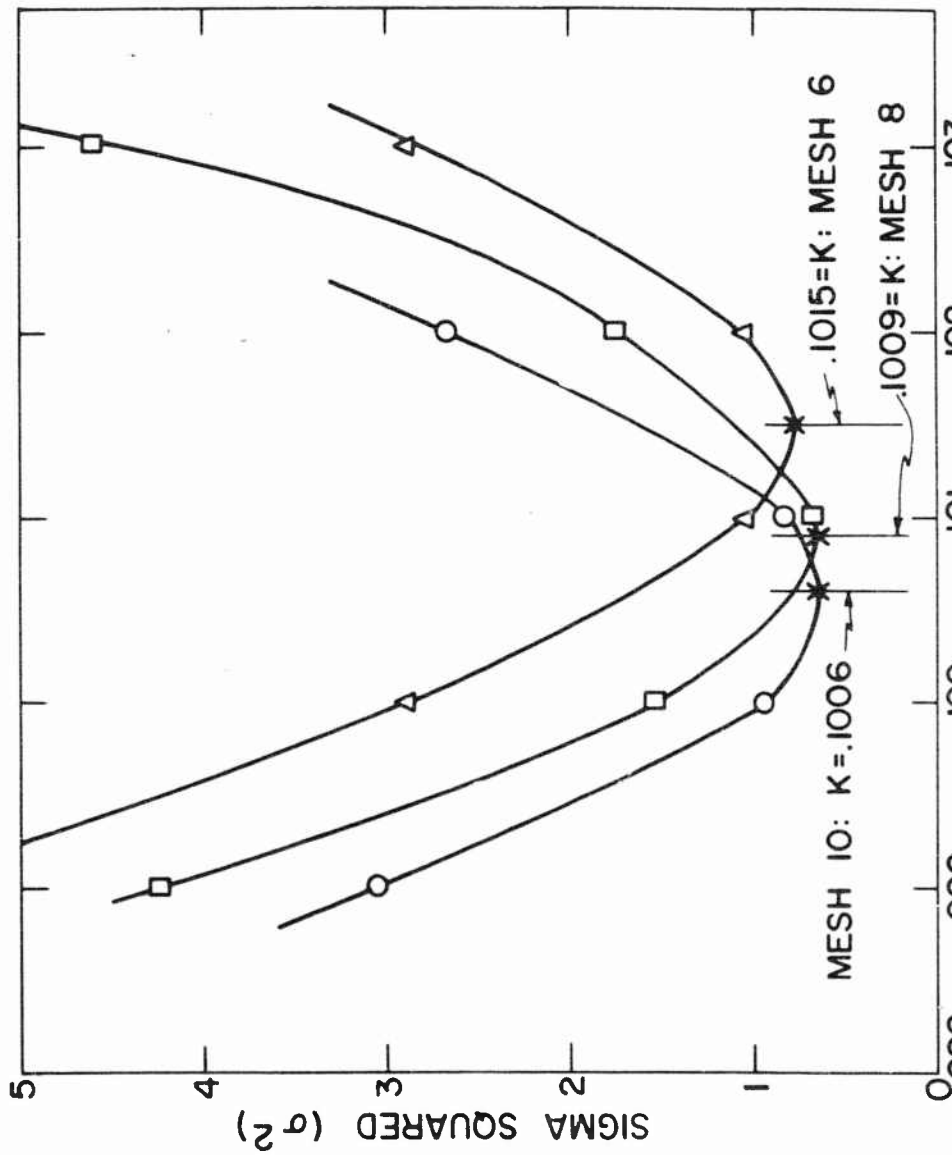

Figure 4. Sigma squared versus k for different mesh sizes

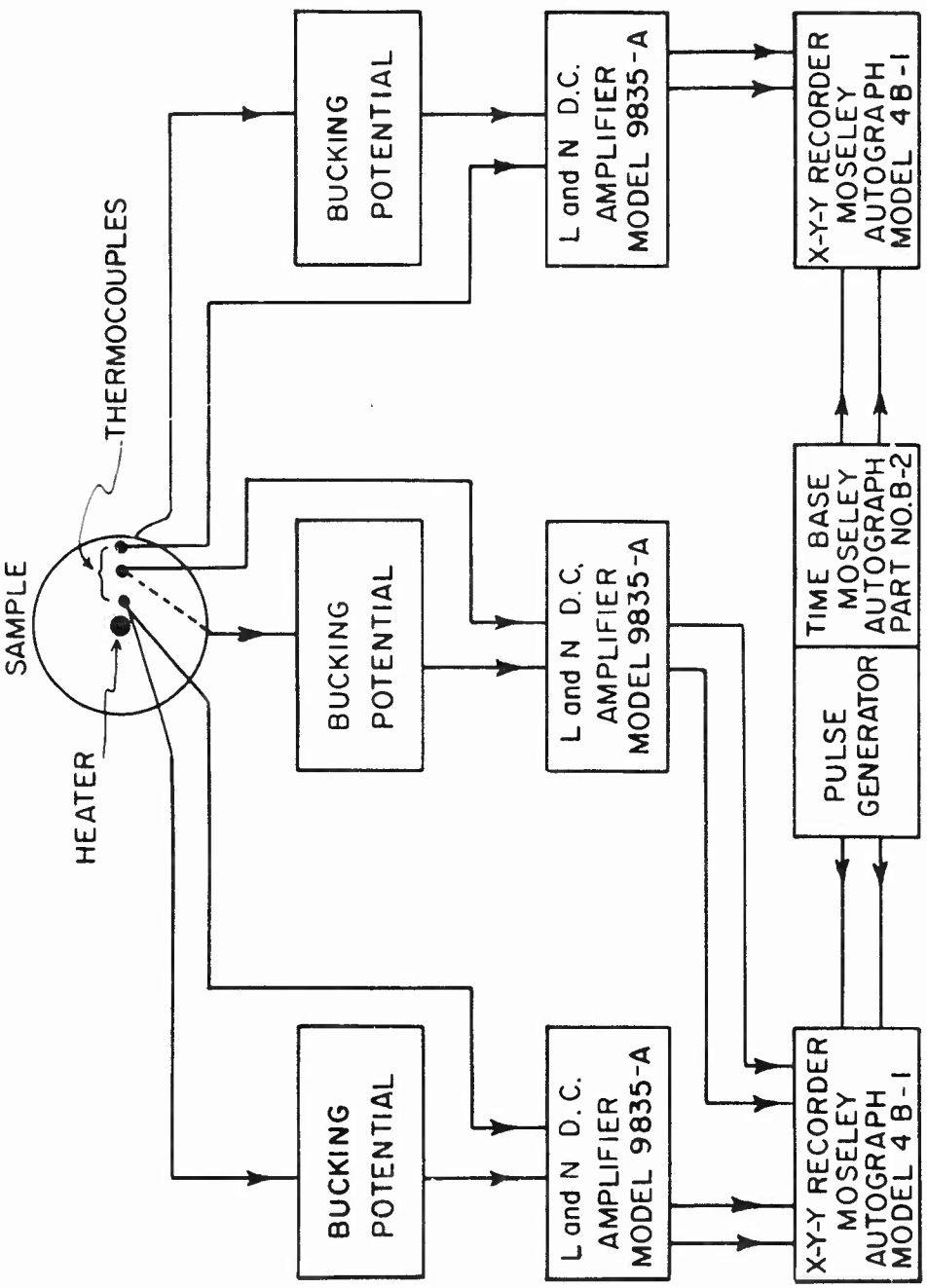

Figure 5. Block diagram of apparatus

A4. SPECIFIC HEAT OF ZIRCONIUM BY A PULSE HEATING METHOD*

by

A. H. Klein and G. C. Danielson
Institute for Atomic Research and Department of Physics
Iowa State University, Ames, Iowa

Abstract

The specific heat of iodide zirconium, from 25°C to the melting temperature of 1845°C, has been determined by a pulse heating method. The α - β transformation from the hexagonal close-packed structure to the body-centered cubic structure occurred at 865°C. For α - zirconium, the specific heat increased from 0.066 cal/g-°C at 25°C to 0.082 cal/g-°C at 865°C. Over the entire temperature range, our results are about three per cent lower than those of Scott. For β - zirconium, where no previous measurements seem to have been reported above 1100°C, the errors were greater than for α -zirconium. Approximate values of the specific heat in the β - range have been determined, however, from our pulse data and from previously known information on the heat of transformation and on the temperature dependence of the resistivity.

PROCEDURE

The specific heat of crystal bar zirconium has been determined from room temperature to the melting point at 1845°C. The sample was fabricated from a piece of iodide zirconium prepared by the de Boer - van Arkel process. An arc-melted fingerling was made and swaged down to 30 mil diameter. After the wire had been annealed at 700°C for two hours in a vacuum better than 5×10^{-6} mm of Hg, it was drawn to 10 mil diameter and cleaned with hydrochloric acid.

---

*. This work was performed in the Ames Laboratory of the U. S. Atomic Energy Commission. Contribution No. 1211.

The pulse heating method has been described in detail by Wallace[1] so only a summary of the procedure is given here. A sample of the zirconium wire 3 cm long was pressure mounted between platinum strips attached to heavy molybdenum electrodes which supported it in the hot zone of a vacuum furnace. The temperature was measured with a Pt - Pt + 13% Rh thermocouple peened into the molybdenum electrode next to the sample.

The sample was placed in the "unknown" position of a Kelvin bridge and supported in a vacuum furnace. It was annealed again at 800°C at 5 x 10^{-6} mm of Hg for an hour and then cooled to room temperature. As the sample was again heated at 50° per hour, resistance-temperature data were taken over the α -range. During this period of heating, the sample was pulsed at 100°C intervals. Each pulse was over a range of 150°C in 35 ms. The unbalance voltage of the bridge during the pulse was displayed on an oscilloscope and photographed. This information was used to calculate the change in the resistance of the sample as a function of time during the pulse. From the resistance-temperature data the change in temperature as a function of time was computed. The known energy input, I^2R/J, was corrected for losses due to radiation and conduction. The heat capacity was then equal to the ratio of the rate of energy input to the rate of temperature change.

RESULTS OF MEASUREMENTS

Zirconium is a member of the fourth group of elements, as are titanium and hafnium. At room temperature it has an

hexagonal close packed crystal structure which is called the α - phase. The β - phase is body centered cubic. Our resistivity data indicated that the transition from α - phase to β - phase took place at 865°C. At 20°C various investigators have obtained values for the resistivity which range from 44 up to 60 μ ohm-cm. Our value was 45 μ ohm-cm, which was typical of crystal bar zirconium after fabrication.

Specific heat values were calculated from the pulse data and resistance-temperature data for α - zirconium. These values were plotted and a curve was fitted to them graphically. Figure 1 shows this curve together with others from the literature. The shape of our curve corresponded quite closely to that of Scott,[2] but was about 3% lower. Earlier work on zirconium had given even higher values than those shown here, especially at high temperatures. As the purity of the zirconium samples improved, however, the curves became lower. Scott's sample was also iodide zirconium from Westinghouse.

Figure 2 shows C_p in cal/mole-deg and the corresponding C_v curve calculated from $C_v = C_p - V\alpha^2 T/\chi$, where V is the atomic volume, α is the volume expansion coefficient, T is the temperature, and χ is the compressibility.

Measuring the properties of β - zirconium presents additional difficulties. β - zirconium is a very efficient getter of nitrogen and oxygen, both of which affect its properties even in very small concentrations. The geometry of our sample - a 10 mil wire about 3 cm long - was such that, even with a vacuum of 5×10^{-6} mm of Hg, the nitrogen and oxygen

impurities picked up in a short time seriously affected the resistance data. Not only did these impurities increase the resistance, but they also changed the shape of the resistance-temperature curve, especially in the region of the transition. Since an accurate knowledge of the resistance-temperature curve was essential to the data reduction for this method, a different approach was tried.

Cook, et al.,[3] measured the resistivity of high and low hafnium zirconium over the range from room temperature to 1400°C. He found a difference in magnitude between the two sets of data, but the shapes of the two curves were very nearly the same. He also found that cold working the zirconium increased its resistivity, but again did not change the shape of the resistivity curve.

In order to get specific heat values in the β - phase, Cook's resistivity and Scott's heat of transformation data[4] were combined with our pulse data. The sample was heated to 800°C, well below the α - β transition, and held at that temperature while it was pulsed thru the transition and well into the β - range. Several pulses were made in this way with pulse times up to 90 ms. During the last pulse the sample was heated to the melting point (1845°C).

Cook's resistivity curve had a constant slope from 950 to 1400°C. For purposes of data reduction this curve was extrapolated to 1845°C. From this resistance-temperature curve and the data from the pulses thru the α - β transition, values for the specific heat of β - zirconium were calculated. A curve was

fitted to these points graphically. It is shown in Fig. 3 with other data on β - zirconium. These data all indicate that the specific heat of β - zirconium just above the transition is lower than that of α - zirconium just below it.

The results given for α - zirconium are estimated to be accurate within 3%. For the β - zirconium the heat loss corrections are much larger because of the wide temperature ranges of the pulses. The use of a calculated resistance-temperature curve also adds to the probable error. For these reasons, the accuracy of the specific heat values for the β - zirconium is placed at 10%.

Work on the thermal diffusivity of zirconium is currently in progress at this laboratory. From this diffusivity data and our specific heat data the thermal conductivity can be obtained from the equation, $K = kcd$, where K is the thermal conductivity, k is the thermal diffusivity, c is the specific heat, and d is the density.

REFERENCES

1. D. C. Wallace, P. H. Sidles, and G. C. Danielson, J. Appl. Phys. 31, 168 (1960).

2. J. L. Scott, A Calorimetric Investigation of Zirconium, Titanium, and Zirconium Alloys from 60 to 960°C, ORNL-2328 (1957).

3. L. A. Cook, L. S. Castleman, and W. E. Johnson, Preliminary Report on the Electrical Resistivity of Zirconium, WAPD-25 (1950).

4. J. L. Scott, loc, cit.

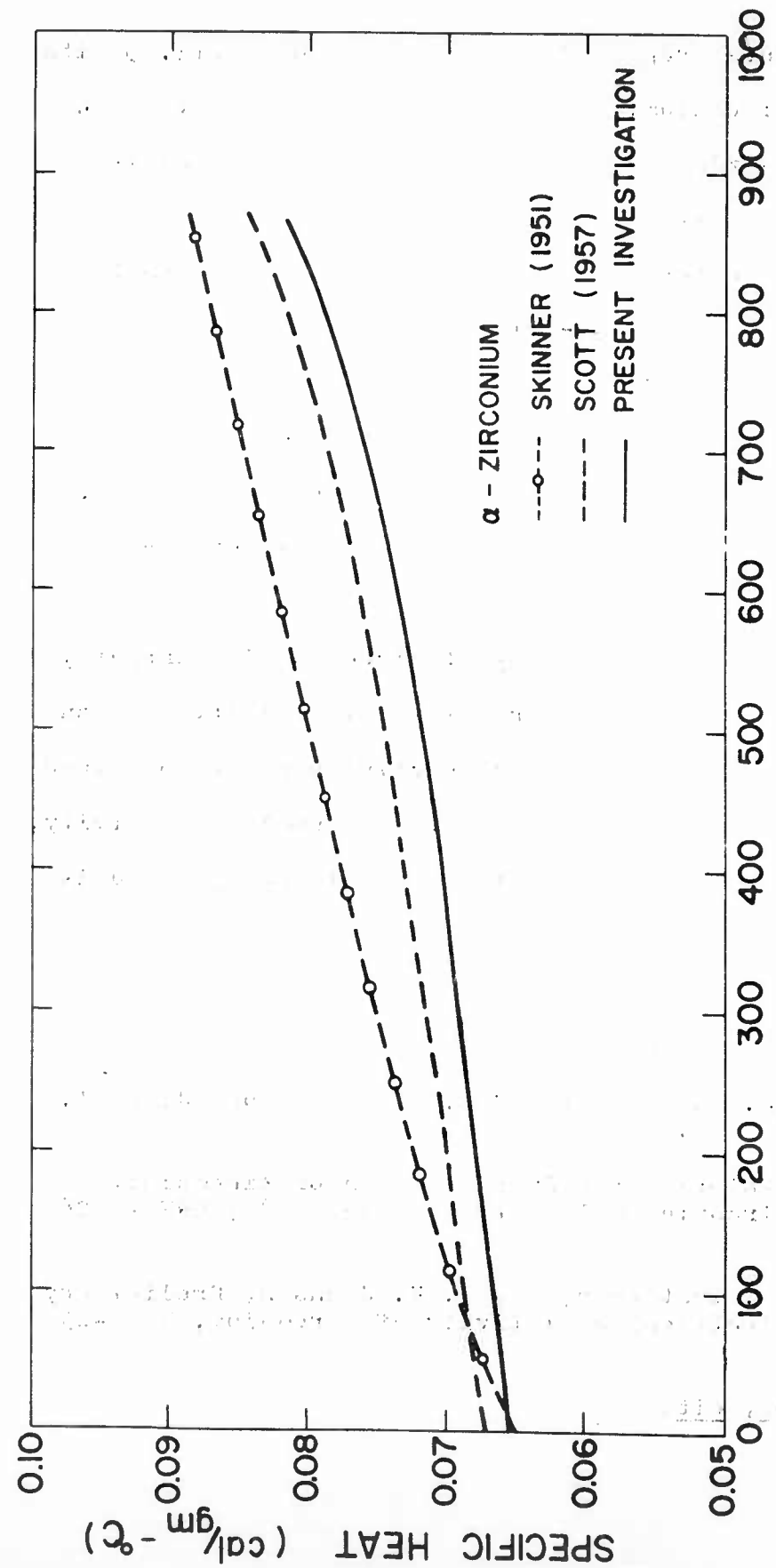

Figure 1. Specific heat of α-zirconium.

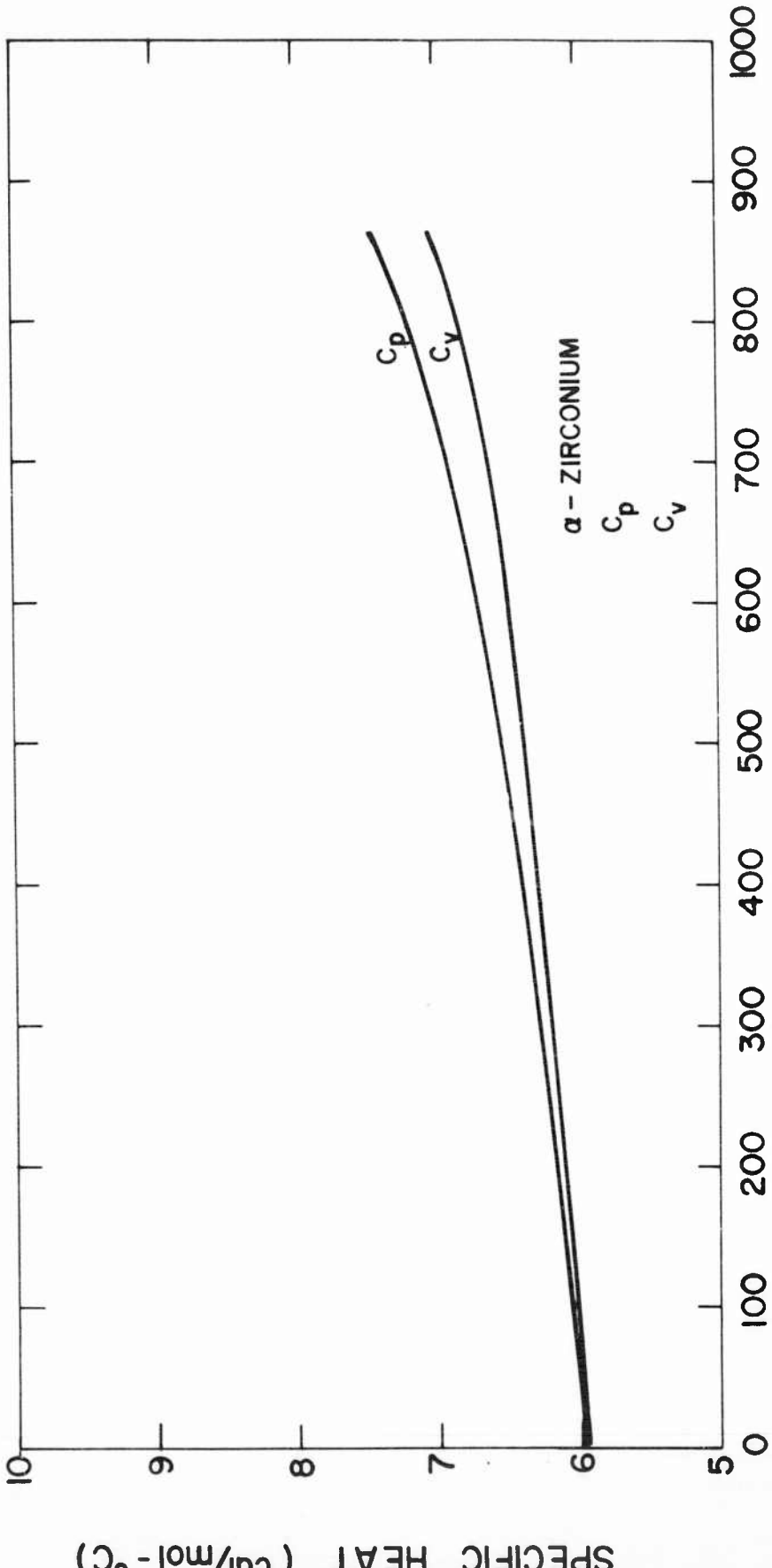

Figure 2. C_p and C_v of α-zirconium.

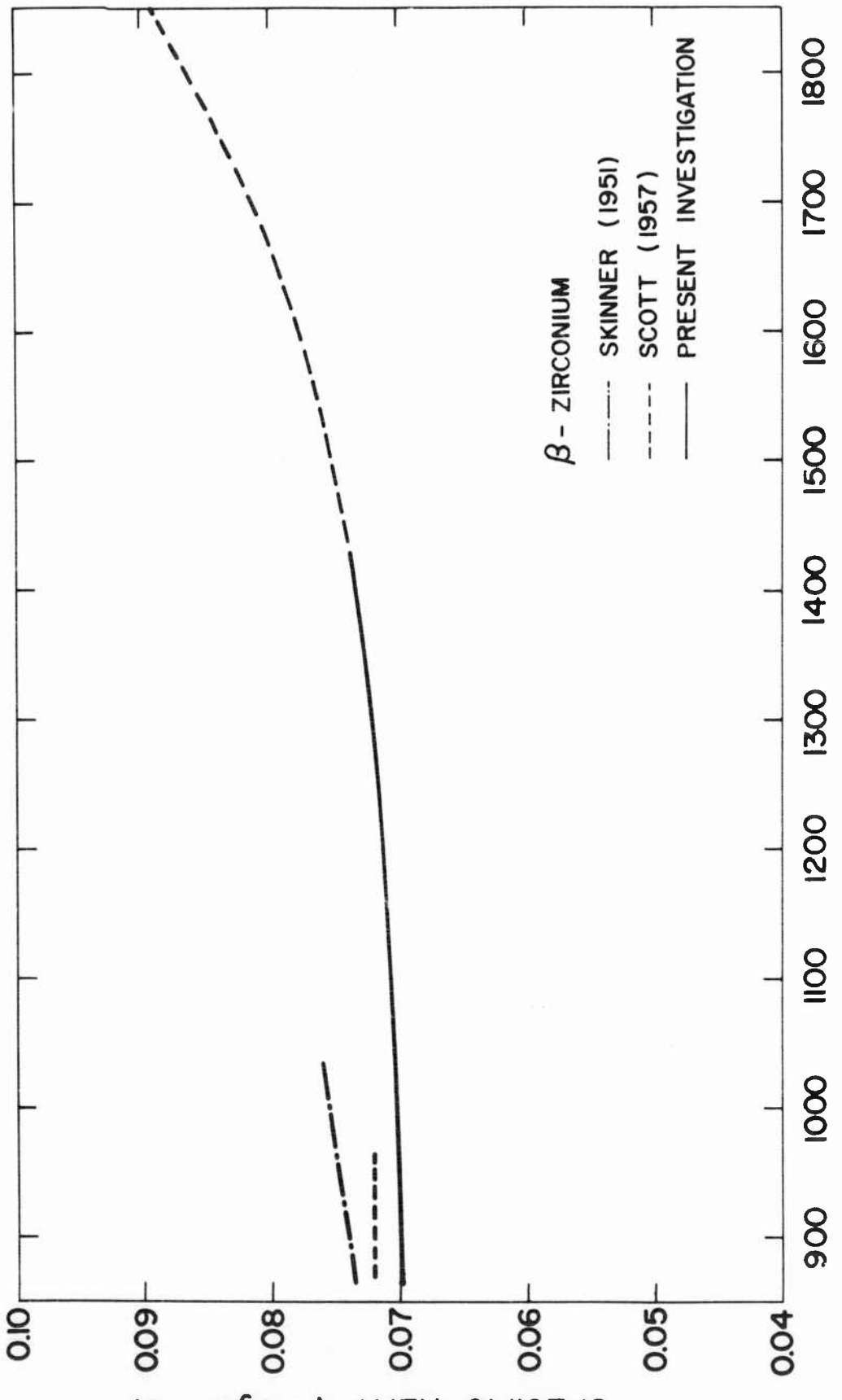

Figure 3. Specific heat of β-zirconium.

B1. (Invited paper) ABSOLUTE MEASUREMENT OF THERMAL CONDUCTIVITY*

by

G. Busch and E. F. Steigmeier**
Laboratorium fuer Festkoerperphysik ETH,
Zurich, Switzerland

Abstract

An apparatus to measure the thermal conductivity by using the absolute method is described. Measurements of single crystals of InSb are given for temperature between 200 and 720°K. The results are shown to agree well with theoretical expectations.

The carrier thermal conductivity has been calculated based on measurements of electrical conductivity, Hall coefficient and Seebeck coefficient of the same samples. The lattice contribution has been determined by deducting the carrier part from the total measured value. A satisfactory explanation may be given for the temperature dependence of the lattice part. The absolute value of the lattice thermal conductivity at 400°K leads to a Grueneisen constant comparable to other group III-V and IV semiconductors.

---

* This work has been reported in Helv. Phys. Acta 32, 463 (1959) and in detail in Helv. Phys. Acta 34, 1 (1961)

** now at RCA Laboratories, Princeton, New Jersey

INTRODUCTION

In 1954 the thermal conductivity of InSb was measured by BUSCH and SCHNEIDER[1]. They found it to rise at high temperature, a fact that could not be explained theoretically. This apparatus has been developed to get more reliable measurements on better materials. The object was mainly to avoid completely losses due to radiation at high temperatures. Results published in the meantime have shown that this is not easy to achieve.

APPARATUS

The absolute method has been used to be independent of any standard materials. Fig. 1 and 2 show the experimental arrangement. The sample is held at its cold end by means of a collet made of copper. A spacing of Copper-Graphite alloy provides a soft transition to compensate for different expansion coefficients. In addition to this, the sample is soldered on top to the collet with indium. The collet is pulled into a conical copper heat sink through which all connections are led. The lower end of the sample carries a small heater inside a silvered copper piece which is soldered to the sample with indium too; three tantalum springs hold it in place at temperatures higher than the melting point of indium. Into the sample we had drilled ultrasonically two holes to fit the thermocouples 10 mm apart (Iron-Constantan, Leeds and Northrup, 0.12 mm thick). The thermocouples were put into these holes and then soldered to the sample with a Tin-Nickel - Germanium alloy. So, every joint is divided into a mechanical and a

thermal connection. The scatter of the measured points is very much dependent on the care these joints are made with. The thermocouples being now in electrical contact with the sample make it impossible to read temperature differences by direct connection. We used the method of the Isolating Potential Comparator by DAUPHINEE[2] (Stevens-Arnold choppers 65 c/s) which proved to be very satisfactory. The emfs were read with a Cambridge Vernier Potentiometer. The heat introduced into heater I was measured electrically.

All thermocouples and leads are thermally connected inside of heater IV to a copper piece to reduce conduction losses and then led without a break from the sample to the ice reference point.

To avoid radiation losses, the sample is surrounded by a radiation shield in which heater II and III maintain the same temperature gradient as in the sample. This can be checked by thermocouples placed at the same level as in the sample. All the time we made the temperatures at T_1 and T_3 equal to those at T_2 and T_4, respectively, to about 0.05°C; the temperature difference ΔT_{78} was then very small too. The radiation shield is built in a manner that direct radiation from the inside is impossible; it is sandblasted inside to prevent reflections. There are four more unheated radiation shields.

Heater IV keeps the heat sink constant to about 0.02°C; since these measurements were taken this has been improved to about 0.005°C. We used a temperature controller similar to

this one described by DAUPHINEE and WOODS[3] but with additional integral control and using Stevens-Arnold choppers. The reference is a Rubicon potentiometer with Zener diode power supply. For temperatures lower than room temperature we used temperature baths; in the meantime the apparatus has been improved to give continuous measurements between 200 and 750°K.

The measurements were taken in a vacuum of better than 5×10^{-5} mm Hg.

ERRORS

Errors arising in this apparatus have been discussed in detail by WETTSTEIN[4]. Conduction losses have been taken into account. Radiation losses are not present up to highest temperatures. Evidence for this is given by the fact that a mismatch of the temperature gradient of the radiation shield (about 0.8 deg/cm) causes a change of only 1-2% in the thermal conductivity at 700°K. Moreover the test-measurements of Armco Iron agree with the data given by POWELL[5] and ARMSTRONG and DAUPHINEE[6] in the interesting temperature range. (see ref. 7). To get around spurious emfs we plotted at every temperature the power of heater I against the temperature difference ΔT_i for three or four settings of the power. The slope of these straight lines is the thermal conductivity at this temperature. We estimate the absolute error of the apparatus to about 4%, the relative being about 2-3%.

MEASUREMENTS ON InSb

Three samples of single crystal InSb have been measured with this apparatus. They have the following impurity concentrations:

Wb p-type 3.3×10^{15} cm^{-3}

Wd n-type 1.2×10^{16} cm^{-3}

We p-type 1.6×10^{15} cm^{-3}

The results are given in Fig. 3. All the three samples show to within 0.6% the same absolute value. The samples were treated for homogeneity. They were prepared from purified indium and antimony, then melted together and zone-refined. Single crystals were pulled using the Czochralski method. The crystals have been cylindrically ground. We show in the same figure the results of some other authors. We disagree with the high temperature rise observed by WEISS[8] and similar to BUSCH and SCHNEIDER[1] which we think was caused by radiation. But we agree with the results of STUCKES[9] and BOWERS et al.[10] within their given error limits of 10%, except that we could not find the absolute value to depend on the carrier concentration (STUCKES[9]).

Fig. 4 shows the Seebeck coefficient of the same samples measured in the same apparatus. To get more reliable results, we used here, too, the method of plotting the emf against the temperature difference ΔT_i and thus getting the Seebeck coefficient from the slope. The results are in good agreement with the measurements of WEISS[8] and the theoretical computed values of EHRENREICH[11]. Our calculated figure of merit (see ref. 7) is about 50% higher than the values given by BOWERS et al.[10]

DISCUSSION

Measurements of electrical conductivity and Hall coefficient of the same samples used for thermal measurements have been made. Method and results are given elsewhere[7]. From Hall coefficient we could determine the carrier concentration and the energy gap (ΔE_o = 0.25 eV) which is in agreement with previous data, (see ref. 7). Fig. 5 gives the electron mobility calculated from the Hall mobility using the scattering factor r(T) computed by EHRENREICH[11]. Agreement between HROSTOWSKI's[12] and our experimental data and EHRENREICH's[11] computed mobilities is excellent for the same assumptions for which good agreement in the thermoelectric power has been found. The step in the mobility curve at 480°K is still unexplained[7,13]. The hole mobility is not well known for high temperatures; therefore, we had to extrapolate low temperature data (ref. given in 7) to high temperatures for lack of better knowledge.

The carrier thermal conductivity can be computed by solving the Boltzmann equation. We get for isotropic scattering

(1)

$$\lambda_{LT}=-K_{7+}+\frac{1}{eT}\left[\frac{K_{5n}^2}{K_{3n}}+\frac{K_{5p}^2}{K_{3p}}\right]-\frac{1}{eT}\frac{K_{3n}K_{3p}}{K_{3+}}\left[\Delta E_T+\frac{K_{5n}}{K_{3n}}+\frac{K_{5p}}{K_{3p}}\right]^2 \quad ; \quad K_{3+}=K_{3n}+K_{3p}=-(\sigma/e)$$

$$K_{7+}=(2\pi k/3)\left[(2kT/m_n^*)^{5/2}\int_0^\infty x_n^{7/2}\tau_n\frac{\partial f_{no}}{\partial x_n}dx_n+(2kT/m_p^*)^{5/2}\int_0^\infty x_p^{7/2}\tau_p\frac{\partial f_{po}}{\partial x_p}dx_p\right] \qquad (1)$$

$$K_{n,p}=(2\pi e/3)(kT)^{1/2}(2/m_{n,p}^*)^{5/2}\int_0^\infty x_{n,p}^{\mu/2}\tau_{n,p}\frac{\partial f_{n,po}}{\partial x_{n,p}}dx_{n,p} \quad ; \quad K_{3n,p}=-(\sigma_{n,p}/e); x_{n,p}=\frac{E_{n,p}}{kT}$$

where ΔE_T means the energy gap at the temperature T, $\tau_{n,p}$ the relaxation time, $f_{n,p}$ the distribution function, and $E_{n,p}$ the kinetic energy of electrons resp. holes. We have now to make assumptions about the relaxation time to solve the integrals. Considering the complicated scattering mechanism in InSb (EHRENREICH[11]) we tried to use the following relaxation time

$$\tau = a\, T^{-l}\, E^{q/2} \qquad (2)$$

q being adjustable temperature dependent parameter. This relaxation holds for acoustical scattering even if the energy bands are non-parabolic; it holds too for optical scattering at high temperatures[14]. Recently EHRENREICH[15] has shown that for polar scattering a relaxation time of this kind fits the results of the variational method down to temperatures comparable to the Debye temperature. Using this formula for τ we get for the carrier thermal conductivity

$$\lambda_{LT}=\frac{k^2}{e^2}\sigma T\left[\frac{A_n\sigma_n+A_p\sigma_p}{\sigma}+\frac{\sigma_n\sigma_p}{\sigma^2}\left(\frac{\Delta E_T}{kT}+B_n+B_p\right)^2\right]$$

$$A_{n,p}=\frac{7+q}{3+q}\frac{F_{\frac{5+q}{2}}(\gamma)}{F_{\frac{1+q}{2}}(\gamma)}-\left[\frac{5+q}{3+q}\frac{F_{\frac{3+q}{2}}(\gamma)}{F_{\frac{1+q}{2}}(\gamma)}\right]^2 \qquad (3)$$

$$B_{n,p}=\frac{5+q}{3+q}\frac{F_{\frac{3+q}{2}}(\gamma)}{F_{\frac{1+q}{2}}(\gamma)} \quad ,$$

where $F_a(\eta)=\int_0^\infty \frac{x_{n,p}^a dx_{n,p}}{e^{x_{n,p}-\eta}+1}$ is the Fermi integral

$q=q_{n,p}$, $\eta=\zeta_{n,p}/kT$, $\zeta_n=\zeta-E_L$, $\zeta_p=E_V-\zeta$.

ζ means the Fermi level, E_v the upper limit of the valence band, E_L the lower limit of the conduction band. Formula (3) reduces for acoustical scattering and parabolic energy bands ($q = -1$) to the expression[16,17]

$$\lambda_{LT} = (k^2/e^2)\sigma T\left[2 + \frac{\sigma_{n,p}}{\sigma^2}\left(\frac{-ET}{kT} + 4\right)^2\right] \qquad (4)$$

The Fermi level at each temperature has been determined from effective masses given by WEISS[13]. For the energy gap we accepted a temperature dependence of $\Delta E_T = \Delta E_o - 2.7 \times 10^{-4} T$ (eV). The mobility is given by the formula

$$\mu_{n,p} = (e/m^*_{n,p})\overline{\tau}^{E}_{n,p} = (e/m^*_{n,p})\frac{\int_0^\infty \tau_{n,p} x_{n,p}^{3/2} \frac{\partial f_{n,po}}{\partial x_{n,p}} dx_{n,p}}{\int_0^\infty x_{n,p}^{3/2} \frac{\partial f_{n,po}}{\partial x_{n,p}} dx_{n,p}} \qquad (5)$$

Using the relaxation time (2) this leads to

$$\mu_{n,p} = (ea'_{n,p}/m^*_{n,p})(q+3/3)T^{\frac{q-2}{2}} \frac{F_{\frac{q+1}{2}}(\eta)}{F_{\frac{1}{2}}(\eta)} = \text{const } T^{a}_{n,p} \qquad (6)$$

This equation has been solved graphically for different q values. From Fig. 5 we read for every temperature the related exponent α_n. Going with α_n and T into this graph we know how q depends on the temperature. The results are given in Table I. This makes it possible to compute the Lorenz factors $A_{n,p}$ and $B_{n,p}$. The

results are shown in Fig. 6. This procedure has been done only for electrons assuming the same relationship to hold for the holes; this is satisfying because of the small contribution of the holes due to the high mobility ratio. For the same reason, no values for A_p are given.

This whole computation of the carrier thermal conductivity is of course only a rough estimate; but we expect it to be better than to accept complete degeneracy or nondegeneracy. Furthermore this backward determination may cause cancelling effects of erroneous assumptions. The results are compiled in Table II for sample We.

Fig. 7 shows a plot of the total measured thermal conductivity against the absolute temperature (upper curves). The lower curves give the lattice part computed by deduction of the carrier contribution from the upper curves. The big limits of inaccuracy at 700°K have been caused especially by the Lorenz factors and the hole mobility. Due to this fact we cannot make a further analysis of the lattice thermal conductivity at high temperatures where in addition to 3-phonon processes there may be some other scattering mechanism involved such as 4-phonon processes or electron-phonon scattering. Between 200 and 400°K we find a relationship $\lambda_g \sim T^{-1.1}$.

We have furthermore computed the lattice thermal conductivity at 400°K using the formula given by LEIBFRIED and SCHLÖMANN[18] for 3-phonon processes and $T > \Theta$:

$$\lambda_g = \frac{12}{5}\, 4^{1/3} \left(\frac{k}{h}\right)^3 \frac{aM\Theta^3}{\gamma^2 T}$$

Using a Debye temperature of 202.5°K we can fit our measurements with a Grueneisen constant $\gamma = 1.94$. BEERS, CODY and ABELES[19] got 1.95 for GaSb, 1.97 for GaAs, 1.55 for AlSb, 1.80 for Si and 1.86 for Ge. We believe the agreement between theory and experiment to be satisfactory.

In conclusion, one may say that this absolute method is able to give precise and reliable measurements of the thermal conductivity for temperatures up to 700°K. It can well be expanded to about 900°K by improving the shielding against radiation losses.

ACKNOWLEDGMENT

The authors would like to thank E.WETTSTEIN* for his help with the measurements. We are much indebted further to R. G. MORRIS** for many important suggestions and discussions as well as for preliminary experiments.

---

* Ebauches S.A., Neuchatel, Switzerland

** South Dakota School of Mines and Technology, Rapid City, South Dakota.

REFERENCES

1. G. BUSCH and M. SCHNEIDER, Helv. Phys. Acta 27, 196 (1954).
2. T. M. DAUPHINEE, Canad. J. Phys. 31, 377 (1953).
3. T. M. DAUPHINEE and S. B. WOODS, Rev. Sci. Instr. 26, 693 (1955).
4. E. WETTSTEIN, Diplomarbeit ETH 1959 (not published).
5. R. W. POWELL, Proc. Phys. Soc. 46, 659 (1934).
6. L. D. ARMSTRONG and T. M. DAUPHINEE, Canad. J. Research A 25, 357 (1947).
7. G. BUSCH and E. STEIGMEIER, Helv. Phys. Acta 34, 1 (1961).
8. H. WEISS, Halbleiter and Phosphore (Garmisch conference 1956), Braunschweig 1958 p. 497.
9. A. D. STUCKES, Phys. Rev. 107, 427 (1957).
10. R. BOWERS, et al. J. Appl. Phys. 30, 930 (1959).
11. H. EHRENREICH, J. Phys. Chem. Solids 9, 129 (1959).
12. H. J. HROSTOWSKI et al., Phys. Rev. 100, 1672 (1955).
13. H. WEISS, Z. Naturf, 11a, 131 (1956).
14. D. J. HOWARTH and E. H. SONDHEIMER, Proc. Roy. Soc. A219, 53 (1953).
15. H. EHRENREICH, Phys. Rev. 120, 1951 (1960).
16. B. DAVYDOV and I. SHMUSHKEVITCH, Uspekhi Fiz. Nauk 24, 21 (1940).
17. P. J. PRICE, Phys. Rev. 95, 596 (1954), Phil. Mag. 46, 1252 (1955).
18. G. LEIBFRIED and E. SCHLOEMANN, Nachr. Akad, Wiss. Goettingen IIa/4, 71 (1954).
19. D. S. BEERS, G. D. CODY and B. ABELES, Exeter conference, 1962.

TABLE I

q	α_n	T*
0	-1.2	~300°K
-1	-2.5	~560
-1.5	-3.0	~700

* This is the temperature where the α_n related to a certain q may be observed experimentally.

TABLE II

THERMAL CONDUCTIVITY OF InSb (SAMPLE We)

p-Type $n_s = 1.6 \times 10^{16}$ cm^{-3}

T °K	σ Ω^{-1}cm^{-1}	μ_n cm^2/V·sec	μ_p cm^2/V·sec	b	$\frac{\lambda \Delta E}{\lambda_{LT}}$ %	λ_{LT} cal/cm·s·°K	λ cal/cm·s·°K	λ_g cal/cm·s·°K
200	6.5	77,000	1380	55.8	---	---	0,0617	0,0617
250	64	81,350	1060	76.7	---	---	0,0483	0,0483
300	200	70,200	810	86.7	40.2	0,000464	0,0400	0,03954
350	426	57,900	627	92.4	32.6	0,00099	0,0343	0,03331
400	704	46,550	498	93.5	27.4	0,00169	0,03005	0,02836
450	1013	38,000	402	94.6	23.5	0,00249	0,0270	0,02451
500	1367	31,350	335	93.7	20.1	0,00347	0,0246	0,02113
550	1765	26,300	280	94.0	17.5	0,00447	0,0228	0,01833
600	2005	21,600	239	90.7	15.9	0,00547	0,0215	0,01603
650	2248	17,500	204	85.8	14.7	0,00645	0,0205	0,01405
700	2435	13,850	178	77.9	14.5	0,00734	0,0197	0,01236
715	2475	12,970	173	75.1	14.5	0,00758	0,0195	0,01192
	c)	c)			a)	b)	c)	d)

a) Ambipolar Part in Percent of the Carrier Thermal Conductivity

b) Carrier Thermal Conductivity Computed

c) Measured

d) Lattice Thermal Conductivity $\lambda_g = \lambda - \lambda_{LT}$

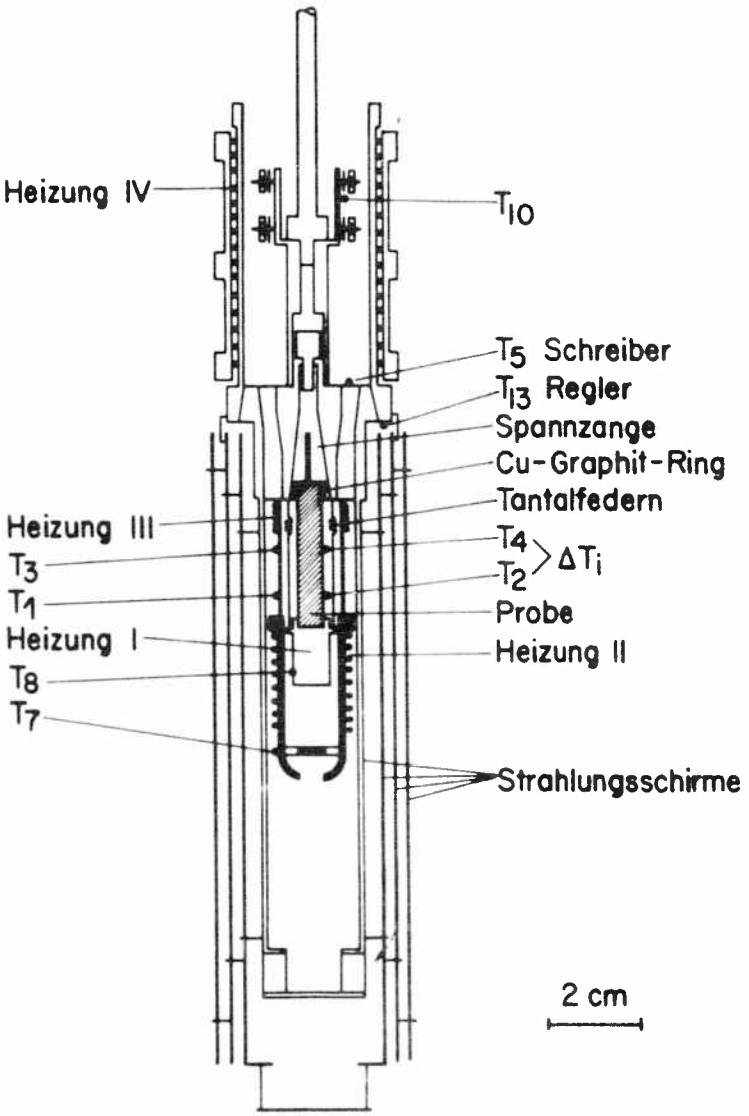

Fig. 1

EXPERIMENTAL ARRANGEMENT

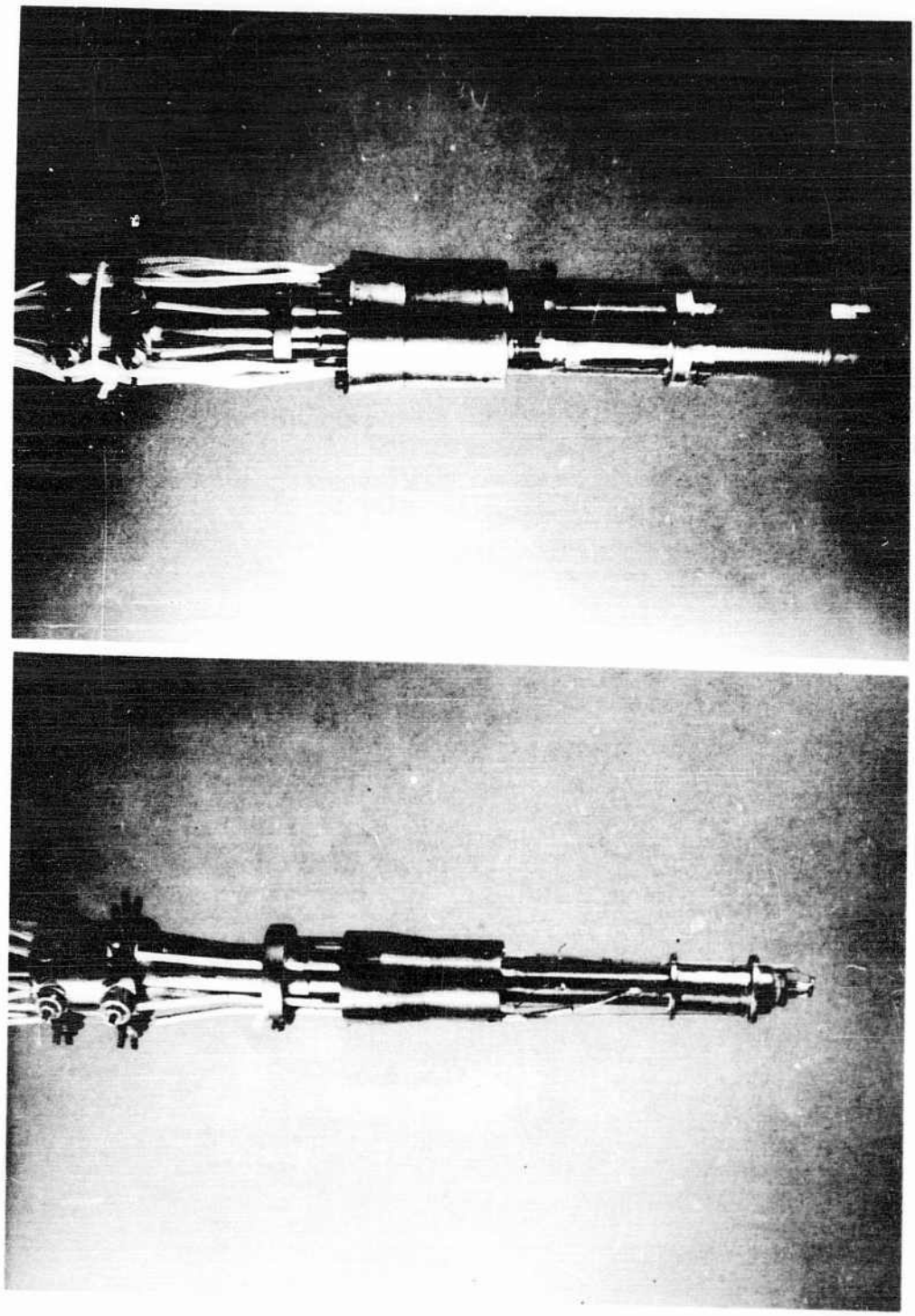

Fig. 2 SAMPLE MOUNTED IN SAMPLE HOLDER (a) AND HEATED RADIATIONSHIELD (b).

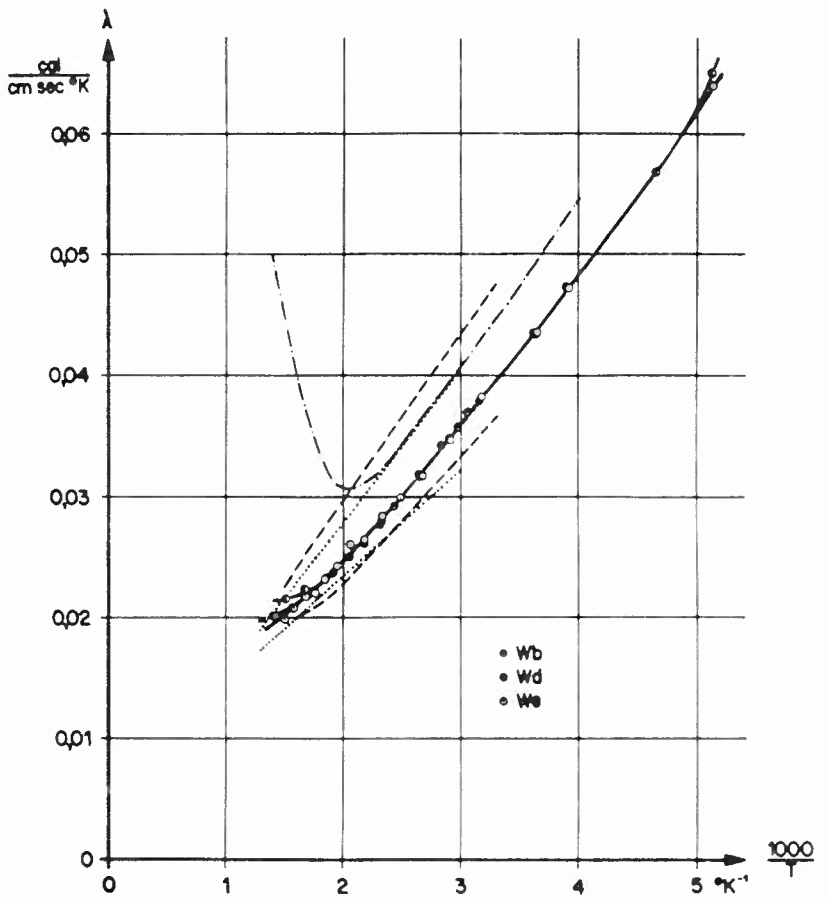

Fig. 3

THERMAL CONDUCTIVITY OF InSb

——— OUR MEASUREMENTS

-·-·-·- WEISS

- - - - STUCKES (2 DIFFERENT SAMPLES)

. . . . BOWERS ET AL. (90% LIMITS)

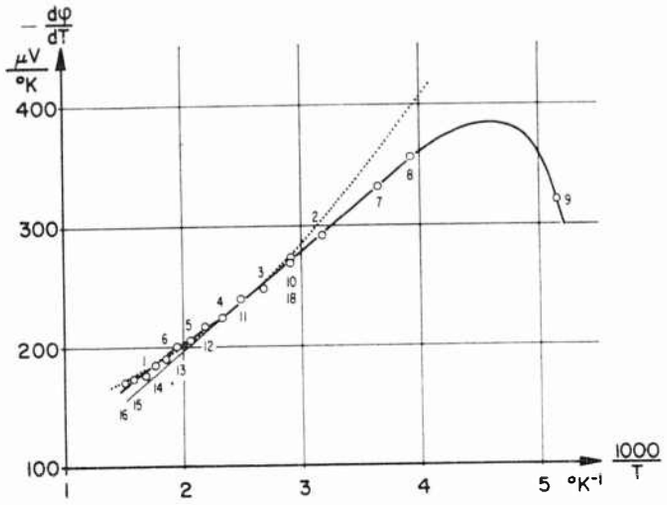

Fig. 4

ABSOLUTE SEEBECK COEFFICIENT OF InSb (SAMPLE We)
NUMBERS INDICATE SEQUENCE OF MEASUREMENTS
·····THEORETICAL VALUES (EHRENREICH e* = 0.20)

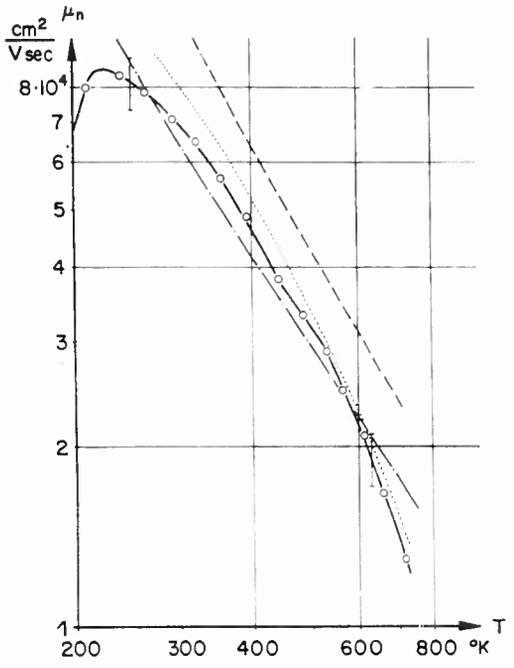

Fig. 5

ELECTRON MOBILITY OF InSb (SAMPLE We)
——— OUR MEASUREMENTS
····· HROSTOWSKI ET AL.
-·-·-·- THEORETICAL VALUE (EHRENREICH e* = 0.20)
- - - - THEORETICAL VALUE (EHRENREICH e* = 0.13)

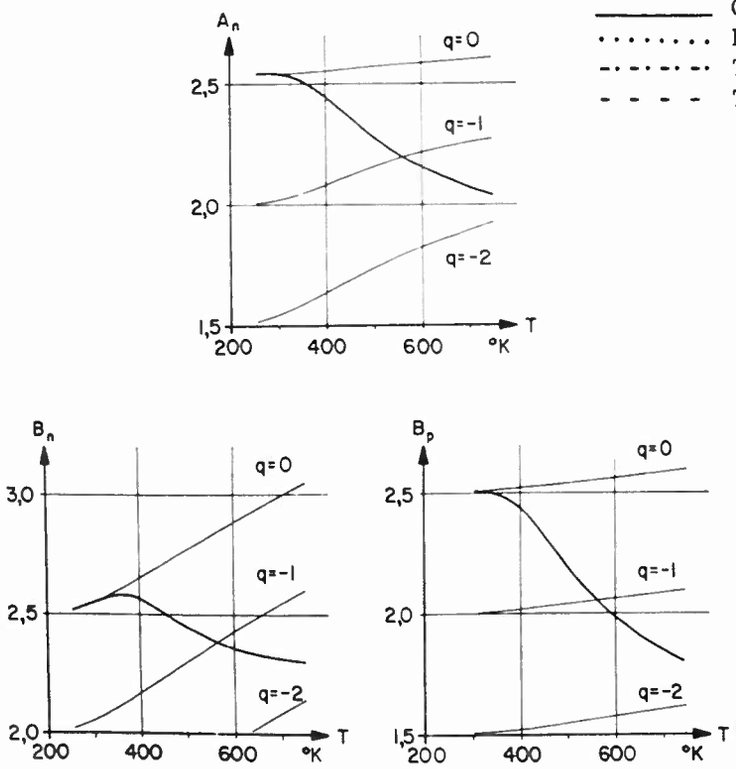

Fig. 6

LORENZ FACTORS

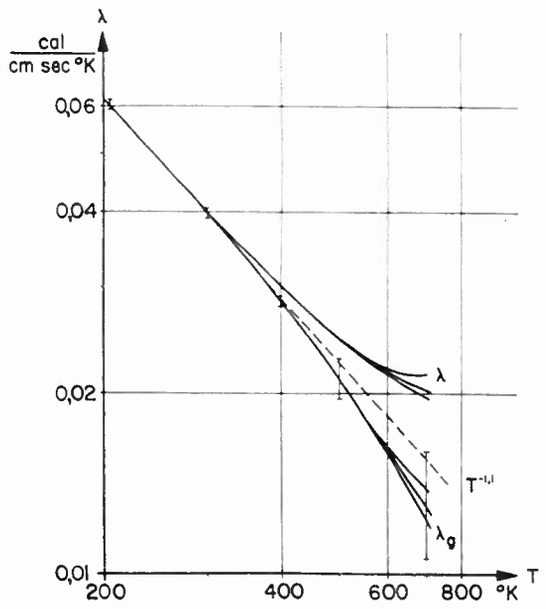

Fig. 7

EXPERIMENTAL VALUES OF THERMAL CONDUCTIVITY λ of InSb
AND COMPUTED LATTICE THERMAL CONDUCTIVITY λ_g
-------λ_g PROPORTIONAL TO $T^{-1.1}$

B2. THERMAL MEASUREMENTS ON FERROELECTRIC BARIUM-CALCIUM TITANATE CERAMICS

by

Donald D. Glower
Sandia Corporation, Albuquerque, New Mexico

INTRODUCTION

There is very little experimental information available which deals with the thermal properties of ferroelectric ceramics; quite the opposite is true for data concerned with electrical properties. The data clearly reveal that the electrical properties vary considerably from one experimental ceramic specimen to another; this variation caused by differences in atomic and crystalline composition, procedure for fabrication, and measuring techniques. The information available in the literature concerning thermal properties reflects this same variation.

Previous data on the thermal conductivity of barium titanate indicate that, for one particular ceramic,[1] the thermal conductivity increased proportional to the temperature, and in another experiment it is essentially independent of temperature.[2] The theory for dielectric crystals indicates that the thermal conductivity should rise according to a 1/T law as the temperature falls below the Debye temperature. In amorphous solids, where no long range order exists, boundary scattering predominates and the phonon free path length is temperature independent. Approximate calculations indicate that $C_p - C_v \sim 0$ for this

ceramic. Using this calculation and the specific heat data of Rase and Rustum,[3] one expects the Debye temperature to be around 160°C for barium titanate. The measurements discussed in this paper are below this temperature and show an increase in the thermal conductivity as temperature decreases, but the increase is not according to the 1/T law.

PREPARATION OF SAMPLES

The ceramic specimens were prepared in a manner customary for barium-calcium titanate ceramics. The specimen geometry was a short cylinder 3/4 inch in diameter and 1 inch long. Two 0.030 inch diameter holes were then drilled, 1/4 inch apart, from the surface to the cylinder axis. The thermal diffusivity was measured according to the modified Angstrom method as developed by Sidles and Danielson.[4]

These cylinders were next cut perpendicular to the axis so that thin disks were obtained. The faces of these disks were lapped parallel on a lapmaster lapping machine using a medium grade grinding compound. The technique for measuring the thermal conductivity is essentially the same as reported by Lucks[5] and Deem. The method as used, however, requires only two different thicknesses of material, while the method previously reported used three or more thicknesses. The method is also similar to that used by Yoshida[6] with the exception that a vacuum and radiation shield are eliminated as well as the large pressures.

THEORY OF THE THERMAL CONDUCTIVITY MEASUREMENT

Heat is conducted from a heat source to a heat sink if the source and sink are connected by a heat conducting material. A

heat balance in a round high conductivity rod, free to radiate to the surrounding air, reveals that the heat conducted down the rod plus the heat lost by radiant and convective transfer must equal the heat supplied by the source. Many longitudinal heat flow methods attempt to eliminate the convective and radiant heat transfer by making them essentially zero. This is not necessary in the temperature range under consideration, 0 to 150°C, if the thermal conductivity of the rod is accurately known. The thermal conductivity, the temperature along the rod axis, and the slope of the temperature versus distance along the rod length provide adequate information for determination of the heat flux at any point along the rod. This approach will give the heat flow into and out of a thin disk placed between the two rods. The thermal conductivity of the disk material can then be determined if the temperature drop across the disk is known.

The longitudinal heat flux along the axis of a rod obeys to a close approximation of Fourier's equation,

$$Q = q/A = -k\frac{dT}{dx}. \qquad (1)$$

The area A and thermal conductivity k are known quantities for the rods with the temperature gradient a quantity to be determined from a graph of temperature versus distance along the rod. The temperature can be measured by placing a number of thermocouples along the axis of the rod. If desired, the heat loss due to convection and radiation between any two points along the rod length can be determined by graphing the heat flux, Q, versus length. The difference in magnitude of the heat flux at the two points determines these modes of heat transfer.

The thermal conductivity can be determined by inserting a disk of the material to be investigated between the two rods.

It is convenient if the disk has the same diameter as the meter rods. A positive force applied to the rods assures a tight fit against the disk. The application of a heat source and sink at the rod ends provides a temperature gradient along the rods. The measurement of temperature along the length of the rods, the temperature gradient, and the knowledge of the thermal conductivity of the rods, furnishes adequate information to allow determination of the heat flux out of one rod face and into the other and the temperature at each face.

The temperature drop between the ends of the rods consists of the drop across the films and the temperature drop through the disk. The thermal conductance of an air film depends upon its thickness, which thickness in turn is dependent[7,8] upon the finish of the surfaces in contact and the pressure applied to force them together. This means, then, that the temperature drop across the two films can be determined by making measurements with two disks of different thicknesses provided that (1) they have identical surface finishes, (2) the faces are parallel, (3) the same pressure is applied in both measurements, (4) the heat flow through the disks is equal, and (5) the average thermal conductivity across each disk is the same. These five requirements are not difficult to approximate. Items 1, 2, and 3 can be achieved with ease. Note that ultrafine finishes of the rod and/or disk faces are not stipulated and they are not necessary, consistency being the important factor. Fulfilling the requirement of equal heat flow through the disks can be ascertained by means of a graph of Q versus ΔT, the total temperature difference between the rod faces. The magnitude of ΔT can be read from the graph for an identical Q for each determination of k. The

fifth requirement can be achieved by adjusting the temperature of the source and heat sinks.

Using these conditions, Equation 1 may be written for the disks 1 and 2 of different thicknesses as

$$Q_1 = Q_2 = -k_1 \left(\frac{\Delta T}{\Delta x_1}\right) = -k_2 \left(\frac{\Delta T}{\Delta x}\right)_2 \qquad (2)$$

where

$$\Delta T = \Delta T_{Total} - \Delta T_{films}. \qquad (3)$$

The average temperature across the disks is equal and so $k_1 = k_2$ and Equation 2 reduces to

$$\Delta T_{film} = \frac{\Delta T_{T_1} - \Delta T_{T_2}\left(\frac{\Delta X_1}{\Delta X_2}\right)}{1 - \Delta X_1/\Delta X_2} \qquad (4)$$

Equation 4 includes the assumption that the films are of identical thickness, at the same average temperature, and, therefore, have the same temperature drop to support the heat flux. After the measured quantities are substituted and Equation 4 is solved for the temperature drop due to the films, Equation 2 is rewritten as Equation 5 and the thermal conductivity of the disk material is determined,

$$k_1 = k_2 = \frac{Q\Delta X_1}{\Delta T_{T_1} - \Delta_{T_f}} = \frac{Q\Delta X_2}{\Delta T_{T_2} - \Delta T_f}. \qquad (5)$$

A schematic of the apparatus as used is shown in Figure 1.

The technqiue used here differs from that of Lucks[5] and Deem in that the temperature difference across the film is actually evaluated. Lucks and Deem write the equation for the

total temperature drop between the two thermocouples, in the rods adjacent to the specimen, as

$$\Delta T_{Total} = \Delta T_{r,u} + \Delta T_{f,u} + \Delta T_{s} + \Delta T_{f_1} + \Delta T_{r,l} \qquad (6)$$

where the subscripts indicate as follows: r = rod, f = film, s = unknown specimen, u = upper, and l = lower. Assuming then that Q is a constant through the specimen,

$$\frac{\Delta T_{Total}}{Q} = \frac{1}{K_s} \Delta X_s + R \qquad (7)$$

where R is the sum of the known and unknown resistances. Now a graph of $\Delta T_{Total/Q}$ versus ΔX_s, for a number of specimens, should result in a straight line, the slope of which is the reciprocal of the conductivity.

EXPERIMENTAL RESULTS

The thermal diffusivity was measured on ceramics of the molecular equation $Ba_{1-x}\ Ca_x\ Ti\ O_3$, when x = 0, 9.9%, and 19%. The results of these measurements are shown in Figure 2. There is some scatter of the points, but they all fall within 10% error about the lines as drawn. The method as used for the measurement sends a heat wave through the material. Since the ceramic is a very poor conductor of heat, it was necessary to have temperature differences of about 10°C, in some instances, between the two thermocouples. Diffusivity is graphed at the average between these two temperatures.

Figure 3 shows the results of measurements on the thermal conductivity. The precise determination of the curve through

the transition points appears to be beyond the capabilities of the measuring technique, primarily since there was a temperature drop across the specimen of about 10°C; the Curie point is a rather sharp transition in these materials. The data on Figure 3 is next graphed to show the effect of adding calcium to the magnitude of the thermal conductivity.

The specific heat, as calculated using the density as independent of temperature for this region, is shown in Figure 5. The void space on the curve represents the unresolved curve in the transition region.

The electrical properties are exemplified by the curves shown in Figure 6. This data, for barium titanate, is typical for reasonably good ceramic ferroelectrics. The dielectric constant at room temperature is slightly higher than 1500, the value considered typical of good ferroelectrics, and the residual polarization, Pr, measured from hystereses loops, is low at 7.13 μ coul/cm^2. The curie constant, determined from the intercept of the reciprocal of the dielectric constant for temperatures beyond the Curie point is 103°C. Data from the various ferroelectrics at 30° C.are listed in Table 1.

Ceramic (% Ca)	ρ (gm/cm^3)	ε	Pr (μ coul/cm^2)	Ec $\left(\frac{KV}{cm}\right)$
0	5.9	1800	7.13	2
3.4	5.8	1650	7.6	1.9
9.9	5.6	1500	8.2	2.1
19	5.28	1300	5.3	3.32

Table 1. Room temperature electrical properties of the barium calcium titanate ceramics.

DISCUSSION

The thermal data, as shown by the graphs, for good quality ferroelectrics are consistent within about ±10%. The thermal diffusivity measurements indicate a significant decrease in the ability of the material to transmit heat, which occurs with rising temperature as the material passes through a phase change. Previous specific heat data and the thermal conductivity data indicate an anomalous increase in these parameters at the transition between tetragonal and cubic crystal structure. Further work is needed to resolve whether or not these magnitudes are identical so as to provide a smooth transition curve for the thermal diffusivity. The data as presented here do not answer this question, but it is hoped that data from further measurements will. The measurements on the thermal conductivity indicate that there is a slight decrease in magnitude as the temperature causes the crystal to enter the cubic phase. These measurements also indicate that the correction for porosity, as applied by Yoshida[2] and Nomura, will not account for the discrepancy in magnitude of the thermal conductivity. The barium titanate ceramics as used here were almost of theoretical density, while the ceramics used in the experiment referred to above[2] were about 87% of theoretical density.

The error of the thermal measurements are estimated to be less than ±10%. The data points for the thermal diffusivity were believed to be within this error, so the lines as drawn should be somewhat more accurate. The measurement of thermal conductivity depended on the knowledge of the properties of the

metering rods, as well as thermocouple calibration, specimen size measurements, and the determination of the temperature drop across the films. The conductivity of the armco iron is believed known absolutely within ±5%. Indirect measurements of the diffusivity indicated that this was indeed the case. The thickness of the specimens were known to within ±0.0005 cm. The thermocouples were calibrated and data measurements indicated a smooth temperature profile along the rod. We believe the overall error to be within ±15%. This is further justified by the figure concerning specific heats. The specific heat for barium titanate as calculated is 3% greater than the value measured directly.[9] This adds strength to the accuracy of the measurements, although the thermal conductivity is 22% larger than reported in the literature.[2]

REFERENCES

1. S. S. Todd and R. E. Lorenson, Heat Capacities at Low Temperatures and Entropies, at 298.6°K of Metatitanates of Barium and Strontium, J. Am. Chem. Soc., 74, 2043-5 (1952).

2. I. Yoshida and S. Nomura, J. Phys. Soc. Japan 13, 1550 (1958

3. D. E. Rase and R. Rustum, Phase Equilibria in the System BaO - TiO_2, J. Am. Ceram. Soc. 38 (2) 102-113 (1955).

4. P. H. Sidles and G. C. Danielson, J. Appl. Phys, 25, 58 (1954).

5. C. F. Lucks and H. W. Deem, ASME Paper No. 56-SA-31, ASME Semiannual Meeting, Cleveland, Ohio (1956).

6. I. Yoshida, J. Phys. Soc. Japan 15, 2211 (1960).

7. L. C. Laming, Thermal Conductance of Machined Metal Contacts, International Developments in Heat Transfer, Part 1, p. 65, ASME, 1961.

8. H. Fenech and W. M. Rohsenow, N.Y.O.-2136, May 1959.

9. C. F. Lucks, (private communication) Battelle Memorial Institute, Columbus, Ohio.

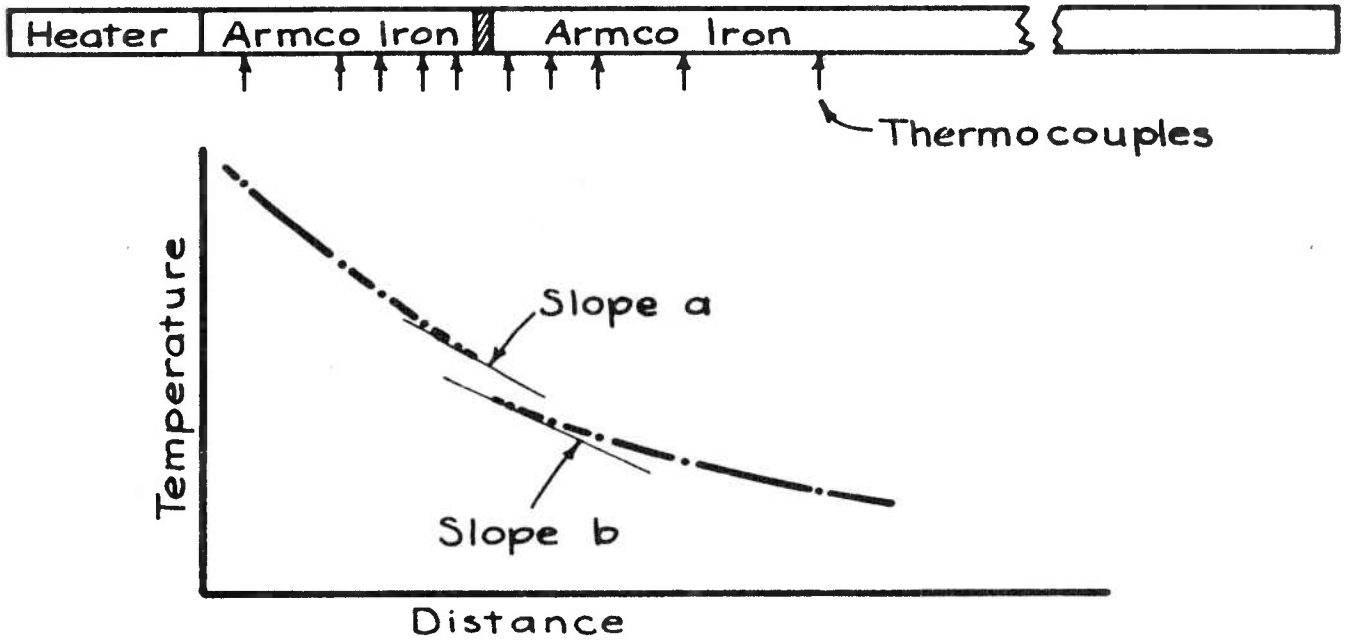

$$Q_a = \frac{q_a}{A} = -\left(k\frac{\Delta T}{\Delta X}\right)_a$$

$$Q_b = \frac{q_b}{A} = -\left(k\frac{\Delta T}{\Delta X}\right)_b$$

$$\frac{Q_a + Q_b}{2} = Q \text{ sample}$$

Sample with thickness t_1

$$Q_1 = \frac{-k_1\left(\Delta T_{T_1} - \Delta T_{f_1}\right)}{\Delta X_1}$$

$$Q_2 = \frac{-k_2\left(\Delta T_2 - \Delta T_{f_2}\right)}{\Delta X_2}$$

When $Q_1 = Q_2$

$$\Delta T_{f_1} = \Delta T_{f_2}\left(\frac{\Delta X_1}{\Delta X_2}\right)$$

$$\Delta T_f = \frac{\Delta T_{T_1} - \Delta T_{T_2}\left(\frac{\Delta X_1}{\Delta X_2}\right)}{1 - \frac{\Delta X_1}{\Delta X_2}}$$

Fig. 1. Experimental technique

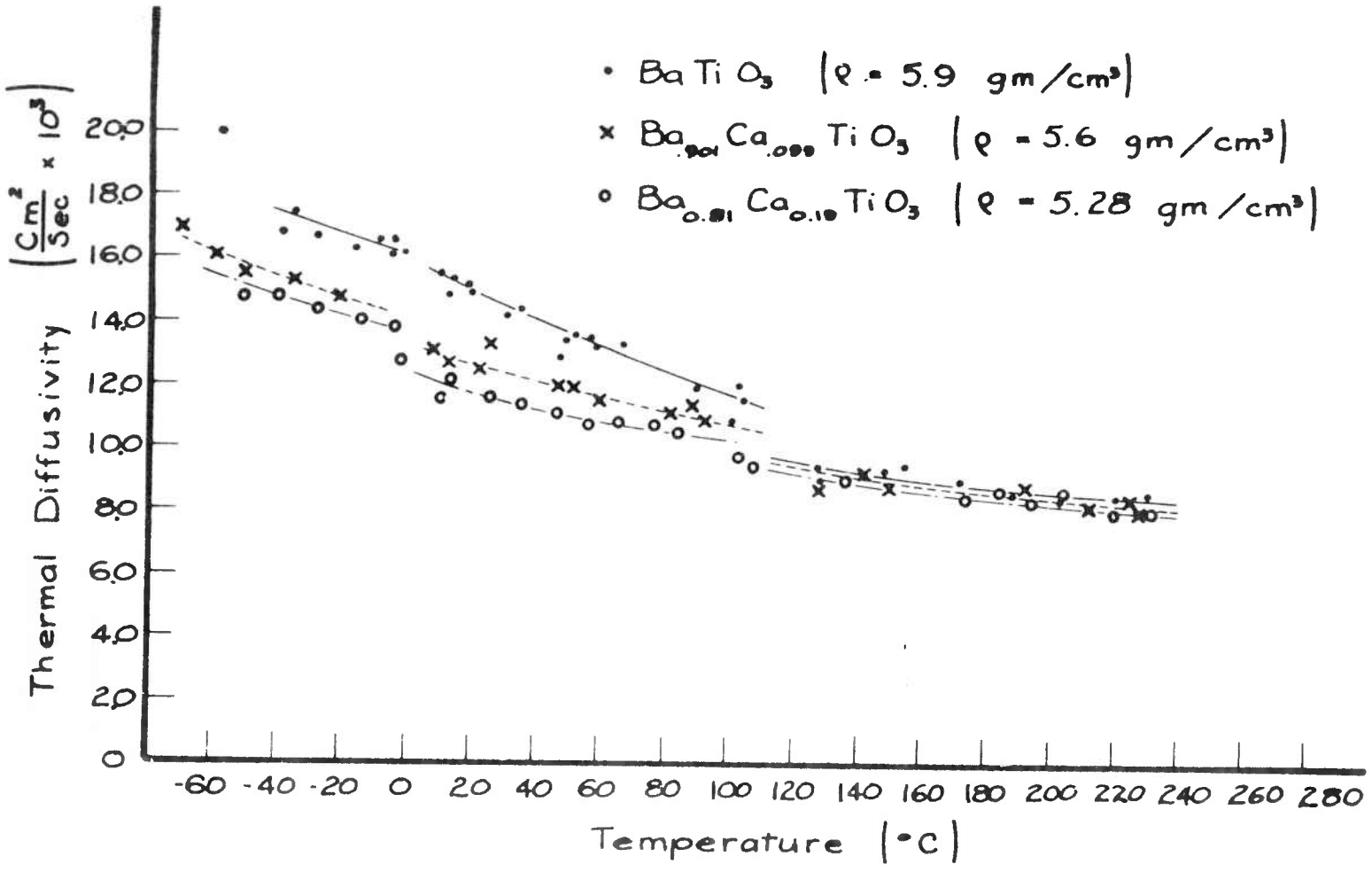

Fig. 2. Thermal Diffusivity of Barium-Calcium Titanate Ceramics

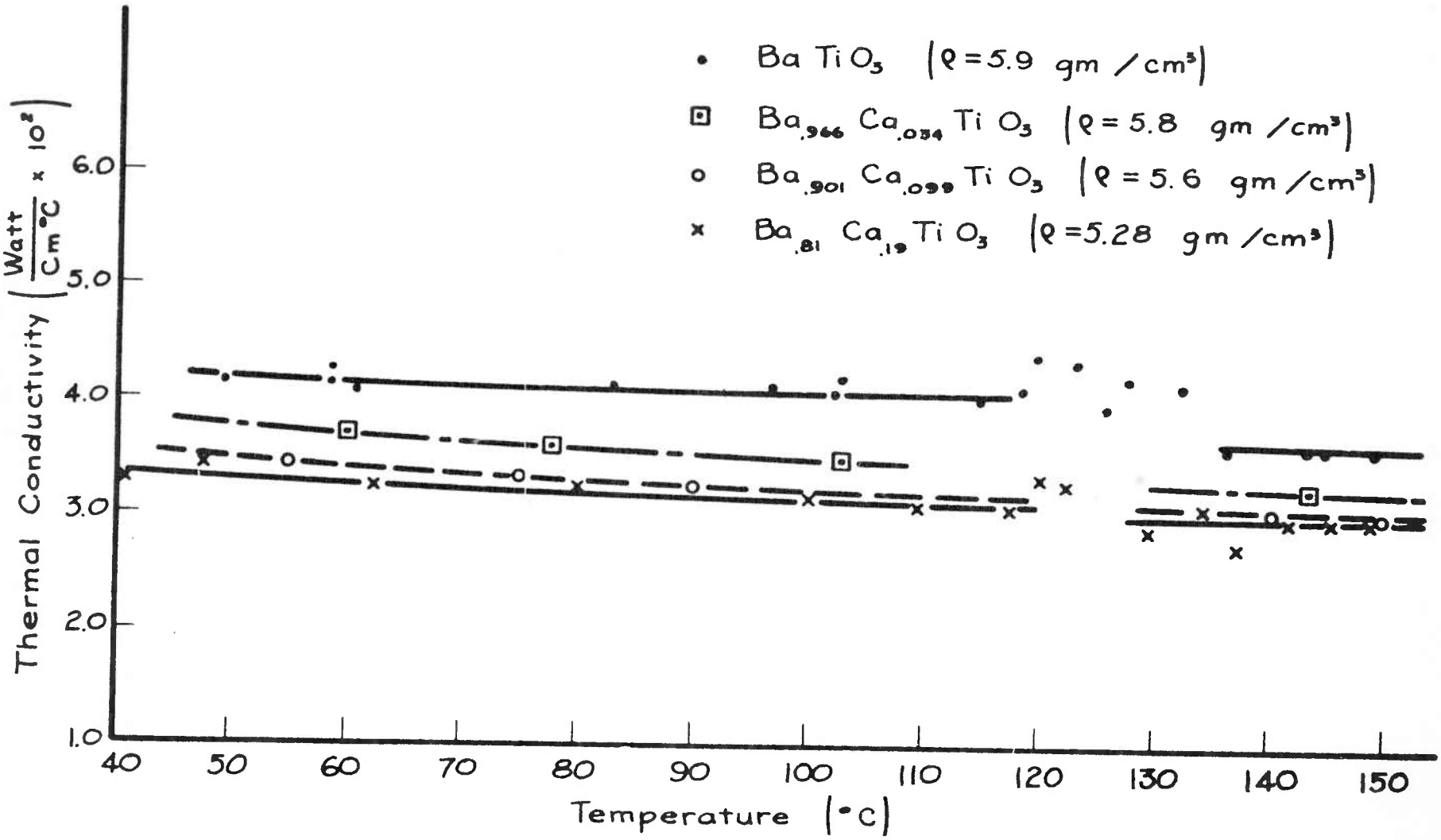

Fig.3. Thermal conductivity of barium-calcium titanate ceramics as a function of temperature

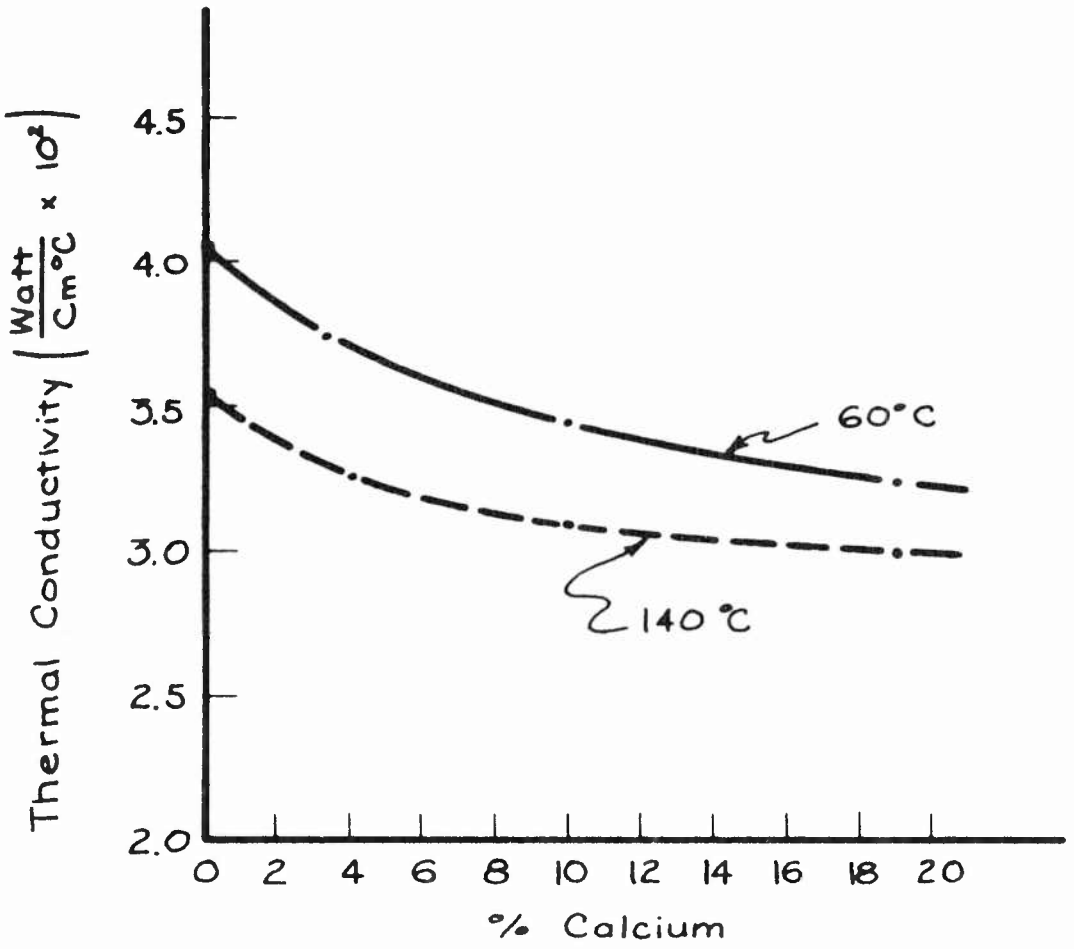

Fig. 4. The effect of calcium additive on the magnitude of the thermal conductivity

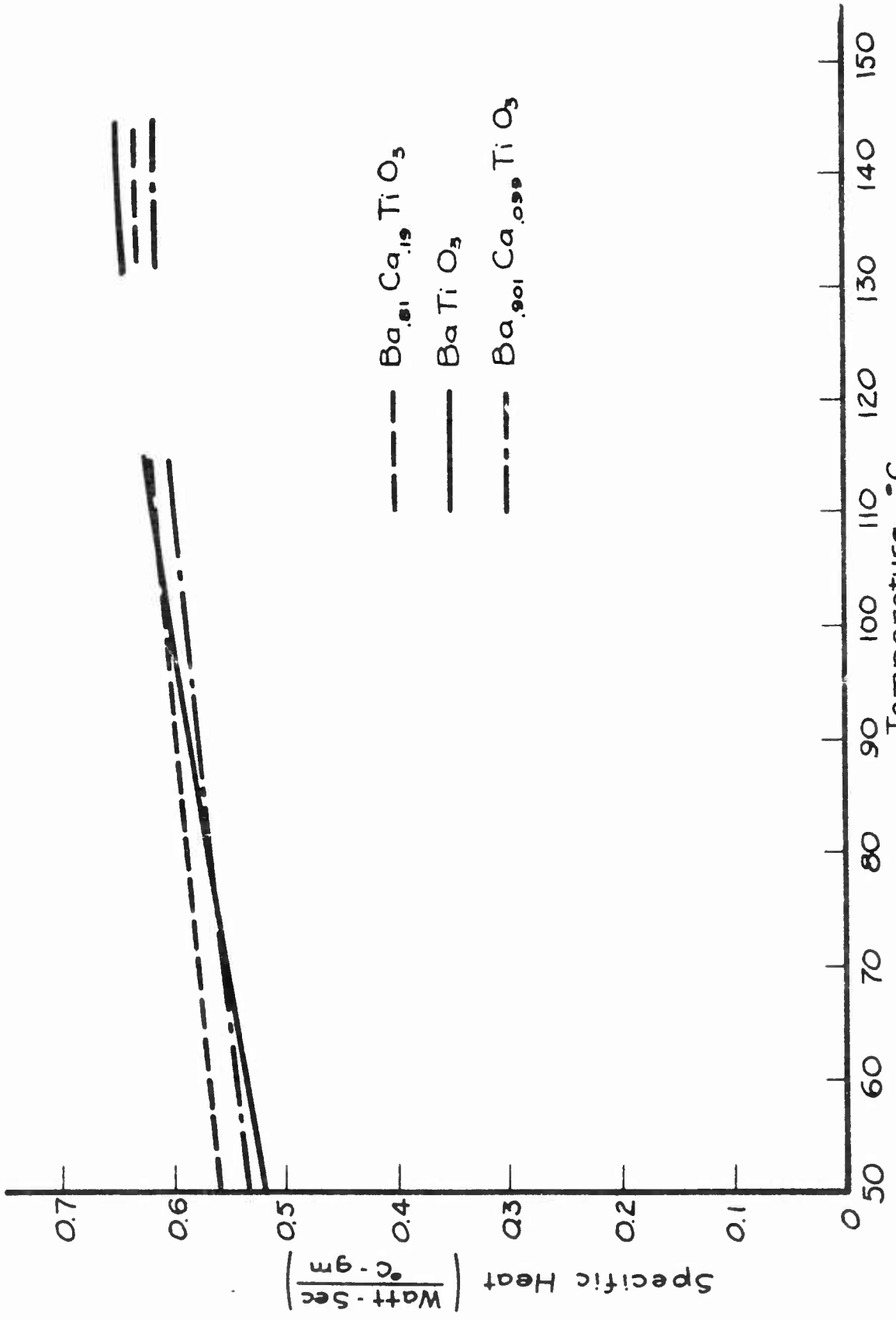

Fig.5. Specific heat as calculated from thermal conductivity and diffusivity measurements

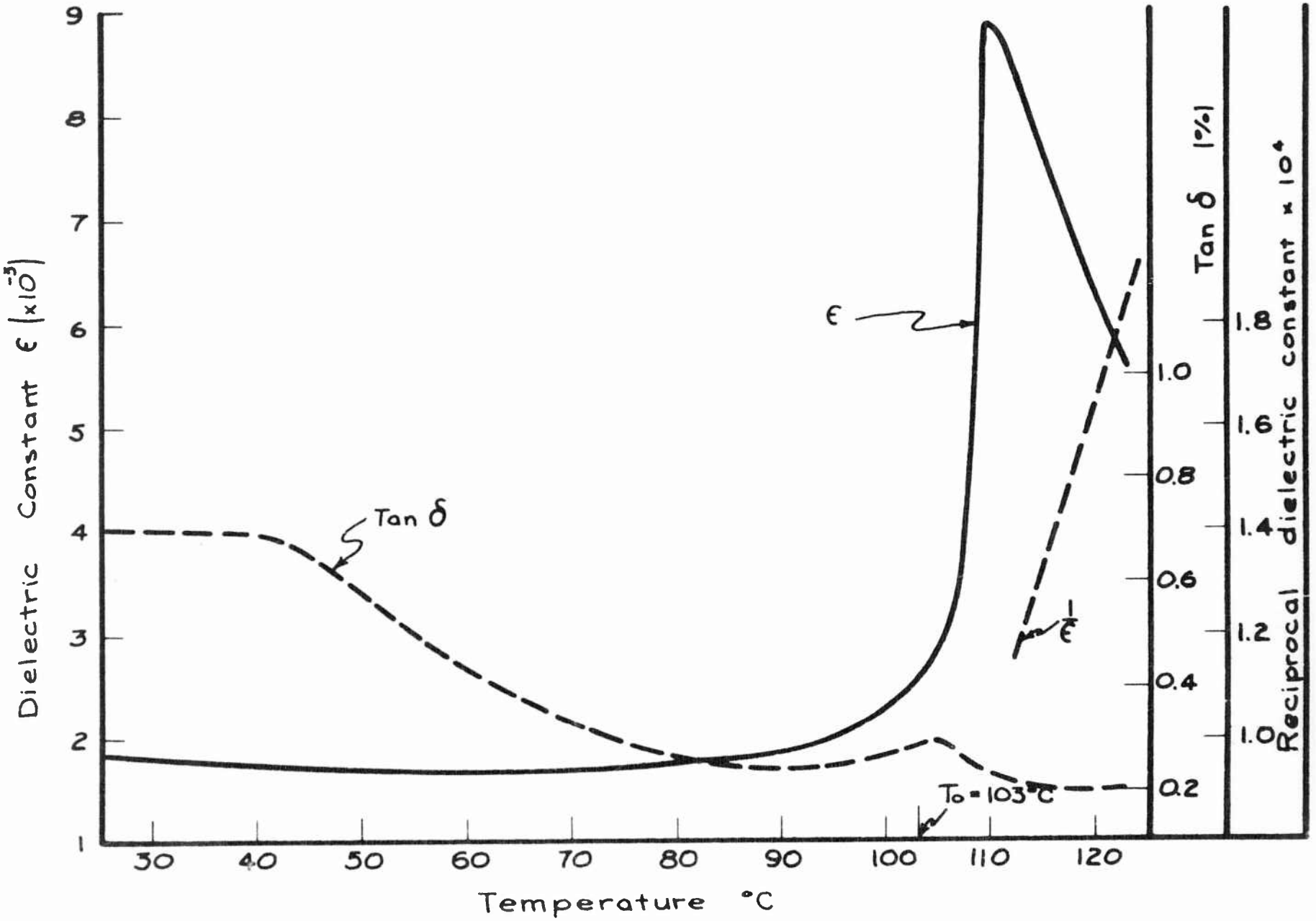

Fig. 6. Electrical properties of the $BaTiO_3$ specimen

B3. SERIES COMPARATIVE MEASUREMENTS OF THERMAL CONDUCTIVITY WITH THERMISTORS*

by

William G. Delinger, Francis W. Kalkbrenner+ and Robert G. Morri
South Dakota School of Mines and Technology, Rapid City

The series comparative method of determining the thermal conductivity depends on the measurement of temperature differences. In conductivity work it is wise to keep the thermal gradients low across both the sample and contacts to minimize radiation error. Low gradients imply near-isothermal conditions Therefore, the temperature differences to be measured will be small. Thermocouples are usually employed as temperature sensors in thermal conductivity measurements. Since thermocouple emf's vary only 6 to 40 microvolts/deg C an error of 10% in determining small temperature differences would not be unusual.

The thermistor, or thermally sensitive resistor, has characteristics which make it suitable for precision temperature difference measurements. It can be made small in size (0.11 cm and smaller) and has a high temperature coefficient of resistanc ($\approx$-5%/deg C at 25°C). For comparison, the resistance of platinum varies only +0.4%/deg C. The literature contains a number of references to results which have been obtained in

---

* This work supported in part by the Office of Naval Research and by a Special Research Appropriation by the State of South Dakota.

+ Present Address: Boeing Company, Seattle 24, Washington

practice for thermistor stability, but it is difficult to draw any very definite conclusions from these as they are to some extent conflicting. Beck[1], however, quotes an accuracy of the order of 0.01°C in a temperature difference of 6 - 12°C over a short period of time. An investigation of the resistance R - vs - T temperature curve was made for typical commercial thermistors. The data show the curve is repeatable within less than 1% as the temperature is cycled many times to 250°C and back to 25°C. The slopes of the curves for thermistors of the same type at the same temperature have also been found to be nearly identical.

The thermal conductivity of a sample is determined by the series comparative method used in this laboratory[2]. However, thermistors are cemented to the sample and standards in place of thermocouples. A Wheatstone bridge is used to measure the difference in temperature ΔT between two thermistors as shown in Fig. 1. Let us first assume two identical thermistors are placed in adjacent arms of the bridge and it is balanced for the case of zero heat flow. When heat is allowed to flow the thermistors will assume different resistances and the bridge will be in an unbalance condition. The degree of unbalance is indicated by the current through the null detector. For small temperature differences, the unbalance current is proportional to the difference in resistance ΔR between the two thermistors. At balance $I_g = 0$ and $X_1R_2 = X_2R_1$ (with $X_1 = X_2$).

For unbalance

$$I_g = \frac{ER(a-b)}{2R(X+a)(X+b) + R^2(2X+a+b) + R_G(X+R+a)(X+R+b)}$$

when X_1 changes to X+a and R changes to R+b. a and b are both much less that X and R.

Knowing $\Delta R = a-b$ we find $\Delta T = \Delta R/(dR/dT)$. The derivative of R with respect to T at T_1 is found by differentiating a polynomial obtained by fitting the least squares on an IBM 1620 computer previously measured Resistance and Temperature values for the thermistors.

Although thermistors of the same type have nearly identical values for dR/dT, they do not have identical resistances. However, by a technique due to Godin[3] both R and dR/dT for a thermistor pair may be matched precisely at any given temperature. This method of matching thermistors uses a resistor in parallel and one in series with one thermistor. (See Fig. 2). A calculation shows that a typical 3000-ohm pair can be matched exactly at $T_1 = 297°K$ and agree within 2 ohms for a temperature range of 5 degrees on either side of T_1 although the difference in resistance between the thermistors may be as much as 100 ohms.

The sensitivity of a Wheatstone bridge near a balance condition has been taken into account in the design of the direct-reading temperature-difference bridge. A graph of the thermistor resistance X-vs-S max/S sensitivity ratio has been plotted in Fig. 3. The optimum ratio for the resistance of the thermistor to the nonthermistor arms of the bridge can be determined for different values of X from this graph.

The thermistors that are used for the temperature sensors are made by Fenwal Electronics, Inc., Framingham, Massachusetts. These are GA51J1 glass coated bead type of thermistors with a

nominal resistance of 100,000 ± 15% ohms. They have a temperature coefficient of resistance of -4.6%/deg C at 25°C and -1.5%/deg C at 250°C. The small ellipsoidal beads have a minor axis of 0.11 cm. For maximum stability, the beads should not be used above a temperature of 300°C. The temperature range is from 25°C to 250°C.

A 9834 Leeds and Northrup electronic DC null detector with an input resistance of 25,000 ohms is used as the galvanometer in the Wheatstone bridge.

The resistances used for the nonthermistor arms of the bridge are 4745 Leeds and Northrup 0-10,000 ohm decade boxes.

REFERENCES

1. A. Beck, "The Stability of Thermistors," J. Sci. Instr. 33, 16 (1956).

2. Robert G. Morris and Jerome G. Hust, "Thermal Conductivity Measurements of Silicon from 30° to 425°C," Phys. Rev. 124, 1426 (1961).

3. M. C. Godin, "A Method of Equalizing Thermistors," J. Sci. Instr. 39, 241 (1962).

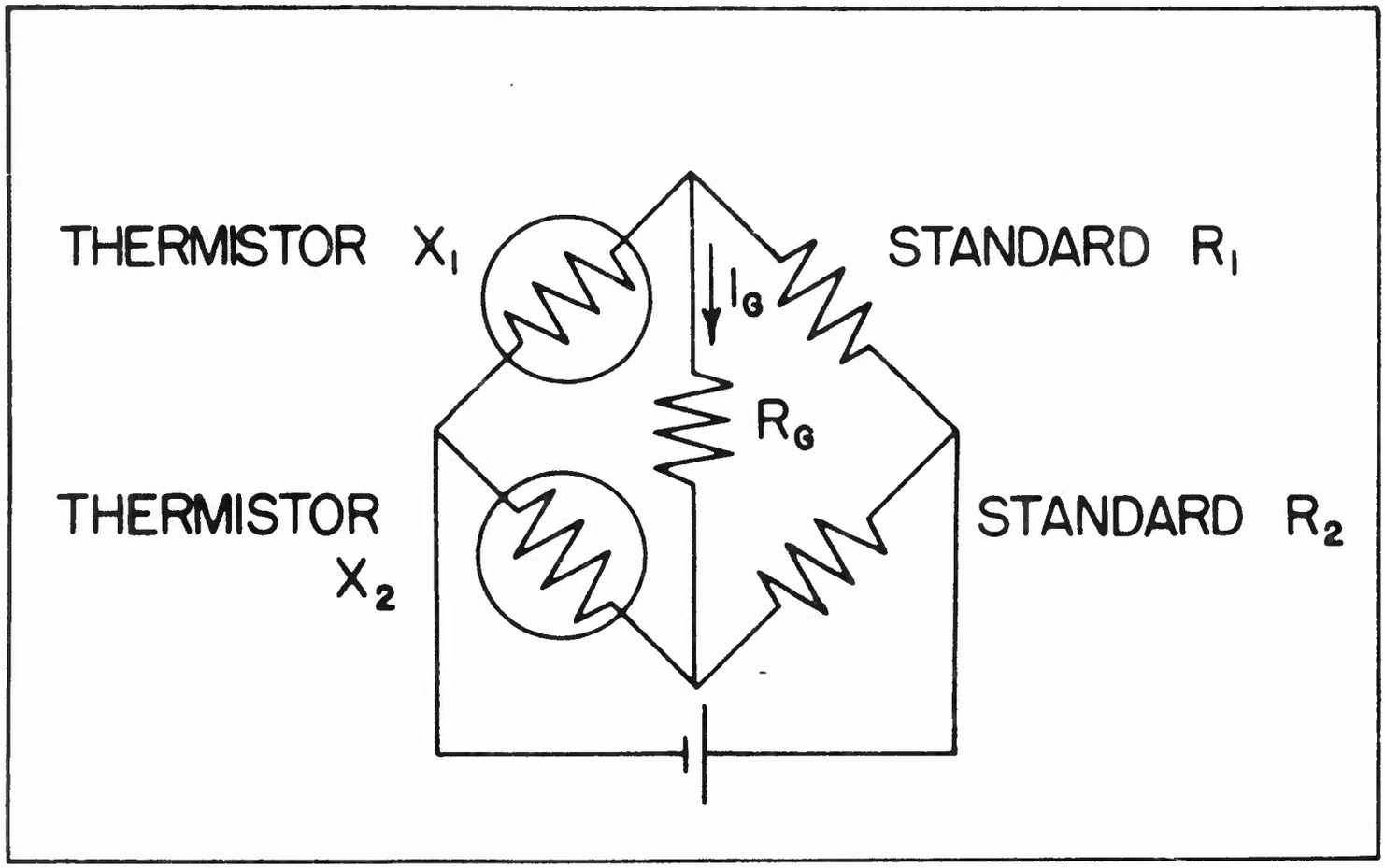

Fig. 1 Thermistor Bridge Circuit

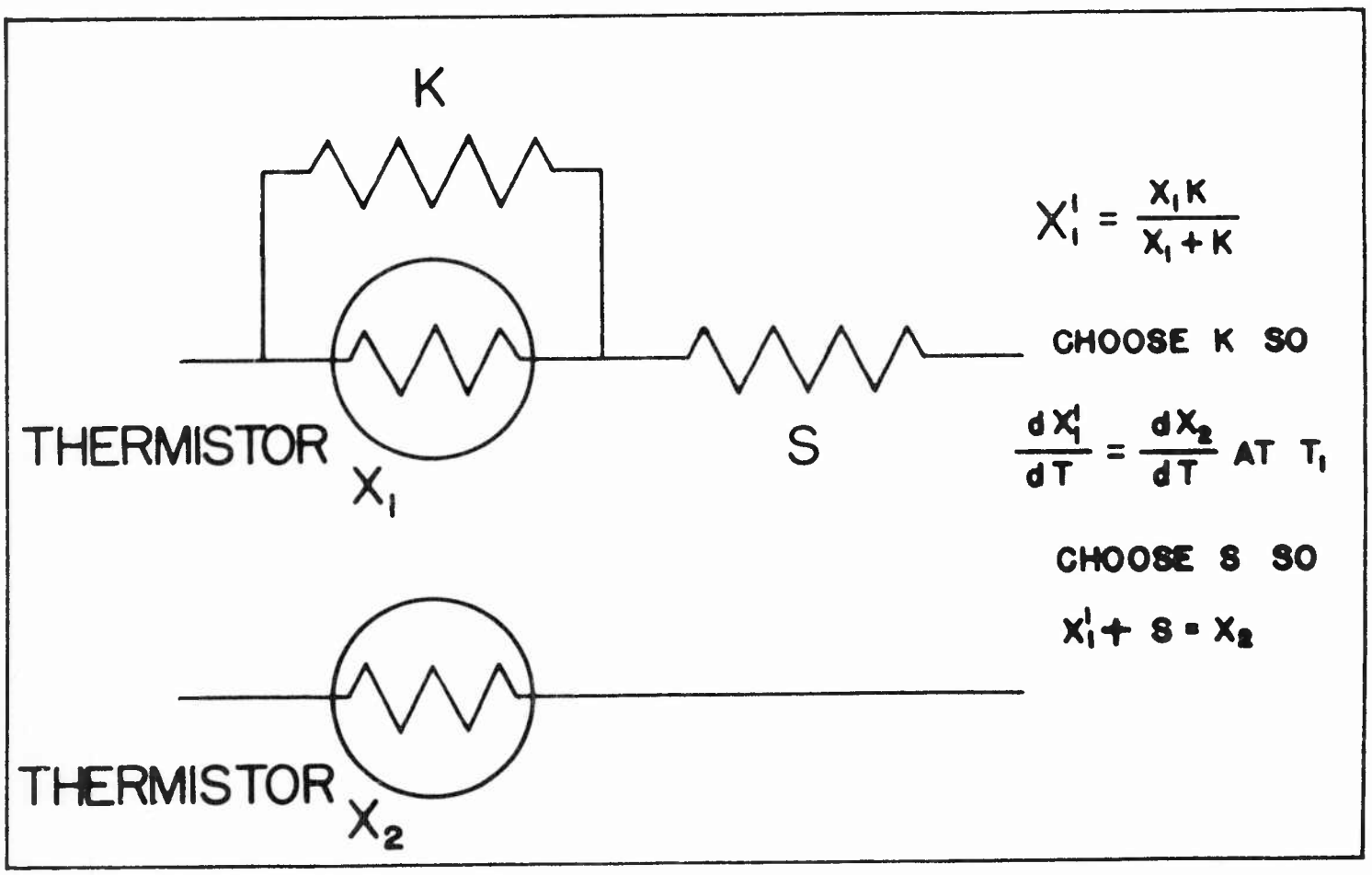

Fig. 2 Godin Technique for Matching Thermistors

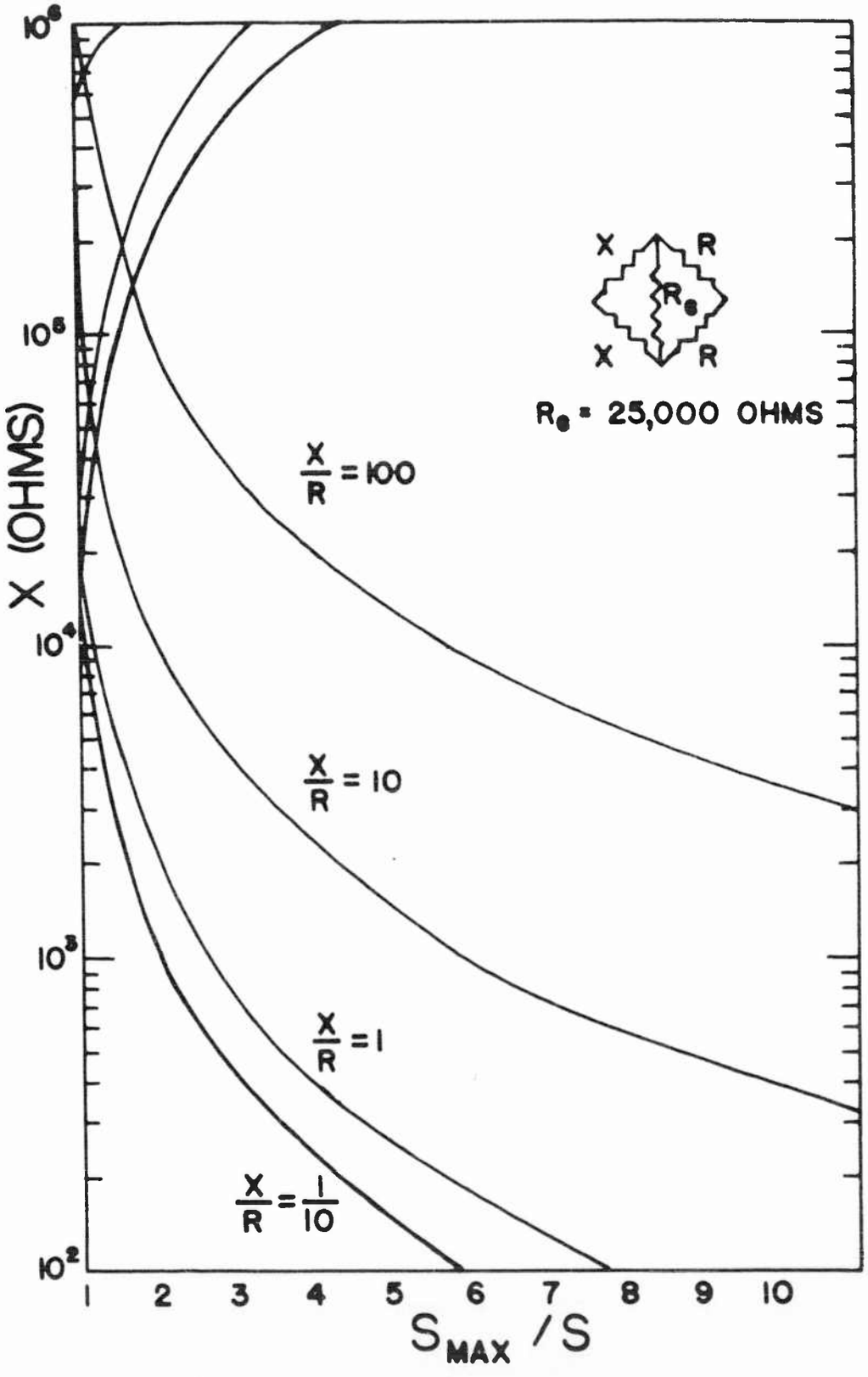

Fig. 3 Bridge Sensitivity as Function of X/R

C1. (Invited paper) THERMAL CONDUCTIVITY MEASUREMENTS BY THE THERMAL-COMPARATOR METHOD

by

R. W. Powell
(Basic Physics Division, The National Physical Laboratory, Teddington, Middlesex, England)

ABSTRACT

An account is given of the use of the original two-ball form of the thermal comparator for thermal conductivity determinations on solids, liquids and powders. An analysis of the conditions governing the flow of heat from the ball to a plane test surface shows the temperature at the point of contact to be quickly established, to change relatively slowly with time and to be a function of the thermal conductivity of the test material. A thermal comparator based on the measurement of this contact temperature would be direct reading and independent of load and surface finish. Two such direct-reading thermal comparators are described and have given useful results although the temperature so far measured departs from that of the contact and is still dependent on load and surface finish. Much smaller specimens can however be tested before the reading becomes size dependent. Results are given for several ceramic and semiconducting materials and the new method is considered particularly suitable for comparative thermal conductivity determinations on samples of such materials for which this property often varies considerably from sample to sample.

Introduction

One of the interesting demands arising from many of the developments of modern technology has been for fairly precise thermal conductivity data for many materials over a wide temperature range. In the inter-war period the laboratories equipped for the measurement of thermal conduction could probably be counted on the fingers of one hand. Today, many laboratories in the countries engaged on modern technological

advances are striving to answer the question "What is its thermal conductivity"? The question is a very relevant one in the field of semiconductors forming the subject of this Conference but it arises just as much with regard to metals, ceramics and thermal insulants. And it is not proving an easy question to answer. As one who has spent over thirty years in attempting to make accurate or reasonably accurate thermal conductivity determinations I know only too well the difficulties that can arise and the time involved in making such measurements. Progress is being made, however, and reliable measurements will be made more extensively as materials of known thermal conductivity become increasingly available and are intercompared in the course of this precise work. Erroneous values in the literature are gradually being put right, beryllium[1], iridium[2], rhodium[2], indium[3] and rhenium[4] are instances with which the writer has been concerned, and gaps in existing knowledge are gradually being filled. The present need is for the provision of a range of materials of agreed thermal conductivity in the region 1000° to 2000°C and even higher.

In recent years I have had the satisfaction of introducing and working on a method[5,6] that is providing a useful means for simple and rapid comparative measurements of thermal conductivity. I am about to tell you of this work, what has been achieved and some of our hopes for the future. But let me emphasize that it is a comparative method. It can never displace the need for precise conventional measurements, but, when used with

intelligent discretion and with suitable standard materials the answer to that question, what is the thermal conductivity, can often be obtained both cheaply and quickly.

The thermal comparator method to which I refer, was introduced as a means of giving quantitative expression to the qualitative assessment of thermal conductivity often made by merely handling a range of materials and arranging them in order of increasing thermal conductivity according to their coldness. This was over five years ago and the method is now fairly generally known. However, it is hoped you will be patient whilst some familiar ground is covered, some theoretical considerations[7,8] presented and, finally, details given of a modified direct-reading form of the thermal comparator on which work is still in active progress and which should have definite advantages, both for routine tests made at normal temperatures and for the measurements to higher temperatures that it is hoped soon to undertake.

The Thermal Comparator and it use for thermal conductivity determinations

The original form of the thermal comparator is shown in Figure 1. It consists of two similar phosphor-bronze or other metal balls securely mounted in a block of thermal insulating material. The balls are usually about $\frac{1}{4}$" in diameter and one projects slightly beyond the surface of the block so that it can be brought into contact with a test material. Two metal studs complete a 3-point contact and ensure stability and

reproducibility but these need not rest on the test material if another co-planar surface is provided. Each ball has a securely attached thermocouple and these are usually connected differentially and the emf observed on a vernier potentiometer reading to 1 μV.

The thermal comparator is heated to an excess temperature of some 40°C and then placed on a test sample at normal temperature. Both balls commence to cool, but the cooling of the contacting ball is augmented by the transference of heat to the test sample. This causes the differential emf to increase approximately linearly for at least 10 seconds the normal period of the experiment. (see Figure 2).

The reading observed after such a fixed time is a measure of the heat flow, and this in the main is a function of the excess temperature, the geometry of the contact (which depends on the load) and the thermal conductivity of the test material. Provided the conditions of the experiment are such that the last mentioned quantity is the only variable there should be a direct correlation between the observed differential emf and the thermal conductivity.

Figure 3 shows the results of tests made at room temperature using materials of known thermal conductivity and ranging from aluminium to plasticized PVC. This range, from 2.39 to 0.0021 J cm/cm^2 sec degC, would require at least two quite different methods of the conventional type. By plotting the thermal comparator reading against the square root of the thermal

conductivity, two straight lines are obtained intersecting at high-alloy steel (0.11 Jcm/cm^{2}sec degC).

The importance of this result is that once calibrating tests have been made on two or three materials of suitable and known thermal conductivity, a very simple method becomes available for making thermal conductivity measurements on an unknown material to an accuracy of about 5 per cent. Examples of such tests for two different types of solid materials are shown in Figures 4 and 5. Figure 4 relates to tests made on discs cut from metal rods that had been used for tests by the conventional longitudinal heat flow method and were thus of known thermal conductivity. One face of each disc was left in the machine-finished state, the other surface was lapped. For each condition, three calibrating materials were chosen of the extreme and an intermediate thermal conductivity and a straight line drawn through plots of the comparator readings against the square roots of the thermal conductivities. The lines for the two surface conditions are quite distinct, indicative of the dependence of the reading on the surface finish and emphasizing the need for test and calibrating surfaces to be closely similar. The experimental points obtained for the other discs are similarly plotted and are seen to be grouped along the appropriate calibration lines the majority of the derived thermal conductivities agreeing with the previously determined values to within 5 per cent.

Figure 5 depicts the results of measurements made on the lapped surfaces of several discs of glass. In this instance the

calibration was obtained for the poorest conducting of the glasses and a similar disc of fused silica. For five of the seven glasses the derived and conventionally determined thermal conductivities agreed to within 1 per cent; for the other two the differences amount to +2.4 and -3.8 per cent.

Figure 6 shows the degree of correlation obtained between the surface finish of a plane steel surface, expressed as CLA values in microinches, and the comparator reading.

Dependence of readings on sample size

In the above two series of comparative tests the shape and size of the standard and test samples have been constant. As this may not always be possible, experiments have been undertaker to ascertain how great a reduction in size could be tolerated without affecting the reading of the comparator. The results of such measurements on discs of mild steel 1 inch in diameter but covering a range of thickness are shown in Figure 7. Similar measurements for glass are in Figure 8. The thickness for which the reading becomes independent of thickness is seen to decrease as the thermal conductivity increases. The influence of disc diameter on the reading was similarly investigated. The results obtained for a particular thermal comparator and method of use are summarized in Table 1.

Table 1

Minimum disc sizes for reading to be independent of size

Material	Thermal conductivity (Watt/cm degC)	Thickness (in)	Diameter (in)
Copper	3.8	0.016	0.3
Mild steel	0.5	0.032	0.35
High alloy steel	0.11	0.050	-
Borosilicate glass	0.011	0.0128	2.5

For good conductors, the sizes required are remarkably small, but the glass used is seen to be comparable in thermal conductivity with some of the poorer conducting of the semi-conductor materials e.g. silver-indium selenide, and then the question of specimen size may need to be watched. It will either be necessary to have both test and calibration samples in the same smaller size and to ensure that they are mounted to have similar heat transfers across the under-sized dimension, or to make some subsidiary tests to enable correction to be made.

On the other hand, provided the sample is in temperature equilibrium, the method enables tests to be made on quite large samples, or even built in parts of a machine. All that is required is the preparation of a small area of surface on which contact can be made.

Consideration of influence of directional effects claimed to arise with dissimilar materials

Experimental evidence has been produced, first in the USA[9],

and later in Bristol[10], indicating that under certain circumstances the resistance to heat flow at the interface of dissimilar metals can vary with the direction of heat flow. The American workers, using plane surfaces 3 inches in diameter found the interface conductance between aluminium alloy and steel to vary with the applied load and to be 2 to 3 times greater when heat flowed from aluminium to steel than for the reverse direction. Thermal warping of the surfaces was thought to be a contributory cause. The workers at Bristol used smaller surfaces of 1 inch diameter and did not vary the applied load. They found a similar but much reduced effect, the interfacial conductance from aluminium alloy to steel being 20 per cent greater than from steel to aluminium alloy. The effect was considered to be associated with the mechanism of conduction at the points of metallic contact, for instance, with metals having different values of the work function it was suggested that a potential barrier might be created reducing the drift of free electrons in one direction and increasing it in the other. This conclusion would appear to introduce an additional parameter likely to influence the rate of heat transfer and hence the reading of the two-ball thermal comparator. Tests to determine if this was so were therefore made.

That no such complicating effect was apparent for the very much smaller contact area of this thermal comparator can be seen from Figure 9. This figure shows the results of several series of experiments in which a thermal comparator fitted with steel

balls was applied to an aluminium alloy surface. The thermal comparator reading noted 10 seconds after contact is plotted against the initial temperature difference between the two metals. The direction of heat flow was reversed by either placing a warm comparator on an aluminium sample at room temperature, (points shown as crosses) or, warming the aluminium and placing a cold comparator on it (ringed points).

The two types of points will be seen to lie within ±7 per cent of the straight line drawn to pass through the origin and to be reasonably evenly distributed about the line. They gave no support for the claim that the heat transfer from aluminium to steel (ringed points) is greater than that from steel to aluminium alloy (crosses). The experiments under reduced load were carried out to give an effective load per unit area comparable with that of the Bristol work (122 lb/cm^2).

Having made these tests for the metallic combination studied elsewhere it was considered of interest to make similar tests for a semiconductor in which most of the heat flow occurs by phonon or lattice waves, and the still more extreme case of an electrical insulator in which there can be no heat conduction by electrons. Thus, when the warm thermal comparator is applied, the heat will flow from steel, for which the bulk of the heat flow occurs by electrons to another material in which there is little or no heat flow by electrons, but the major portion, or total heat flow is by phonons. When a cooler comparator is applied, these conditions will be reversed and heat flow predominantly by phonons will become one predominantly by electrons.

Results are shown in Figure 10 for germanium and a soapstone ceramic and it will be seen that even for these extremely different materials and types of heat transport no directional effect is involved.

In Figure 11 thermal comparator readings for materials of known thermal conductivity, Armco iron and high alloy steel, have been included and plotted in the usual way to enable the thermal conductivity of the germanium sample to be derived from the results of the previous figure. The value obtained in this way is 0.58 Jcm/cm^2 sec degC, which agrees well with a room temperature value of about 0.6 Jcm/cm^2 sec degC reported by Slack and Glasbrener[11]. The thermal conductivity of the soapstone ceramic material has been measured independently and this gives a point on a line of lower slope as found previously.

Theoretical treatment

Only a very approximate analysis has been made of the transfer of heat from the thermal comparator to the test sample[7,8]. The full analysis would be one of considerable complexity since the sphere cools by radiation and by air conduction as well as by conduction through the restricted area at the solid to solid contact. At normal temperatures radiation can be neglected but not conduction through the surrounding air. However, in the first instance only the conduction through the solid constriction has been considered. This problem has been reduced to that of the heat flow in two semi-infinite regions, $0 < z < \infty$, $0 > z > -\infty$, having thermal conductivities k_1 and

k_2 and initial temperatures V_o and 0 respectively which are in contact over a small radius r_1. (The sphere can be considered a semi-infinite solid since its diameter is some two orders of magnitude greater than the diameter of the contact area).

Regarding the comparator as a steady-state device, the temperature in region (1) is given by

$$V_1 = V_o - V_1'$$

where $V_1 = V_o$ at $z = \infty$

$V_1' = 0$ at $z = \infty$

and V_1 satisfies the equation

$$\frac{\partial^2 V_1}{\partial r^2} + \frac{1}{r}\frac{V_1}{r} + \frac{\partial^2 V_1}{\partial z^2} = 0$$

V_1 is found to be given by

$$V_1 = V_o - \frac{2V_o k_2}{\pi(k_1+k_2)} \int_0^\infty e^{-\lambda z}(\sin \lambda r_1) J_o(\lambda r)\frac{d\lambda}{\lambda}$$

The contact temperature $V_1(0)$ is found to be given by

$$V_1(0) = \frac{V_o k_1}{k_1 + k_2} \qquad (1)$$

and is seen to be independent of the radius of contact and uniform over the contact area.

The quantity of heat Q, passing from one region to the other is given by

$$Q = \frac{4k_1 k_2 V_o r_1}{k_1 + k_2} \qquad (2)$$

which varies linearly with the radius of contact.

R, the total resistance of the constriction is given by

$$R = \frac{V_o}{Q} = \frac{k_1 + k_2}{4k_1k_2r_1} \qquad (3)$$

which is the expression obtained by regarding it as the sum of the constructional resistances $\frac{1}{4k_1r_1}$ and $\frac{1}{4k_2r_1}$ in series.

Now although in the above treatment the sphere of the comparator was treated as semi-infinite, it does contain a finite amount of heat, and, regarding the sphere as a capacitor containing heat, gives

$$\rho c\Omega \frac{dV}{dt} + \frac{V}{R} = 0 \qquad (4)$$

where V is the average temperature of the sphere, of density ρ, specific heat c and volume Ω.

For such a capacitor

$$V = V_o e^{-\frac{4k_1k_2r_1t}{(k_1+k_2)\rho c\Omega}}$$

and the cooling rate

$$\frac{dV}{dt} = -\frac{4k_1k_2V_or_1}{(k_1+k_2)\rho c\Omega} e^{-\frac{4k_1k_2r_1t}{(k_1+k_2)\rho c\Omega}}$$

When r_1 and t are small, say 10 seconds,

$$\frac{dV}{dt} = -\frac{4k_1k_2V_or_1}{(k_1+k_2)\rho c\Omega} \qquad (5)$$

Consideration of the transient term

In the case of good thermal conductors the transient term is known to have a smaller influence, so it will only be considered for poor conductors. Now equation (1) shows that when k_2 is small the contact temperature differs but little from the sphere temperature whilst equation (2) reduces to

$$Q = 4k_2V_or_1 \qquad (6)$$

Henc any temperature gradients in the sphere may be neglected and, as an approximation the circular source of heat at temperature V_o can be replaced by a hemi-spherical source of heat of radius r_1. The heat flow will then be radial and the temperature will satisfy the equation

$$\frac{1}{K_2}\frac{\partial V}{\partial t} = \frac{\partial^2 V}{\partial r^2} + \frac{2}{r}\frac{\partial V}{\partial r}$$

where $K_2 = k_2/\rho_2 c_2$, the thermal diffusivity.

Under these conditions the heat flow Q is given by

$$Q = 2\pi V_o r_1 k_2 \left\{1 + r_1\sqrt{\frac{\pi c}{\pi k_2 t}}\right\} \qquad (7)$$

in which the steady state term, $2\pi V_o r_1 k_2$, differs only from equation (6) in the numerical coefficient.

By evaluating equation (7) with t = 10 seconds, the transient term is found to amount to 3 per cent of the steady state term for glass and to 6 per cent for ebonite.

This approximate analysis confirms that the effect of the transient term can normally be neglected and the thermal comparator can virtually be accepted as a steady state device.

Similar conclusions have been reached by Dahl and Jones[12] and by Ginnings[13].

Consideration of the influence of an interfacial resistance

Unless the purpose is to study the properties of a surface deposit any test surfaces will be as clean as possible, but, since most metals acquire an oxide layer of up to 100 Å thick shortly after cleaning, the influence of such a film should be considered. If 'a' is the thickness of the film, it will be small compared with r_1. Also the thermal conductivity k_3 of an oxide film will usually be less than k_2 so that any spreading of the heat flux along the film can be neglected. Under these conditions

$$Q_F = \frac{k_3 \pi r_1^2 V}{a}$$

where V is the temperature drop across the film.

Thus the thermal resistance of the film becomes

$$\frac{V}{Q_F} = \frac{a}{k_3 \pi r_1^2}$$

and the effect of the film is to increase the total resistance R_T to

$$R_T = \frac{1}{4k_1 r_1} + \frac{1}{4k_2 r_1} + \frac{a}{\pi k_3 r_1^2} \qquad (8)$$

This modifies the heat flow Q to

$$Q_F = \frac{4k_1 k_2 V_o r_1}{k_1 + k_2 + \frac{4k_1 k_2 a}{\pi k_3 r_1}} \qquad (9)$$

which reduces to equation (2) when a = 0.

The effect of most normal films is small, but, if Q and Q_F are determined from comparator measurements made without and with a film which is sufficiently thick to modify the heat flow whilst still obeying the above restrictions, then

$$Q - Q_F = \frac{16k_1^2k_2^2aV_or_1}{(k_1+k_2)^2\pi k_3r_1 + 4k_1k_2a(k_1+k_2)} \qquad (10)$$

The evaluation of r_1 from the comparator measurements is discussed later, so equation (10) offers a possibility of determining either 'a' or k_3 when the other is known.

The loads would need to be sufficiently small that the film is not damaged. Also, as shown later, such measurements would need to be conducted under vacuum conditions to avoid complications arising from the air conduction component.

Such tests have not yet been attempted, but the method is mentioned as offering a possible method of approach to what could be a very difficult problem, the determination of k_3.

Comparison of theory of heat flow through a solid constriction with experiment

In Figure 12, the cooling rate as given by equation (5), using the known values for the excess temperature and the volume and properties of the phosphor bronze sphere and assuming values of 0.003, 0.004 and 0.005 cm can be compared with the comparator readings of Figure 3 for a range of values of k_2.

For high values of k_2 the theoretical curve is of similar shape and corresponds with the experimental curve when r_1 has a

value of 0.0046 cm. Deviations can be expected since the single thermocouple does not necessarily measure the average temperature of the sphere.

For low values of k_2 the departures are much greater and the curves no longer approximate to the same shape. These differences are greater than would seem likely to result from ignoring the transient term.

Figure 13 shows a similar comparison made for results obtained under different conditions for the series of metal discs (See Figure 4).

An attempt was made to calculate the likely effect of the air conduction component and the corrections needed to allow for this are indicated in Figures 12 and 13. The thermal comparator reading is seen to have been considerably augmented by this component. When testing aluminium it amounts to some 14 per cent and for high alloy steel to some 61 per cent. Measurements have since been made inside an enclosure that could be evacuated and an experimental determination made of the air conduction component. Some preliminary results obtained are included in Figures 12 and 13. They are seen to confirm that the air component is often a major factor.

Remembering that the comparator determinations reproduced in Figure 13 gave the straight line of Figure 4 when the comparator reading was plotted against the square root of the thermal conductivity, this result and the change of slope of Figure 3 would now seem to have arisen rather fortuitously from a complex combination of different factors.

The air conduction component will have caused the foregoing values of r_1 to be too large. It is also believed to be largely responsible for the high rate at which the critical size increases with decrease in thermal conductivity.

The thermal comparator used for thermal conductivity determinations on liquids and on powders

The two-ball thermal comparator has been found suitable for comparative tests on liquids. By retaining the test liquid in a shallow glass dish and tautly stretching a thin plastic membrane over the rim so that the liquid is in contact with the underside of the membrane, the thermal comparator, at a known excess temperature can be applied to the upper surface of the membrane and the test conducted in the normal way.

Figure 14 shows the results of such measurements made on liquids of known thermal conductivity[14]. The departure from a smooth curve is relatively small, and suggests that this simple method yields values that can be relied on to about 5 per cent. This is sufficient for most practical purposes, and, in fact compares well with that of many earlier so called absolute determinations.

When a similar procedure of working through a diaphragm was tried for measurements on powders and other soft materials the results proved less reproducible, presumably due to the intervening air film. However, the foregoing analysis had suggested that an alternative method might be applied to powders and some preliminary results shown in Figure 15 indicate that this is quite promising and worthy of further attention.

On the basis of equation 7, the heat flow Q from a hemisphere when embedded in a medium of low thermal conductivity is seen to be approximately proportional to the thermal conductivity of the medium. A thermal comparator was therefore used in which two tungsten carbide spheres of 1 cm diameter were each half embedded in the block of balsa wood and were sufficiently far apart for one of the exposed half-spheres to be buried in the cooler test powder whilst the other remained in air. The differential cooling 10 seconds afterwards was observed in the usual way for a constant initial temperature excess and is plotted in Figure 15 against the known thermal conductivities of the various powders tested. The points are seen to conform fairly well to a straight line which cuts the zero ordinate at about the thermal conductivity of air.

A similar method was later tried for liquids, but was not so successful. One sphere was embedded in the retaining block of thermal insulation and the other half exposed. The lower surface of the block was coated with a waterproof cement and the idea was simply to float the block on the surface of the liquid and observe the initial cooling of the half submerged sphere. A method of this type would probably be applied to oils and other liquids of low vapour pressure, but unduly high readings were obtained for carbon tetrachloride and other liquids of high vapour pressure. This could no doubt be attributed to lowering of the temperature of the liquid by evaporation. Incidentally this is a source of trouble which would be minimized in the method previously used by the covering of plastic sheeting.

A more responsive, direct reading form of thermal comparator.

The two-ball form of the thermal comparator has been shown to have gone a long way towards reducing the difficult and costly measurement of thermal conductivity to a simple and relatively inexpensive test. Indeed, it has been the means of promoting the property of thermal conductivity to join the relatively few properties of use to the non-destructive test technician[6,15]. A disadvantage of the present method as a non-destructive routine test is the need for the twofold measurement of time and emf; also a test of only 10 seconds duration is unduly long. This last criticism becomes aptly true when applications at high temperature are considered[12]. Radiation transfer is then likely to assume complicating proportions and is best reduced by a reduction of the test time.

Now the foregoing analysis has shown that the contact temperature, V_c is quickly established, and, according to equation (1) is a function of the thermal conductivity of the test material:- $V_c = V_o k_1/(k_1+k_2)$. This suggested that a thermal comparator based on the measurement of the contact temperature would be likely to give the required improved performance.

Clark, when working at the NPL, had made some preliminary observations of the contact temperature by means of the experiment indicated in Figure 16. In this experiment the phosphor-bronze sphere and the nickel surface with which it made contact formed the two elements of a phosphor-bronze and nickel thermocouple. When calibrated by insertion in an enclosure

maintained at various known temperatures, 16.9 μV was found to be equivalent to 1 degC over the working range. Figure 17 shows a plot of the observed contact temperature against time for an initial excess temperature of 43°C. The observed value was in reasonable agreement with the value predicted from equation (1). Furthermore the rate of change of V_c of about 1 degC in 10 sec is sufficiently small for the contact temperature to be regarded as relatively constant for the first few seconds.

The experiment was then repeated under similar conditions and dV/dt determined in the normal way. Equation (5) can be written as

$$r_1 = \frac{\rho c \frac{dV}{dt}}{4k_2 \frac{V_o k_1}{k_1 + k_2}} = \frac{\rho c \frac{dV}{dt}}{4k_2 V_c} \qquad (11)$$

For loads ranging from 93 to 360 g on the contacting sphere the values of r_1 determined in this way ranged from 0.0061 to 0.0082 cm, yet the experimentally measured value of V_c proved to be independent of load, as required by equation (1).

These measurements had confirmed the suitability of a method based on the measurement of V_c. It would be quick, the required reading would change relatively slowly with time and should be independent of load and surface roughness. All very desirable attributes.

The problem is to measure V_c in the general case, for, when the test sample becomes the main variable, it can no longer serve

as one of the thermoelements, and the thermocouple must form an integral part of the applied probe.

Figure 18 shows a diagrammatic representation of a form that has been partially successful. Two differentially connected thermocouples are shown attached to a suitable metal probe in such a way that the resultant emf, ΔV, is a function of $V_o - V_c$, that is

$$\Delta V = fV_o k_2/(k_1 + k_2) \qquad (12)$$

Some guidance in the choice of probe materials can be gained from Figure 19 which shows curves of k_2 plotted against $k_2/(k_1+k_2)$, a quantity proportional to the theoretical reading of the differentially connected thermocouples for values of the probe conductivity of 4.0, 1.0 and 0.25 J cm/cm^{2}sec degC. It is clear that for best sensitivity when testing materials of high thermal conductivity, the probe material should also be of high conductivity. On the other hand a probe of lower thermal conductivity, such as constantan ($k_1 = 0.25$) is preferable for tests on materials of low conductivity, for instance glass and many semiconductors. To measure V_c by the introduction of a second metal is proving difficult owing to the smallness of the contact area. When the actual thermo-junction is located a little away from the surface it does not conform to equation (1). Also its reading is dependent on load and surface finish. However, although the ideal form is proving elusive, some quite useful direct-reading forms have been produced. Two are shown in Figures 20 and 21. Both these probes are of constantan. One

is of the conical form already shown, with a fine insulated chromel wire threaded through a small axial hole. A slightly oversize bead was formed on the end of the chromel wire by an electric arc, and this bead was discharge welded to the constantan (Figure 20a), and the excess metal of the bead ground off whilst retaining a curved surface on which contact is to be made (Figure 20b). The chromel-constantan junction is clearly slightly removed from the point of contact. Thus unit mounted in a block of balsa wood is the comparator used for most of the measurements detailed in the next section.

The other probe has the chromel wire peened in a hole drilled normally in a small projecting cylinder of the main constantan probe and the excess metal again ground away (Figure 20c). With this design the junction can be formed closer to the point of contact, but the presence of the connecting wire makes it difficult to produce the required spherical contour and the reading is sensitive to load and small changes of aspect. A photograph of this form, before being mounted in balsa wood, is shown in Figure 21.

Thermal conductivity determinations with a direct-reading form of the thermal comparator

The two types just described have been used for measurements on several samples of known thermal conductivity. The thermal comparators were heated in a temperature-controlled oven to an excess temperature of about 53°C and then placed on the samples at room temperature. For materials of high thermal

conductivity, a definite steady reading was established almost as soon as contact was made, but with poor conductors the reading was slightly time dependent, since the initial reading was followed by a small drift to a lower value. The drift becomes increasingly apparent as the thermal conductivity decreases and is probably associated with the transient term.

The reproductions from the recorder traces shown in Figure 22 illustrate the nature of the reading and its dependence on time or the thermal conductivity of the test sample. In general, however, the measurements have been made on a vernier potentiometer. By taking successive readings, the setting of the potentiometer can soon be set to give no deflection, or a small change of a microvolt or two, on contact being made. We have usually attempted to obtain this reading within a second or so of contact, but so long as a standard procedure is adopted any uncertainty arising from the small drift should be taken care of in the calibration. A merit of this new form of comparator is that it has a large heat capacity and five or six applications, each lasting a few seconds, can be made before the reading starts to change by more than a microvolt or so. When contact with the test specimen is broken the reading quickly returns to zero.

Figures 23 and 24 show some results obtained by these two types of probe. Thermal conductivity is plotted against the comparator reading and both sets of curves are seen to be of the general form predicted in Figure 19. The conditions of test were

closely similar and the form with the thermojunction located in the small projection is seen to have given appreciably higher readings (Figure 23), but the reproducibility was not so good particularly for tests on good conducting metals. The effective chromel-constantan junction would seem to be closer to the point of contact in this form, but the actual point of contact is probably less definite owing to its nonspherical shape. The readings of both forms are dependent on the surface finish of the test sample and on the load.

Work is continuing in the hope of producing a form of comparator still less dependent on these variables. Several examples of measurements made with the less sensitive form of Figure 20 can however be quoted, and these indicate that for many purposes a reasonably acceptable device is already available.

Plotting the reading against the thermal conductivity yields a curve. This is rather less satisfactory than the linear relationship often obtained with the two-ball comparator and requires calibration with rather more samples of known conductivity or for the conductivities of test and standard to be fairly close together.

Measurements on some ceramic materials

The readings obtained with this comparator on materials of known thermal conductivity are plotted as ringed points in Figure 24 and show a scatter from the mean curve comparable with that of the original two-ball comparator. The main departure

occurs for a sample of boron nitride. Two 1/2 inch diameter rods of this material had been included of density 2.14 g/ml, the axis of one being parallel to the direction of pressing and that of the other perpendicular to this direction. Thermal conductivity measurements made by a conventional longitudinal heat flow method had confirmed the thermal conductivity measured with the pressing direction perpendicular to the direction of heat flow to be greater by some 75 per cent. This is the sample for which the thermal comparator reading is displaced from the curve. Further work is however necessary, both to test the homogeneity of this particular sample, and to assess the performance of the comparator method on other anisotropic materials. The question of homogeneity could arise since the comparator measurements were made on one end of the rod, whilst the conventional method was applied to a mid section.

This figure also contains the results of measurements made on a few samples of unknown thermal conductivity. These are shown by crosses and mainly relate to refractory ceramic materials for which no estimate of the thermal conductivity could be made from any other property such as electrical resistivity.

Table 2 contains the values of their thermal conductivities as read from the curve of Figure 24, the degree of reproducibility of successive readings made at various points on the surface of each sample can be judged from the range indicated for the readings. The larger variations found for the unbaked steatite and the low density silicon nitride are consistent with the non-homogeneity of these materials.

Table 2

Thermal conductivity values (Jcm/cm^{2}sec degC) at about 30°C as determined by the modified thermal comparator and derived from Figure 24

Material	Reading (μV)			Thermal conductivity
	Number	Mean	Range	
Steatite, baked	4	193	3	0.032
Steatite, unbaked (Soapstone)	5	299	6	0.233
Magnesium-aluminium silicate	3	166	1	0.018
Silicon carbide Δ = 2.36 g/ml	3	333	3	0.69
Silicon nitride Δ = 3.16 g/ml	3	285	1	0.185
Silicon nitride Δ = 2.34 g/ml	5	225	10	0.050

Measurements on glasses and fused silica

The materials in Figure 24 marked A, C, F and H are fused silica and some of the glasses previously described and tested in connection with the earlier form of the comparator.

The results obtained with the direct reading comparator are reproduced more clearly in Figure 25, and should be compared with those of Figure 5. A greater degree of sensitivity will be noted, since the present readings are about three times larger. The differences between the derived thermal conductivities and those given by the conventional method are about the same as in the two figures. Glass G again shows a departure of about -4 per cent, whilst the others all agree to within 2 per cent. The accuracy appears to compare well with that of the conventional method.

These highly satisfactory results are in part due to the ease with which the comparator could be applied in a reproducible manner on the 3-inch diameter discs and in part due to the consistency of their surface finish. With smaller samples difficulty can arise in ensuring that the three contact points, the probe and the two studs, rest on coplanar surfaces. This, however, is not a major difficulty, but rather an essential requirement of the method. The question of surface finish is more likely to give trouble.

The results for the glasses are indicative of the order of accuracy obtainable for good specimens of materials of the same class, but it can often happen that a test is required to judge the degree of consistency of a particular product, or to study the effect of small compositional changes. In such cases the surface finish resulting from a standard method of preparation is not likely to vary, and, if good, differences of 2 per cent and more in the thermal conductivity should be apparent when tested by this method.

Measurements on some semiconductors

The final series of measurements includes samples of several semiconducting materials of various shapes and sizes. For this series of tests the same comparator was used, but the load had been increased to ensure greater stability. The calibration and test results are given in Figure 26 and Table 3. The largest face of each test material had been ground flat by a standard procedure, but the presence of small holes in some materials and small cracks in others precluded a truly smooth surface being obtained in all cases.

Table 3

Thermal conductivities of samples of semiconducting materials as indicated by measurements with the modified thermal comparator

Material		Approximate dimensions (inches)			Description of surface	Comparator Readings (μV)			Thermal conductivity (Jcm/cm^{2}sec degC)	
No.	Name	Test surface Length	Test surface Breadth	Thickness		Number	Mean	Range	Derived from Curve of Fig. 26	Reported elsewhere
1	$AgInSe_2$	½	½	½	Good: few fine cracks	4	98	1	0.005	-
2	$AgInTe_2$	½	3/8	½	Good	4	130	1	0.010_5	0.0079[a]; 0.012[b]; 0.04544[c]
3	Bi_2Te_3 (single crystal)	¼	1	3/8	Good (ground face)	6	149	4	0.015	0.006-0.024[d]; 0.030-0.036[e]; 0.016[f]; 0.016[g]
	"	3/8	1	¼	Good (shiny unground perpendicular to above)	6	138	5	0.012_5	0.020[h] (also values as low as (d) and as high as (e))
	"	¼	1	3/8	Good (unground, opp. ground)	4	149	2	0.015	
	"	3/8	¼	1	Good (unground end face)	8	128	4	0.010	
4	CdTe	½	5/16	3/8	Good	4	245	5	0.108	0.055[i]
	"	½	3/8	5/16	Rough ground, flat, (perpendicular to above)	4	221	5	$> 0.069_5$	
5	$CuAlTe_2$	3/4	½	½	Good with few cracks and voids	4	192	6	0.032_5	
6	$CuInSe_2$	5/8	½	½	Good with few cracks and very small voids	4	202	4	0.043	0.037[b]
7	$CuInTe_2$	1	1	½	Good, but with lots of very tiny holes - clearly a porous sample	4	212	3	0.057	0.049[b]; 0.06098[c]; 0.07395[c]
8	CuFeSnTe	½	1¼	¼	Fair: many voids and striations	8	214	8	0.059	0.029-0.036[a]
9	Hg_3CdSe_4	3/4	5/8	¼	Good, but few pits (probably crystals torn from surface. Not voids indicating porosity)	8	114	5	0.007_5	0.0125[a]
10	Hg_2TeSe	5/8	5/16	5/16	Good	4	159	2	0.018	0.018[a]
11	PbTe	5/16 diameter		11/16	Good (end face of cast rod)	4	163	4	0.019_5	0.015[g]; 0.016[g]; 0.019[f]; 0.020_5[j]; 0.019-0.031[k]; 0.033-0.040[l]
12	$ZnSnAs_2$	½	7/16	½	Good, but with lots of tiny holes (approaching condition of $CuInTe_2$)	4	229	7	0.081_5	-

(a) H. J. Goldsmid (Private communication)
(b) Radio Corporation of America value for lattice thermal conductivity[16]
(c) New York University value[17]
(d) H. J. Goldsmid[18]
(e) C. B. Satterthwaite & R. W. Ure, Jr[19]
(f) R. C. Miller & R. W. Ure[20], lattice thermal conductivity
(g) T. de la Perrelle[21]
(h) T. C. Harman, J. H. Cahn & M. J. Logan[22]
(i) R. P. Chasmar, E. W. Durham & A. D. Stuckes[23]
(j) A. D. Stuckes[24]
(k) R. R. Heikes[25]
(l) E. D. Devlatkova[26]

The requirement that calibrating and test materials should have comparable thermal conductivities, necessitated the use of materials of rather low conductivity as standards. Only two metals were used, a stainless steel and a titanium alloy. These were given the same surface preparation as the test samples but the glasses and the ceramic materials had been ground and lapped by a different technique. One of the latter, a soapstone and alumina ceramic, had a known thermal conductivity within about 1 per cent of that of the titanium alloy and it is of interest to note that the comparator readings obtained for these two very different materials agreed to within 2 μV in 230 μV. Also the two sets of measurements made on the sample of Bi_2Te_3 on equivalent ground and unground faces are in agreement. Another point studied in connection with these tests has been the effect of sample size. By good fortune Dr. A. J. Moulson of the British Ceramic Research Association had provided a disc measuring 0.5 inch thick x 2.5 inches diameter that had been formed from a mixture of diatomaceous earth with a suitable binding material. This disc had good smooth surfaces and proved to give consistent readings that were a little below the lowest reading obtained for the semiconductors and indicated that it had a thermal conductivity of 0.004_5 Jcm/cm^{2}sec degC. From this disc, samples of successively smaller size were cut and tested with the comparator. The results obtained for the same excess temperature of 33°C are given in Table 4.

Table 4

Effect of sample size on the reading of a comparator of the direct reading form, for a material of low thermal conductivity (about 0.0045 Jcm/cm^{2}sec degC)

Sample size (in inches)		Comparator reading		
Thickness	Surface dimensions	Number	Mean	Range
			μV	
5/8	2 1/2 diameter	8	94	4
5/8	2 1/2 " other face	8	94.5	5
5/8	1 1/2 x 1 1/2	8	94.5	4
5/8	1 x 1	9	94.5	5
3/8	1 x 1	7	94.5	2
3/8	3/4 x 3/4	10	94	4
3/8	1/2 x 1/2	8	93.5	3
3/16	1 x 1	4	94.5	2
3/16	3/4 x 3/4	7	94	4
3/16	1/2 x 1/2	8	91.5	5

No appreciable change in reading was obtained until the surface dimensions were reduced from a square of 3/4 inch side to one of 1/2 inch side, when for the 3/8 inch thickness the reading only decreased by about 1 μV, but for half this thickness the decrease was about 3 μV. It would seem that size-effect is not likely to cause any noticeable error with the specimens listed in Table 3. The lowest reading under the same test conditions was 98 μV for the sample of $AgInSe_2$, and although its test surface measured about 1/2 inch by 1/2 inch, its thickness was also 1/2 inch. The reading is not likely to be more than 1 μV low. The 1/4 inch x 1 inch Bi_2Te_3 is the only other sample of questionable size, but, as its conductivity is

two to three times that on which the size tests were made, any correction should again be quite small. The differences in the readings for the three directions studied can certainly be related to the anisotropy of this material.

When these critical sizes are compared with those given in Table 1 for the readings of the two-ball form of the thermal comparator after 10 seconds some striking differences are obtained. Extrapolation is necessary to lower thermal conductivities and from logarithmic plots a critical size of about 4 inch diameter by 0.175 inch thickness is indicated for a material of K_2 = 0.005 Jcm/cm^{2}sec degC. Quite large corrections for the size effect would have been required had the original comparator been used for determination on some of the present series of semiconductors. Thus these experiments have brought out another advantage of the modified form of the thermal comparator. It gives size-independent readings on smaller samples, certainly for low conductivity materials and probably for materials of high conductivity as well.

It only remains to consider the derived thermal conductivity values obtained for the semiconductors listed in Table 3.

The odd shapes and small sizes meant that in only a few instances would it be possible to check these results on the same materials by any conventional thermal conductivity measurements. No such measurements have been attempted. Also, some of the samples contained cracks and voids and the results would be expected to vary from sample to sample and to be below the value for a maximum density material.

It is necessary to state that the derived thermal conductivity values given in the penultimate column relate only to the particular sample tested.

The last column includes some values obtained by other workers. These are relatively few. Even so, they embrace a wide range, emphasizing either the possible variations in nominally the same material, or, the uncertainty of some thermal conductivity determinations. The degree of uncertainty that exists is perhaps more readily apparent from Figure 27 where the thermal conductivities as derived from Figure 26 are plotted against the values of other workers.

Since an increase in surface roughness tends to reduce the comparator reading and these surfaces tended to be rather rougher than the standard materials the values derived from the comparator might be expected to err on the low side. Of the nine materials included in Figure 27, only the value for the sample of Hg_3CdSe_4 however appears to be decidedly low, those of six samples are in the main in fair agreement, whilst those of the other two, CuFeSnTe and CdTe, are much higher than the other determinations. The thermal comparator readings for these two materials were confirmed by repeat readings taken subsequently and certainly imply very marked material differences or that the earlier investigators had obtained too low values. The present sample of CdTe was of highly crystalline appearance and might even be a single crystal, whilst the workers who obtained the lower value stated that their sample had the appearance of a

sintered material. The lower density of such a material can be accepted as a likely cause of the lower thermal conductivity.

In this connection attention might be drawn to a statement by Harman, Cahn and Logan[22] when presenting their measurements of thermal conductivity which utilized the Peltier effect and which were made on samples of Bi_2Te_3. "Measured thermal conductivity values have been as high as those reported by Satterthwaite and Ure and as low as those reported by Goldsmid. It is believed that these are real variations from ingot to ingot, which may be due to temperature, convecting stirring or mechanical variations during the recrystallization process."

There seems to be little doubt that the thermal conductivity of many semiconductors varies considerably from sample to sample, and that many of the differences evident in Table 3 and Figure 27 arise from this cause.

For the samples of the semiconductor materials for which no previous thermal conductivity values were located the thermal comparator measurements indicated the following values:- $AgInSe_2$ 0.005, $CuAlTe_2$ 0.032_5 and $ZnSnAs_2$ 0.081_5 Jcm/cm $sec^2 degC$. These values should be correct to within 10 per cent.

Further work proposed

The attempt to design a direct reading form of the thermal comparator that is less dependent on load and surface finish will be continued. Further work will also be directed to studies involving the use of the thermal comparator at temperatures other than normal. Given a suitable range of standards of known

thermal conductivity, the method should prove well suited for measurements at both low and high temperatures. As already indicated, the shortening of the test time that has resulted from the introduction of the direct reading form of the thermal comparator, should result in considerable less trouble from radiation when measurements at high temperature are attempted. The best form for measurements at high temperature will probably comprize two probes of platinum alloy, or other non oxidizable material, each similarly equipped with a thermojunction at or near the point of contact, these being connected differentially and the probes being so mounted that the loss of heat by radiation and conduction from each is small and approximately the same, whilst one probe can be brought into contact with the test material in the usual way. The differential emf at the time of contact should be a function of the thermal conductivity of the test material, whilst the design should minimize the influence of other factors on this reading.

Conclusions

An improved form of thermal comparator has been developed giving a direct reading within a very short time of contact being made, which has been shown to be a function of the thermal conductivity of the contacted material. The method has been applied to metals, refractory ceramics, glasses and to semiconductor materials comprising a wide range of thermal conductivities. For materials of not too high a thermal conductivy and when surfaces of comparable surface finish are available the method

allows thermal conductivities to be measured to an accuracy of two per cent or so, indeed to an accuracy that often compares well with the conventional methods.

At present the method is not independent of load and of surface finish and is likely to give too high values on soft materials and too low values on materials having a relatively poor surface finish.

The dependence of the reading on sample size has been shown to be much less than that of the two-ball form of the thermal comparator. This has allowed the method to be applied to a range of materials of moderately low conductivity and of small size.

The two main advantages of the present form over the two-ball thermal comparator are the shortening of the test time and the smaller size of test sample needed.

These advantages are likely to make the present form of the thermal comparator a much more suitable device for measurements at other than normal temperature in particular at high temperatures.

Whilst at present the direct reading form of the thermal comparator has only been used for tests on solid materials, the above advantages should also make it a more desirable form for thermal conductivity measurements on liquids. The reduction in time will allow less opportunity for convection currents to be set up, whilst the smaller sample will be more quickly brought to the required initial temperature and will be an asset for liquids only available in limited quantities.

In the particular instance of semiconductor materials it would appear that the thermal conductivity is often likely to vary from sample to sample. It is for just such materials that a test method is required which can readily be applied, initially to samples resulting from variations in the production technique, and subsequently to the material as produced by the optimum production method, rather than to a specially prepared test specimen. The direct reading thermal comparator method that has been described, with its simplicity, its speed and its adaptability to almost any specimen form, seems well suited for this purpose.

Acknowledgements

Acknowledgement is made to the able assistance given throughout this work by Mr. R. P. Tye, and to help at various stages by Miss Margaret J. Woodman, Mr. W. T. Clark, now at the AEI Research Laboratories, Aldermaston, Mr. B. W. Jolliffe and Mr. A. E. Langton.

The samples of the semiconductor materials listed in Table 3 were kindly supplied by Dr. H. J. Goldsmid of the GEC Hirst Research Centre, Wembley.

The work has formed part of the research programme of the Basic Physics Division of the National Physical Laboratory and this account is published by permission of the Director of the Laboratory.

References

1. R. W. Powell,
The thermal and electrical conductivities of beryllium.
Phil. Mag., 44, 645, 1953.

2. R. W. Powell and R. P. Tye,
Thermal conductivity measurements down to -190°C:
Iridium and Rhodium, Proc. of the 9th International
Congress of Refrigeration, 1, 2083, 1955.

3. R. W. Powell, Margaret J. Woodman and R. P. Tye,
The thermal conductivity and electrical resistivity of
indium, Phil. Mag. In press.

4. R. W. Powell, R. P. Tye and Margaret J. Woodman,
The thermal conductivity and electrical resistivity of
rhenium, J. Less-Common Metals. In press.

5. R. W. Powell,
Experiments using a simple thermal comparator for measurements of thermal conductivity, surface roughness and thickness of foils or of surface deposits. J. Sci. Instrum.,
34, 485, 1957.

6. R. W. Powell and R. P. Tye,
The thermal comparator in non-destructive testing.
"Techniques of non-destructive testing" p.175, Butterworths
Scientific Publications Co., 1960.

7. W. T. Clark,
"Investigation and applications of a simple thermal comparator, Project Report for Diploma of Technology in
Applied Physics, Brunel Technical College, Oct., 1959.

8. W. T. Clark and R. W. Powell,
"Measurements of thermal conduction by the thermal
comparator", J. Sci. Instrum. In press.

9. M. E. Barzelay, K. N. Tong and G. F. Holloway,
"Effect of pressure on thermal conductance of contact
joints", N.A.C.A., TN.3295, 1955.

10. G. F. C. Rogers,
Heat transfer at the interface of dissimilar metals,
Internal J. Heat and Mass Transfer, 2, 150, 1961.

11. G. A. Slack and C. Glasbrener,
The thermal conductivity of germanium from 3°K to 1020°K,
General Electric Research Laboratory, Memo Report No.
P-208, Nov., 1959.

12. A. I. Dahl and D. W. Jones,
Thermal-Conductivity studies with the Powell method.
A.S.M.E.-A.I.Ch.E. Heat Transfer Conference, Buffalo, NY,
Aug., 1960, Paper 60-HT-30.

13. D. C. Ginnings,
Powell comparator method for determining thermal conductivities. A discussion, "Progress in International Research on Thermodynamic and Transport Properties", p.474, A.S.M.E., Academic Press, NY, 1962.

14. A. R. Challoner and R. W. Powell,
Thermal conductivities of liquids: new determinations for seven liquids and appraisal of existing values, Proc. Roy. Soc., A.238, 90, 1956.

15. R. W. Powell,
Thermal conductivity and its contribution to materials examination, Materials Research, 1, 72, 1962.

16. J. W. Davisson and J. Posternak,
"Status report on thermoelectricity",
NRL Memorandum Report 1241, p.30, Jan., 1962.

17. J. W. Davisson and J. Posternak,
"Status report on thermoelectricity",
NRL Memorandum Report 1177, p.97, July, 1961.

18. H. J. Goldsmid,
The thermal conductivity of bismuth telluride,
Proc. Phys. Soc., B.69, 203, 1956.

19. C. B. Satterthwaite and R. W. Ure, Jr.,
Electrical and thermal properties of Bi_2Te_3,
Phys. Rev., 108, 1164, 1957.

20. R. C. Miller and R. W. Ure, Jr.,
"Thermoelectric generator materials", Scientific Paper 414 FR 801-P1 of 1st Aug., 1960 (Westinghouse Research Laboratories. See "Status report on thermoelectricity", NRL Memorandum Report 1177, p.138, July, 1961.

21. T. de la Perrelle,
Notes on a preliminary investigation of thermoelectric materials, and on the measurement of material properties and generator efficiency. Royal Aircraft Establishment (Farnborough) Technical Note No. RAD.804, Sept., 1961.

22. T. C. Harman, J. H. Cahn and M. J. Logan,
Measurement of thermal conductivity by utilization of the Peltier Effect. J. App. Phys., 30, (9), 1351, 1959.

23. R. P. Chasmar, E. W. Durham and A. D. Stuckes,
"The thermal and electrical properties of cadmium and mercury tellurides", Proceedings of the International Conference on Physics and Semiconductors, Prague 1960 (Prague Publishing House of Czechoslovak Academy of Sciences) p.1018, 1961.

24. A. D. Stuckes,
Measurement of thermal conductivity of semiconductors at high temperatures, British J. of Applied Physics 12, 675, 1961.

25. R. R. Heikes and R. W. Ure, Jr.,
"Thermoelectricity: Science and Engineering",
Interscience Publishers, p.411, 1960.

26. E. D. Deviatkova,
A study of the thermal conductivity of lead telluride,
Soviet Phys. Tech. Phys., 2, 414, 1957.

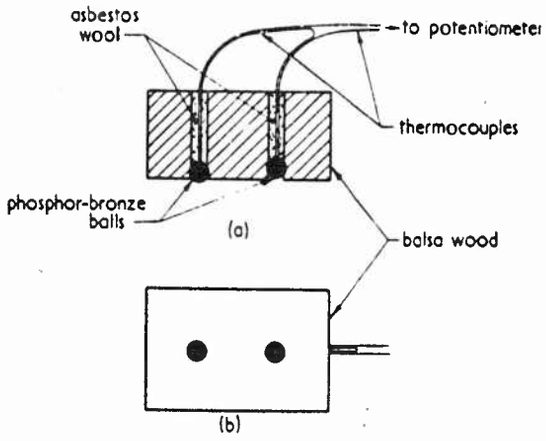

Fig. 1. Diagram of thermal comparator No. 1
(*a*) side view; (*b*) base view.

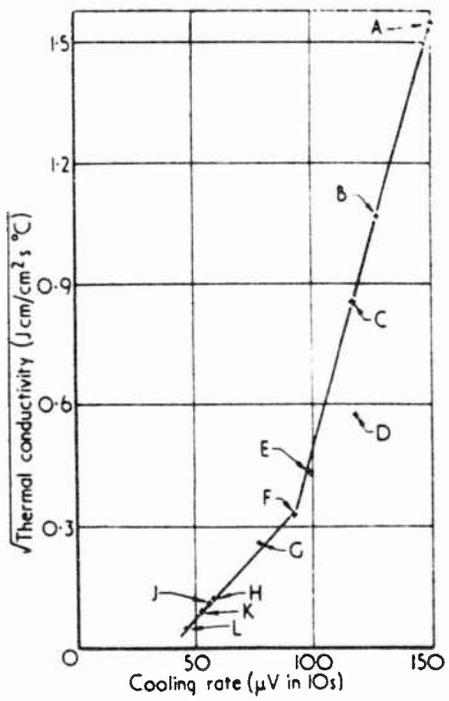

Fig. 3. Thermal comparator No. 5 loaded with 100 g weight. Initial rate of cooling plotted against the square root of the thermal conductivity

A, aluminium; *B*, brass; *C*, iron; *D*, lead; *E*, alumina; *F*, high alloy steel; *G*, quartz; *H*, silica; *J*, borosilicate glass; *K*, bonded mica; *L*, plasticized P.V.C.

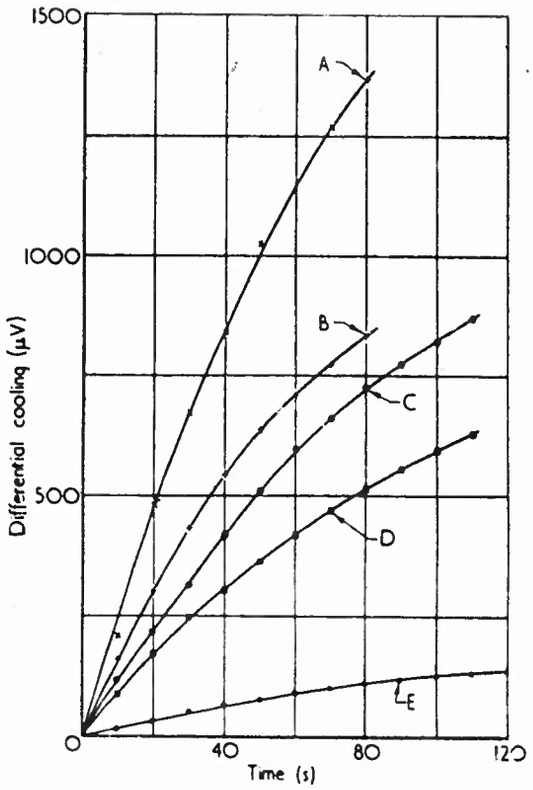

Fig. 2. Typical curves obtained from measurements with thermal comparator No. 1 applied to various materials and when freely cooling in air

A, aluminium; *B*, iron; *C*, alloy steel; *D*, high alloy steel; *E*, air.

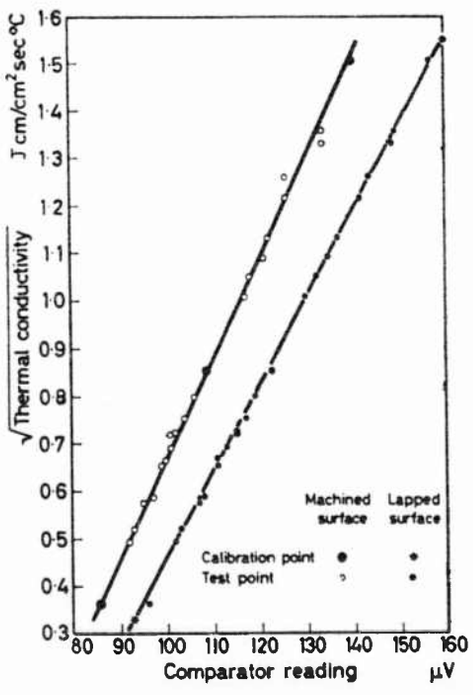

Figure 4. Use of thermal comparator for thermal conductivity determinations on alloy discs

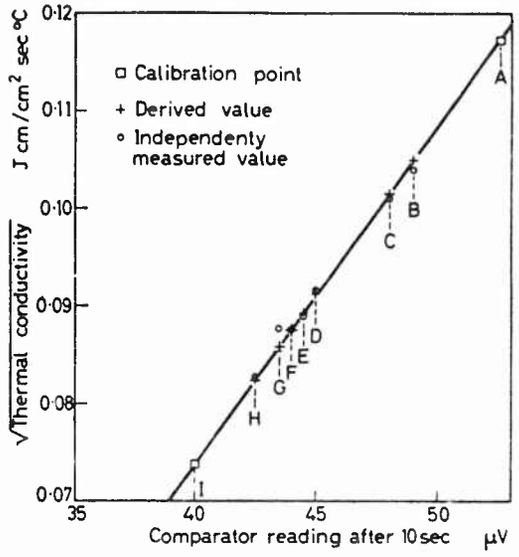

Sample	Composition %										
	SiO_2	K_2O	Na_2O	PbO	Sb_2O_3	As_2O_3	B_2O_3	Al_2O_3	ZnO	CaO	BaO
A	100	—	—	—	—	—	—	—	—	—	—
B	72·7	14·5	4·0	—	0·4	—	7·7	0·4	0·4	—	—
C	71·2	8·9	7·6	—	0·8	—	2·9	0·1	3·0	5·5	—
D	54·2	7·1	2·4	34·2	2·0	0·2	—	—	—	—	—
E	40·5	—	—	—	0·3	0·2	6·5	1·8	7·7	—	42·9
F	49·8	8·5	2·9	5·9	0·7	0·2	—	—	7·8	—	24·2
G	46·0	9·2	—	44·8	—	0·1	—	—	—	—	—
H	35·6	4·4	—	59·7	—	0·2	—	—	—	—	—
I	20·0	—	—	80·0	—	—	—	—	—	—	—

Figure 5. Use of thermal comparator for thermal conductivity determinations on glass discs

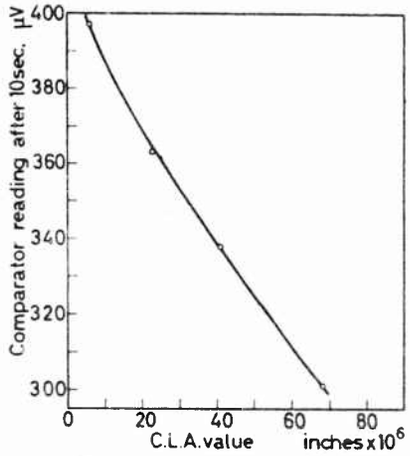

Fig. 6. Graph of thermal comparator reading against C.L.A. values of four samples of K9 cast steel (phosphor–bronze ball comparator $\frac{1}{4}$ inch in diameter)

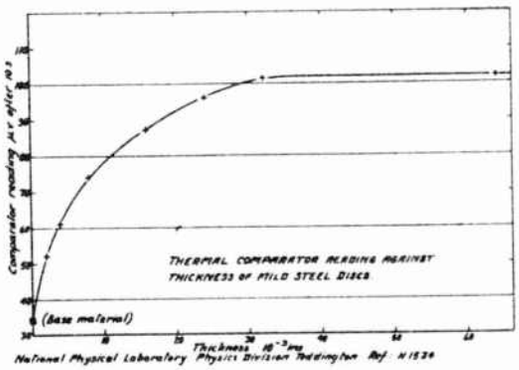

FIG. 7

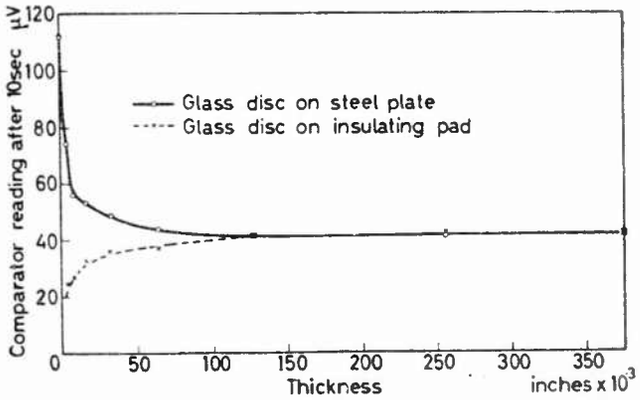

Figure 8 Thermal comparator reading against thickness for glass discs

FIG.9. THERMAL COMPARATOR MEASUREMENT ON SAMPLE OF ALUMINIUM ALLOY

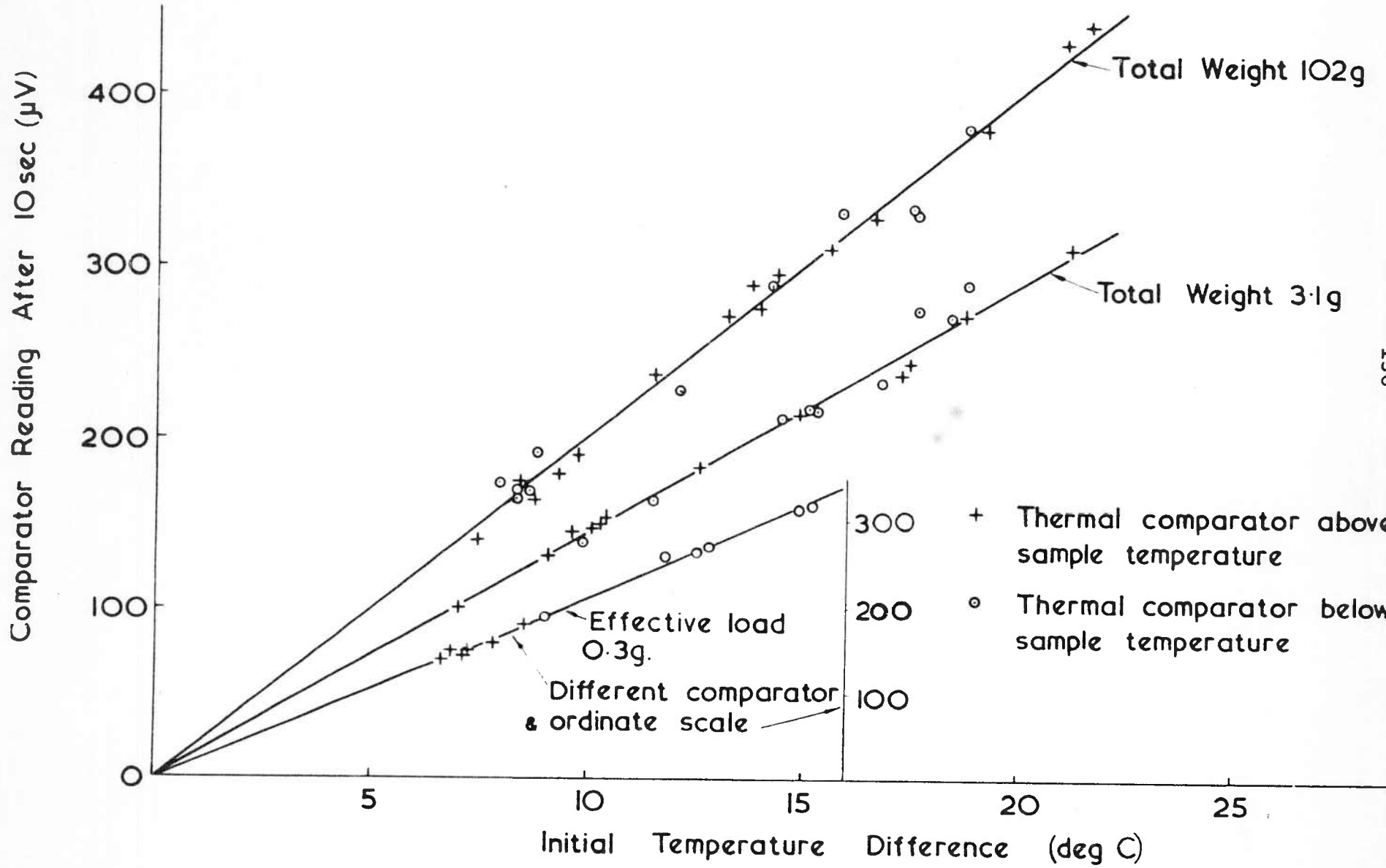

FIG. 10. THERMAL COMPARATOR MEASUREMENTS ON VARIOUS MATERIALS.

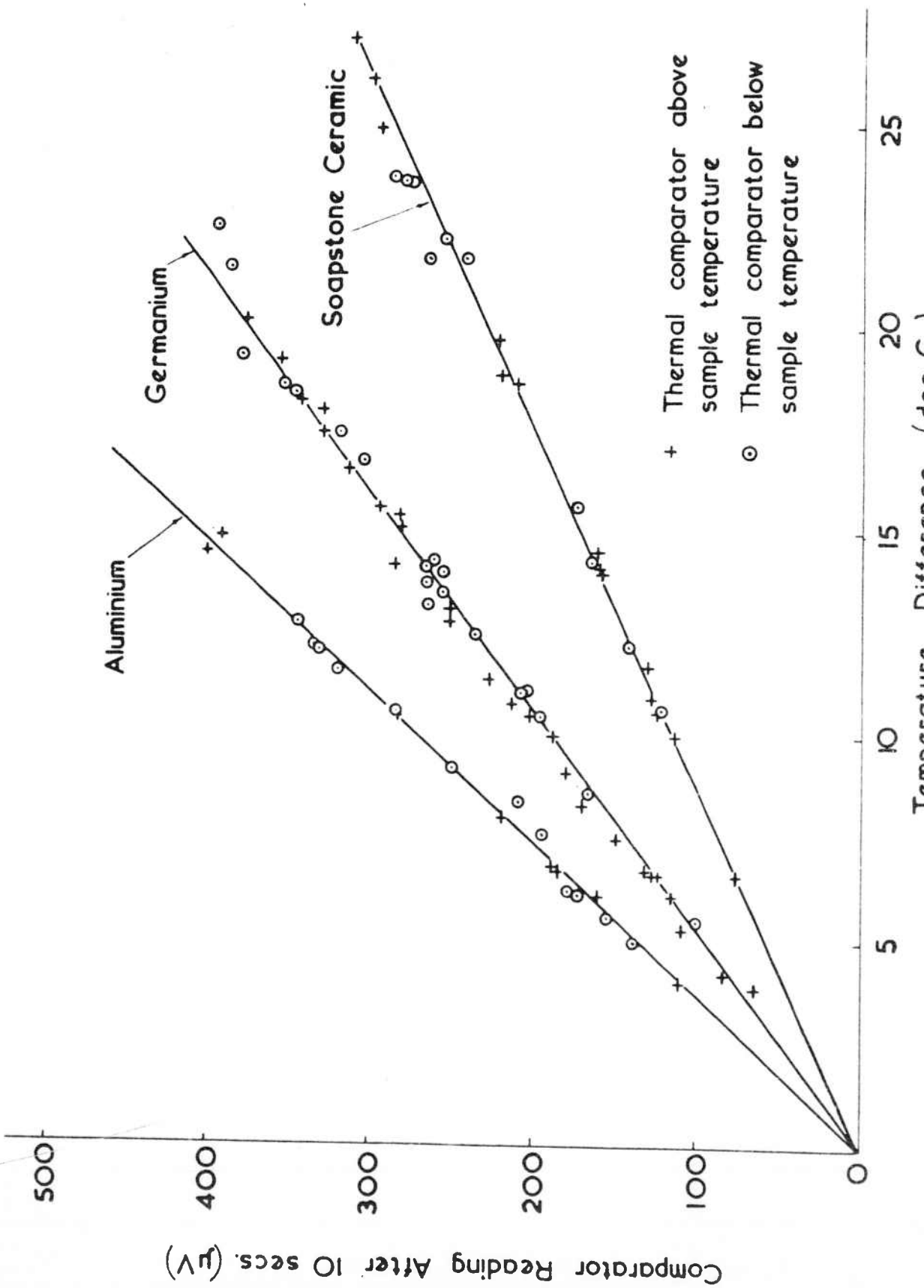

FIG. 11. THERMAL COMPARATOR READING AGAINST $\sqrt{K}$ TO ESTIMATE THE THERMAL CONDUCTIVITY OF GERMANIUM

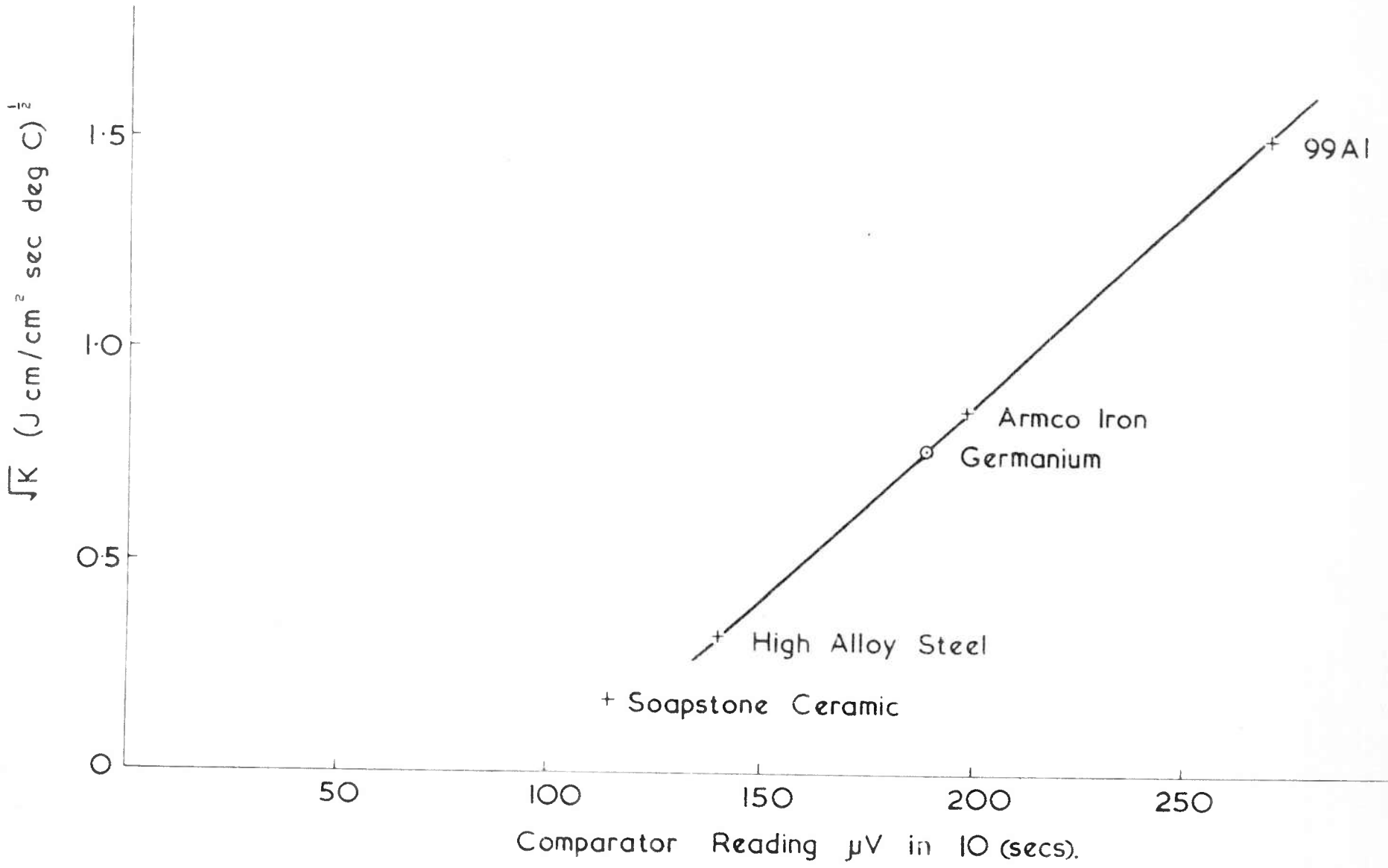

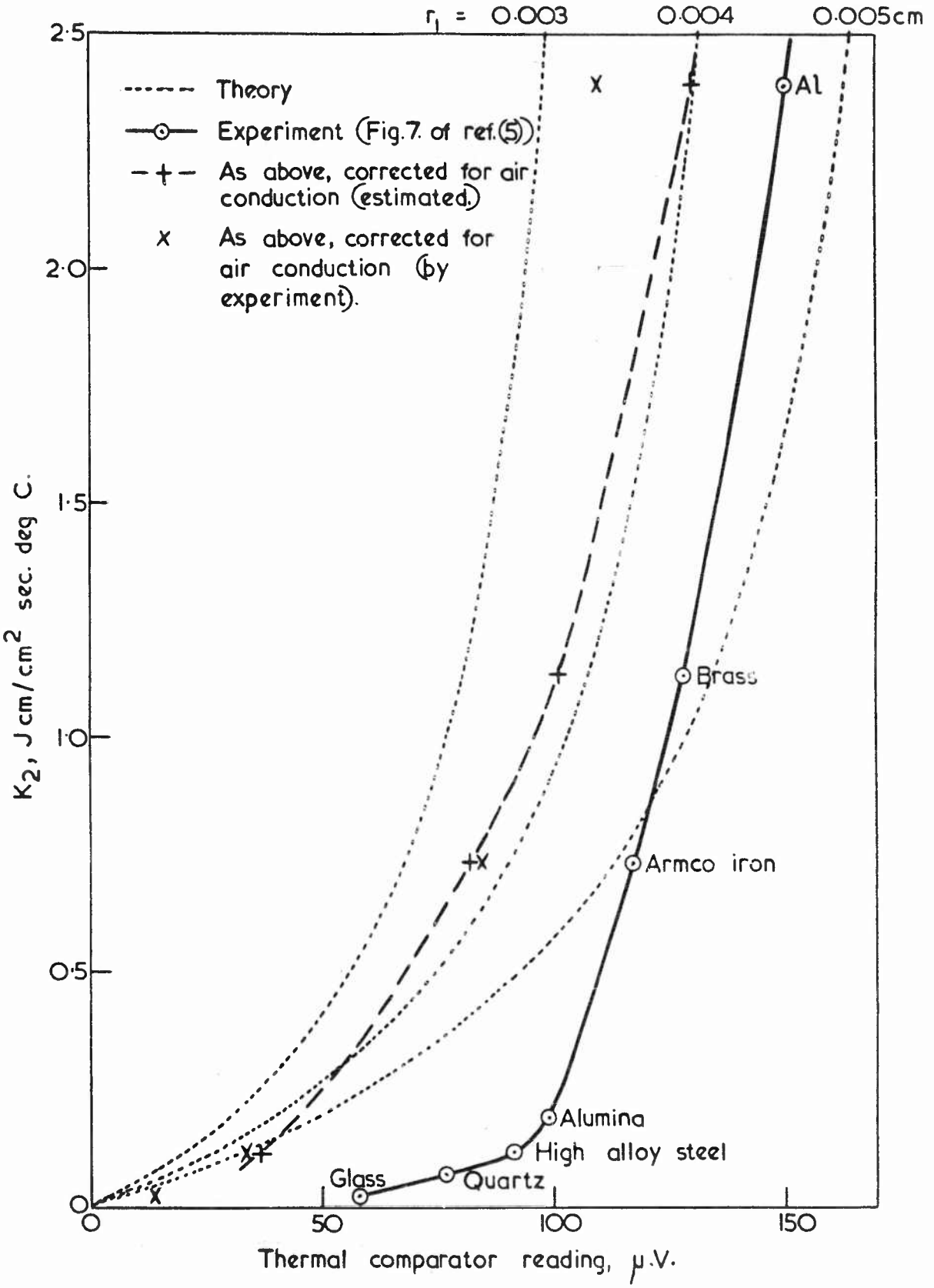

FIG. 12. COMPARISON OF THEORY WITH EXPERIMENT (FIG. 7. OF REF. (5))

FIG. 13. COMPARISON OF THEORY WITH EXPERIMENT (TABLE 3, POWELL (1957))

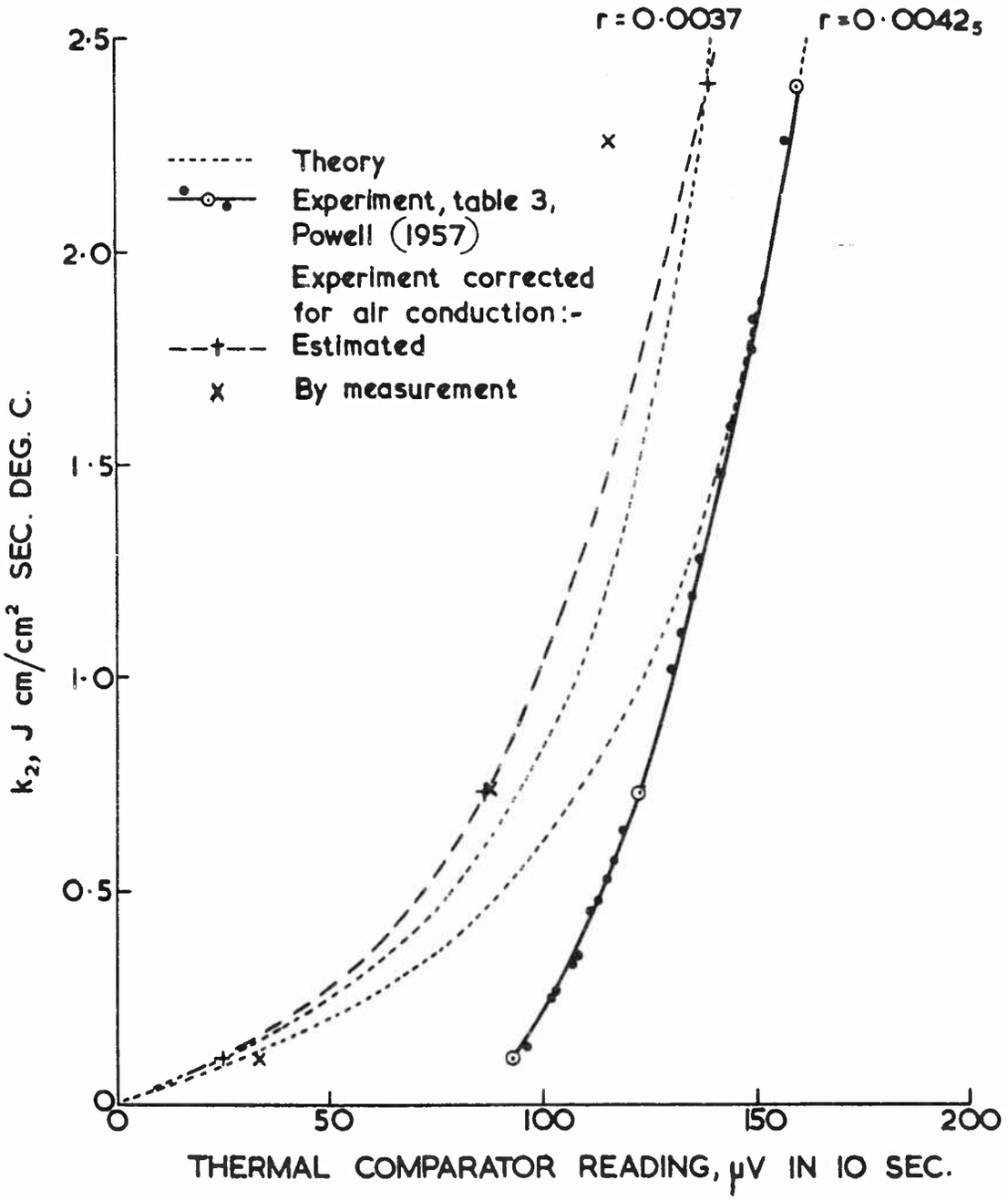

FIG. 14. THERMAL COMPARATOR METHOD APPLIED TO VARIOUS LIQUIDS OF KNOWN THERMAL CONDUCTIVITY

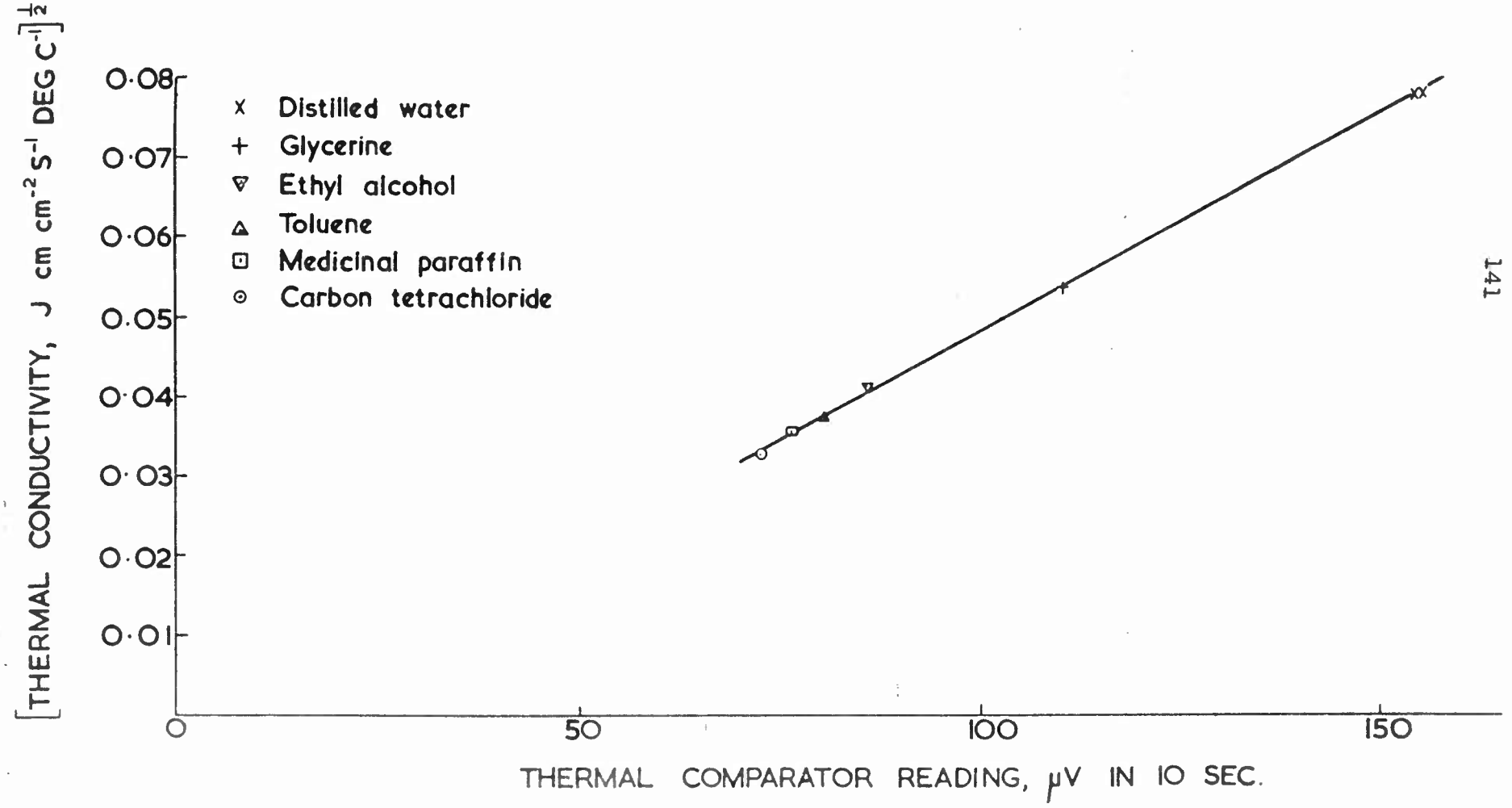

FIG 15 THERMAL COMPARATOR METHOD APPLIED TO POWDERS

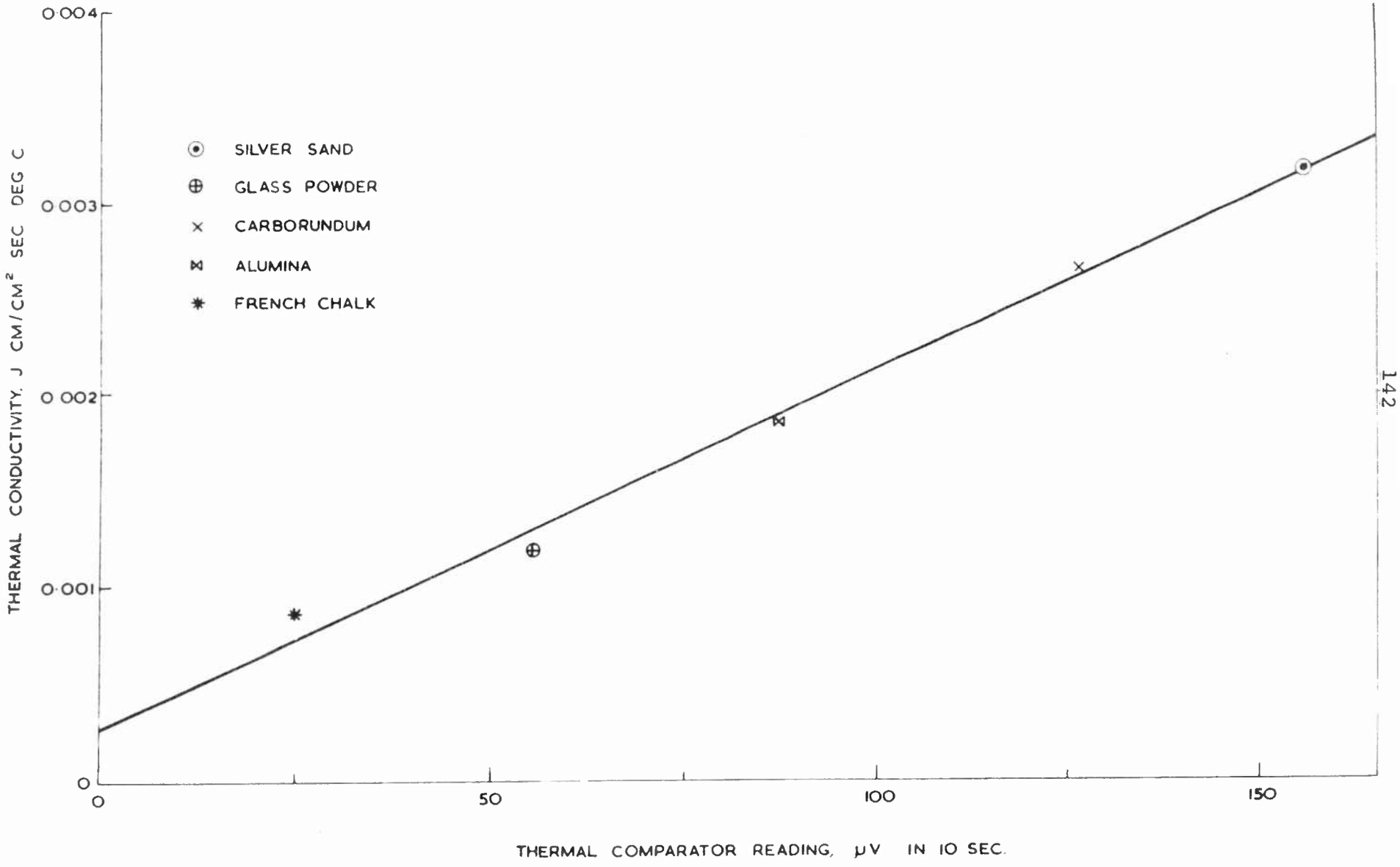

FIG. 16. EXPERIMENTAL ARRANGEMENT SHOWING CONTACT THERMOCOUPLE FOR MEASUREMENT OF Vc

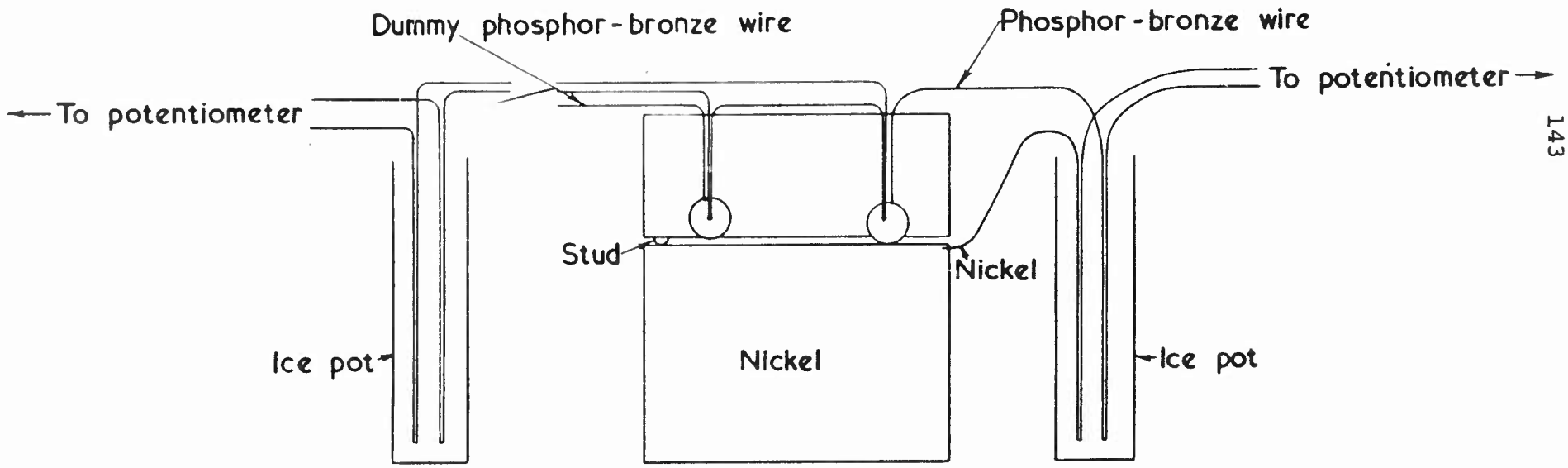

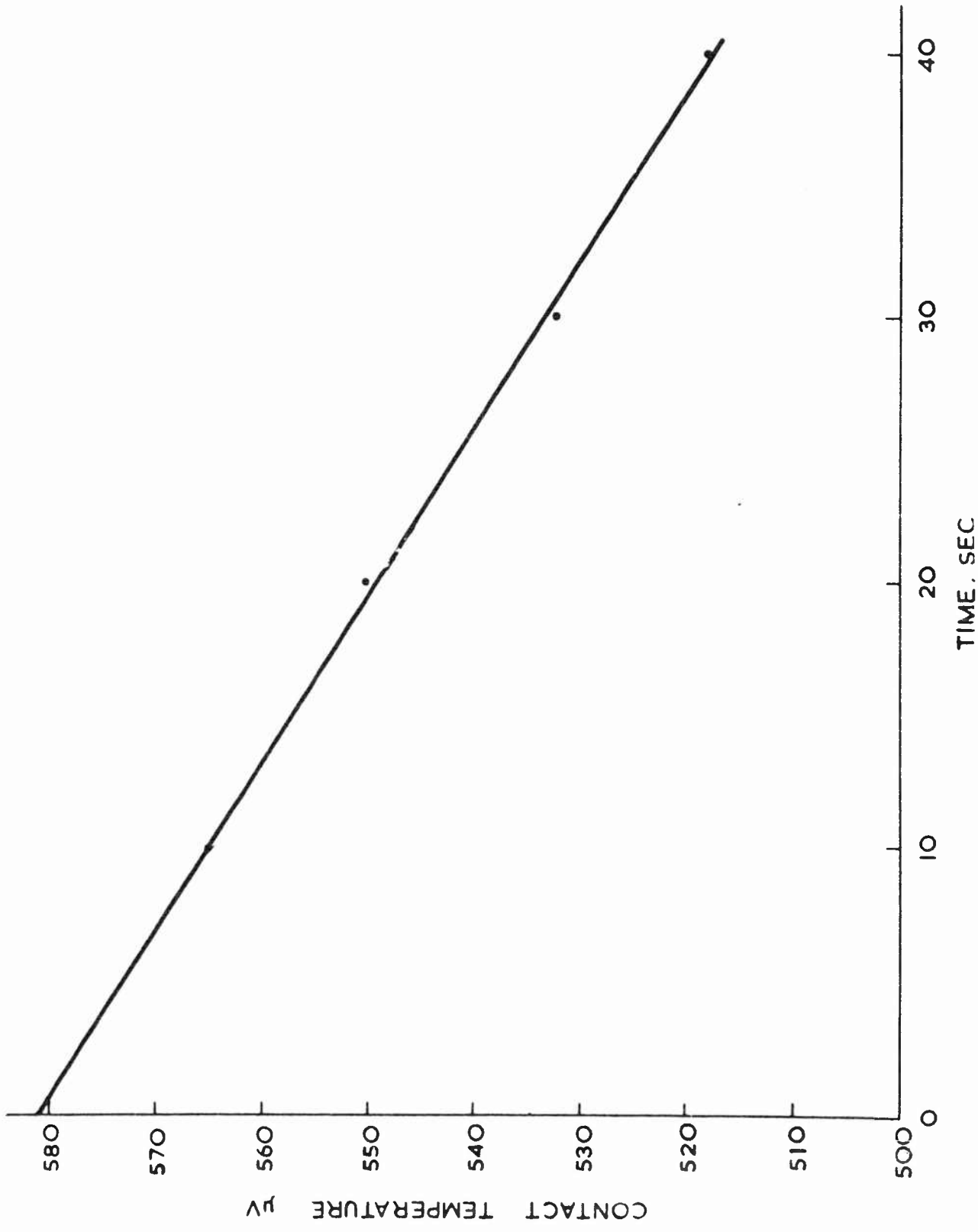

FIG.17. VARIATION OF CONTACT TEMPERATURE WITH TIME

FIG. 18. SUGGESTION FOR MODIFIED THERMAL COMPARATOR, GIVING DIRECT READING $\Delta V \propto k_2/(k_1 + k_2)$

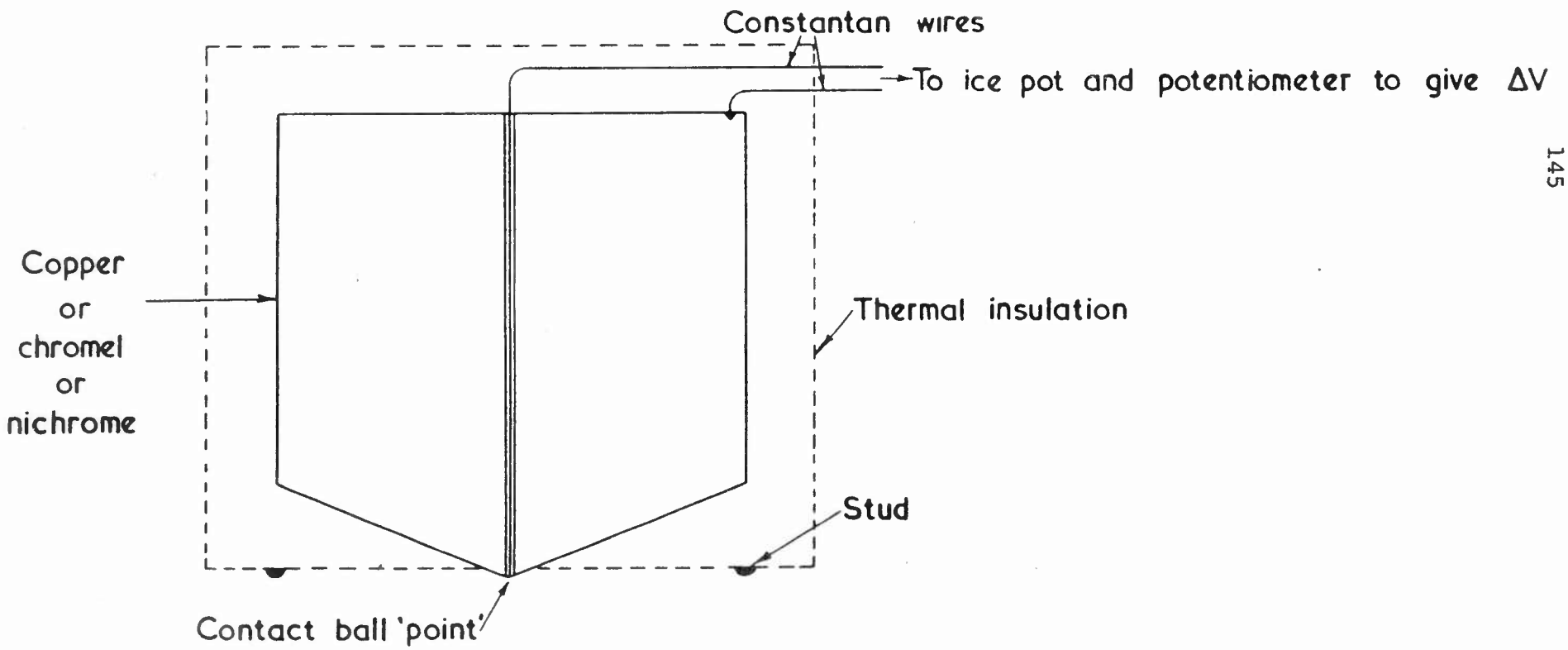

FIG.19. k_2 AS A FUNCTION OF $\frac{k_1}{k_1 + k_2}$

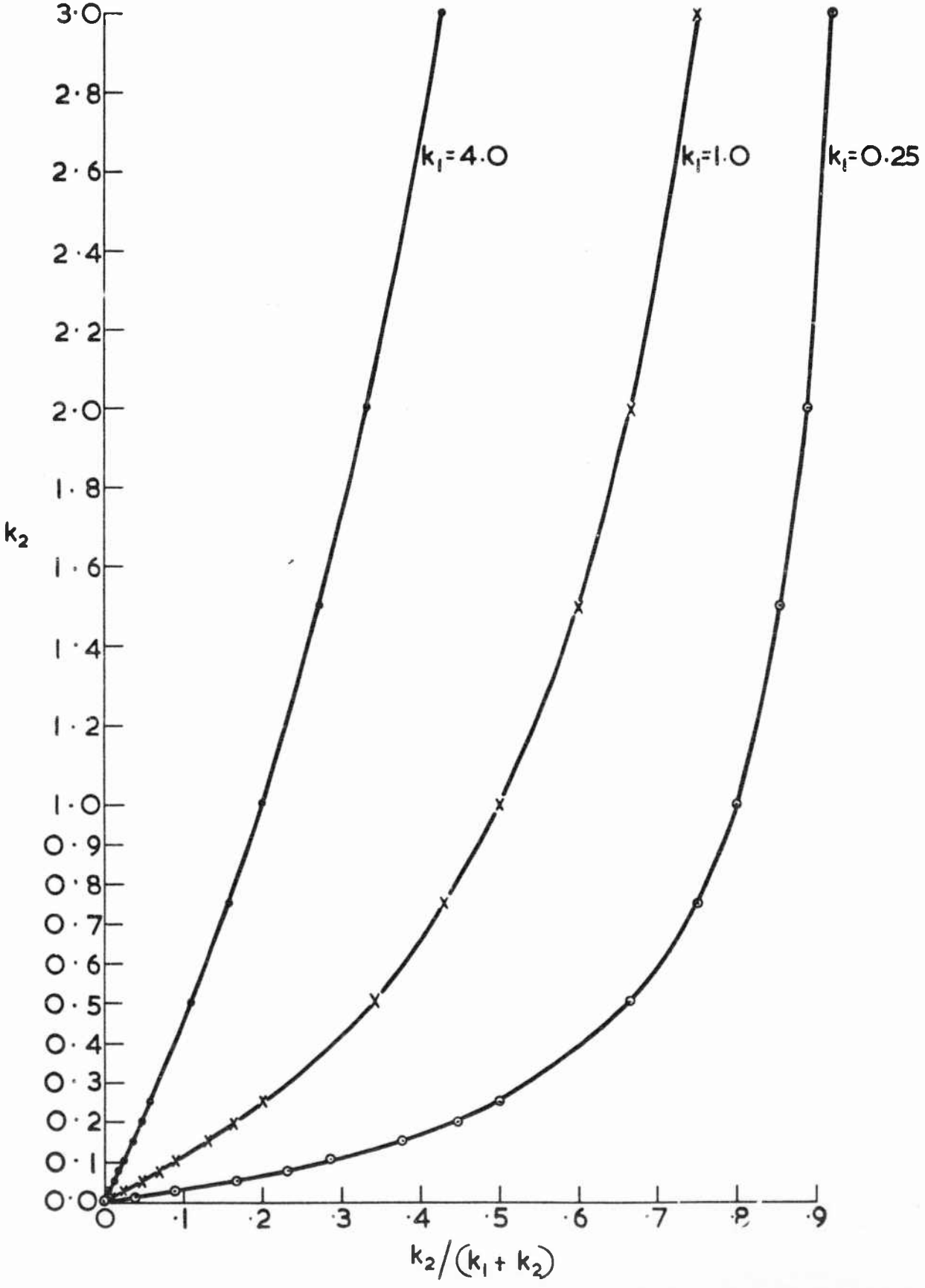

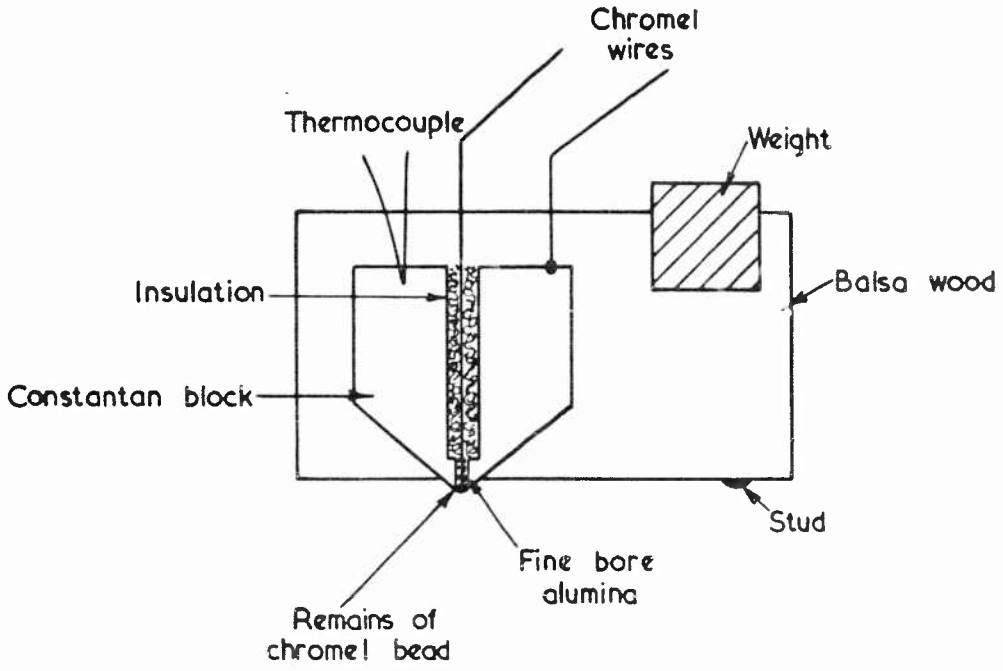

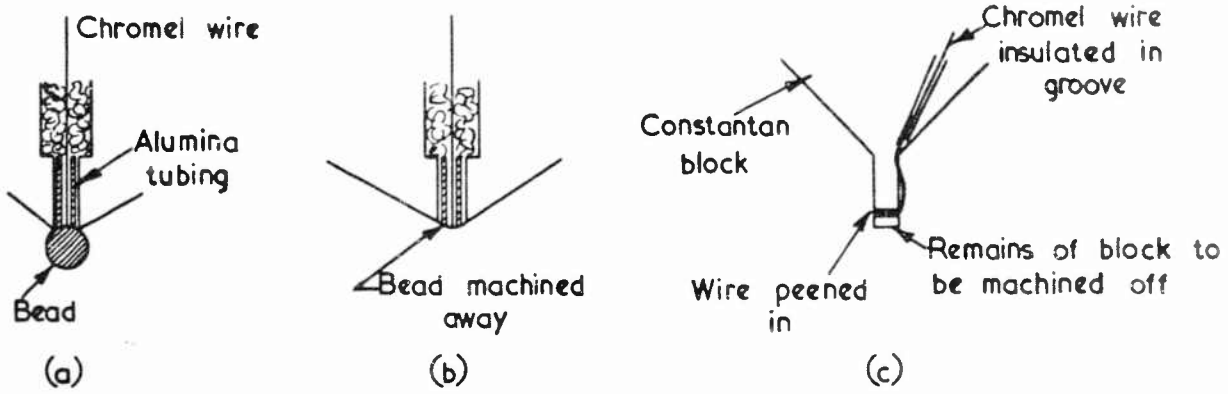

FIG. 20. DIRECT - READING FORMS OF THERMAL COMPARATOR

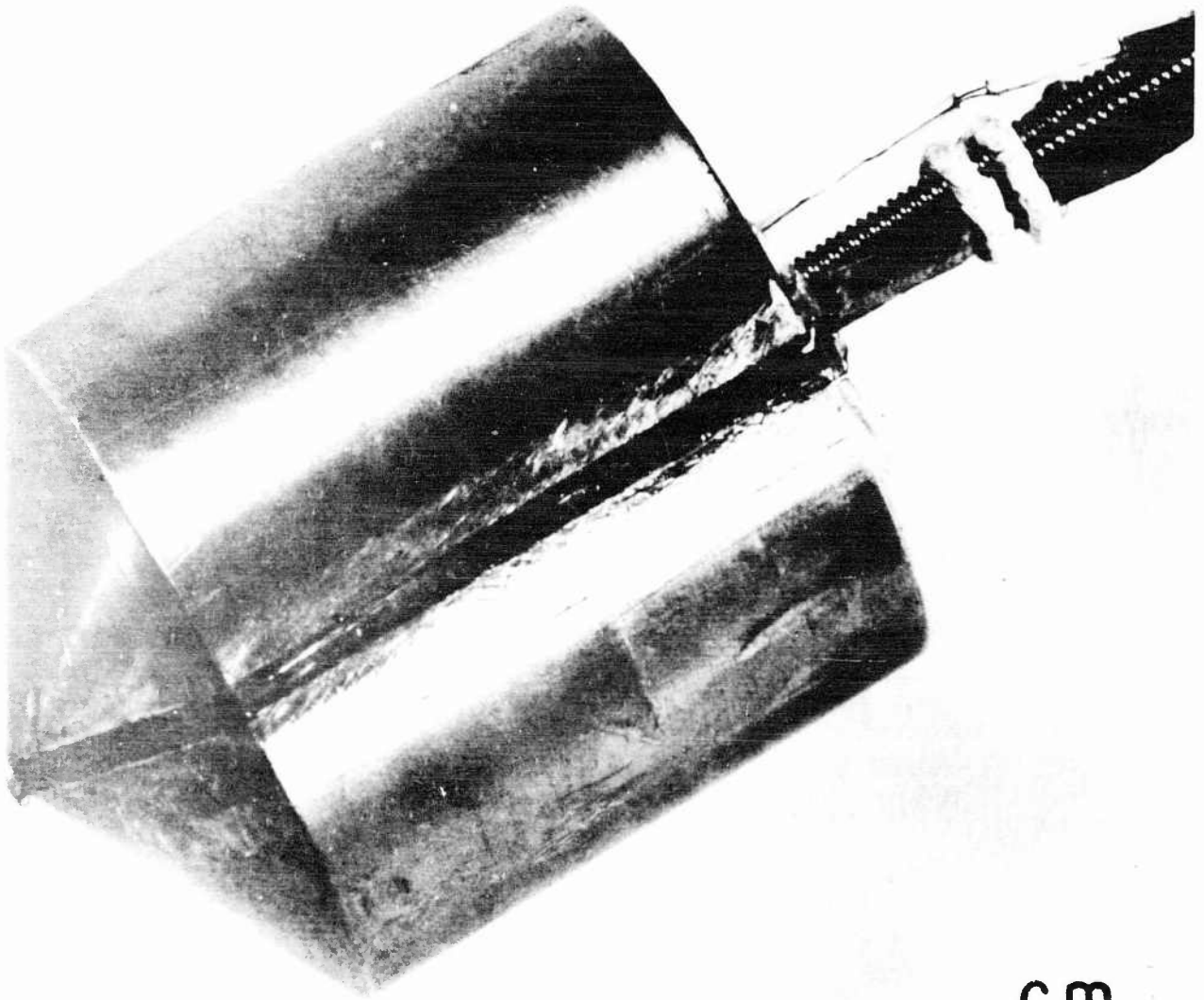

FIG. 21. PROBE UNIT OF THERMAL COMPARATOR OF TYPE SHOWN IN FIG. 20c.

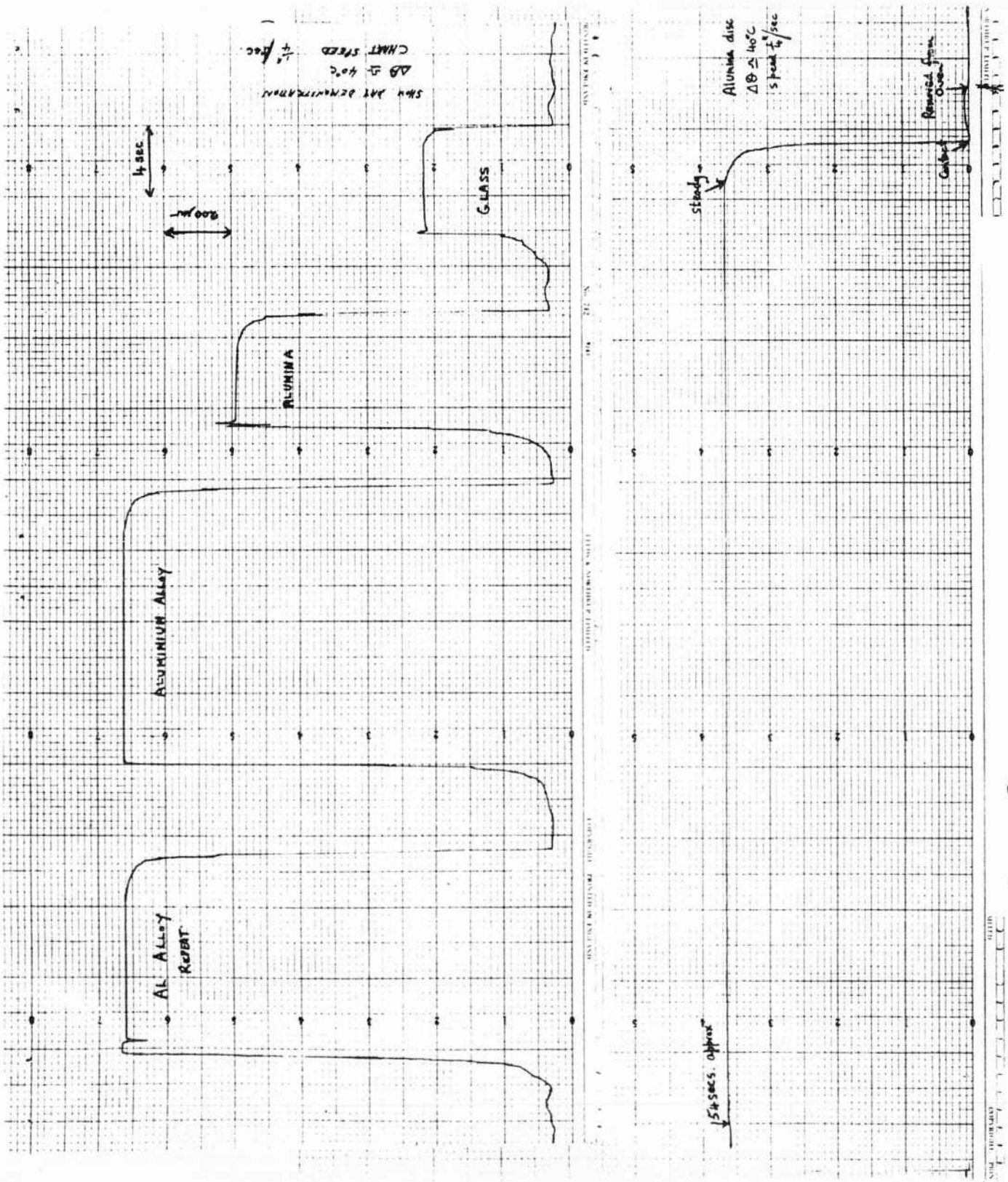

FIG. 22. RECORDER TRACES USING THERMAL COMPARATOR OF TYPE SHOWN IN FIG. 20c.

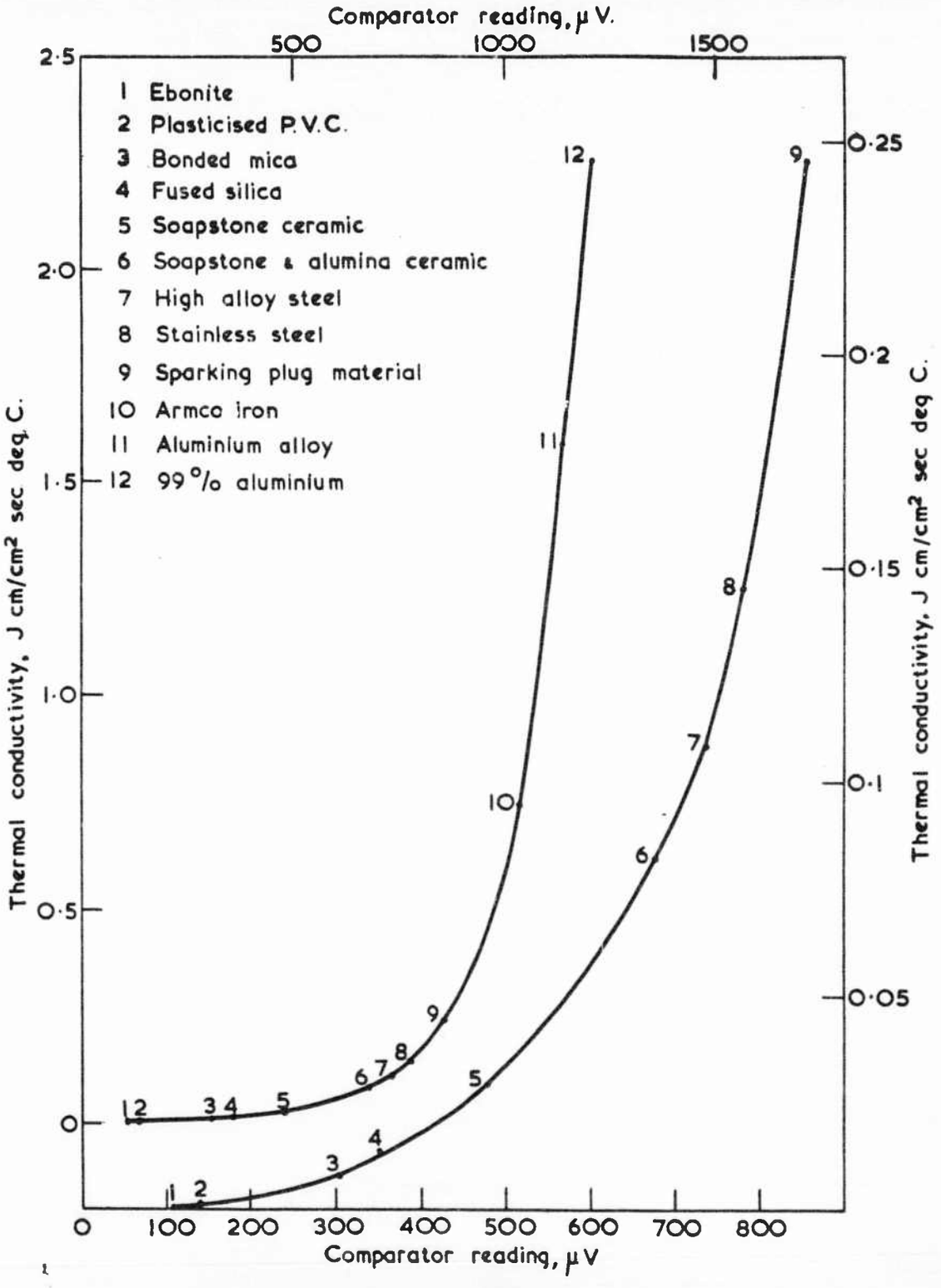

FIG. 23 CALIBRATION CURVE FOR DIRECT-READING THERMAL COMPARATOR (FIG. 20C)

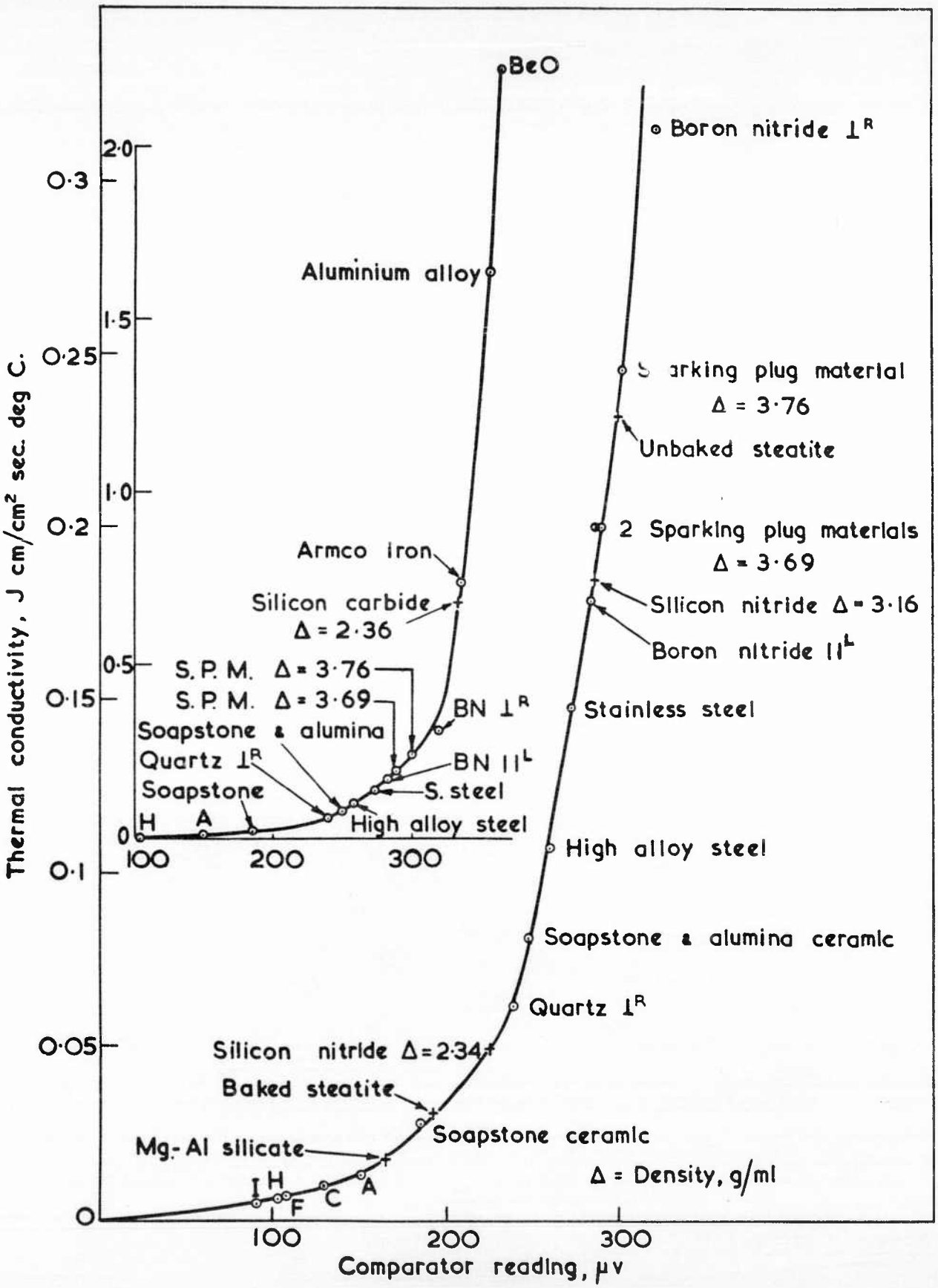

FIG. 24. CALIBRATION CURVE FOR DIRECT READING THERMAL COMPARATOR (FIG. 20 b) : USE FOR CERAMIC MATERIALS

FIG.25. THERMAL COMPARATOR READING v THERMAL CONDUCTIVITY FOR A SERIES OF GLASSES

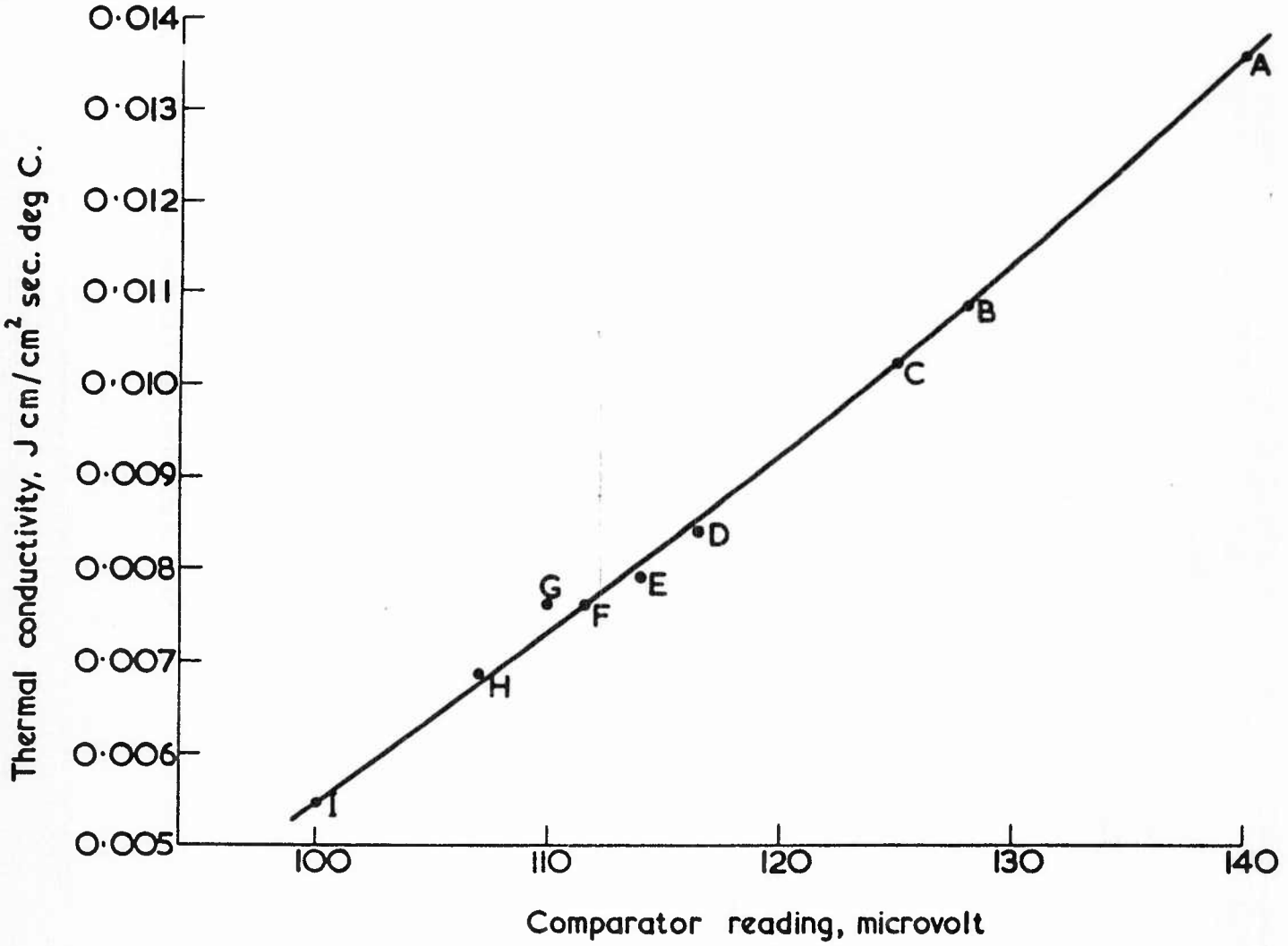

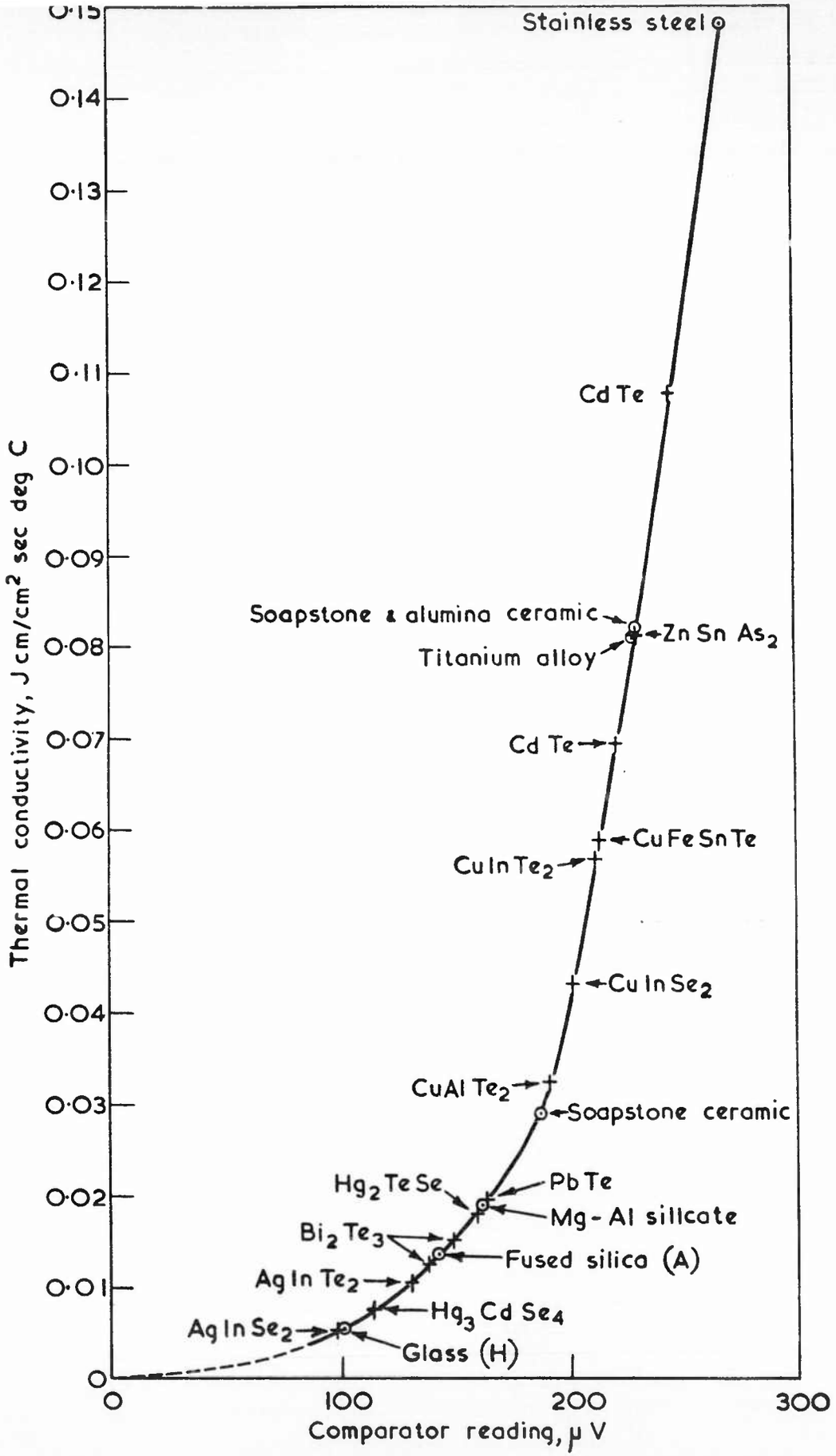

FIG. 26. THERMAL CONDUCTIVITY OF SEMI CONDUCTORS BY DIRECT-READING THERMAL COMPARATOR

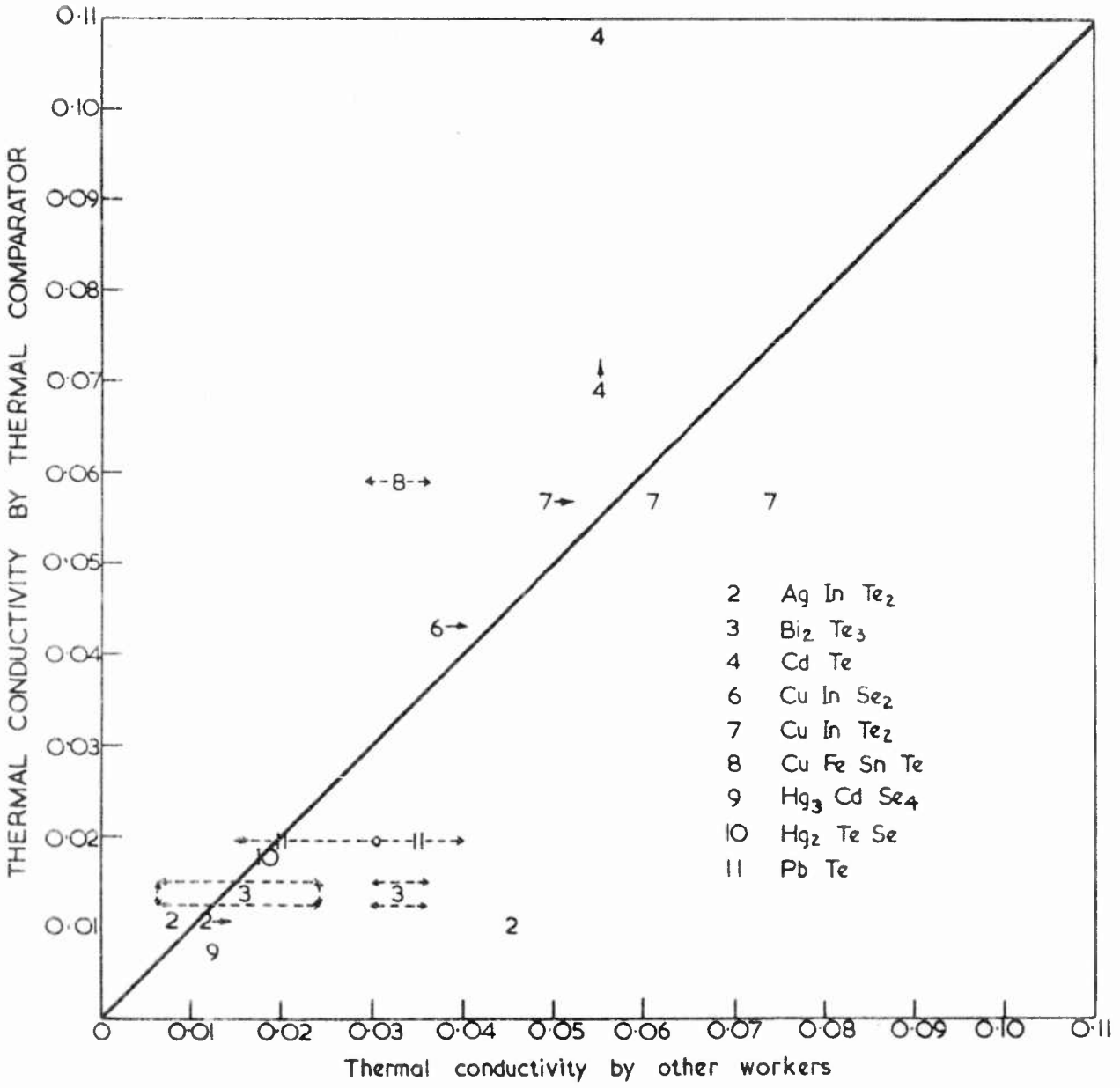

FIG. 27. THERMAL CONDUCTIVITY OF SEMI CONDUCTORS: COMPARISON OF VALUES DERIVED FROM FIG. 26. WITH THOSE OF OTHER WORKERS

C2. MICROWAVE HALL MOBILITY IN GERMANIUM*

by

Y. Nishina[/] and G. C. Danielson
Institute for Atomic Research and Department of Physics
Iowa State University, Ames, Iowa

ABSTRACT

Hall mobilities of germanium single crystals have been measured at a frequency of 9000 Mc over the temperature range 30 - 300°K. The rectangular sample was placed on the wall of a rectangular cavity which was doubly degenerate in the TE_{101} mode and in the TE_{011} mode at a single resonance microwave frequency. Measurements on n - type germanium were in quantitative agreement with the theoretical analysis by Liu, Nishina, and Good. Measurements on p - type germanium were more difficult to interpret and quantitative discrepancies between the microwave Hall mobility and the corresponding dc Hall mobility were found. The magnetic field dependence of the microwave Hall mobility in p - type germanium was in qualitative agreement with the analysis of dc measurements by Willardson, Harman, and Beer.

The measurement of mobility at microwave frequencies has been made by means of a rectangular cavity which was doubly degenerate in the TE_{101} mode and TE_{011} mode at a single resonance microwave frequency. The theoretical analysis of the apparatus has been reported by Liu, Nishina, and Good[1] and the experimental method has been described in detail by Nishina and Danielson.[2] Measurements of the Hall mobility at microwave frequencies were compared with the dc Hall mobility between 30

---

*This work was performed in the Ames Laboratory of the U. S. Atomic Energy Commission.

[/]Present address: National Magnet Laboratory, Massachusetts Institute of Technology, Cambridge 39, Massachusetts.

and 300°K. For n - type germanium the agreement was excellent, but for p - type germanium quantitative discrepancies were found.

Recently, N. Watanabe[3] has also measured the Hall effect in n - type and p - type germanium at microwave frequencies. He used a double mode cavity, but cylindrical rather than rectangular in shape. He also found excellent agreement between the Hall mobility at microwave frequencies and the dc Hall mobility for n - type germanium, but found some discrepancies for p - type germanium. He assumed acoustical mode scattering between room temperature and 100°K, and considered both light and heavy holes.

It is clear that further work on the microwave measurement of Hall mobility is desirable. At lower temperatures one will have predominantly impurity scattering rather than acoustical mode scattering. The importance of the energy dependence of the relaxation time, as discussed in detail by Watanabe, can then be examined.

With sufficiently low temperatures and high frequencies, the dependence of mobility upon frequency should be observable. In the research program at Iowa State University it is planned to increase the frequency from 10 Gc to 100 Gc and to lower the temperature from 20 to 1°K. Both n - type and p - type semiconductors will be studied.

REFERENCES

1. S. H. Liu, Y. Nishina, and R. H. Good, Jr., Rev. Sci. Instr. 32, 784 (1961).

2. Y. Nishina and G. C. Danielson, Ibid. Journal 32, 790 (1961).

3. N. Watanabe, J. Phys. Soc. Japan 16, 1979 (1961).

C3. ELECTRICAL RESISTIVITY MEASUREMENTS AT LOW TEMPERATURES

by

R. V. Colvin and S. Arajs
Edgar C. Bain Laboratory for Fundamental Research
U. S. Steel Corporation, Monroeville, Pennsylvania

Originally it was intended that this paper would be primarily on the electrical resistivity measurements that have been made on the rare earth metals below room temperature. In view of the nature of the conference and the interests of the people that are attending it would seem more appropriate to stress the equipment and use the results obtained with it as an illustration of what can be done with such equipment.

Our recent measurements on uranium and chromium are perhaps more interesting and for this reason we are including a couple of figures showing these results.

In the first figure you see a scale drawing of the heat-leak chamber we use to obtain sample temperatures between 1.3°K about 400°K. You will note that the sample chamber is made of high conductivity copper and is wrapped over its length with a heater and is equipped with carbon and copper sensing elements.

In the next figure you see the heat-leak chamber in the cryostat filled with liquid N_2 or He. The sample holder which is not shown is essentially an insulated flat piece of copper attached to a stainless steel tube. Current and potential leads are spot welded to the sample which is clamped against the copper. A thermocouple is glued to the center of the sample. Thermal

contact between the sample chamber and the sample is obtained by pumping out the chamber and filling with helium gas to a pressure between 1mm and 100 microns. The sample temperature is controlled by the amount of heat supplied to a heater wound on the sample chamber. Since a vacuum is maintained around the outside of the sample chamber, a constant temperature may be obtained by supplying heat equal to the conduction losses along the stainless steel and the radiation losses to the bath. The copper or carbon resistor is in one arm of a bridge circuit, with the input of a Brown Servo Amplifier connected at the null detector position. This amplifier controls a helipot with its servo motor. An externally programable power supply connected to this helipot supplies power to the heater. One thus obtains temperature control of the sample chamber. It is also possible to control temperature on an on-off basis with another servo motor equipped with an arm that operates a switch.

Since it is useful to change sample temperatures as quickly as possible, automatic switching apparatus has been incorporated so that it is possible to heat the sample chamber quickly to a preselected temperature, cool to the desired temperature, cycle on-off to stabilize and then switch to proportional control with the servo mechanism positioned properly to begin control. The reverse mode of control is also possible for measurements made with decreasing temperatures.

The measurements are made by the standard potentiometer method. Voltage drops on the sample are measured with a microvolt potentiometer and sample current is measured with a Rubicon

type B. A current controller, heavy copper reversing switches, saturated standard cells in a thermostated box and a temperature controlled laboratory area contribute a great deal to the precision of the measurements.

Thermocouple emf's are measured with a Diessel horst potentiometer which will measure to .1 micro-volt.

We have a number of figures (Fig. 3 - 5) on some of the work we have done that illustrates the results one can obtain. Anomolous behavior is seen in all of these resistivity curves. Other physical properties have been measured on these elements and they also indicate anomolous behavior in the same temperature region as does the electrical resistivity. For those of you who may be interested in seeing some of the published work on this work we suggest the following.

Electrical Resistivity of the Heavy Rare Earths
Phys. Rev., 120, 741-745 (1960).

Electrical Resistivity of La, Pr, Nd, and Sm
Phys. Rev., 121, 1637-1639 (1961).

Initial Study of Electrical Resistivity of a Chromium Single Crystal
J. Less Common Metals, 4, 46-51 (1962).

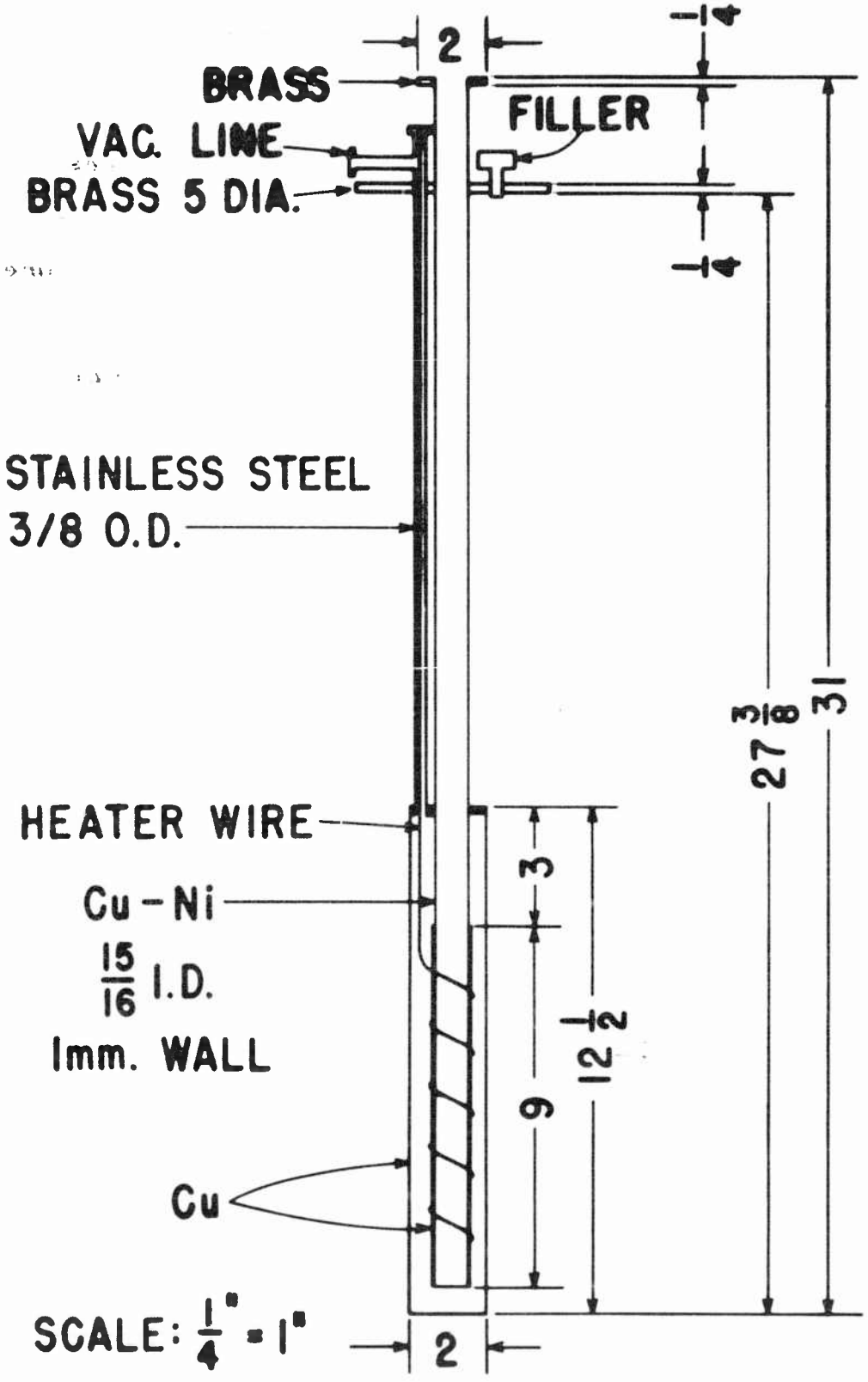

Fig. 1 Heat-Leak Chamber

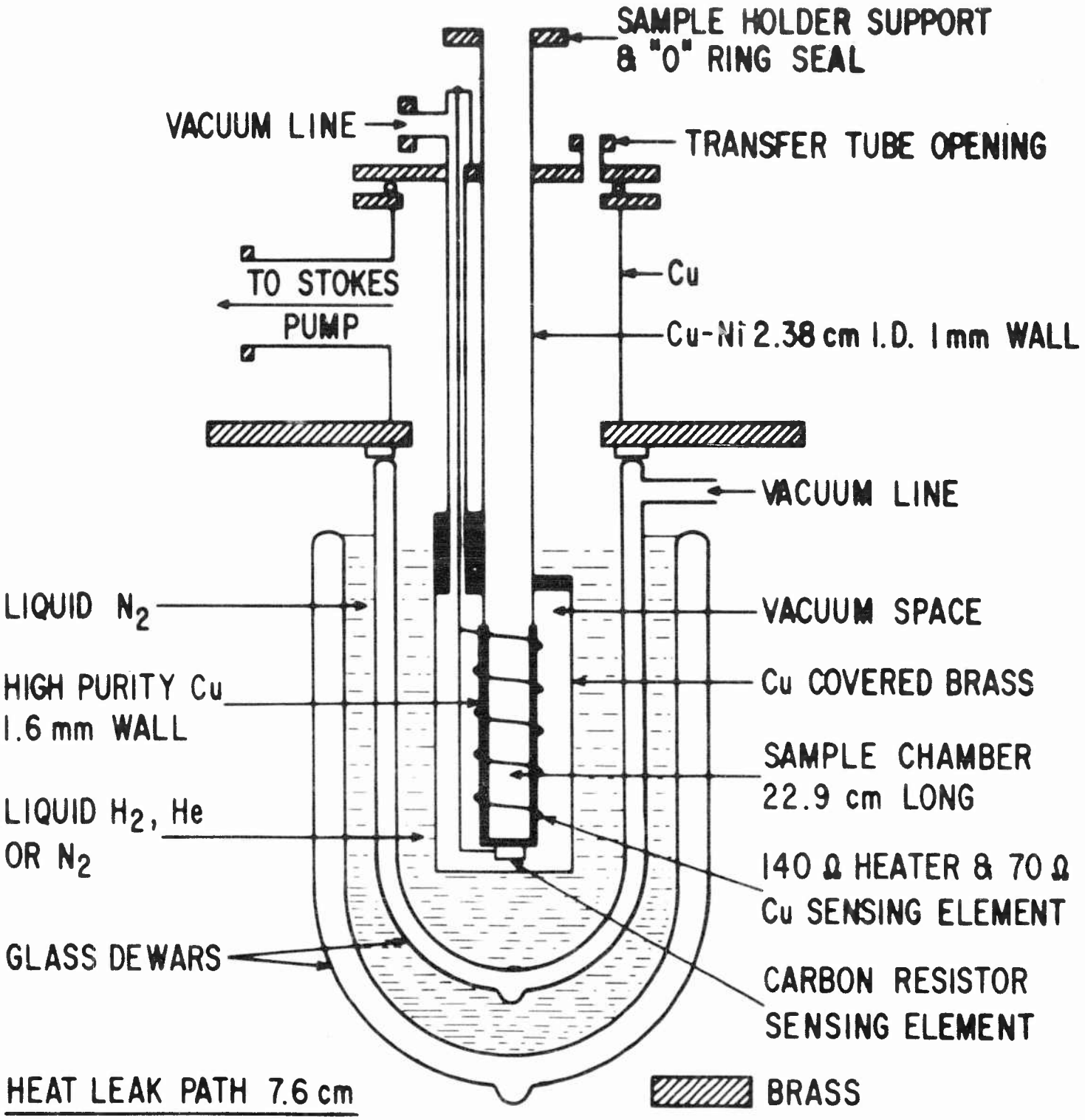

Fig. 2 Heat-Leak Chamber Mounted

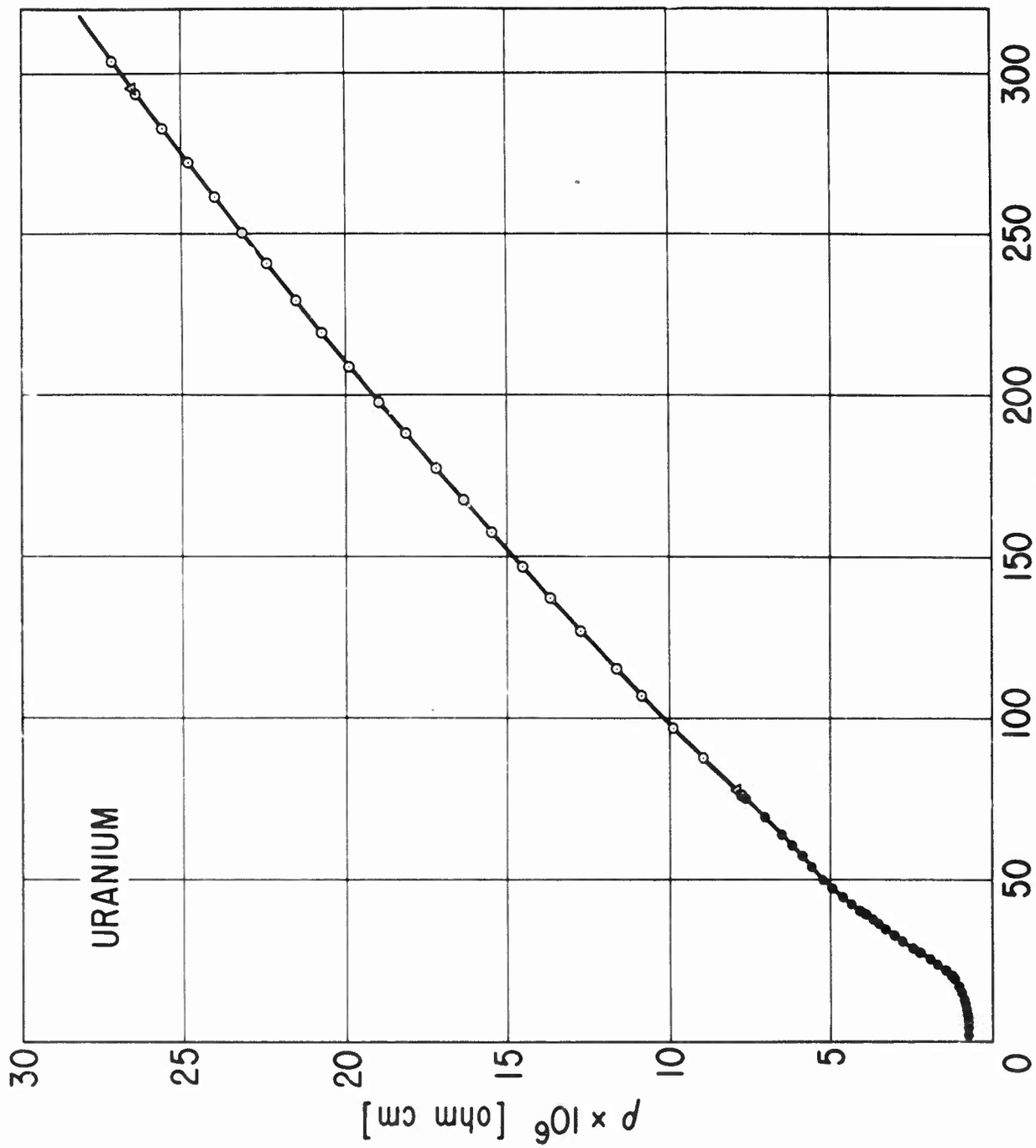

Fig. 3

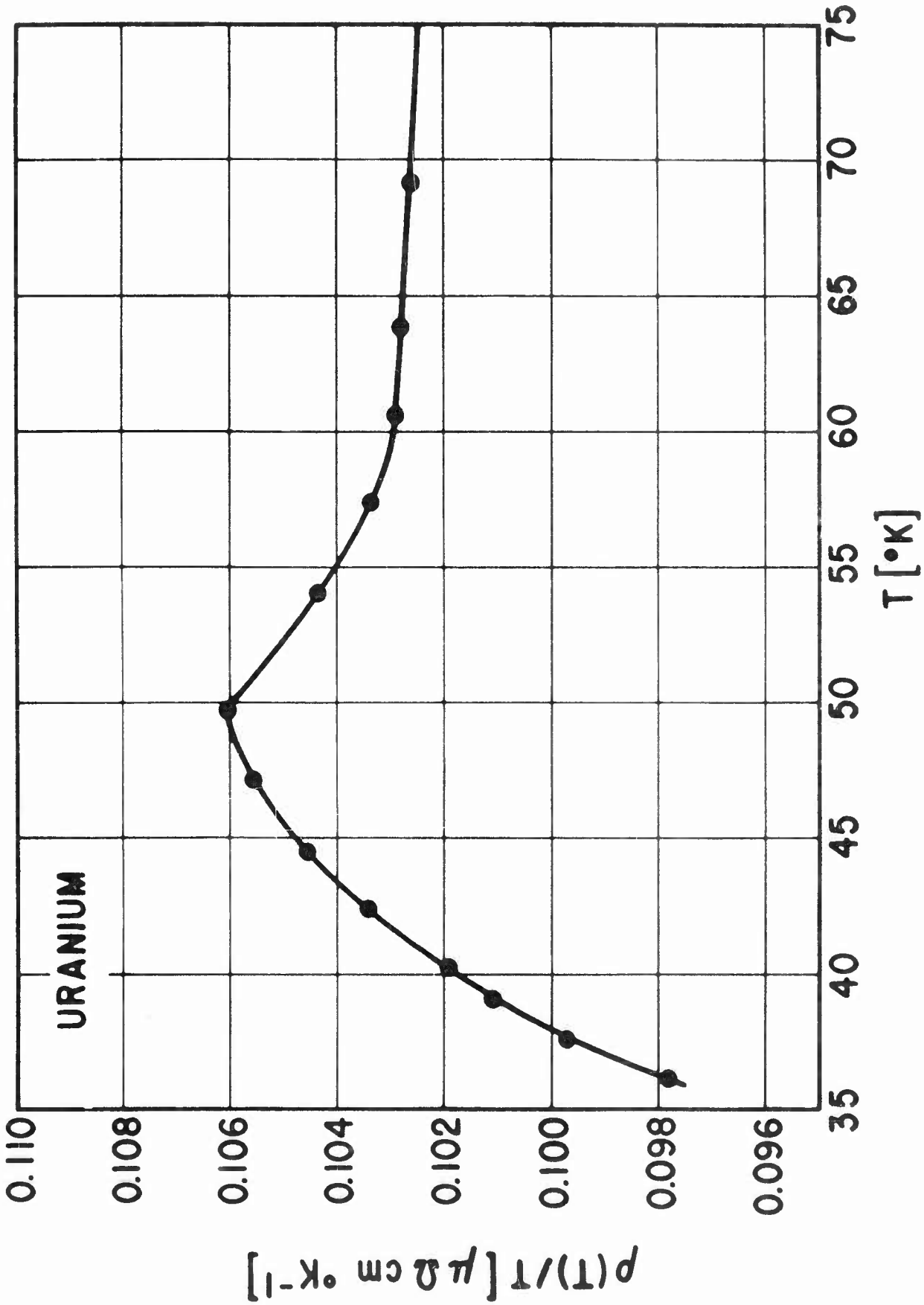
URANIUM
0.110
0.108
0.106
0.104
0.102
0.100
0.098
0.096
35
40
45
50
55
60
65
70
75
T [°K]
ρ(T)/T [μΩ cm °K⁻¹]

Fig. 4

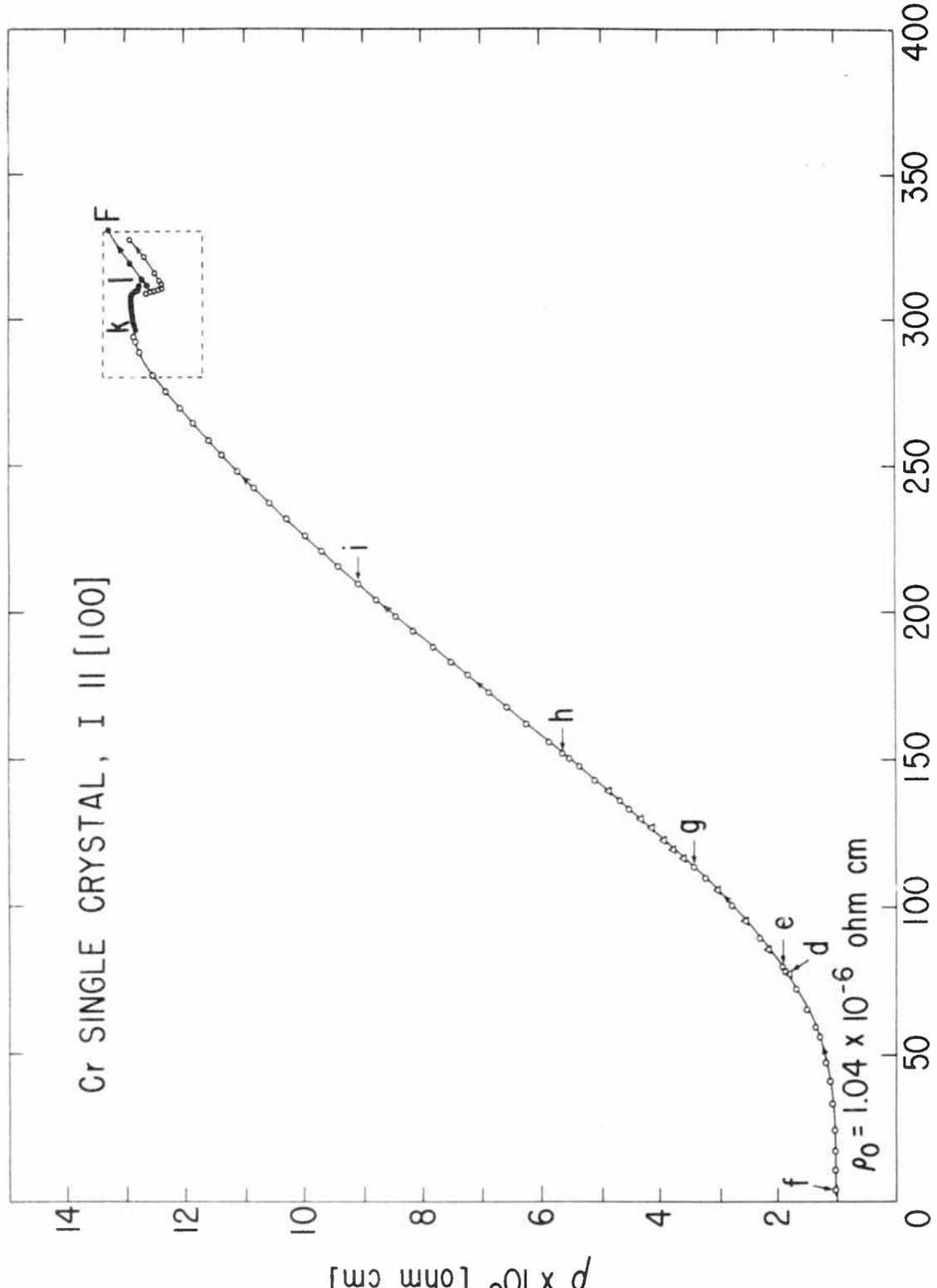

FIG. 5 -- ELECTRICAL RESISTIVITY OF CHROMIUM SINGLE CRYSTAL FROM LIQUID HELIUM TEMPERATURES TO 330°K.

D1. THE THEORY OF ELECTRICAL AND THERMAL CONDUCTIVITY OF SOLIDS

by

P. G. Klemens
Westinghouse Research Laboratories
Pittsburgh 35, Pennsylvania

It is clearly impossible to give a comprehensive review of electrical and thermal conduction in solids within the time allocated to me. Let me stress a few random points, keeping to the foundations of the theory, and speak of a recent development.

I. Lattice Thermal Conductivity

Some of the points which will be made here are also of relevance for the electronic conduction properties.

The basis of the transport theory is the theory of equilibrium properties. It would be natural to describe the vibration of the atoms in terms of motion of single atoms about their equilibrium sites, but since the motion of neighboring atoms is coupled, this is not a good description. Instead, one represents the atomic vibrations as a superposition of lattice waves. In a perfectly regular crystal with harmonic interatomic forces and without boundaries, these waves are normal modes, i.e., the energy residing in each wave or normal mode is a constant of motion. In order to treat equilibrium properties it is usually assumed that these waves are only approximately normal modes, that there is a slow interchange of energy among them (due to anharmonicities, lattice defects, boundary irregularities), and then one invokes a principle of extreme randomness to get an

equilibrium distribution of energy, as in all applications of statistical mechanics. It is unnecessary to specify the nature or strength of this energy interchange--this does not affect the equilibrium properties. We need know only the lattice wave spectrum--the number of normal modes in a given frequency interval.

As soon as we consider transport phenomena, we require (1) all the information needed to understand the equilibrium properties, and (2) an exact knowledge of how energy is interchanged among the normal modes, and in particular how fast this interaction restores a non-ecuilibrium situation to equilibrium.

Since our theoretical knowledge of the second point (the interaction rate) is so very crude and approximate, it is usually not considered worth while to include into the transport theory any refinement relating to (1) --thus instead of using the true lattice wave spectrum one usually uses the Debye spectrum. This is somewhat inadequate, but one usually makes worse approximations in calculating interaction rates.

Both in the equilibrium and the nonequilibrium theory one must do two things: (1) treat the energy of each normal mode as quantized, i.e., made up of discrete quanta or phonons of energy $\hbar\omega$; (2) consider the discretness or atomicity of the lattice. These two refinements of the theory are entirely distinct: one can forget about quantization only at high temperatures, but one can replace the discrete lattice by an elastic continuum only for long waves, i.e., only at low temperatures. See Table I.

TABLE I

Range of Validity of Theories of Lattice Vibrations

	Continuum	Discrete Lattice
Classical	Sound and Ultrasonics	High Temperatures
Q-Mechanical	Low Temperatures	Completely Valid

To calculate the conductivity, we set up a Boltzmann equation which balances the rate of change of energy (or number of phonons) in a given mode due to interactions with other modes, against the change due to a temperature gradient. The rate of change due to interactions (disregarding fluctuations) must of course vanish if all modes are excited to their equilibrium value (this being the condition for equilibrium), so that a steady rate of change, to counteract the effect of the temperature gradient, requires a steady deviation from equilibrium, which is anisotropic. This anisotropic distribution carries a heat current, proportional to the temperature gradient, and the solution of the Boltzmann equation thus defines the thermal conductivity.

Formally, one can show that the thermal conductivity tensor is given by

$$\kappa_{ij} = \sum_{\underline{q}} S_{\underline{q}} v_i v_j \tau_{\underline{q}} \qquad (1)$$

where the summation is over all modes (specified by a wave-vector $\underline{q}$ and the polarization) v_i, v_j are the components of the group velocity, $S_{\underline{q}}$ the specific heat of a normal mode, and τ the

relaxation time. The relaxation time is defined as follows. Consider the steady-state nonequilibrium distribution under the influence of a temperature gradient*, and let the perturbing temperature gradient be suddenly switched off. The distribution will then revert to equilibrium. If E is the energy in a normal mode, E_o its equilibrium value, then τ is defined in terms of the initial rate of E, i.e.,

$$dE/dt = (E_o - E)/\tau \qquad (2)$$

It is thus always possible to speak of a relaxation time; however, in cases when dE/dt depends not only on E of the mode considered, but also on the value of E of all other normal modes, which in turn depends on the solution of the Boltzmann equation, it may be necessary to solve an integral equation to deduce τ. In that case τ has only a formal significance, but in many cases it is a good approximation to calculate τ as if all other modes were at equilibrium, making the relaxation time a practical concept.

The crux of the problem is, of course, the calculation of dE/dt for various interactions (defects, anharmonic interactions, etc.). All calculations that have been done to date have one common feature: they are based on perturbation theory. In other words, one assumes an almost perfect crystal**. We

---

*or the electron distribution in the presence of an electric field in the case of electric conduction.

**Another case which can be treated is the scattering of long waves in glass. Here one assumes a perfect elastic continuum, with small local fluctuations of the elastic constants superimposed, which in turn are again treated by perturbation theory.

simply do not have the means to treat strong disturbances, though in practice it is often found that the range of validity of the perturbation theory seems to extend further than one would have expected on purely theoretical grounds.

Thus one considers a small local fluctuation in density, elastic properties, or the corresponding atomic quantities. A lattice wave passing this disturbance will give rise to secondary waves in all directions, and thus loose energy. When calculating the radiation by secondary waves, one assumes that the wave-form at the disturbed region is unaffected by the perturbation (Born approximation).

In this way one can calculate the scattering of lattice waves by any static perturbation. In practice such calculations have been performed with reasonable certainty only in the case of single atoms whose mass differs from the mean mass (isotope or quasi-isotope scattering). Cases where the disturbance of the lattice extends over several sites (such as wrong linkage forces, distortion effects) are not only more difficult to calculate, because one must take account of spatial interference effects, but the basic parameters that would be needed in a proper theory are not as well known. Thus if we put a K ion into NaCl we know the mass difference between K and Na quite well, but we have little information about the radial distortion introduced because of a difference in ionic radii.

However, there are cases when we know the strain field of an extended imperfection (for example we know the strain field around a dislocation except for its value near the dislocation

core), and provided we can resolve such extended imperfections into Fourier components, we can handle the problem of spatial interference.

However, the scattering by a strain field involves the concept of anharmonicities. If a crystal is strained, all elastic properties are slightly altered, such that

$$v = v_o(1+\gamma\epsilon) \qquad (2')$$

where v is an elastic constant, v_o its value in the unstrained crystal, ϵ the strain, γ an anharmonicity coefficient. The above definition applies only to a homogeneous strain, and the appropriate coefficient γ for homogeneous strain can be deduced from properties such as thermal expansion and higher order elastic constants. Now a homogeneous strain does not scatter phonons, because it does not destroy the regularity of the lattice. Scattering arises from inhomogeneous strains, such as due to lattice defects or thermal fluctuations. At this point the difficulty arises that one must try to deduce the anharmonic effects of an inhomogeneous strain by extrapolation from the observed effects of a homogeneous strain, but such extrapolation procedures, although plausible, are by no means unique, unless we can make use of a detailed model of interatomic forces. Therefore we cannot calculate the scattering of phonons by inhomogeneous strain fields with confidence.

A clear example of this difficulty is provided by the low temperature thermal resistance due to dislocations. This resistance, which can be identified by its temperature dependence, has been correlated in some cases with dislocation

densities determined by other means (stored energy, etch pit counts, electron micrographs), and the scattering cross-section has been compared with theory. In all cases one found the cross-sections substantially larger than the theoretical values. Whether this is due to our inadequate knowledge of the anharmonicites, or due to special arrangements of the dislocations and consequent reinforcement of their strain fields, is still an open question.

Now let us consider the anharmonic scattering of lattice waves due to thermal fluctuations, which is usually the major source of resistance at ordinary and high temperatures. The simplest approach would be to consider thermal fluctuations in density (or other strains), treat them as if they were static perturbations, and calculate the scattering of lattice waves. This was the original approach of Debye, who first treated this problem. Note that the atomic nature of the solid must be considered, for every unit cell is treated independently of every other unit cell. At low temperatures, where the thermal motion is mainly due to lattice waves, and the motion of neighboring atoms is correlated, this is certainly not correct, but at high temperatures it is, in fact, not a bad approximation.

The proper theory, as developed by Peierls, is much more elaborate. The thermal fluctuations are not static: they arise to lattice waves, so that it is appropriate to treat the scattering process as an interaction between lattice waves. Cubic anharmonicities, in the lowest order perturbation theory, are treated as the sum of interaction processes, each process

involving three lattice waves. Only certain triplets of lattice waves can interact: if and and $\underline{q}$ are the frequency and wave-vector of a lattice wave, interactions are allowed only if two conservation conditions are fulfilled, i.e.,

$$\omega + \omega' = \omega'' \qquad (3)$$

$$\underline{q} + \underline{q}' = \underline{q}'' + \underline{b} \qquad (4)$$

where $\underline{b}$ is an inverse lattice vector of the crystal, including the special case $\underline{b} = 0$. Processes for which $\underline{b} = 0$ are normal processes (N-processes), other processes are called Umklapp processes (U-processes).

Since N-processes conserve a constant of motion of the lattice waves (or phonon gas), namely the total "momentum" of the phonons, they can never, by themselves, obliterate an anisotropy in the phonon distribution. Thus they are ineffective, or have only a secondary effect, in producing thermal resistance. Their role depends entirely on the nature of the processes which obliterate phonon momentum. Finding the effective relaxation time in the presence of N-processes is quite a complicated problem, which has not yet been properly solved in general. N-processes are particularly important when phonon-scattering by point defects is a significant resistive process. On the other hand, they can be disregarded when calculating the high temperature resistance due to U-processes.

One can show fairly generally that the thermal resistance varies as T at sufficiently high temperature, and one can determine which are the relevant parameters determining its magnitude.

Thus the intrinsic thermal conductivity at high temperature is of the form

$$K = AM\alpha\Theta^3/T \qquad (5)$$

where A is the numerical constant, M the mean atomic mass, α the interatomic distance, Θ the Debye temperature.

The calculation of A is however extremely difficult, involving a knowledge of the anharmonicities, and more importantly, a summation over all U-processes. A rough estimate has been given by Leibfried and Schloemann. Clearly A decreases as the crystal structure becomes more complex (i.e., as the number of zone boundaries increases). So far it has not been possible to calculate the effect of crystal structure on A.

Thus one may as well have used the original Debye theory to calculate high temperature conductivities. However, one should remember that this theory makes some assumptions, behind which are hidden some difficulties which can only be resolved by the full theory. Furthermore, the proper theory goes over smoothly into the case of low temperatures, where the Debye theory fails.

We may thus summarize the theory of lattice thermal conductivity in the following way. In principle it gives us a good insight into the processes of thermal resistivity, and a qualitative understanding of the temperature dependences and the influence of imperfections and, to a limited extent, of the atomic properties of the crystal. With the exception of the resistance due to some of the simpler imperfections, it fails to give quantitative results except in the most approximate manner.

II. Electron Conduction Properties

Even though the theory of the electronic conduction properties is very different from that of the lattice thermal conductivity, many of the general conclusions still apply. The free electron picture, which at best can apply only to the monovalent metals, is the customary basis of discussion, although some qualitative conclusions of the theory turn out to be independent of the detailed band structure. Again, one considers the scattering of the carriers--this time the electrons--by static imperfections and by thermal fluctuations. Elastic scattering by static imperfections is a temperature-independent mechanism. Scattering due to thermal fluctuations is temperature dependent, and at high temperatures, where the motion of atoms can be simply described by treating each atom as an independent oscillator, it is easily seen that the mean square value of the thermal strain varies as T, so that the electrical resistance varies as T. This is analogous to the high temperature intrinsic resistance in the case of lattice waves.

Again, a more sophisticated treatment is needed if the entire temperature range is to be covered: the thermal fluctuations are expressed in terms of lattice waves, and the scattering of electrons by lattice waves is treated as an interaction, in which an electron emits or absorbs a phonon, and changes its energy and momentum.

Again we have N-processes and U-processes in this interaction, i.e., if an electron has energy E and a wave-function

of wave-vector $\underline{k}$, we have two conditions to satisfy

$$E \pm \hbar\omega = E' \tag{6}$$

$$\underline{k} \pm \underline{q} = k' \pm \underline{b} \tag{7}$$

Again, the scattering probabilities are calculated by perturbation theory, both in the case of scattering by static imperfections, and in the case of electron-phonon interactions, with the sole exception of the scattering by the shielded Coulomb potential of an impurity atom, which has been treated by the method of partial waves, a wave-fitting method which is superior to the Born approximation.

Again, when estimating the scattering either due to an inhomogeneous strain field or due to a lattice wave, one runs into the same difficulty that one had when estimating the anharmonic scattering of phonons, i.e., one must extrapolate the effect of these strain fields from the effect of a homogeneous strain on the electronic states; this extrapolation goes under the name of deformation potential in the literature. We have great difficulty of even estimating a rough magnitude of this interaction except in very simple cases. As an example consider the dispute in the literature as to whether the electrical resistance increase in deformed metals is to be ascribed mainly to dislocations, vacancies, or stacking faults.

Greatest interest lies in the temperature dependence of the intrinsic resistance. We have a quantitative theory only for a spherical Fermi surface and N-processes only. No quantitative estimate has been made so far with any trustworthiness of the effect of U-processes (which must be important at high temperatures), and of the effect of the topology of the Fermi surface

at low temperatures (which is important even in many monovalent metals, and of course most important in the non-monovalent metals).

The electronic thermal conductivity is somewhat easier to treat. In many cases it is simply related to the electrical conductivity by the Wiedemann-Franz law. If the electron gas is highly degenerate, this law holds provided scattering is essentially elastic, and even if it is inelastic, if it is also isotropic. The only case where it breaks down is the intrinsic resistance at low temperatures, though it is possible to conceive of some special situations at high temperatures, where small departures would occur.

In conclusion let me briefly discuss a few refinements of the theory that have been considered recently. One of them is the mechanism of inelastic scattering of electrons by impurities and other lattice defects. The impurity potential is modulated by the lattice wave with a frequency equal to the frequency of the lattice wave. As pointed out recently by Koshino, this leads, according to simple perturbation theory, to processes in which electrons are scattered at the impurity with the emission or absorption of a phonon. This process should lead to pronounced deviations from Matthiessen's rule, in particular to a strong modification of the temperature dependent component of the electrical resistivity at low temperatures.

When studying the effect of the strain field in the immediate vicinity of a defect, it is no longer adequate to suppose that the strain field of a lattice wave is unaffected by

the defect, as one supposes in the Born approximation, and one must use a more careful analysis. It turns out that every defect has a characteristic frequency ω_i. If ω_i is above the continuum of lattice waves, a localized mode is formed. Due to the inelastic scattering mechanism, localized modes can contribute to the electrical resistance. At Westinghouse, D. H. Damon has recently observed indications of this resistance mechanism above room temperature in the Au-Zn alloy.

If ω_i falls in the continuum, no local modes are formed, but the local strain for all modes $\omega > \omega_i$ is enhanced. This is because the defect vibrates <u>out of phase</u> with the applied lattice wave when executing forced vibrations above its resonance frequency. The enhancement of the local strain above the resonance frequency ought to be apparent in an appropriate irregularity of the temperature dependence of the electrical resistance in alloys such as Cu-Pt. This has not yet been put to an experimental test. However, there are other properties which are very sensitive to the local strain around defects (optical absorption in solids involving phonons, spin-lattice relaxation). J. G. Castle and D. W. Feldman at Westinghouse have indeed seen the effect of the enhanced strain for $\omega > \omega_i$ in spin-lattice relaxation, and it seems very likely that this behavior will be observed in the effect of appropriate defects on conduction properties.

E1 MIXED CONDUCTION IN SEMICONDUCTORS

R. K. Willardson, Bell and Howell Research Center
Pasadena, California

Abstract

Studies of transport phenomena in semiconductors are often restricted to cases involving extrinsic conduction by carriers with a single effective mass. In many materials, mixed conduction must be considered, because of the contributions by carriers of several quite different effective masses and mobilities. Light and heavy holes occur as the result of a degenerate valence band. Electrons in different minima of the conduction band can have quite different effective masses, and the relative concentrations of light and heavy electrons will almost always be temperature dependent. At high temperatures conduction involving both light and heavy electrons as well as light and heavy holes has been observed in GaSb and GaAs. The temperature and magnetic field dependence of galvanomagnetic effects are used to evaluate the relative contributions of the various carriers present in mixed conduction.

INTRODUCTION

In semiconductors, two types of current carriers are present in variable proportions: (1) electrons having energies in the conduction band which act as negative carriers; and (2) vacant states or holes in the valence band which act as positive carriers. At low temperatures, impurities will be the source of the carriers which will be either electrons or holes depending on the impurities involved. In this the extrinsic range the concentration of the second type of carrier will be negligible. At high temperatures intrinsic conduction consisting of nearly equal numbers of both electrons and holes results from the thermal excitation of electrons from the valence to the conduction band.

Because of the detailed structure of the valence and conduction bands in semiconductors, electrons and holes with quite different effective masses and mobilities can exist simultaneously and contribute to the electronic transport. Figure 1 shows the band structure of GaAs in the vicinity of the valence and conduction band edges. Theoretical calculations and infrared absorption experiments indicate a triple degeneracy in the valence band of most Group IV and III-V compound semiconductors. Thus, the valence band has several branches. These are commonly referred to as the heavy mass, the light mass, and the split-off valence bands. Since the density of states in the valence band having the larger effective mass is much greater, these holes will always be present in the largest concentrations and will usually predominate in the conductivity. However, the carriers with the lower effective mass have a much higher mobility and can predominate in transport phenomena where carrier mobility is important, particularly in the weak-magnetic-field Hall effect where a carrier's contribution is proportional to the square of the carrier mobility.

Since the heavy mass and light mass bands have maxima occurring at the same energy, little or no variation in the ratio of the numbers of light mass to heavy mass holes would be expected as a function of temperature.

A contribution of the split-off valence band to electronic transport in any semiconductor has yet to be observed.

Evidence that the valence bands in GaAs were similar to those of germanium was furnished by the free-hole absorption measurements of Braunstein[1]. These experiments yielded a value of the spin-orbit splitting of 0.33 ev. as well as ratios of the effective masses in the heavy mass, light mass, and split-off bands.

---

(1). R. Braunstein, J. Phys. Chem. Solids 8, 280 (1959)

Ehrenreich[2] has discussed the band structure of GaAs and other III-V compounds in detail.

Of particular interest in GaAs is the structure of the conduction band. At low temperatures the [000] minimum in the conduction band is predominant. The effective mass of electrons is about 0.07 m_o, and this results in the electrons having an unusually high mobility for a semiconductor with an energy band-gap of 1.53 ev. However, at higher temperatures a second conduction band minimum with a density-of-states effective mass slightly greater than 1 is predominant, and GaAs becomes a semiconductor in which the mobilities of the heavy mass electrons, as well as the light and heavy mass holes, approximate those in silicon.

Most of the details regarding the band structure of semiconductors have evolved during the past 10 years and apparently we still have much to learn. In the sections which follow the transport properties of a number of semiconductors will be discussed in terms of the relative contributions of the various carriers. Effects of warped energy surfaces, carrier lifetime, and impurity scattering are considered.

THE MAGNETIC FIELD DEPENDENCE OF THE HALL COEFFICIENT CROSSOVER

When an electric current flows in a semiconductor, electrons and holes move in opposite directions. The application of a magnetic field tends to deflect the oppositely moving and oppositely charged carriers in the same direction. A counteracting electric field is set up by the initial movement of

---

(2). H. Ehrenreich, J. Appl. Phys. 32, 2155 (1961)

charge. In the steady state, equal numbers of electrons and holes will flow in the direction of the magnetic deflection as required by the condition that the net transverse current be zero in accordance with the principle of charge conservation.

Since the force exerted by the magnetic field is proportional to the product of the electric current and the magnetic field, and the electric current depends on both the number of free carriers and their mobility; the presence of even a few light mass, high-mobility carriers can be significant. This is particularly true at low magnetic fields where the contribution required for the counteracting electric field is proportional to the square of the carrier mobility. However, at large magnetic fields the carrier mobility is no longer important and the transverse electric or Hall field is determined only by the number of carriers.

The dashed line in Figure 2 shows the magnetic field dependence of the temperature for which the Hall coefficient is zero for a semiconductor similar to germanium but which contains no light mass holes.(3) Since, in germanium the mobility of electrons is greater than that of the holes by a factor of 9/4, the crossover temperature should increase with increasing magnetic field. As the magnetic field increases, the relative effect of the higher-mobility electrons decreases and it requires more of them to balance the current of the holes. The experimental data shown for p-type germanium shows the effect of a few percent of light mass holes which have a mobility a little over 3 times greater than that of the electrons. Tabulated values for the basic parameters shown in Figure 2 are given in Table I.(3)

---

(3). R. K. Willardson, T. C. Harman, and A. C. Beer, Phys. Rev., 96, 1512 (1954)

Table I. Tabulated Values of Basic Parameters

Temperature °K	n_2 cm^{-3}	n_1/n_2	n_3/n_2	μ_2^0 $cm^2/volt\ sec$	μ_1^0/μ_2^0	μ_3^0/μ_2^0
205	4.23×10^{13}	0	0.0187	4500	----	7.5
296.7	5.08×10^{13}	0.170	0.02	1900	2.2	8.0
297.7	5.16×10^{13}	0.184	0.02	1895	2.2	8.0
307.2	6.30×10^{13}	0.335	0.0200	1755	2.25	8.0
310.1	6.80×10^{13}	0.386	0.0208	1710	2.25	8.0
312.5	7.29×10^{13}	0.427	0.0206	1685	2.25	8.0
314.8	7.81×10^{13}	0.468	0.0214	1655	2.25	8.0

A similar experiment with GaAs should prove most valuable. Here two regions would be of interest; the first a region around room temperature where the light mass electrons of the [000] minima would predominate; and a curve similar to the dashed line in Figure 2 would be observed. If the experiment were performed very carefully, it should be possible to obtain an interesting set of experimental curves of the Hall coefficient crossover versus magnetic field as the temperature is increased and the number of light mass, high-mobility electrons decreases. The interpretation of such data should prove to be a challenge, particularly if samples of GaAs can be obtained in which the magnitude of the diffusion currents depend on the recombination velocity at the surface and on the lifetime.

The subsidiary conduction band minima in GaSb lies only 0.08 ev. above

the [000] minimum[4] and the valence bands appear to be like those in germanium.[5]

Hence, the effect of the heavy mass electrons become important at much lower temperatures than in GaAs. Also, since the band gap in GaSb is only 0.81 ev. which is about the same as germanium or roughly half that in GaAs, intrinsic conduction occurs at lower temperatures and it is easier to control the crossover temperature of the Hall coefficient.

Again, in the case of GaSb, a careful study of the Hall coefficient crossover should prove rewarding. The major difficulty is getting material of reasonable purity, since most GaSb is p-type with a carrier concentration of 1 to $2 \times 10^{17}/cm^3$.

INFLUENCE OF CARRIER LIFETIME AND SURFACE CONDITIONS

Whenever transport phenomena involving conduction by both electron and holes are considered, the possibility of carrier concentration gradients, giving rise to diffusion currents, must be considered. The usual Hall effect equations apply only if the concentration of carriers is undisturbed. In the presence of a magnetic field the holes and electrons are swept to the same side of the semiconductor. This establishes a gradient of carrier concentrations and gives rise to diffusion currents across the sample. The magnitude of these diffusion currents depends on the recombination velocity at the surface and on the lifetime of the excess carriers in the interior.

---

(4). A. Sagar, Phys. Rev. 117, 101 (1960)

(5). W. M. Becker, A. K. Ramdas, and H. Y. Fan, J. Appl. Phys. 32, 2094 (1961)

The importance of correctly specifying the surface conditions of semiconductors used in studies of galvanomagnetic effects was pointed out a long time ago by Fowler[6] who discussed the extreme case of infinite carrier lifetime. Equation 1 gives the relationship for the Hall coefficient which is appropriate for the case of zero lifetime in which any desired rate of generation or recombination can be maintained without an appreciable change in the carrier concentration. This restriction upon the validity of this relationship is not usually explicitly stated.

$$R = \frac{r}{e} \cdot \frac{p-b^2n}{(p+bn)^2} \qquad \text{(zero lifetime)} \qquad (1)$$

The relationship for infinite lifetime is given in Equation 2.

$$R = \frac{r}{e} \cdot \frac{p-bn}{(p+bn)(p+n)} \qquad \text{(infinite lifetime)} \qquad (2)$$

When the concentration of electrons or holes greatly exceeds that of the other, Equations 1 and 2 become identical. The distinction becomes important in the intrinsic region as is shown for an n-type sample of germanium in Figure 3. In p-type material, of particular importance is the point at which the Hall coefficient is zero and this is quite different in the two cases. The temperature at which the Hall coefficient reversal occurs will be influenced by the lifetime of excess carriers in the particular sample measured. Landauer and Swanson[7] showed that it was possible to determine the lifetimes of the excess carriers on the basis of Hall effect experiments. They derived the Hall coefficient for the general case in which neither the bulk lifetime nor the surface recombination velocity are assumed to have an extra value.

---

(6). R. H. Fowler, Statistical Mechanics (University Press, Cambridge, 1936), 2nd ed.

(7) R. Landauer and J. Swanson, Phys. Rev. 91, 555 (1953).

Hunter et al[8] used the expressions derived by Landauer and Swanson to determine lifetimes of excess carriers in germanium, and from the data shown in Figure 3 they obtain a surface recombination velocity of 370 cm/sec. This value is to be compared to the value of 450 cm/sec obtained by conventional methods. They concluded that this method permits the measurement of lifetimes of excess carriers in germanium as low as 0.1 microseconds, and that changes in lifetime of the order of 0.01 microseconds could be detected.

Of course, since this work was done in 1953, it was not realized that the light mass holes were making a significant contribution to the Hall coefficient measurements. They did, however, use the experimentally determined ratio of drift to Hall hole mobility which made an amazingly appropriate first-order correction. Such experiments should be repeated using the higher-purity germanium which is available today and making the calculations using the present-day knowledge of the band structure in germanium. Similar experiments on GaAs and GaSb would be instructive. Again, as mentioned in the last section, two temperature regions would be of interest; first, the region near room temperature where the light mass electrons would be predominant; and, a region appreciably above room temperature where the electrons in the higher minima of the conduction band would contribute significantly. While the lifetimes of the carriers in GaAs have been low because of the relatively impure material available for these experiments, the higher purity GaAs which which will soon be available should make such interesting experiments practical.

((8). L. P. Hunter, E. J. Huiboregtse, and R. L. Anderson, Phys. Rev. 91, 1315 (1953)

GaAs AT HIGH TEMPERATURES

The two conduction band minima in GaAs result in a mixed conduction above room temperature involving electrons of light and heavy effective masses. This type of mixed conduction in extrinsic semiconductors results in a maximum in the Hall coefficient at high temperatures. Figure 4 is a plot of the fractional change in Hall coefficient against the reciprocal of temperature in the temperature range where this increase becomes noticeable for three n-type GaAs samples of widely different carrier concentrations. It is possible to estimate separation of the conduction band minima from this temperature dependence of the Hall coefficient. Using the data shown in Figure 4, Aukerman and Willardson[9] calculated an activation energy $\Delta e = 0.38 \pm 0.02$ ev. They assumed that the ratio of the hole mobilities in the two bands was 10 and was independent of temperature between 500 and 1500°K. The ratio of the effective masses was taken to be 0.04. At 500°K the concentration of electrons in the upper minimum is approximately 2% of that in the lower minimum; at about 900°K concentrations of electrons in the two minima are equal, but even at the melting point of GaAs the conductivity in the lower minima still predominates because of the much larger mobility of the low mass electrons.

WARPED VALENCE BANDS AND MIXED SCATTERING

The magnetic field dependence of the Hall coefficient is strikingly affected by the charge-carrier scattering mechanisms and by the band structure. The effect of degenerate valence bands on the Hall coefficient

---

(9). L. W. Aukerman and R. K. Willardson, J. Appl. Phys. 31, 939 (1960)

as a function of magnetic field in germanium has been studied by Beer and Willardson[10] and some of the results are shown in Figure 5.

Three points are significant: (1) The 25 to 35% decrease in the Hall coefficient with increasing magnetic field is caused by the decrease in the mobility squared contribution of the fast holes to the Hall coefficient; (2) At liquid nitrogen temperatures impurity scattering is very important, even in the highest-purity germanium and must be considered in th calculations; and (3) The warping of the heavy mass valence band is responsible for the small maxima that occur between 5000 and 15,000 gauss. Calculations were made using the mixed scattering by acoustic-phonons and ionized impurities as well as a single warped heavy mass band.

In Figure 5 agreement of theoretical predictions and experimental values are semiquantitative, but it appears likely that values of the mixed scattering parameter β exist which can bring the curves into a better coincidence. There is good agreement between the theoretical and experimental curves with respect to the slope in the region of rapid change with field and also in the shape of the minimum and maximum in the case of speciman 2-C. The prominence of the maximum depends on the amount of impurity scattering. Magnetoresistance calculations using the same parameters as those shown in Figure 5 also provided a good approximation to the experimental data.

Similar calculations for high-purity p-type silicon are compared with experimental data in Figure 6.[11] Here a prominent maximum is observed. In accordance with theory the magnitude of the maximum increases with additional

---

(10). A. C. Beer and R. K. Willardson, Phys. Rev. 110, 1286 (1958)

(11). R. K. Willardson, J. Appl. Phys. 30, 1158 (1959)

impurity scattering introduced by irradiation with Co^{60} γ rays. It should be mentioned that the germanium-like behavior for the Hall coefficient factor R_H/R_∞ as a function of magnetic field occurs only in the highest purity silicon.

In ordinary silicon no initial decrease is observed, only a maximum similar to those shown for AlSb in Figure 7.(12) This behavior for silicon with appreciable impurity content is in agreement with the theoretical curves shown in Figure 7. There seems to be little question but that with appropriate parameters the theoretical and experimental curves in Figure 6 could be brought into at least semiquantitative agreement. However, the choice of appropriate mixed scattering and warped band parameters is rather critical.

The similar behavior of the Hall coefficient factor in silicon, AlSb, and diamond is in accordance with a general pattern in which the ratio of the mobilities for the light and heavy holes increases with decreasing band-gap. The explanation of this is that for lower mobility ratios the mobility-squared contribution at low magnetic fields is not significant.

POLAR LATTICE SCATTERING

In germanium and silicon the major scattering mechanisms are acoustical mode lattice scattering and ionized impurity scattering. Of the scattering mechanisms that determine the transport properties in III-V compounds at room temperature and above, the most important is the polar interaction. However, there are few cases in which ionized impurity scattering can be neglected. In addition, when reasonably large concentrations of electrons are present in

---

(12). A. C. Beer, J. Phys. Chem. Solids 8, 507 (1959).

the semiconductor these polar interactions are screened.[13]

Fortunately, at large magnetic fields the simple expression given in Equation 3 is still applicable.

$$R \simeq - \frac{1}{e \sum_i n_i} \qquad (3)$$

Much valuable information can be obtained from the magnetic field dependence of the Hall coefficient in polar semiconductors. Both experimental data and theoretical calculations in this area have been badly neglected. This has led to a number of erroneous conclusions in utilizing experimental weak field Hall data.

In polar semiconductors at high temperatures a time of relaxation exists and is proportional to $E^{1/2}$ and R_o can be expressed as:

$$R_o = - \frac{45\pi}{128} \frac{1}{ne} = - \frac{1.104}{ne} \qquad (\tfrac{\Theta}{T} \ll 1) \qquad (4)$$

in the nondegenerate limit. Following Delves[14] the collision operator derived by Howarth and Sondheimer[15] was used and the Boltzmann transport equation was integrated directly to give the results in Figure 8 for $2\Theta \geq T \geq \Theta/2$ and $5 \geq \eta \geq -2$. η is the reduced Fermi level and $\Theta = \nu h/k$ where ν is the frequency of the longitudinal optical mode. Values for Θ/T are indicated for a number of III-V compounds. Since GaAs has an effective mass of about 0.07, carrier concentrations less than 6×10^{16} will result in η being less than -2 or nondegenerate conditions at room temperature and above. On the other hand, electron concentrations greater than 6×10^{16} will result in η being positive at 77°K and below.

---

(13). H. Ehrenreich, J. Phys. Chem. Solids 8, 130 (1959)

(14). R. T. Delves, Proc. Phys. Soc. (London) 73, 572 (1959)

(15). D. J. Howarth and E. H. Sondheimer, Proc. Roy Soc. (London) __, 280 (1960)

The Hall coefficient factor r provides a possible explanation for the Hall mobilities in GaAs which may be higher at room temperature and lower at 77°K for specimens with carrier concentrations on the order of $10^{17}/cm^3$ than for cases in which the carrier concentration is about $10^{15}/cm^3$. Thus, in one sample the degeneracy is significant and the Hall coefficient factor is relatively constant or decreasing with decreasing temperature, while for low carrier concentrations the value of r increases appreciably with decreasing temperature. Of course, impurity scattering should be included in such calculations before a quantitative explanation can be considered. Experimental evidence that the Hall coefficient factor r is significant is shown in Figure 9(16). Here, for a sample containing 1.5×10^{16} carriers/cm^3 at 300°K, decreases of as much as 15% for the Hall coefficient are shown as the magnetic field is increased. The use of higher magnetic fields and samples of high purity will contribute further to the verification of theoretical predictions. The theoretical curves shown in Figure 9 were calculated for the case of mixed impurity and acoustical mode lattice scattering. The comparison of experimental data with the theory is good, but this is probably only because impurity scattering is predominate.

The magnetic field dependence of the Hall coefficient factor is shown in Figure 10 for the case of a nondegenerate polar semiconductor at a temperature $\Theta/3$. The calculations are those of Lewis and Sondheimer(17). The quantity

$$C(Z) = Z^{3/2} e^{1/2z} K_1 (1/2Z)/(e^{\beta}-1)$$

and $\beta = H\tau_\omega/ne$ is a dimensionless parameter proportional to H. The factor $C(Z)\beta$ is proportional to H and independent of Z. At the temperature $\Theta/3$,

---

(16). R. K. Willardson and J. J. Duga, Proc. Phys. Soc. (London) 75, 280 (1960)

(17). B. F. Lewis and E. H. Sondheimer, Proc. Roy. Soc. (London) A227 241 (1955)

C(Z) is 0.34 and β is very nearly μH.

Figure 11 (18) shows the Hall coefficient as a function of magnetic field for a sample on n-type InSb at 77°K which is approximately $\theta/3$. Using a value of 435,000 cm^2/volt sec for σ_∞/ne, a value of 1.48 for C(Z) β corresponds to 1000 gauss. It should be noted then that the decrease in Hall coefficient shown in Figure 11 occurred at the magnetic fields predicted by the theoretical curve of Figure 10. However, the magnitude of the change was only half that predicted, probably because impurity scattering is important and was not used in the calculations. The use of the actual mobility rather than the lattice mobility made the first-order correction for impurity scattering in the magnetic field comparison.

The magnetic field dependence of the Hall coefficient in p-type InSb is shown in Figure 12. Like germanium at large fields the Hall coefficient decreases to about one-half of the weak magnetic field value. Champness (19) assumed a relaxation time independent of energy and spherical energy surfaces to calculate light hole mobilities of 35,000 to 60,000 in InSb at 77°K. He concluded that these values were too low and that ionized impurity scattering must be considered. It appears likely that the light hole mobility in InSb at 77°K is over 200,000 cm^2/volt sec and that it may even be over 1,000,000 cm^2/volt sec and approach that of the electrons. In any event, the magnetic field at which the decrease in Hall coefficient occurs continues to be a measure of the number of defects in the InSb.

Calculations of the light hole mobility in InSb using mixed ionized impurity and optical mode lattice scattering with the appropriate warping of the valence band remains a challenge.

---

(18). A. C. Beer, J. Appl. Phys. 32, 2107 (1961)

(19). C. H. Champness, Phys. Rev. Letters 1, 439 (1958)

SUMMARY

Both theoretical calculations and experimental data are lacking in several regions where such studies should be rewarding:

1. The Hall coefficient crossover in polar semiconductors where both light and heavy electrons and holes contribute to the conduction.
2. The intrinsic or Hall coefficient crossover region where the effect of carrier lifetime and surface conditions are important for semiconductors with both light and heavy electrons and holes.
3. The effects of temperature (Θ/T) on the Hall coefficient in polar semiconductors for various degrees of degeneracy and for ionized impurity and other scattering mechanisms.
4. A determination of the light hole mobilities in InSb, GaSb, AlSb, InAs, InP, GaAs, and GaP.
5. Further studies of Group IV semiconductors, particularly high-purity silicon.
6. More detailed studies of mixed conduction in other compound semiconductors and on the understanding of the Hall coefficient factor in such materials.

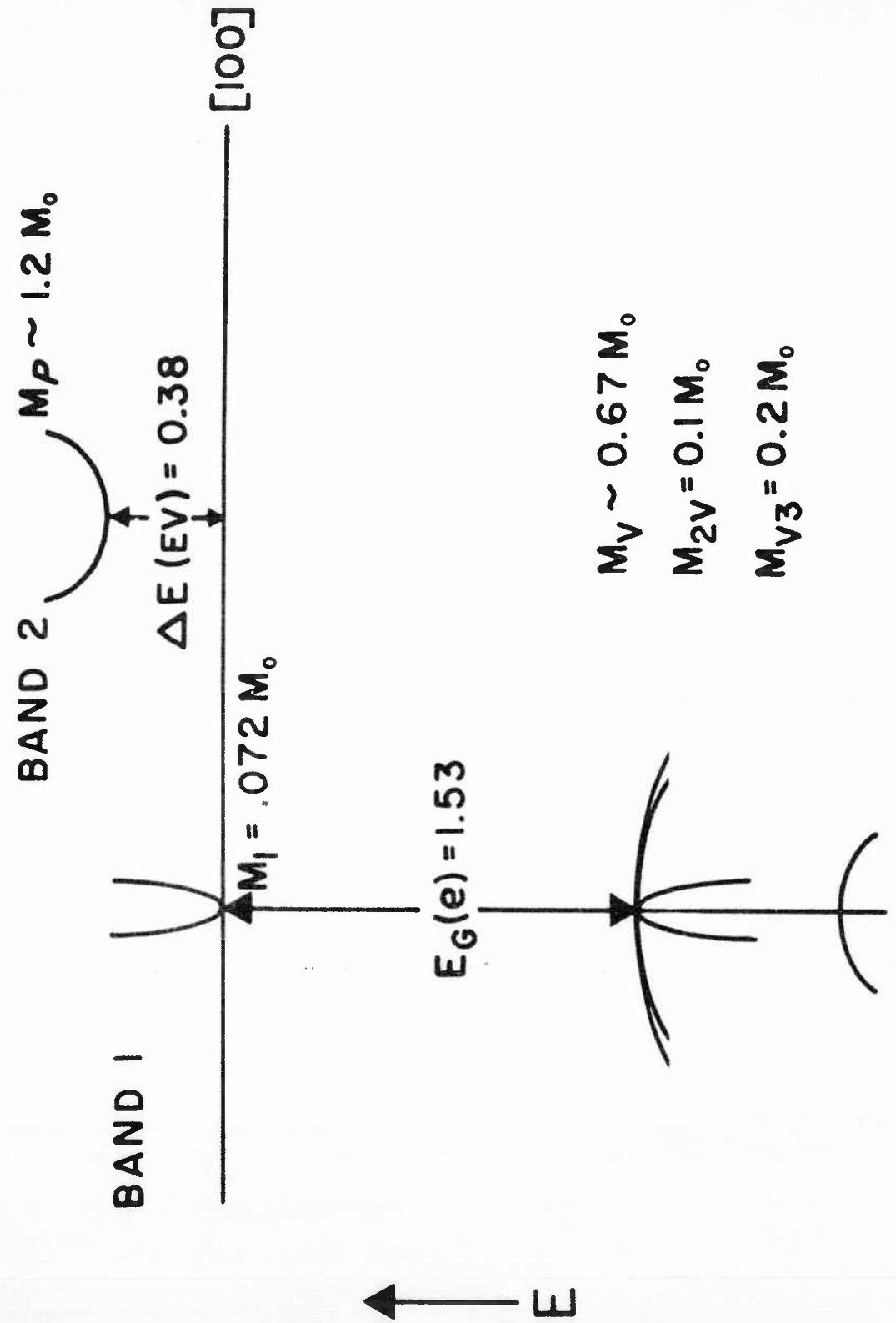

Figure 1 The band structure of GaAs.

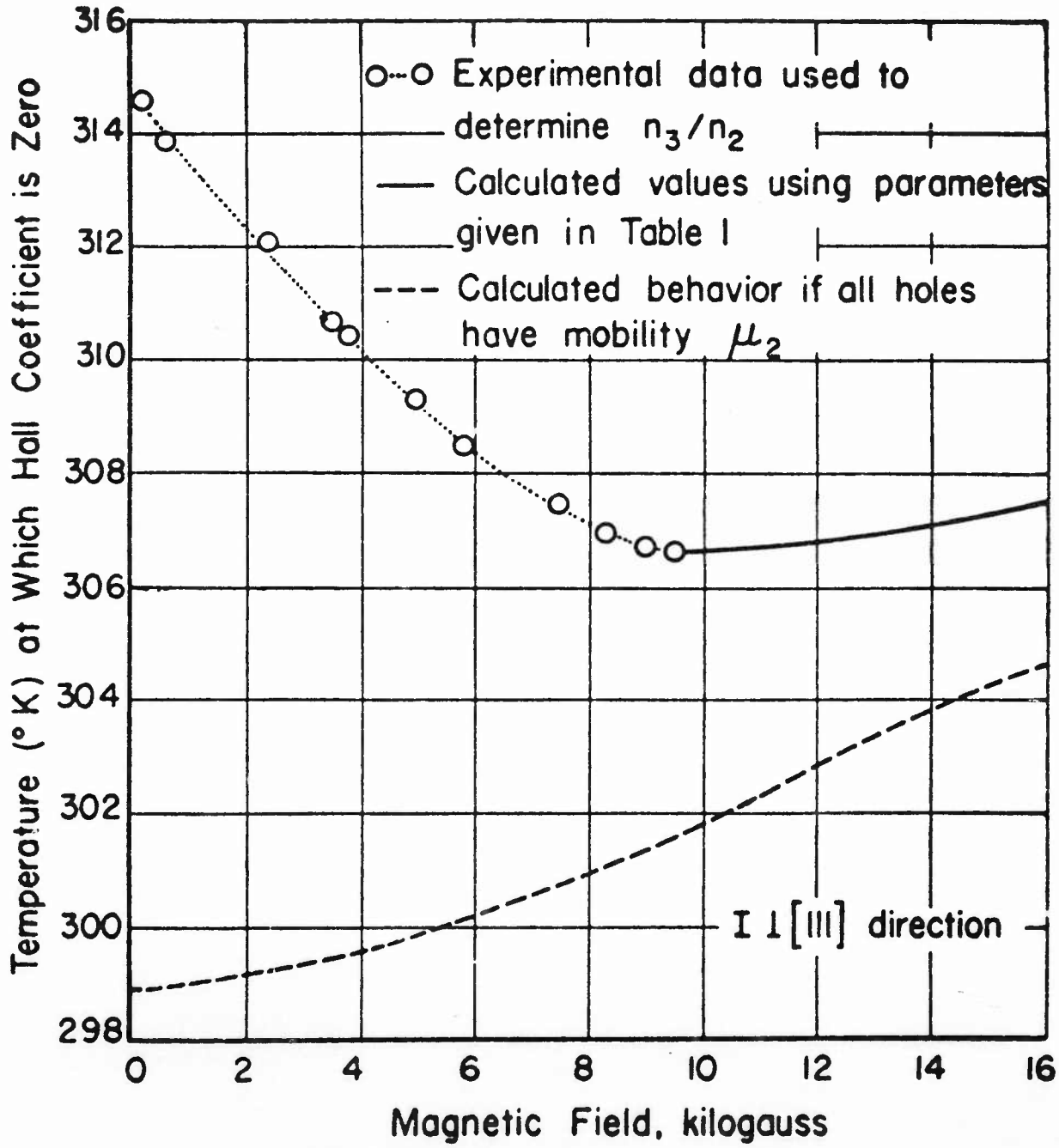

Figure 2 Hall coefficient crossover temperatures in p-type germanium as a function of magnetic field (after R. K. Willardson, T. C. Harman, and A. C. Beer[3]).

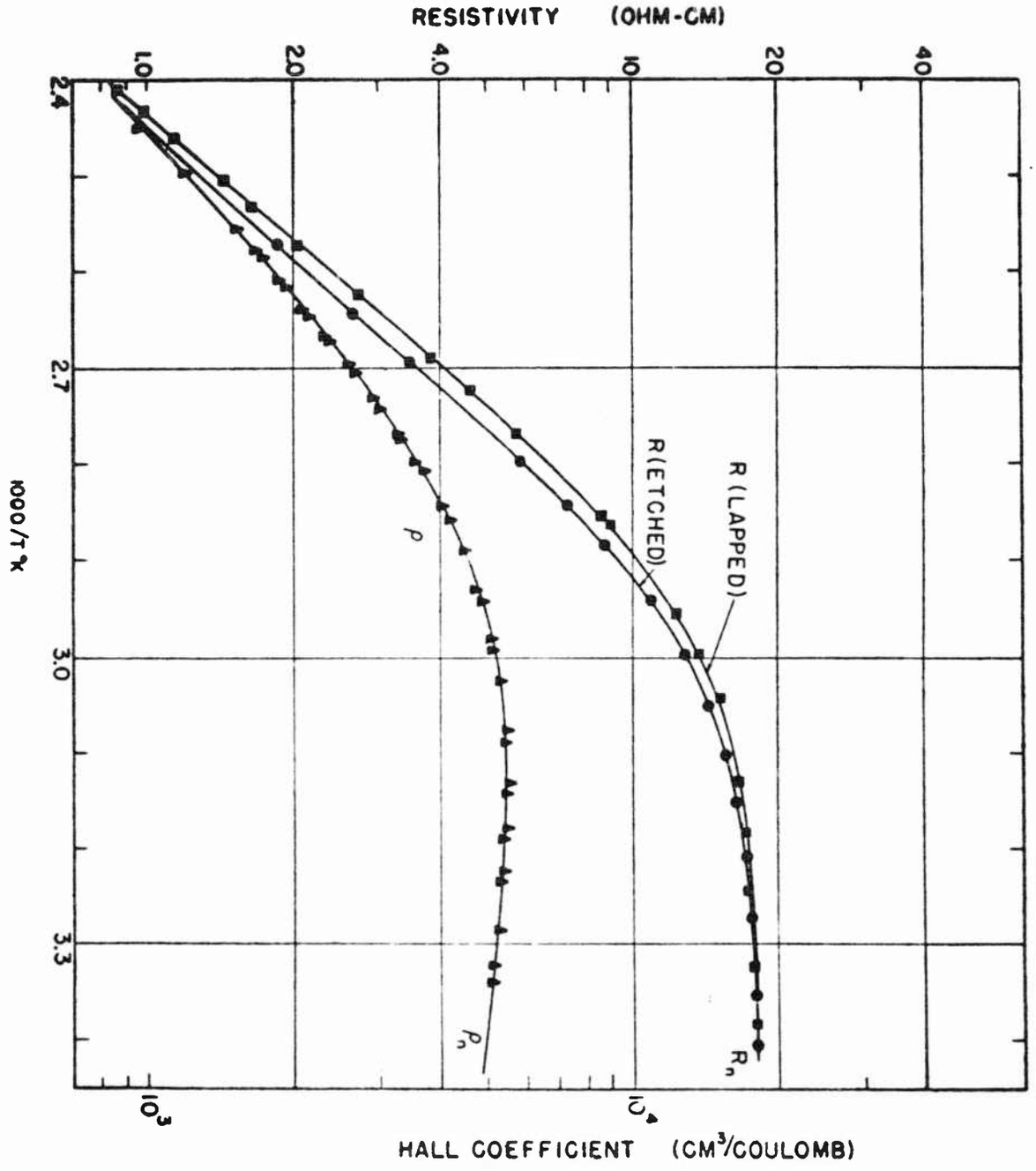

Figure 3 The Hall coefficient as a function of temperature for a sample of n-type germanium with lapped and etched surfaces (after L. P. Hunter, E. J. Huibregtse, and R. L. Anderson[8]).

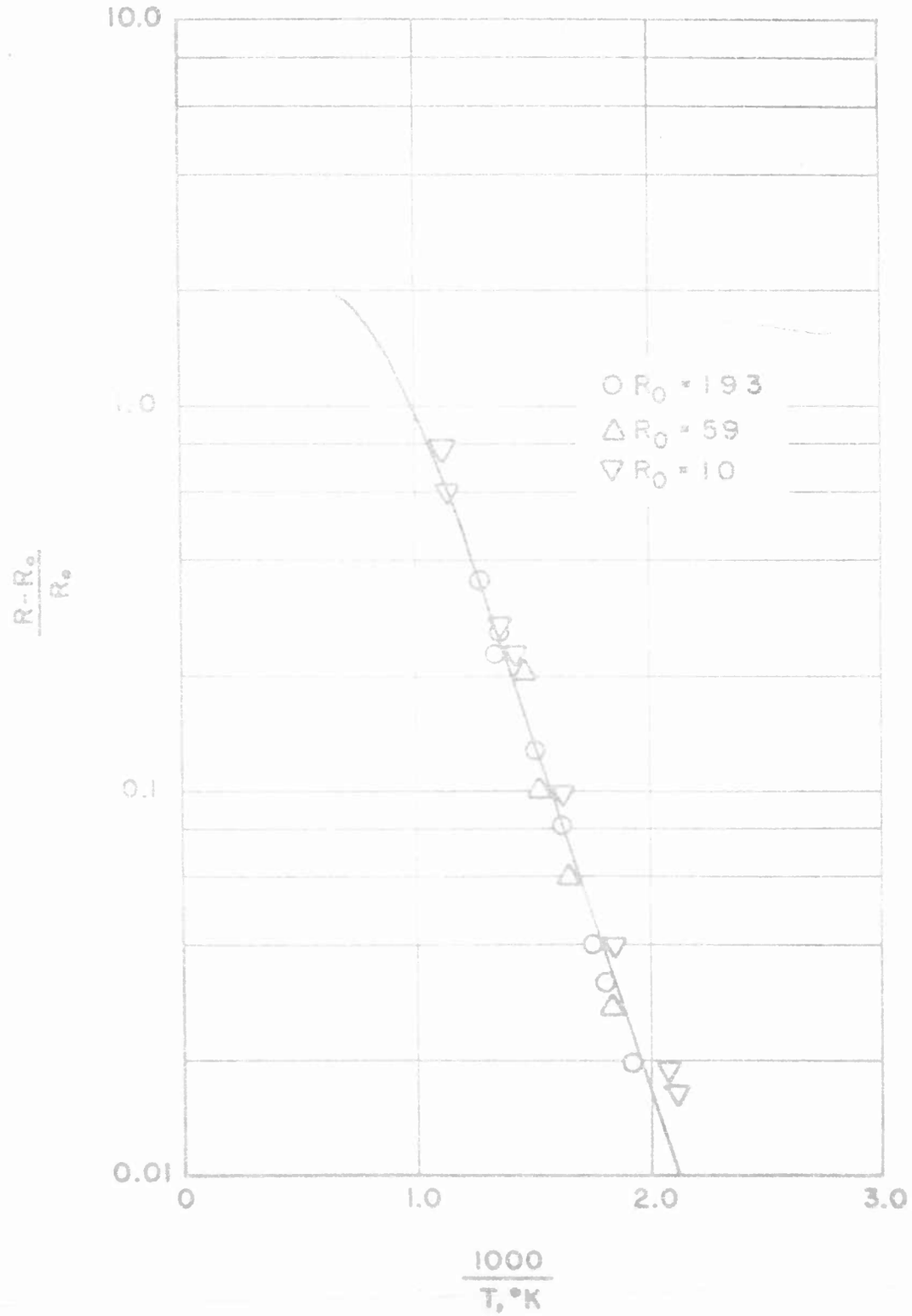

Figure 4 The fractional increase in Hall coefficient as a function of reciprocal temperature for three n-type specimens of GaAs (after L. W. Aukerman and R. K. Willardson[9]).

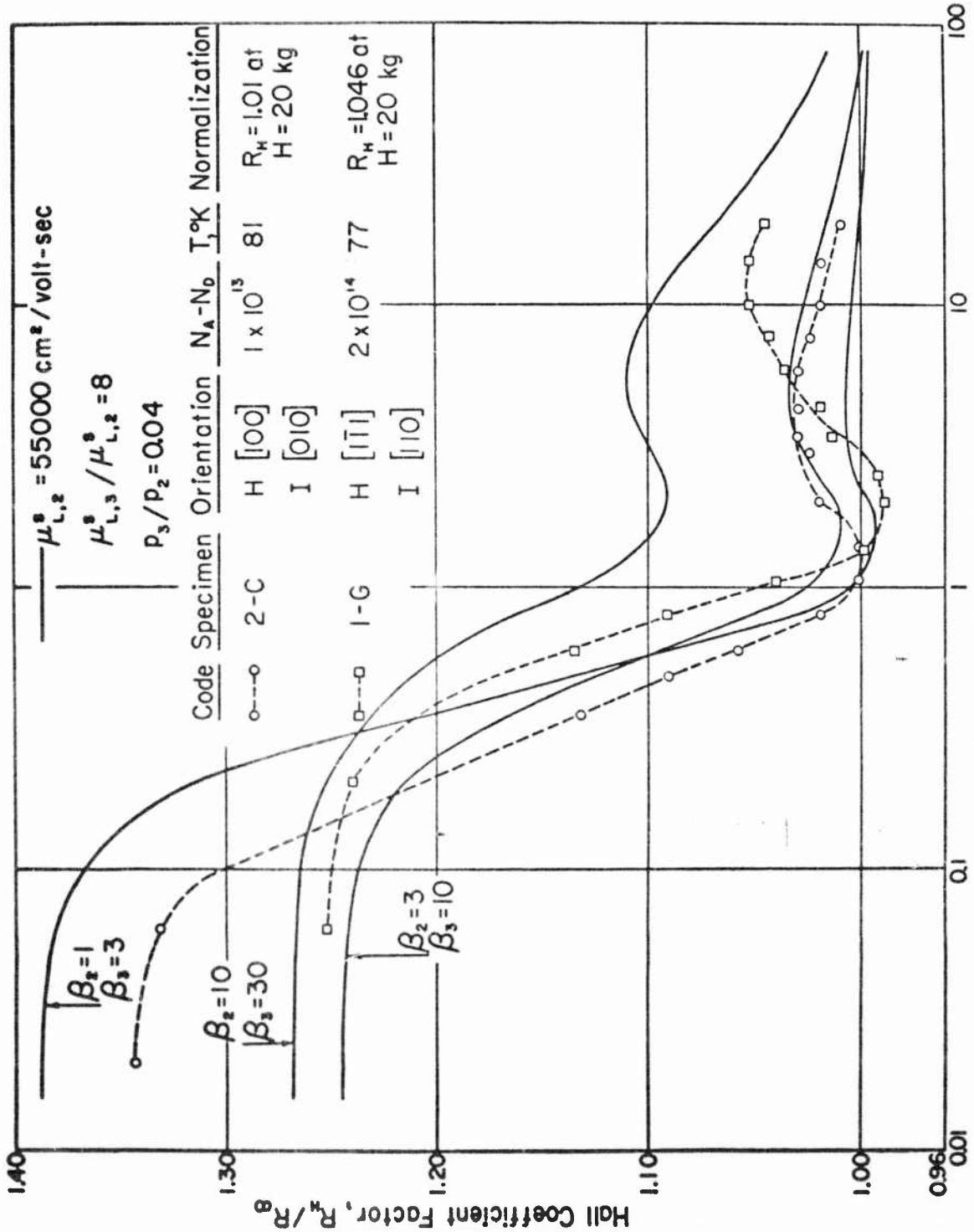

Figure 5 The Hall coefficient factor R_H/R_∞ as a function of magnetic field for a germanium sample at liquid nitrogen temperatures (after A. C. Beer and R. K. Willardson(10)).

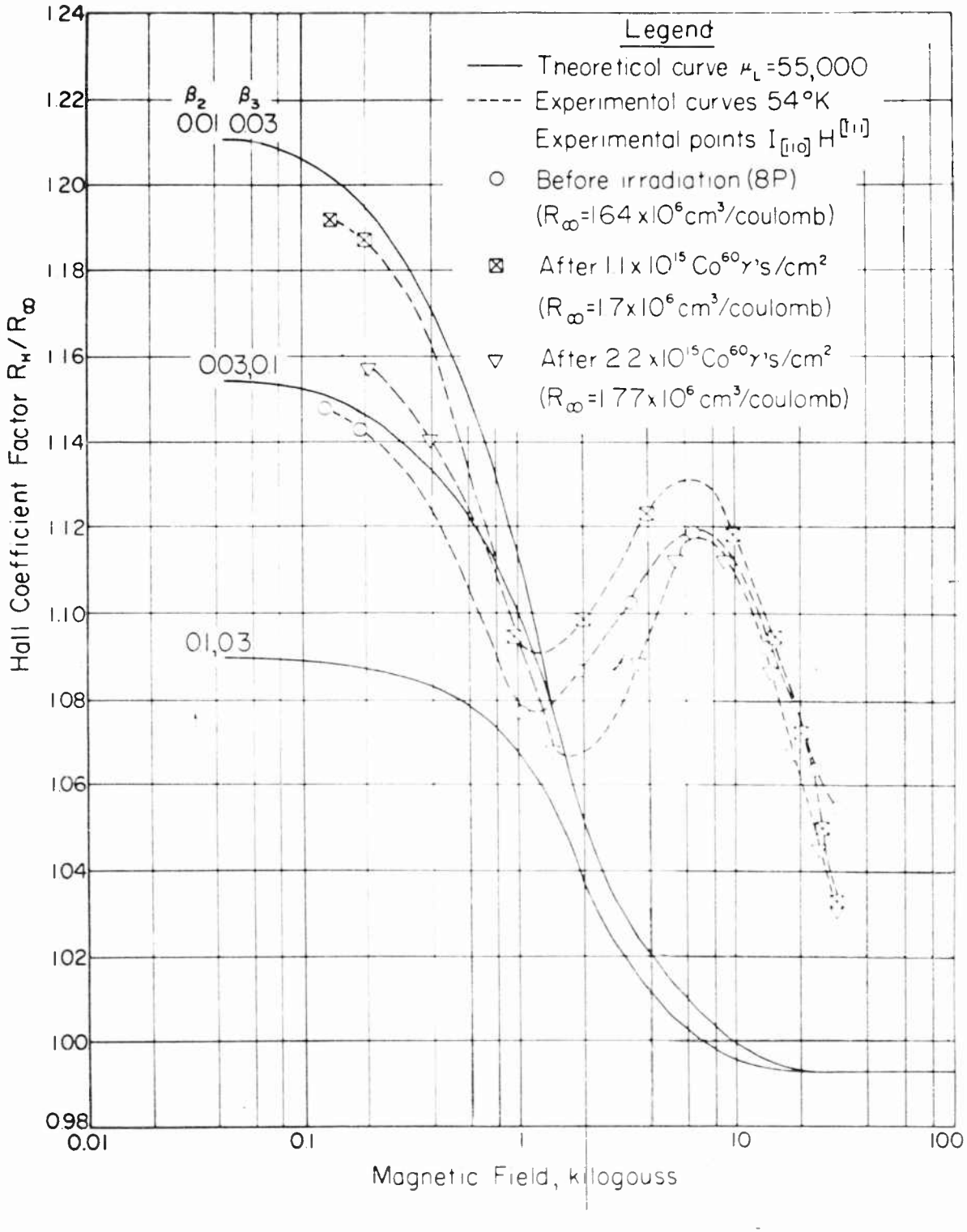

Figure 6 The magnetic field dependence of the Hall coefficient factor R_H/R_∞ in p-type silicon (after R. K. Willardson[11]).

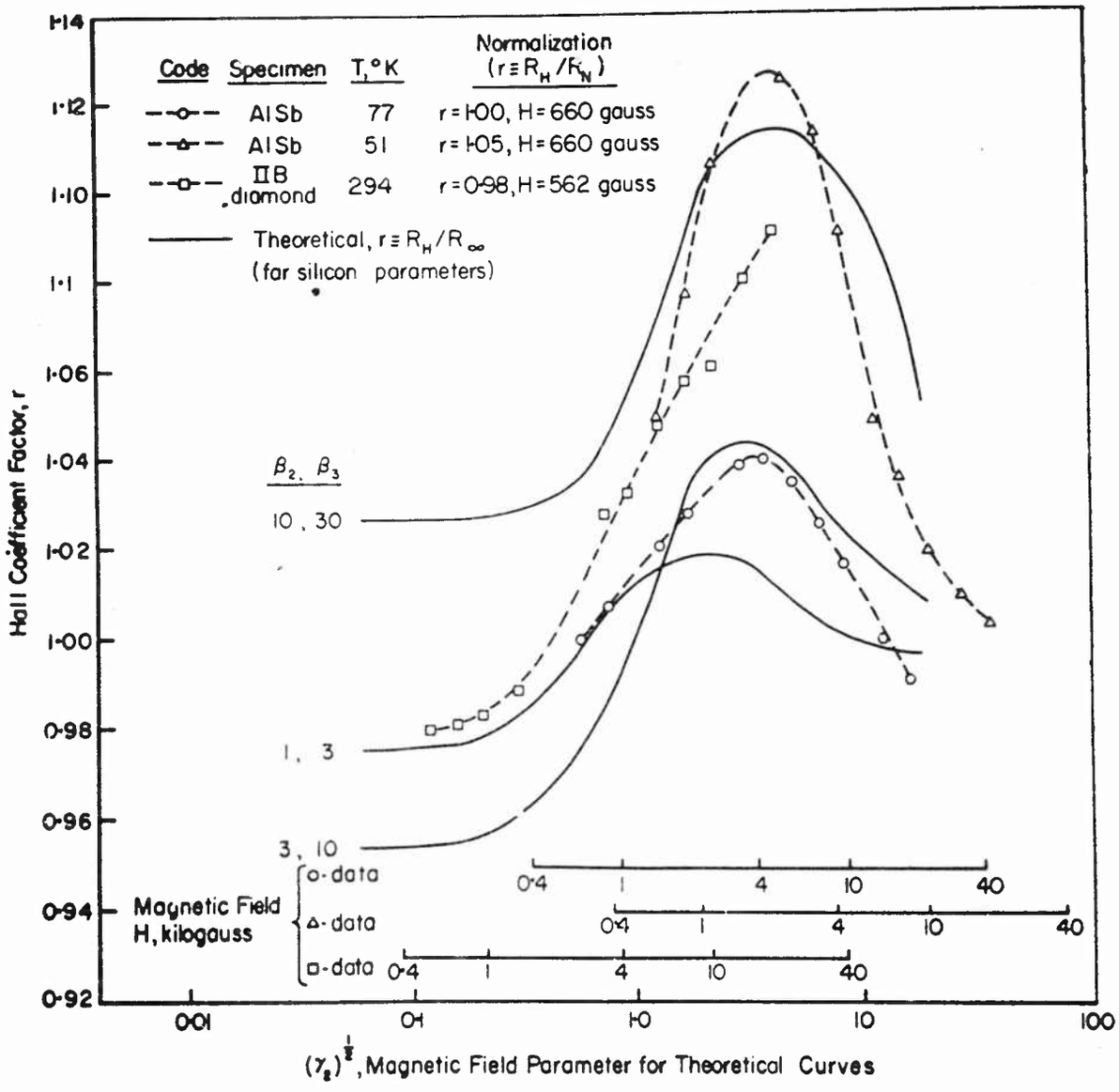

Figure 7 The magnetic field dependence of the Hall coefficient factor for p-type diamond and AlSb (after A. C. Beer[12]).

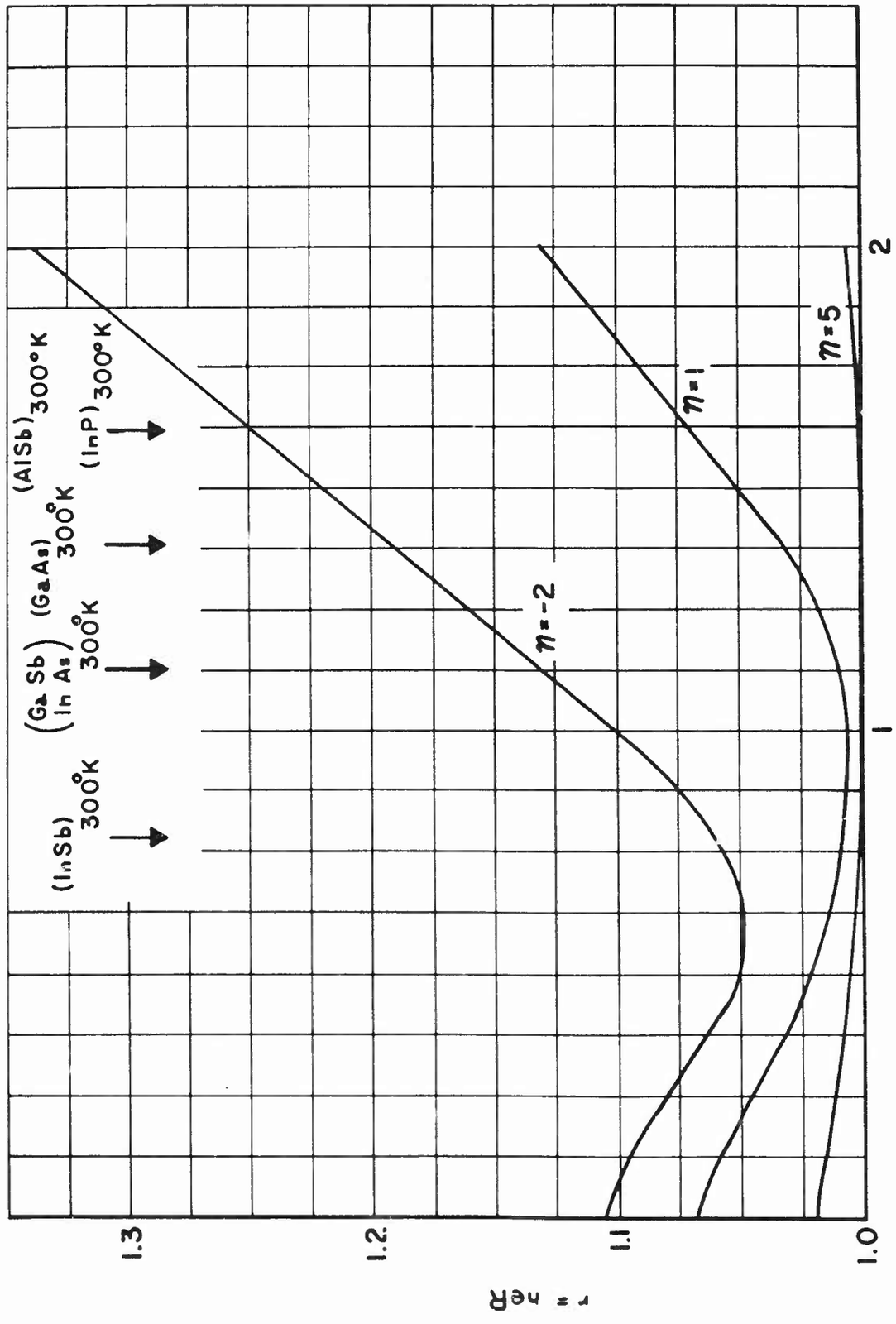

Figure 8 The dependence of the scattering factor r on temperature and degree of degeneracy when polar scattering is predominant.

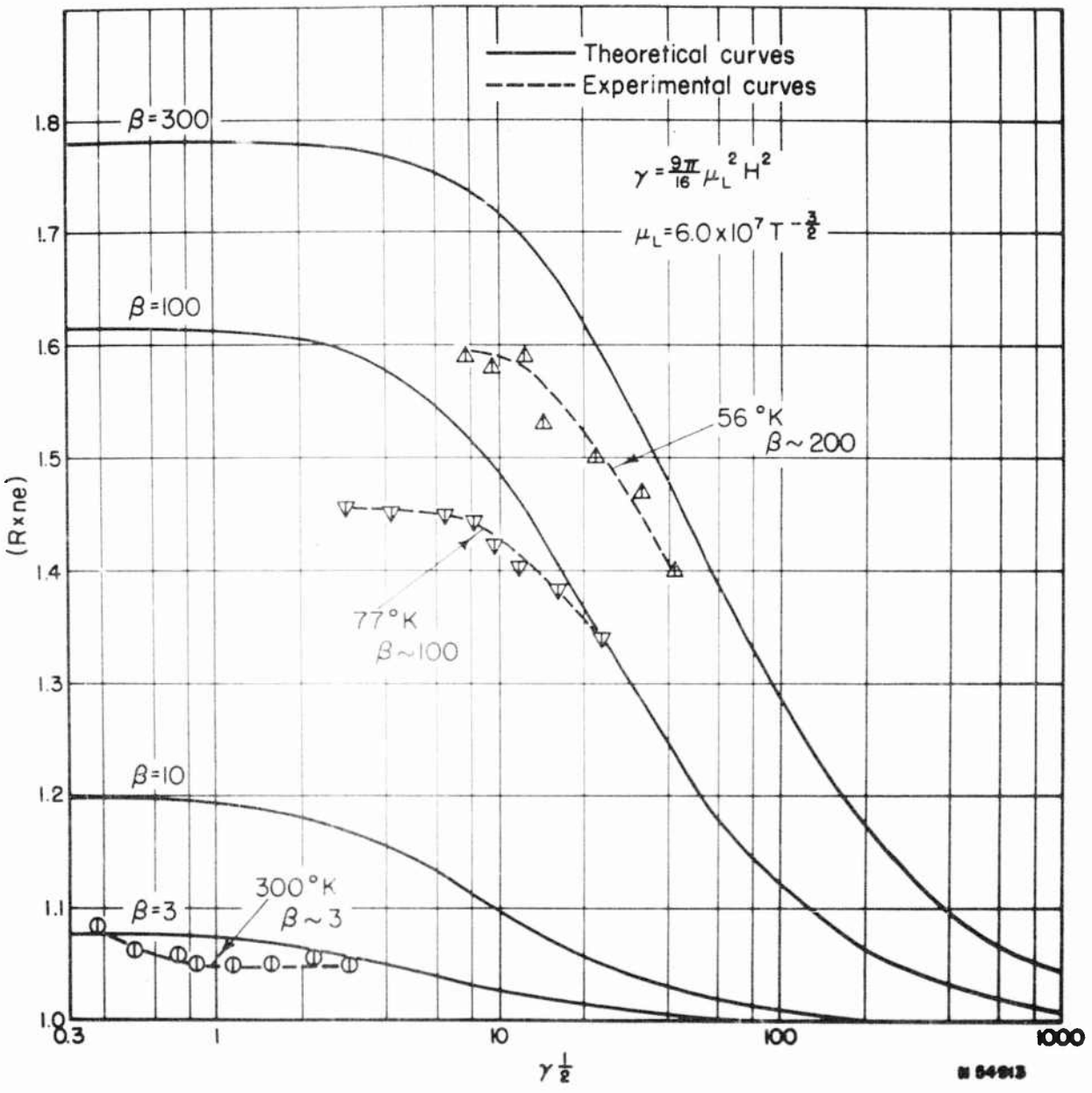

Figure 9 The magnetic field dependence of the Hall coefficient in GaAs (after R. K. Willardson and J. J. Duga[16]).

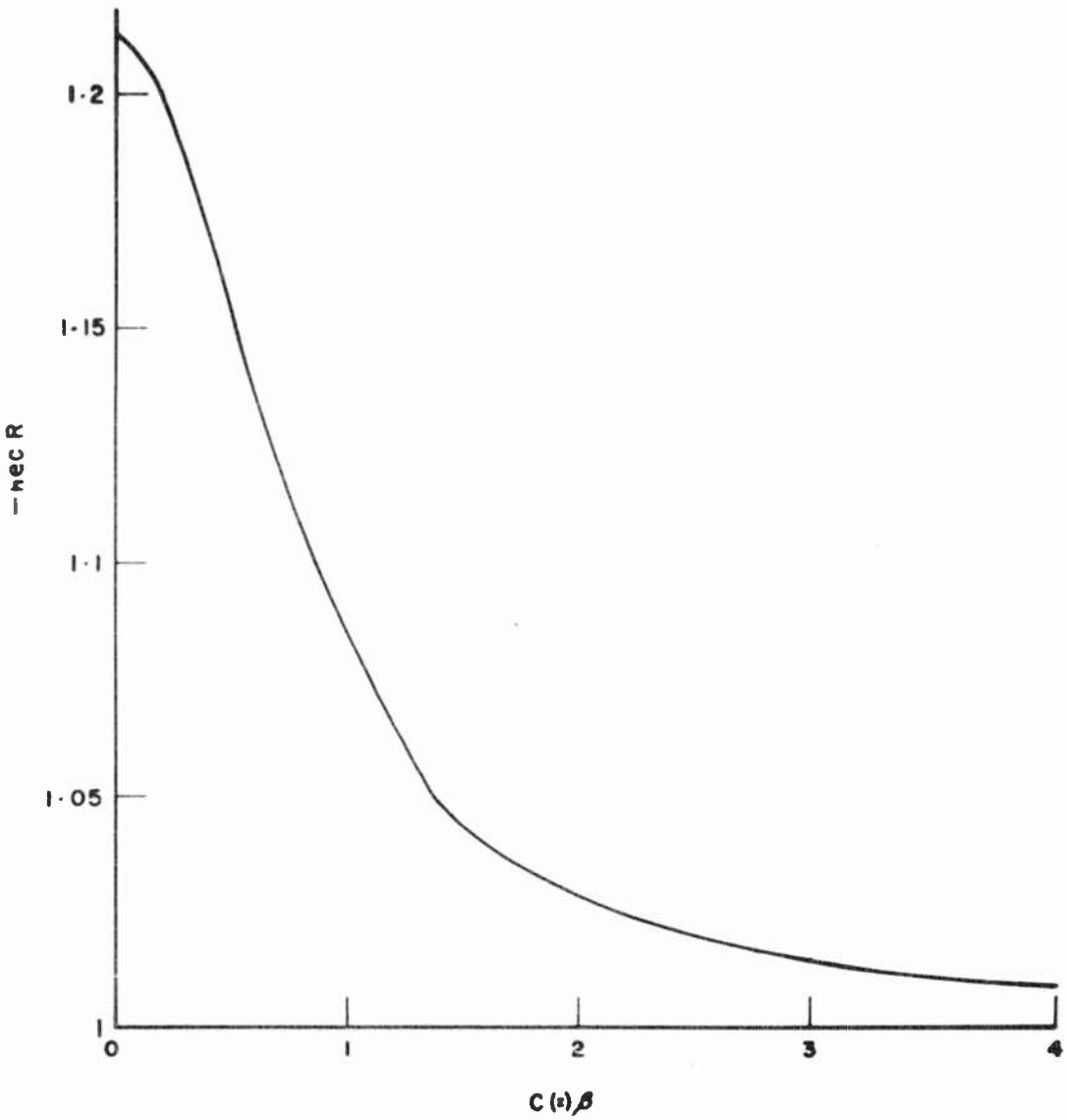

Figure 10 The magnetic field dependence of the Hall coefficient for a non-degenerate polar semiconductor at a temperature θ/3.

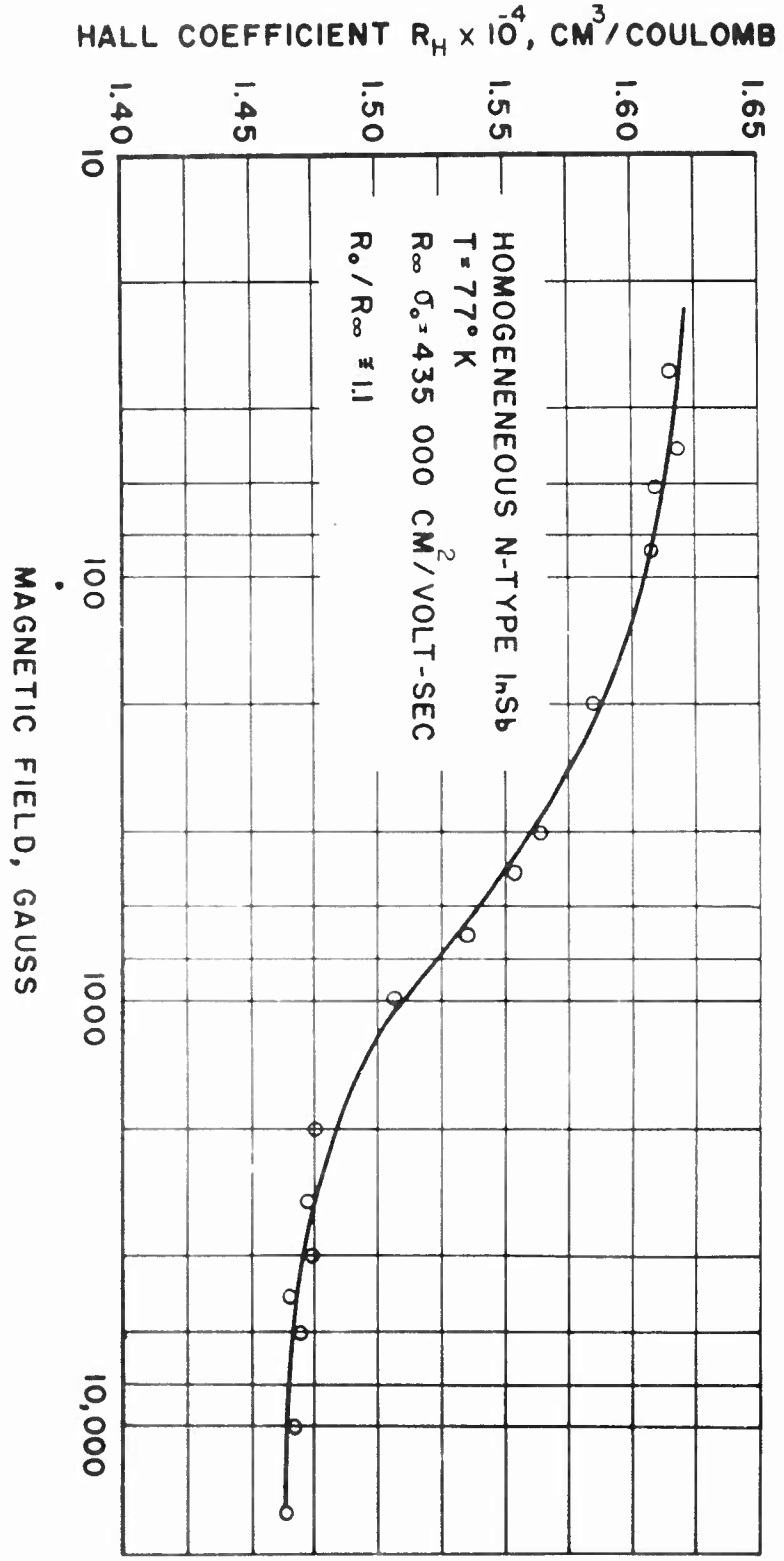

Figure 11 The magnetic field dependence of the Hall coefficient in n-type InSb (after A. C. Beer[18]).

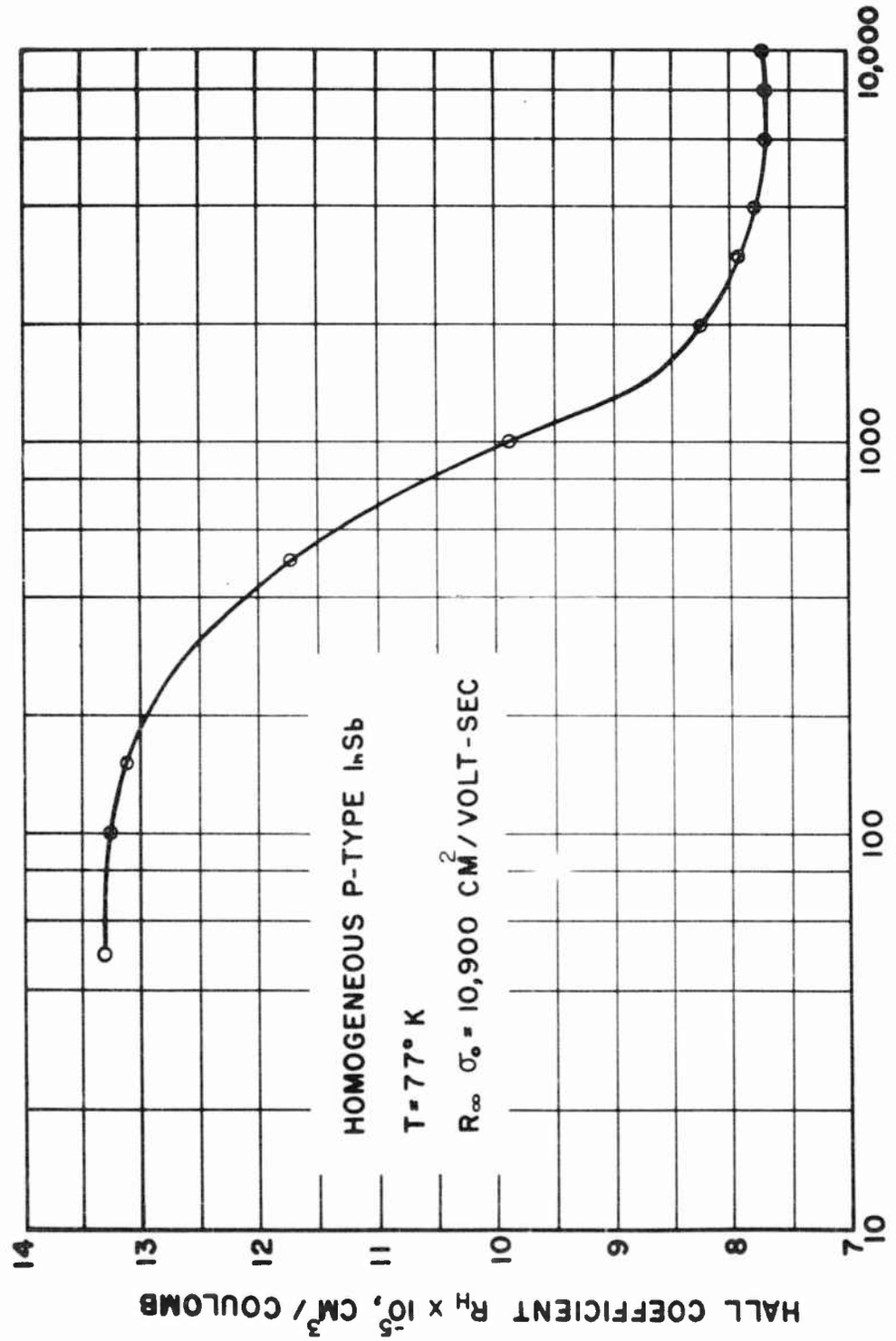

Figure 12 The magnetic field dependence of the Hall coefficient in p-type InSb.

E2. SEMICONDUCTING PROPERTIES OF $Hg_{1-x}Cd_xTe$*

by

M. D. Blue and P. W. Kruse
Honeywell Research Center, Hopkins, Minnesota

Abstract

$Hg_{1-x}Cd_xTe$ is a semiconductor having an energy gap approximately linearly dependent upon x, ranging from 1.45 eV for CdTe to 0.02 eV for HgTe[1].

Optical measurements including transmittance, photoconductivity, the photovoltaic effect, and the PEM effect, are being employed to determine the dependence of the optical gap upon composition, found by chemical analysis.

Hall and resistivity measurements are made between 4.2 and 295°K as functions of magnetic induction. Because of the large hole to electron mobility ratio, the conductivity and Hall coefficient are determined almost entirely by electrons above 200°K in the HgTe rich region. A large dependence of Hall coefficient upon magnetic field is observed.

Electrical data for a sample containing 2 per cent CdTe have been fitted in the mixed conduction region to a band model with a thermal gap of 0.025 eV. The electrical properties of the same sample after conversion from n-type to p-type (by annealing in Hg vapor) have also been measured. Estimates of electron-hole and optical mode scattering indicate these processes may limit the mobility of electrons above room temperature.

Introduction

HgTe and CdTe are semiconductors with the cubic zincblende structure. The lattice parameter is essentially constant (0.3 per cent variation) in this system[2], and the compounds form solid solutions at all compositions[1]. The energy gap varies approximately linearly with composition from a value of 1.45 eV for

---

*Work performed under Contract AF 33(616)-7901 with the Air Force Systems Command.

CdTe[3] to about 0.02 eV for HgTe[4]. The interesting electrical and optical properties of these alloys have been only partially discussed in the literature. In this brief review, we shall emphasize the electrical properties of the HgTe rich alloys.

Optical Properties

Measurements of photoconductive response and optical transmittance are used to determine the relationship of the optical energy gap to alloy composition. A Perkin-Elmer Model 112 single beam dual pass spectrometer employing a NaCl prism is being utilized over the spectral interval from 2 to 15 μ.

If we assume for the present that the energy gaps are given approximately by the point on the transmittance curves which is one per cent of the maxima found at long wavelengths, the relationship between energy gap and composition shown in Fig. 1 is obtained. The slope in this region is greater than the linear interpolation given by the solid line.

Because of the large carrier concentrations in these materials, photo-signals are often of thermal rather than photon origin, although the photo-conductive response on one alloy has been measured to beyond 15 μ[5]. The spectral response and the absorption edge of these alloys is temperature dependent. The temperature dependence of the gap for various compositions is shown in Fig. 2, including the result for CdTe as reported by Bube[3].

Galvanomagnetic Properties

The general dependence of the Hall coefficient and resistivity upon magnetic induction and temperature found in the HgTe

rich alloys is shown in Fig. 3. The small field Hall coefficients exhibit a negative maximum below room temperature. At higher magnetic fields, the Hall coefficient passes through zero to positive values at low temperatures.

This behavior, typical of many samples, parallels that found in InSb. With increasing magnetic induction the temperature of the Hall cross-over increases, and resistivity increases. The effects in InSb have been discussed by a number of authors[6-8]. Satisfactory agreement may be obtained with a theory which assumes the carrier relaxation time to be independent of energy, ignores the effect of degeneracy of the electron gas, and neglects the non-parabolic nature of the conduction band. These effects are negligible or smaller than experimental error for InSb of reasonable purity.

Although the electrical behavior of the HgCdTe alloys has many qualitative similarities to InSb, the simple theory will not fit well our experimental data. Although the variation of R_H with induction in Fig. 3 may be fitted well in some samples, a simultaneous fitting of magnetoresistance data is not possible. In addition, two Hall samples measured during the quarter exhibited negative Hall coefficients whose magnitudes at 4.2°K increased with field. Such behavior in InSb has been found by Bate et al.[9] to be related to internal p-n junctions.

An example of the effects of annealing is shown in Figs. 4 and 5. This specimen, originally p-type, exhibited an n-type Hall coefficient after an 18-hour anneal in Hg vapor at 240°C.

The thermal gap in this sample, estimated from the slope of a np/T^3 plot, is 0.025 eV. Because of the very large free hole density in the p-type sample, the Fermi level may be located by the relation[10]

$$p_o = N_V(T)\ F_{1/2}(\eta)\ . \qquad (1)$$

The hole mass was chosen to be 0.4 m_o by analogy to CdTe[11,12].

A non-parabolic conduction band is indicated by experiment and by analogy to the III-V compounds. We have used the k·p conduction band[13] with a mass of 0.014 m_o to fit the data at room temperature. (If a value of m_e appropriate to the gap were chosen, m_h would be required to be over four times the free electron mass.) This value of m_e agrees with the value found by Rodot at low temperatures[14].

Figure 6 shows the variation of the Fermi level over the calculated temperature range. In the p-type sample, the Fermi level was arbitrarily arrested when it penetrated 2kT into the valence band to simulate the effect of the large acceptor density. The "n-type" sample is also p-type, with a negative Hall coefficient resulting from the high electron mobility.

Electron Mobility

Figure 6 shows the Hall mobility of the "n-type" sample, and the electron mobility calculated to fit to the p-type data of Figs. 3 and 4 using the band model described previously. The steep rise at low temperatures (p-type) is required to fit the Hall zero, but would not occur if the temperature dependence of the gap shown in Fig. 2 were included in the calculation. The

increase in room temperature mobility after annealing is due to the reduction of impurity scattering. The higher value of room temperature mobility agrees with the results of Rodot[14] and Lawson[15] for HgTe. At lower temperatures, mobility is limited by impurity scattering. For the large acceptor concentrations in these samples, the Brooks-Herring formula is no longer suitable for calculating mobilities. This difficulty is related to the dielectric constant approximation and the degree of ionic bonding[16,17].

The mobilities for electron-hole[18] and optical mode polar scattering[19] calculated for this alloy are also shown in Fig. 6. The optical mode temperature (190°K) and the effective charge for scattering (0.08 e_o) were calculated from the few measurements reported for these compounds[12,20,21]. The trend of mobility for constant mass is shown by the dotted lines. The solid lines include the effect of the non-parabolic band obtained by weighting the proper function of the mass of each state by the function of electrons in that state. The combined mobilities agree most satisfactorily with experiment in view of the necessary approximations and suggest that these mechanisms may limit the mobility at room temperature and above in the HgTe rich alloys.

Summary

The effects of anneals on the electrical properties and the general tendency toward positive Hall coefficients at high magnetic fields and low temperatures suggests that deviations from stoichiometry are limitations to purity in the HgTe rich

region. Our data indicate a decreasing residual free hole concentration as the CdTe content is increased. It appears likely that with addition of HgTe to CdTe, the maximum melting point of the ternary deviates from that of a nearly stoichiometric composition. The composition at the maximum melting point will accommodate increasing concentrations of interstitial tellurium, mercury or cadmium atoms on tellurium sites, or mercury or cadmium vacancies. All of these defects should act as acceptors. At low temperatures, the high residual free hole concentrations should result in the formation of an impurity band. The low values of hole mobility found in these alloys (60 cm^2/volt sec in Fig. 4) are much lower than the values found in CdTe below room temperature[12]. The excess acceptor concentration can be partially reduced by annealing as shown in Figs. 4 and 5. However, the annealed samples still behave as mixed conductors (as in Fig. 3), in agreement with the results found for the position of the Fermi level in Fig. 6.

We shall defer further consideration of such topics as optical absorption, material preparation, and band structure. However, the preceding discussion will illustrate the complexity of the electrical properties of the alloys and their interrelation with the thermochemical properties.

REFERENCES

1. W. D. Lawson et al., J. Phys. Chem. Solids 9, 325 (1959).
2. J. C. Wooley and B. Ray, J. Phys. Chem. Solids 13, 151 (1960).
3. R. H. Bube, Phys. Rev. 98, 431 (1955).
4. T. C. Harmon et al., J. Phys. Chem. Solids 7, 228 (1958); J. Black et al., J. Electrochem. Soc. 105, 723 (1958); R. O. Carlson, Phys. Rev. 111, 476 (1958).
5. P. W. Kruse et al., Infrared Physics 2, 53 (1962).
6. C. Hilsum and R. Barrie, Proc. Phys. Soc. B71, 676 (1958).
7. D. J. Howarth et al., Proc. Phys. Soc. 70, 124 (1957).
8. H. P. R. Frederikse and W. R. Hosler, Phys. Rev. 108, 1136 (1957).
9. R. T. Bate et al., J. Appl. Phys. 32, 806 (1961).
10. J. S. Blakemore, Semiconductor Statistics (Pergamon, 1962).
11. F. A. Kröger and D. de Nobel, J. Electronics 1, 190 (1955).
12. S. Yamada, J. Phys. Soc. Japan 15, 1940 (1960).
13. E. O. Kane, J. Phys. Chem. Solids 1, 249 (1957).
14. M. Rodot et al., J. Appl. Phys. 32, 2254 (1961).
15. W. D. Lawson et al., J. Phys. Chem. Solids 9, 325 (1959).
16. L. Stelbans, J. Phys. Chem. Solids 8, 123 (1959).
17. R. J. Cherry and J. W. Allen, J. Phys. Chem. Solids 23, 163 (1962).
18. F. J. Morin and J. P. Maita, Phys. Rev. 94, 1525 (1954).
19. H. Ehrenreich, J. Phys. Chem. Solids 8, 130 (1959).
20. A. Mitsuishi et al., J. Phys. Soc. Japan 13, 1235 (1958).
21. T. C. Harman et al., Phys. Rev. Lett. 7, 403 (1961).

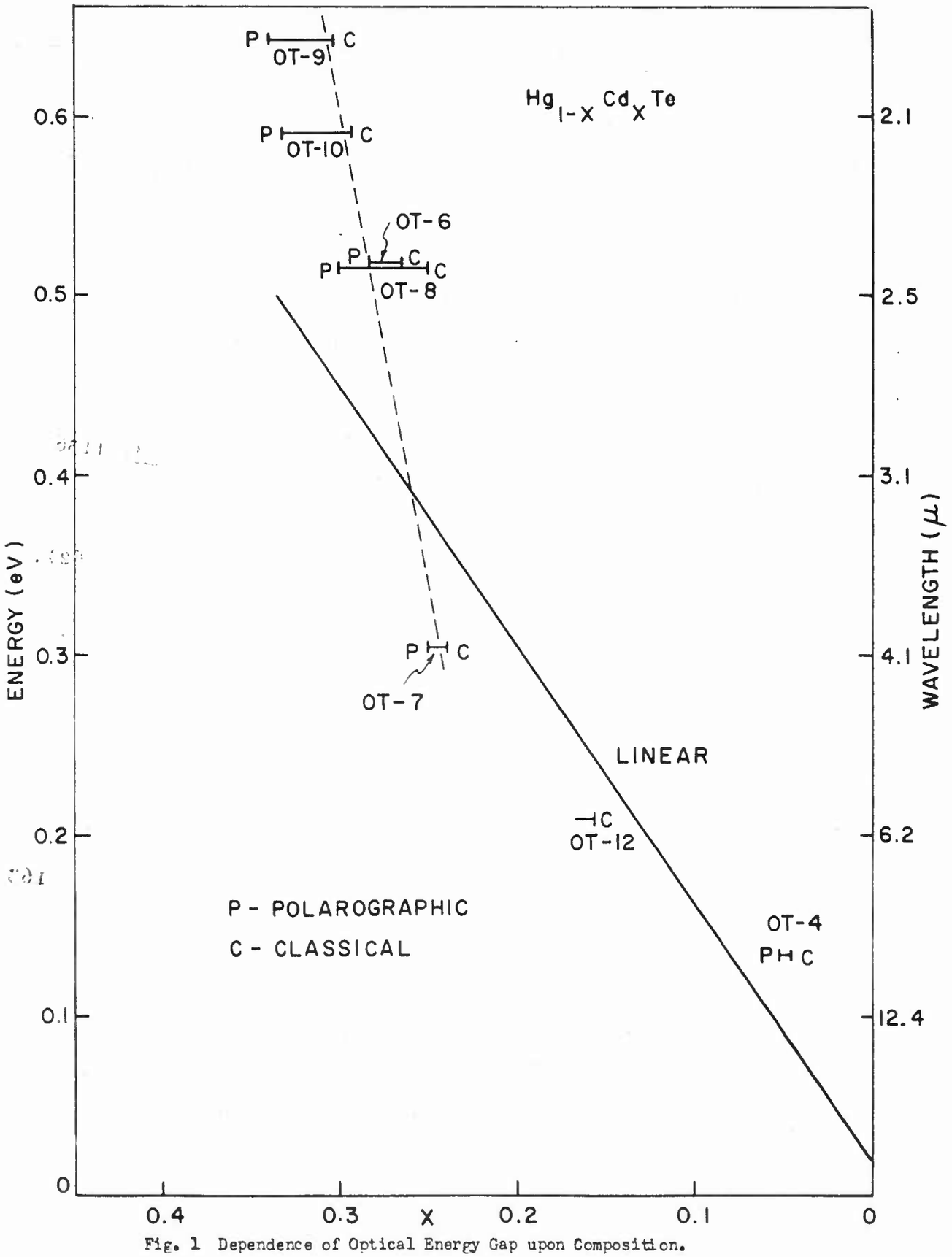

Fig. 1 Dependence of Optical Energy Gap upon Composition.

P and C refer to chemical techniques of sample analysis.

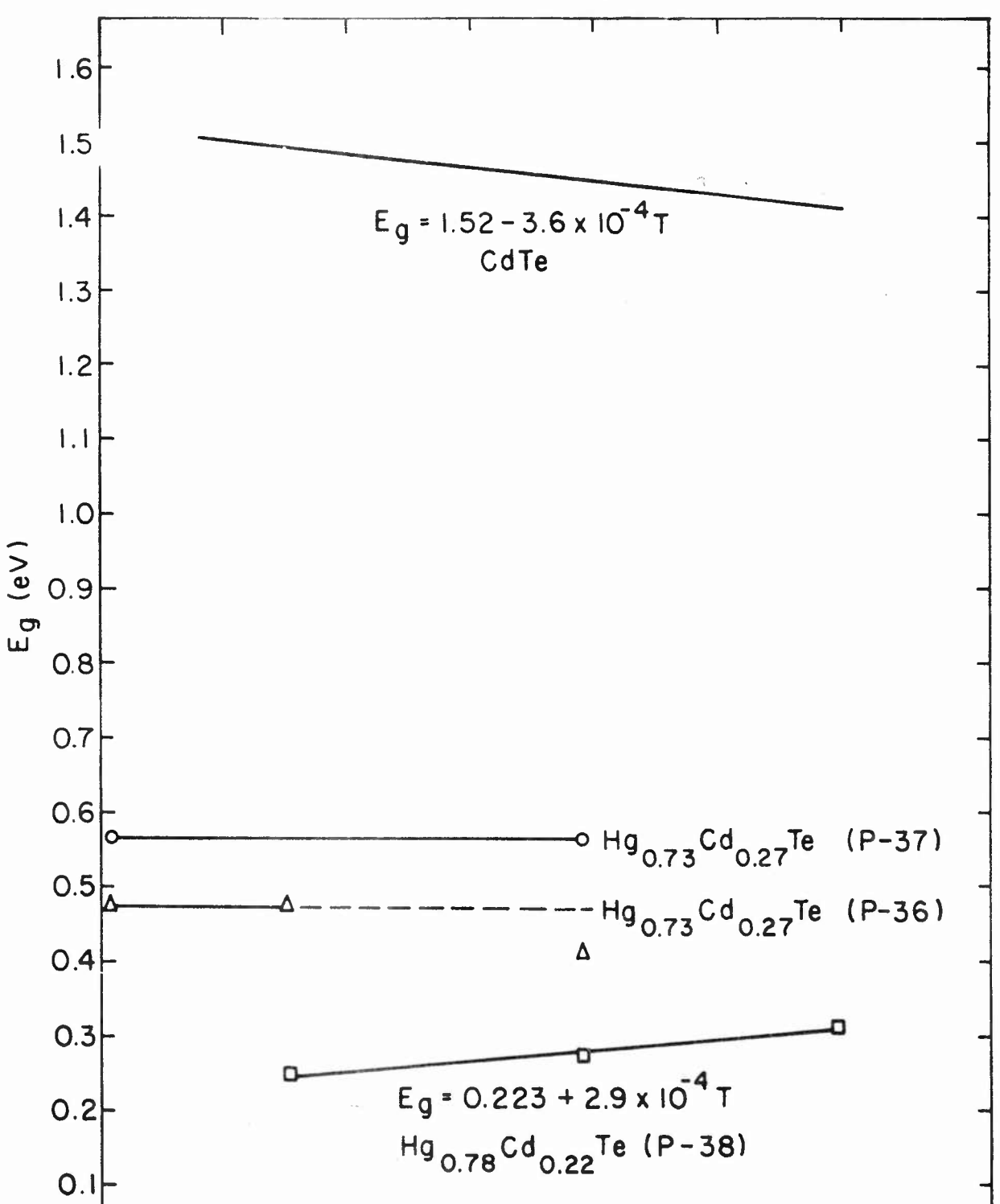

Fig. 2 Temperature Dependence of the Energy Gap.

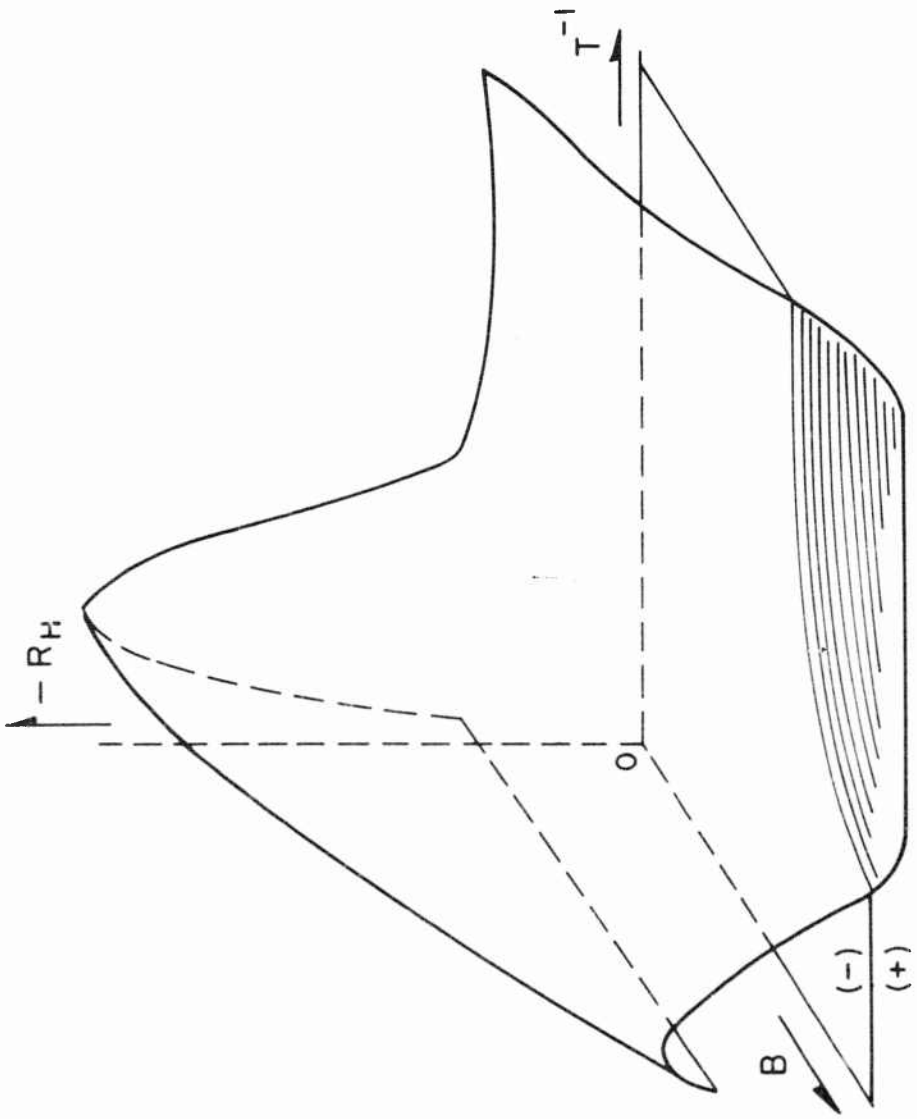

Fig. 3 Dependence of the Hall Coefficient of HgTe Rich Alloys upon Magnetic Induction and Temperature.

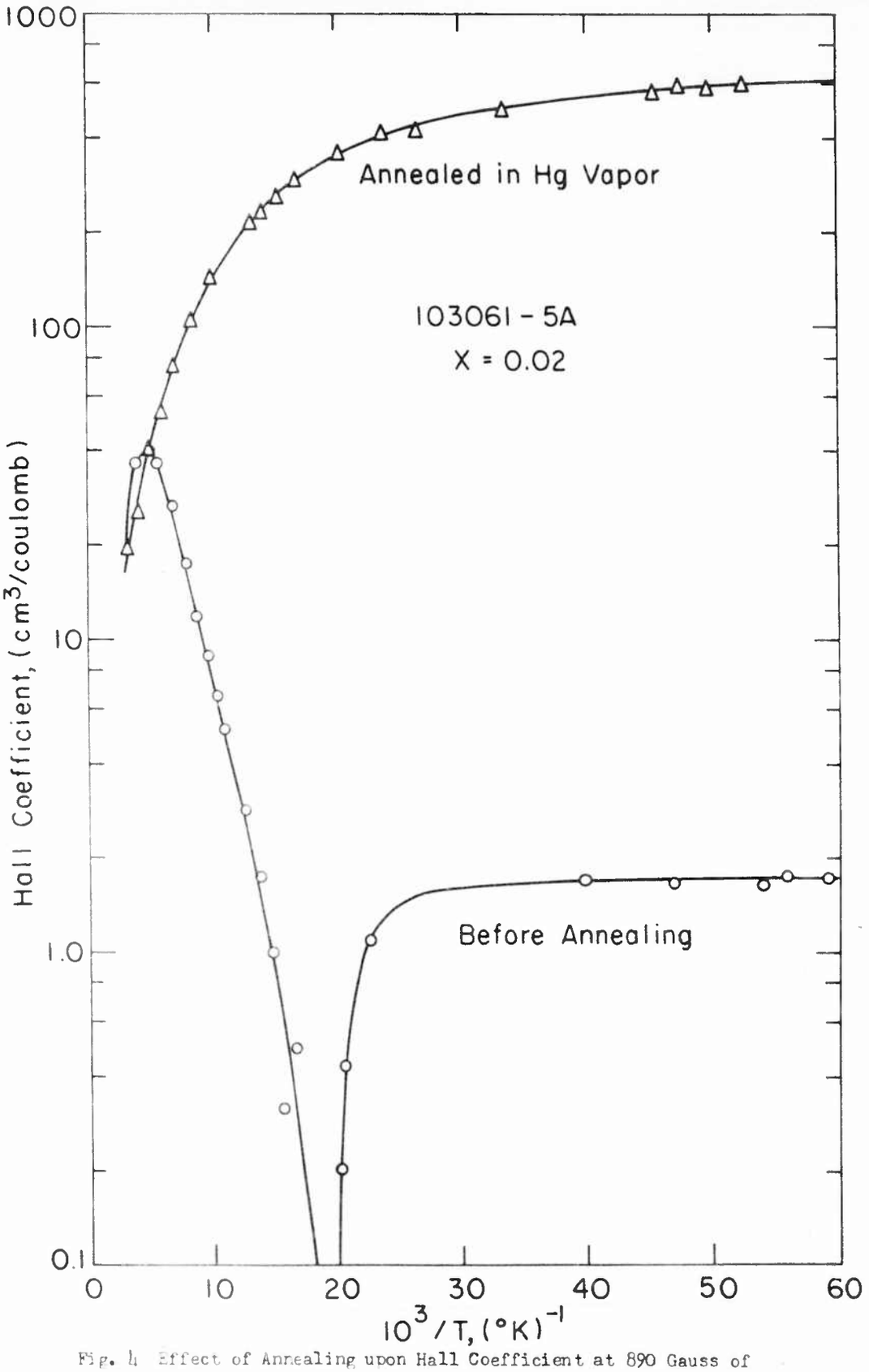

Fig. 4 Effect of Annealing upon Hall Coefficient at 890 Gauss of $Hg_{0.98}Cd_{0.02}Te$.

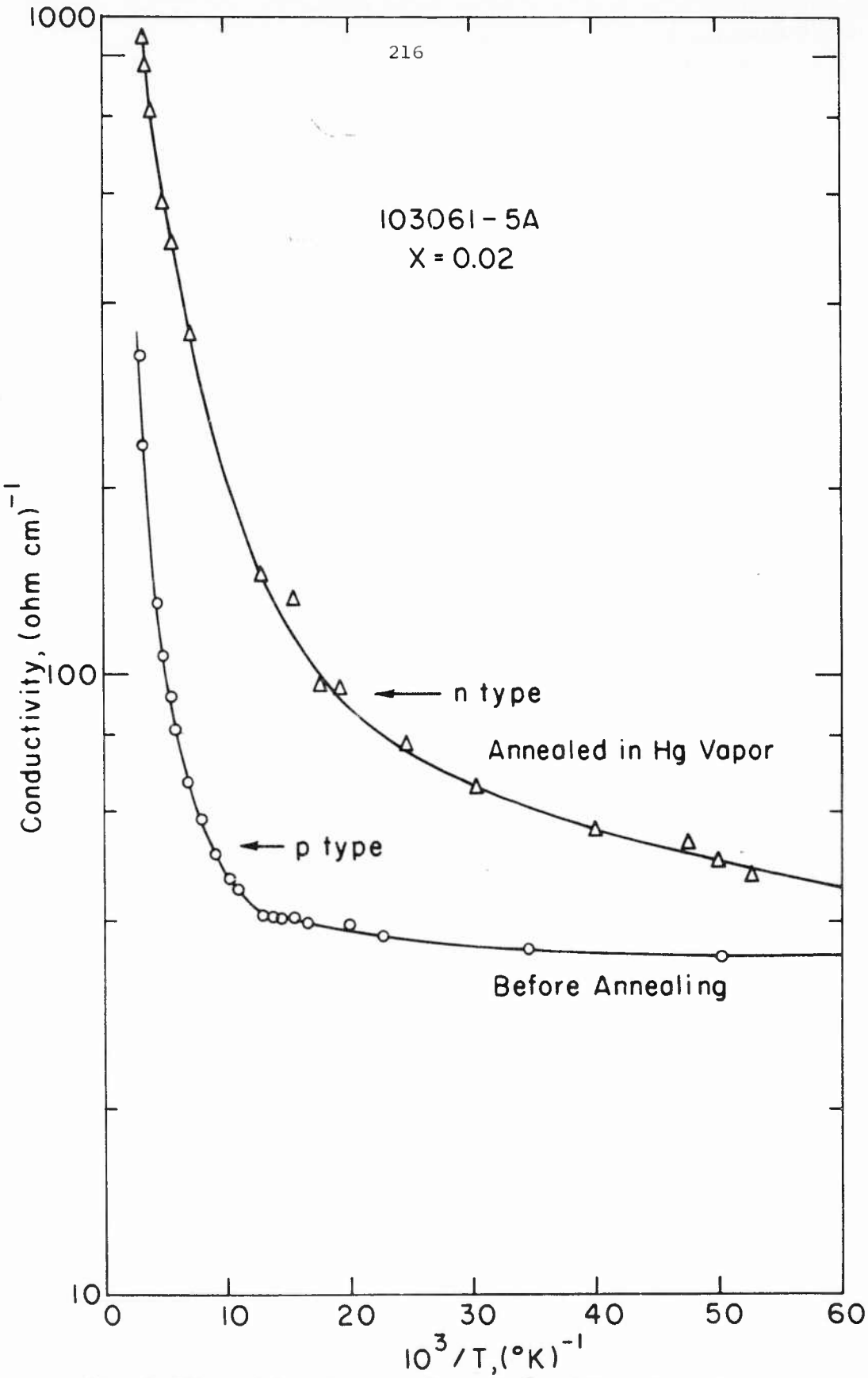

Fig. 5 Effect of Annealing upon Conductivity of $Hg_{0.98}Cd_{0.02}Te$.

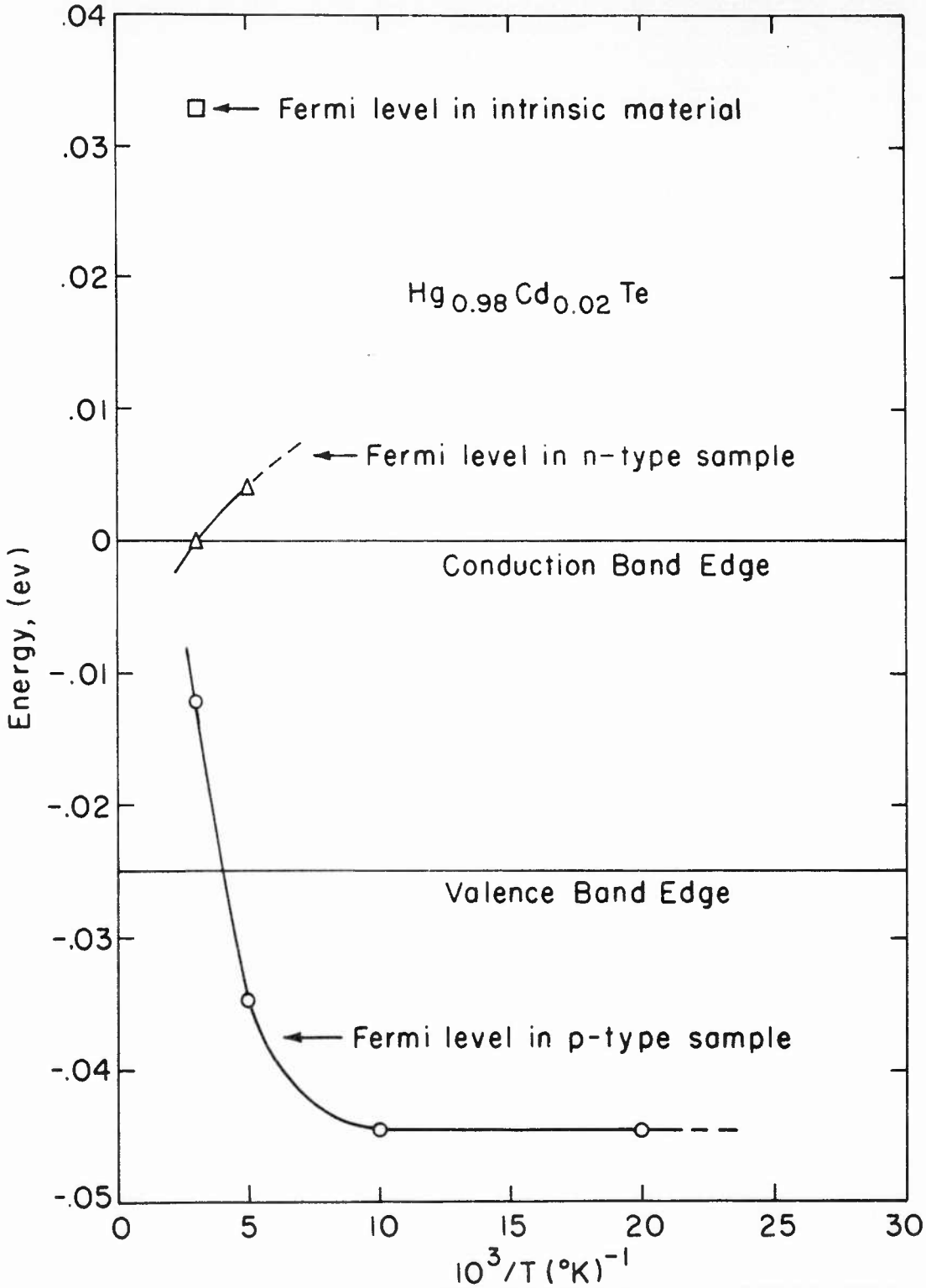

Fig. 6 Temperature Dependence of Fermi Level in $Hg_{0.98}Cd_{0.02}Te$.

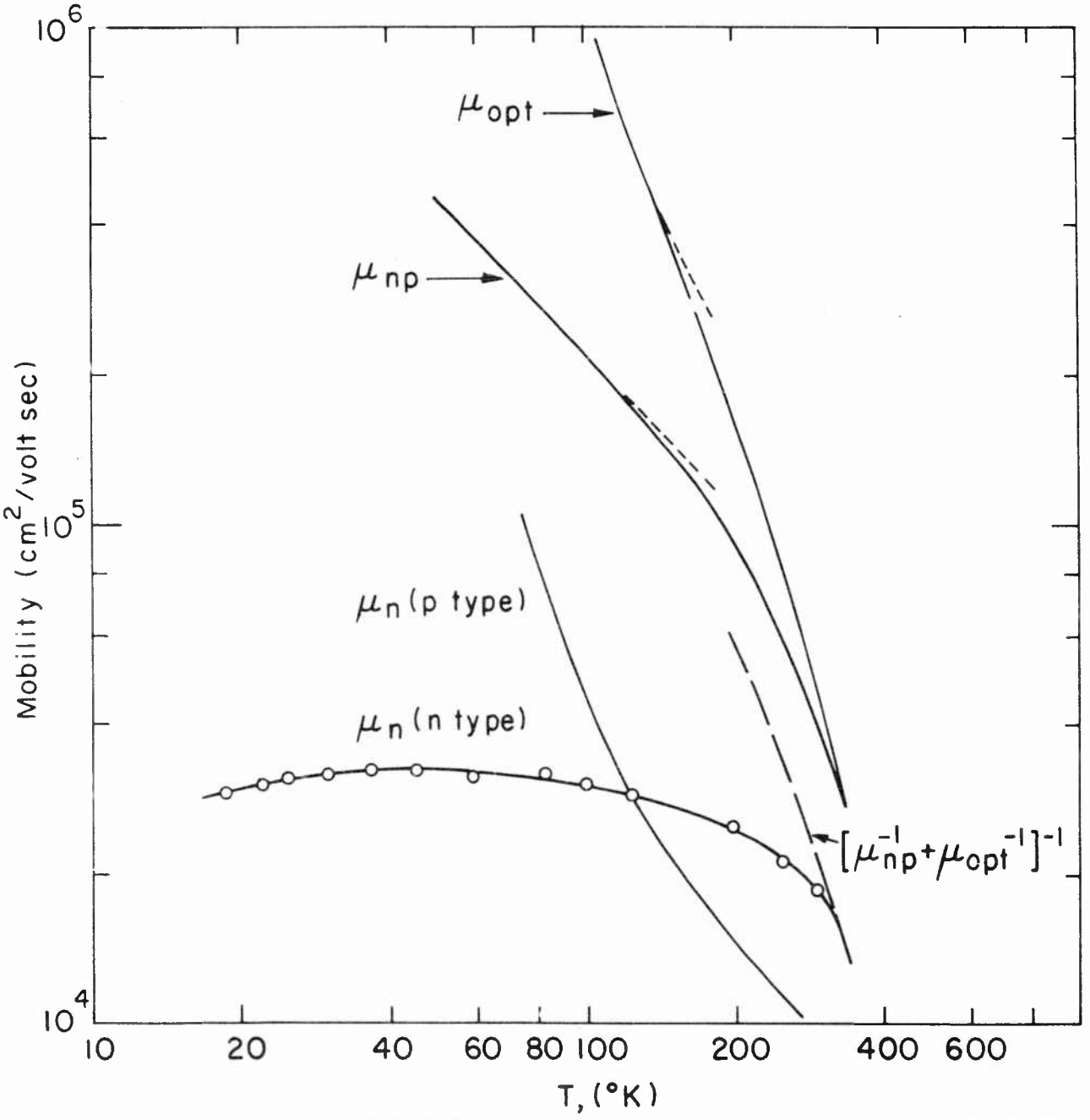

Fig. 7 Temperature Dependence of Electron Mobility of $Hg_{0.98}Cd_{0.02}Te$.

E3. DYE-SENSITIZED PHOTOCONDUCTIVITY OF ZINC-OXIDE FILMS*

by

L. I. Grossweiner and S. J. Dudkowski
Department of Physics
Illinois Institute of Technology

INTRODUCTION

Electronic processes in solids can be sensitized to wavelengths longer than the fundamental absorption of the host crystal by the presence of light absorbing additives, either on the surface or in the bulk. Putseiko and Terenin[1] have reported the sensitization of zinc oxide photoconductivity by adsorbed eosin dye. This paper reports the current progress of a further investigation of the kinetics and mechanism of this process on zinc oxide thin films. The results are interpreted by an elementary model which is consistent with the qualitative knowledge of photoprocesses in pure zinc oxide and eosin films.

EXPERIMENTAL DETAILS

Zinc oxide films in the form of 1.3 cm diameter discs were prepared by evaporating zinc (spectroscopic grade, Jarrell-Ash Co.) on flat glass plates which had been flashed with copper to improve adhesion. The zinc films were heated in air to produce ZnO and then two gold electrodes were evaporated on each film near the circumference. The film thickness was estimated as 800 to 1000 Å by evaporating silver over a representative film and

*Work supported by the U. S. Atomic Energy Commission.

its glass substrate and measuring the step height with two-beam interferometry. Eosin (National Aniline, C.I. No. 768) was adsorbed on the zinc oxide film by heating the film to 600°K at 10^{-5} mm Hg for 12 hours, cooling, and admitting an air-free ethanolic solution of the dye. Excess dye was removed from the electrode area. The surface conductivity of the zinc oxide film was investigated, where one face of the film was on the glass substrate and the other was partially covered with adsorbed dye.

A 30-watt tungsten filament lamp with a Corning C.S. No. 4-64 filter was the irradiation source for the eosin layer (eosin light), and an Osram HBO 109 mercury-arc lamp with a Corning C.S. No. 7-39 filter was the irradiation source for the zinc oxide layer (zinc oxide light). Current measurements were made with a General Radio Type 1230-A D.C. electrometer. A 45 volt battery was used with a 10,000 ohm load resistor. The samples were contained in a holder which was evacuated to 10^{-5} mm Hg and which could be maintained from 80°K to 400°K.

RESULTS

Fig. 1 shows the optical absorption spectra of undyed (a) and eosin-dyed (b) zinc oxide films measured at 80°K. The visible bands of the dyed film at 500 and 530 mμ are close to the maxima obtained in dilute ethanolic solutions at 495 and 532 mμ. The shorter wavelength band has been associated with dimer molecules and the longer wavelength band with monomer molecules[2]. The spike near 380 mμ on the undyed film is absent on the dyed film, suggesting that it is a surface effect,

possibly a perturbation of the zinc oxide fundamental absorption by the surface, i.e. it is related to the alpha bands of alkali halide crystals[3].

Fig. 1(c) shows the excitation of photoconductivity at 300°K as measured with narrow-band filters. Maximum photoconductivity occurs on the eosin monomer band and on the zinc oxide absorption edge, where eosin is almost transparent. Fig. 2 shows that the sensitized photoeffect increases monotonically with temperature, in contrast to the "fast" effect in zinc oxide films where there is a slow increase from 80 to about 300°K and a rapid increase at higher temperatures[4]. The dark conductivity of the dyed film is also shown; the numerical values have been matched at 373°K to indicate that the temperature dependence of the dark and sensitized photoconductivity is the same above 273°K.

Fig. 3 shows consecutive build-up and decay cycles of the sensitized photo-effect. Although the dark conduction increased slightly after each irradiation with eosin light, the net change was constant within the experimental error. The dependence of the sensitized process on dark current was further investigated by exposing the films to prior zinc oxide-light irradiation, which induced a temporary increase in dark current that persisted for many hours. It was found that the magnitude of the sensitized photoeffect is independent of the dark current for changes in the latter by a factor of 5. The "fast" photoconductivity in pure zinc oxide films varies with the two-thirds power of the dark current[5].

The sensitized photoeffect varies with a constant power of the eosin-light intensity, between 0.48 and 0.52 for different runs (Fig. 4). By contrast, the "fast" photoeffect in zinc oxide films varies with approximately the one-third power of the light intensity, where the specific relationship depends on the light intensity and dark current[5]. Fig. 5 shows the dependence of the total photocurrent on zinc oxide-light intensity for different constant eosin-light intensities. At high eosin-light intensities, the total photocurrent is almost independent of the zinc oxide-light intensity.

The build-up and decay processes shown on Fig. 3 were investigated as a function of temperature, dark current, and light intensity. Fig. 6 shows that the build-up at 300°K is an exponential function of time after an initial rapid rise, and that the first-order rate constant is independent of light intensity. Fig. 7 shows that the decay at 300°K is exponential in time after an initial rapid fall, and that the first-order rate constant is independent of the initial steady-state value. Table I shows that the half-time for decay is independent of dark current, as modified by prior zinc oxide-light irradiations, but that the half-time for build-up increases with decreasing dark current. Table II shows the build-up and decay half-times at different temperatures. (The dark current for this data was from 1 to 3 μamps, accounting for the considerably longer half-times compared to Table I.) Surprisingly, the rates of build-up and decay are substantially independent of temperature. For the "fast" process in zinc oxide films, the initial slope of the

Table I. Dependence of Build-up and decay half-time on dark current.

Dark Current (μamp)	Half-time for Build-up(sec)	Half-time for Decay(sec)
3.8	57	48
6.1	34	60
11.4	32	40
52	15	45
71	14	30
97	13	42

Table II. Dependence of build-up and decay half-time on temperature.

Temperature (°K)	Half-time for Build-up(sec)		Half-time for Decay(sec)		
	Run 1	Run 2	Run 1	Run 2	Run 3
368	221	234	67	56	48
296	175	142	41	66	59
275	190	155	47	53	35
200	230	202	19	42	51
86	142	86	28	20	27

build-up curves vary approximately with the first power of the dark current[4] and accurately with the first power of the light intensity[6]. However, Fig. 8 shows that the initial slope for the sensitized photoeffect varies with the one-half power of the eosin-light intensity and approximately the four-thirds power of the dark current.

DISCUSSION

The sensitized photoeffect differs considerably from the "slow" and "fast" processes in pure zinc oxide films, particularly in the dependence on temperature, dark current, and light intensity. In fact, the data of Fig. 5 shows that the two processes are competitive in a dyed film, because at high eosin-light intensities the total photocurrent no longer increases with increasing zinc oxide-light intensity. The kinetics are characterized by a first-order build-up and decay and a one-half power dependence of the steady-state photocurrent on eosin-light intensity. This indicates that the sensitization of photoconduction is a two-step process: a light-induced generation of carriers with a fast second-order decay and a slower capture of carriers which enhances the zinc oxide conductivity. Nelson[7] has shown that erythrosin is a p-type photoconductor and since eosin has the same structure except that the iodine atoms are replaced by bromine atoms, we shall assume that hole conductivity predominates in eosin. To explain the one-half power dependence on light intensity, it is assumed that the holes generated by light absorption in the eosin layer recombine with trapped

electrons in a fast process:

$$D + \text{light} \xrightarrow{I} D^- + p \ ,$$

$$D^- + p \xrightarrow{k_1} D.$$

It is necessary to explain how holes generated in the dye layer can increase the electrical conductivity of the ZnO layer. We postulate that the holes which migrate into the zinc oxide layer are captured at interstitial Zn^+ , converting them to Zn^{++}, and enhancing the zinc oxide conduction electron lifetime. This mechanism was first proposed by Mollwo[8] to explain the photoeffect in zinc oxide films, but has been superseded by other models based on the results of field effect measurements[6,9]. However, hole-capture by Zn^+ is consistent with the assumption of p-type conductivity in eosin and with the temperature dependence of the sensitized photoeffect, which appears to be an enhancement of the dark conduction.

A simple volume-kinetic analysis gives results in agreement with the observed rate equations. The current is assumed to be given by:

$$i = A(Zn^+)_o + (B - A)\ (Zn^{++}) \ ,$$

where (Zn^+) and (Zn^{++}) are the interstitial ion concentrations, the subscript refers to dark conditions, and $B > A$. The extent of sensitization is controlled by hole-capture and release:

$$Zn^+ + p \underset{k_2}{\overset{k_2'}{\rightleftharpoons}} Zn^{++} \ .$$

The rate equations are given by the solutions to:

$$d(Zn^{++})/dt + \left[k_2(I/k_1)^{1/2} + k_2'\right]\ (Zn^{++}) - k_2(I/k_1)^{1/2}(Zn^+)_o = 0,$$

where it has been assumed that the rate of hole generation in the eosin layer is photostationary. If it is further assumed that $k_2' \gg k_2(I/k_1)^{1/2}$, then:

$$\underline{\text{Steady-state}} \quad i_{ph}^{*} = (B\text{-}A)(k_2/k_2')(I/k_1)^{1/2}\,(Zn^{+})_o \ ,$$

$$\underline{\text{Build-up}} \quad i_{ph} = i_{ph}^{*}\,(1 - \exp\text{-}k_2't) \ ,$$

$$\underline{\text{Decay}} \quad i_{ph} = i_{ph}^{*}\exp\text{-}k_2't \ .$$

The above equations predict correctly that the initial rate of build-up and the steady-state photocurrent vary with the one-half power of the light intensity and that the build-up and decay are exponential in time. They are not in good agreement with the dark current effects. There is increasing evidence that the "fast" photoeffect in zinc oxide films and crystals depends on dark current because of a surface electron-trap distribution[6,9]. If this is the case, then $(Zn^{+})_o$ is constant for a particular condition of oxygen and eosin adsorption and the rate constants for build-up and decay should be identical and independent of dark current, which is not in agreement with the data of Table I. However, the non-dependence of the build-up and decay rate on temperature indicates that neither process is thermally activated and suggests that k_2 and k_2' are not hole-capture and release coefficients in the usual sense. The observations indicate that a <u>statical</u> condition occurs, in which holes move short distances across the interface under the action of illumination and return when the excitation is removed. Thus, k_2 and k_2' could depend on the interfacial space charge layer, which in turn varies with the filling of the surface traps.

The energetics of sensitization can be shown on a diagram based on the two-band model. For simplicity, the secondary influence of adsorbed oxygen on the undyed region of the surface is neglected and it is assumed that no barrier potential exists between the zinc oxide and eosin layers in the dark. Fig. 9 shows the energy level scheme based on this model. The eosin band gap (2.3 ev) is taken from the absorption maximum of the dyed film and the photoelectric work function (5.5 ev) is taken as approximately the same as erythrosin[10]. The photoelectric work function of zinc oxide (6.3 ev) is taken from the measurements of Wilessow and Terenin[11] on evacuated powder at room temperature. The donor energy level for neutral, interstitial zinc is taken as 0.05 ev from the work of Hutson[12], and the Zn^+ level is taken from the activation energy of 2.3 ev as obtained by Pohl[13] for the high-temperature electrical conductivity of zinc oxide crystals in equilibrium with oxygen. It is interesting to note that the eosin valence band lies close to the interstitial Zn^+ levels, but this may be coincidental and not essential to the model since other dyes can sensitize zinc oxide photoconductivity.

REFERENCES

1. E. K. Putseiko and A. N. Terenin, Zhur. Fiz. Khim. 23, 676 (1949)

2. P. Pringsheim, Fluorescense and Phosphorescence (Interscience, New York, 1949) pp. 353-55

3. C. Delbecq, P. Pringsheim, and P. Yuster, J. Chem. Phys. 20, 746 (1962)

4. H. Weiss, Z. Physik 132, 335 (1952)

5. E. Mollwo, Ann. Physik (6) 3, 230 (1948)

6. E. Mollwo, Solid State Physics Vol. 8 (Academic Press, New York, 1959) pp. 193-323

7. R. C. Nelson, J. Chem. Phys. 29, 388 (1958)

8. E. Mollwo, Photoconductivity Conference (John Wiley & Sons, New York, 1956) pp. 509-528

9. G. Heiland, J. Phys. Chem. Solids, 22, 227 (1961)

10. R. C. Nelson, J. Opt. Soc. Amer., 51, 1186 (1961)

11. F. Wilessow and A. Terenin, Naturwiss. 46, 167 (1959)

12. A. R. Hutson, Phys. Rev. 108, 222, (1957)

13. R. Pohl, Diplomarbeit, University of Erlangen, 1955

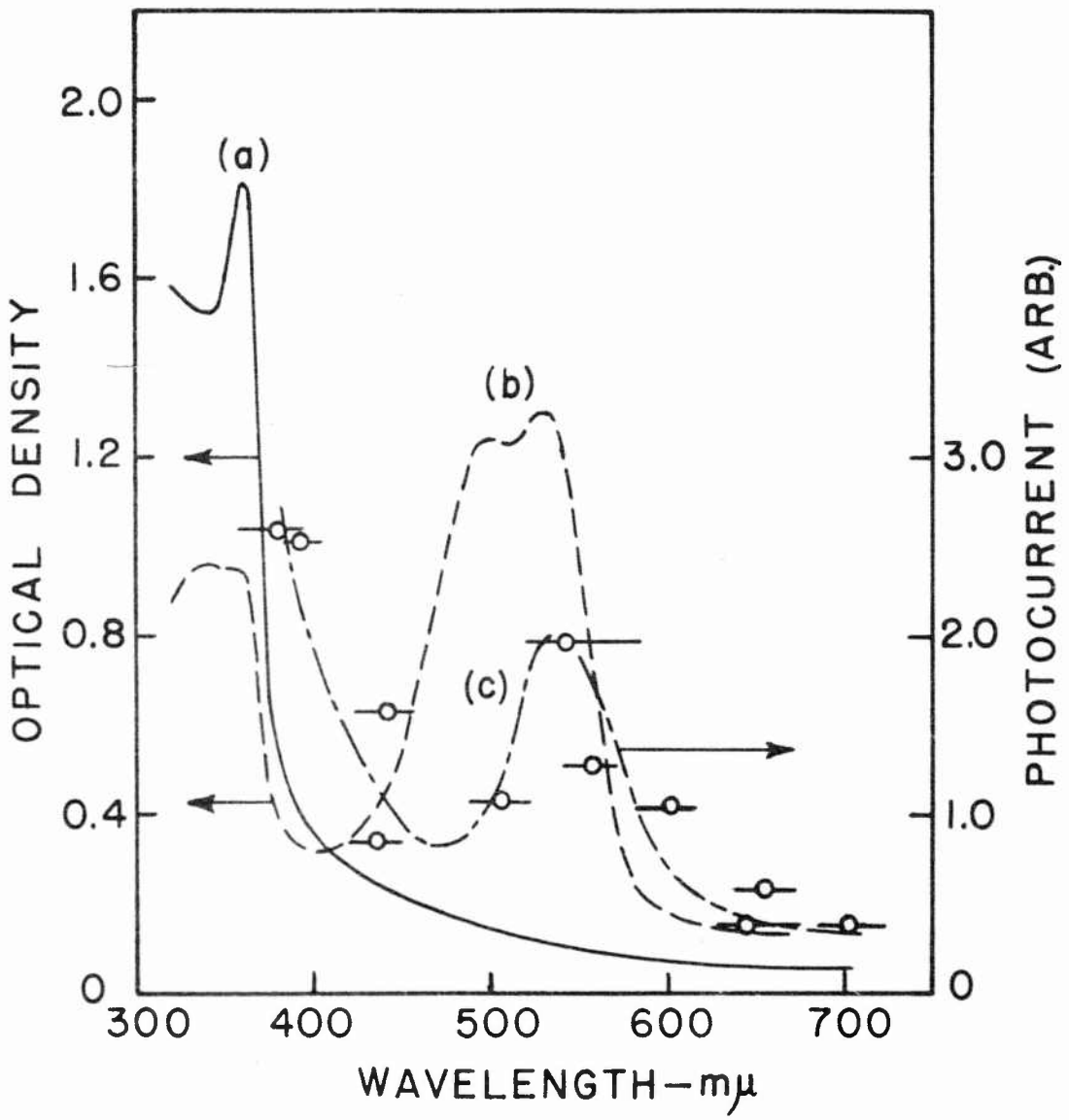

Figure 1. Optical absorption spectra of zinc oxide (a) and eosin-dyed zinc oxide (b) films and the excitation spectrum of photocurrent (c) as measured with narrow-band filters.

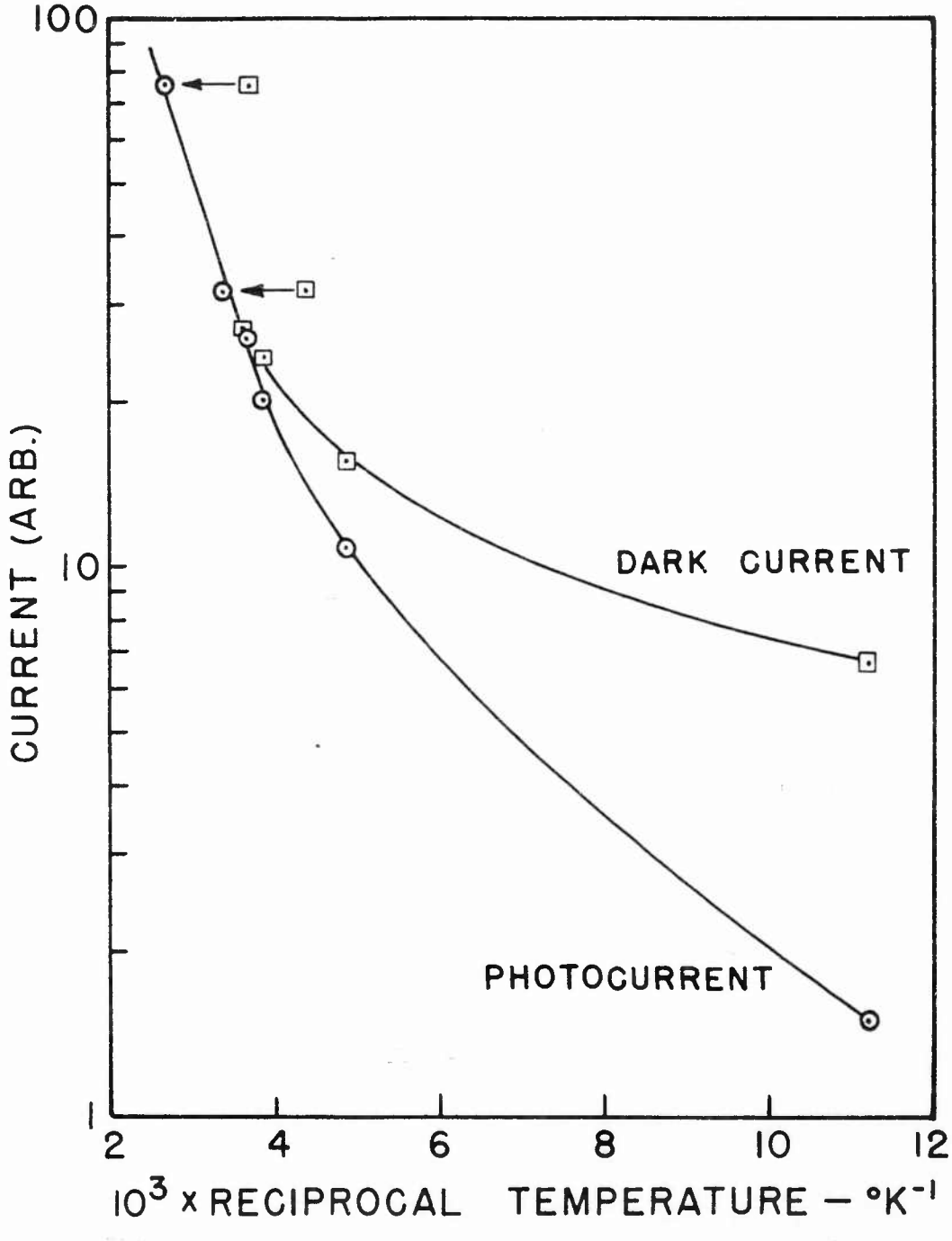

Figure 2. Temperature dependence of dark current and sensitized photoeffect of eosin-dyed zinc oxide film.

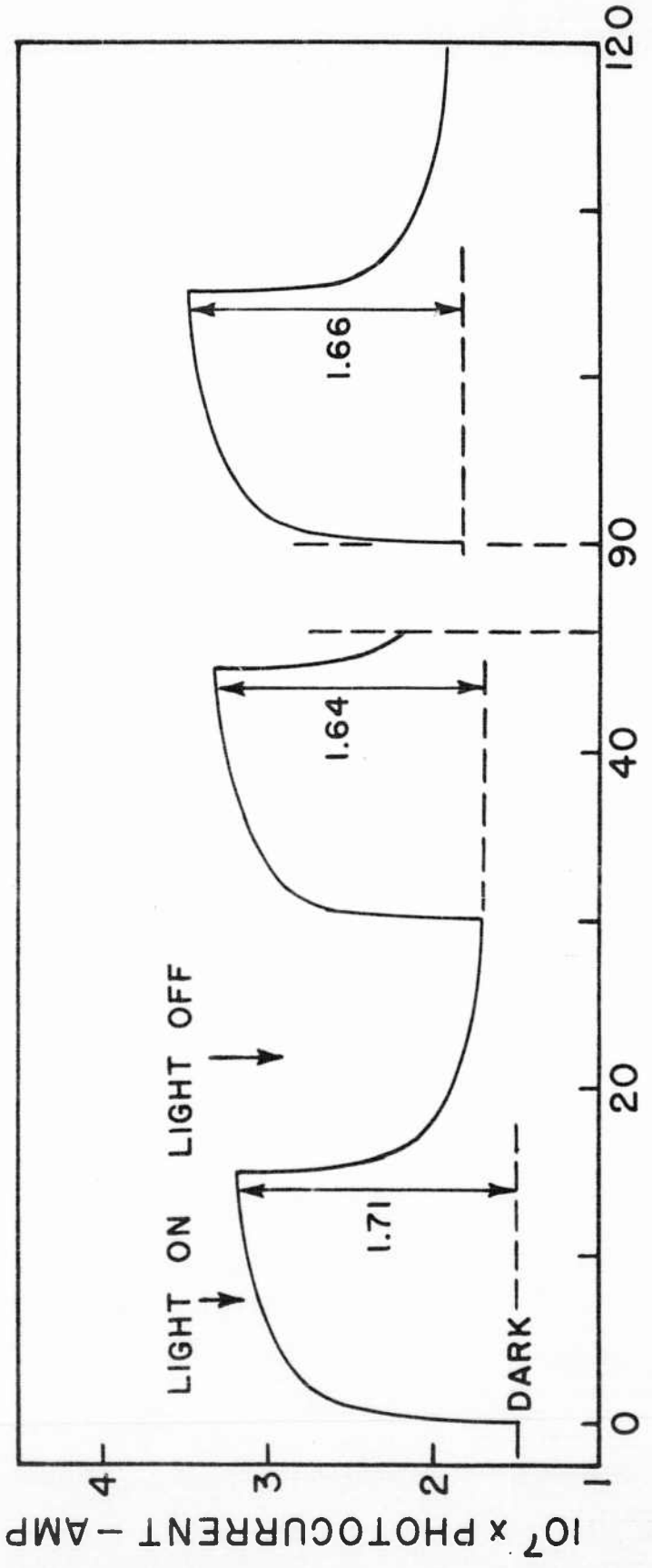

Figure 3. Build-up and decay of sensitized photoeffect at 300°K.

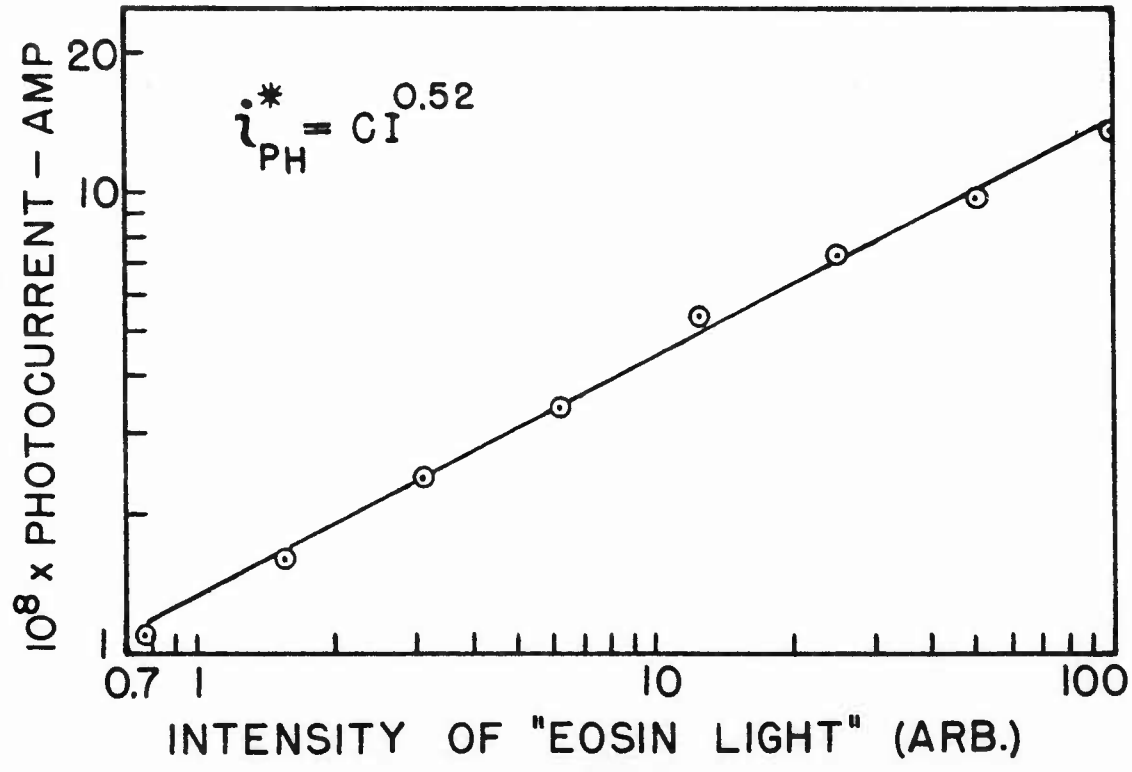

Figure 4. Dependence of sensitized photoeffect on light intensity at 300°K.

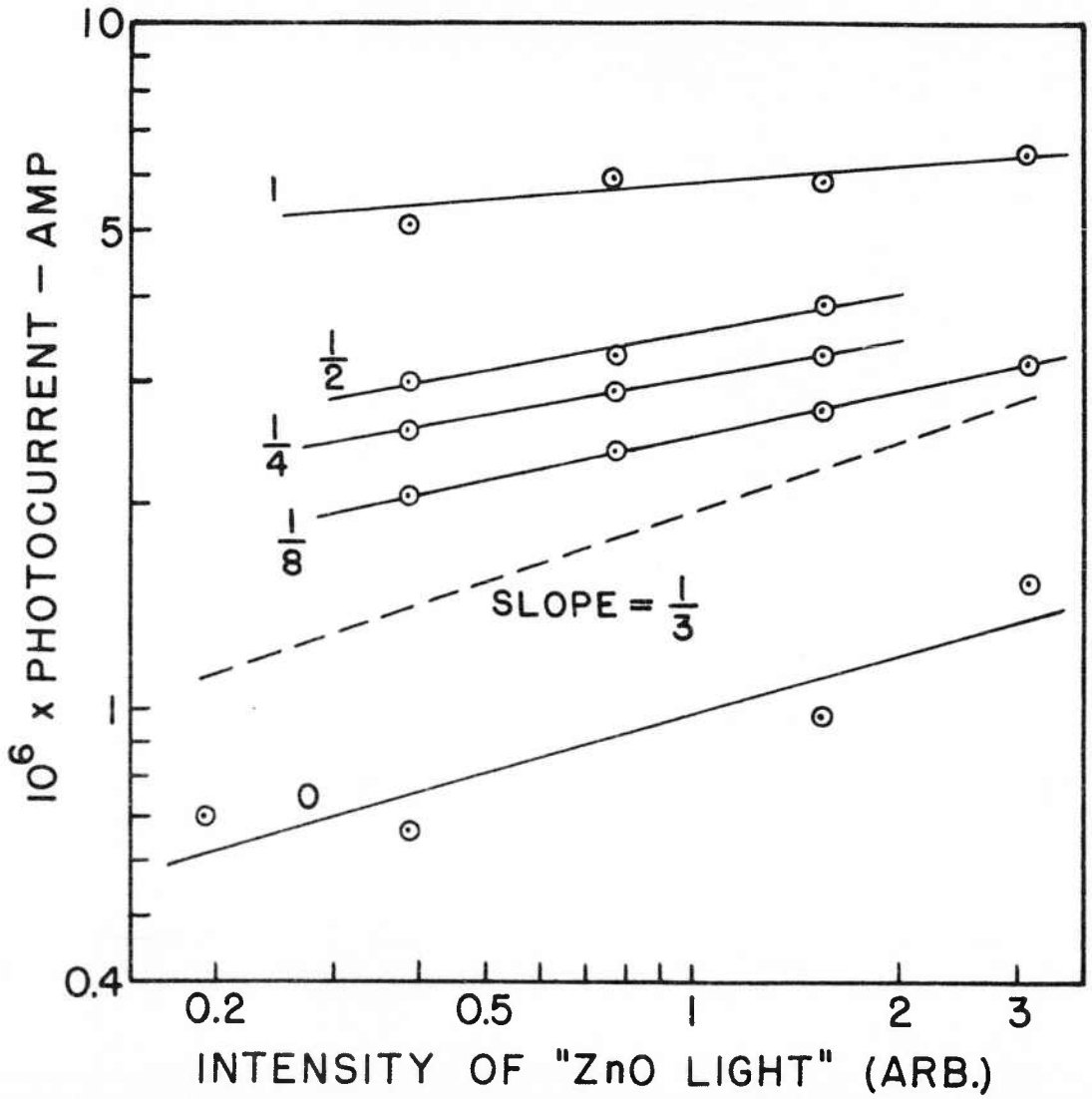

Figure 5. Dependence of total photocurrent on zinc oxide-light intensity at constant eosin-light intensities. The number to the left of each line denotes the relative eosin-light intensity.

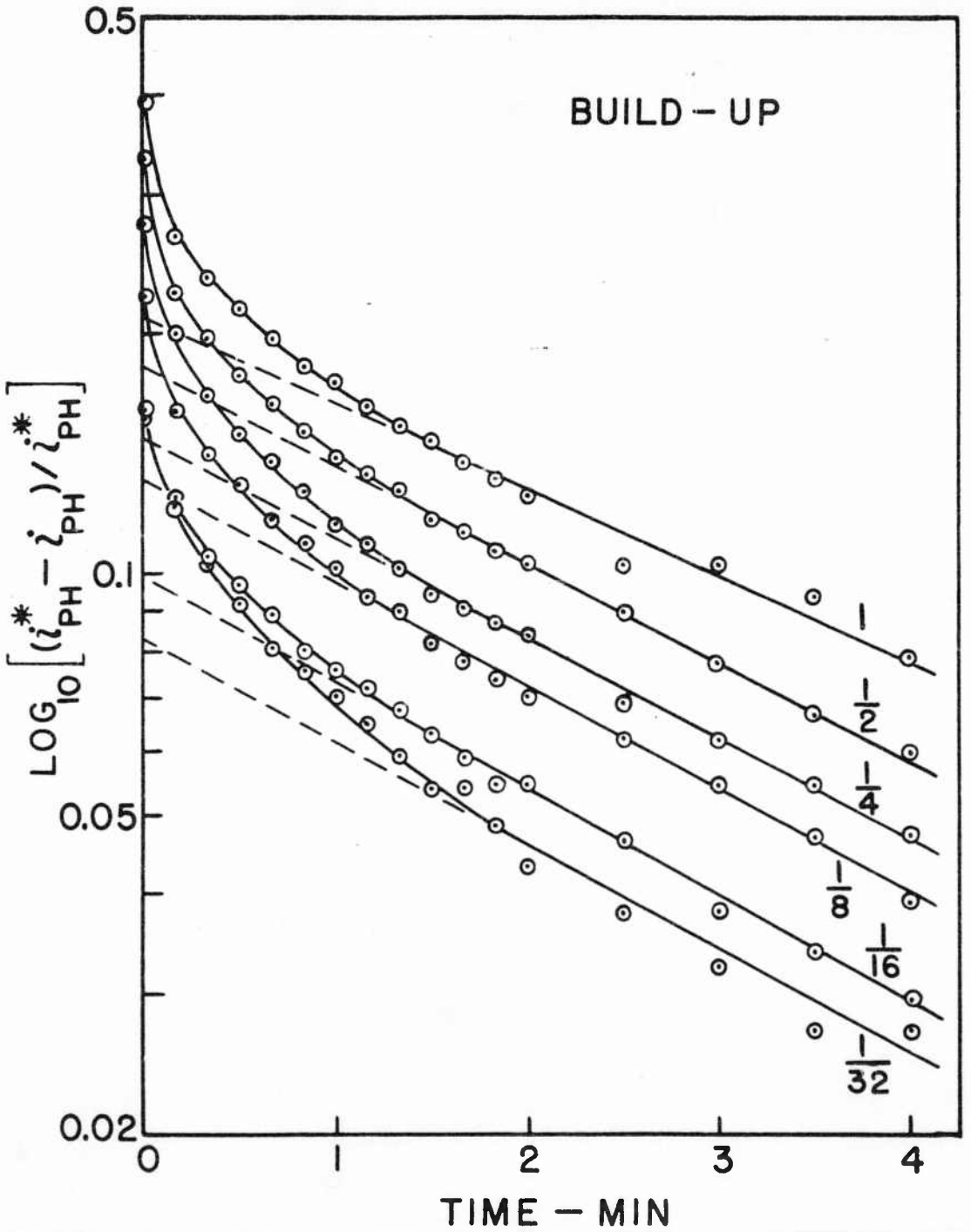

Figure 6. Build-up of sensitized photoeffect at 300°K as a function of eosin-light intensity.

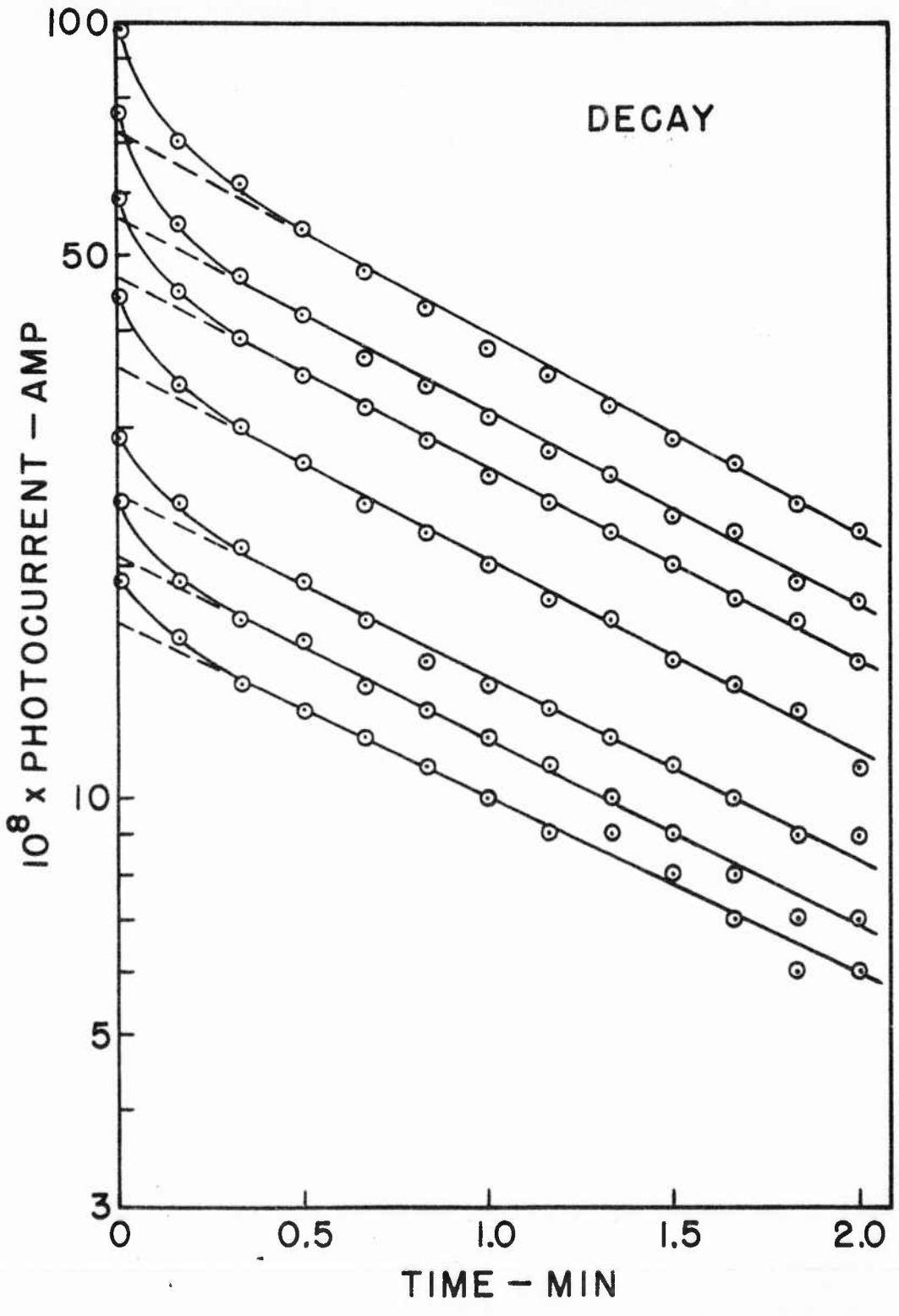

Figure 7. Decay of sensitized photoeffect at 300°K.

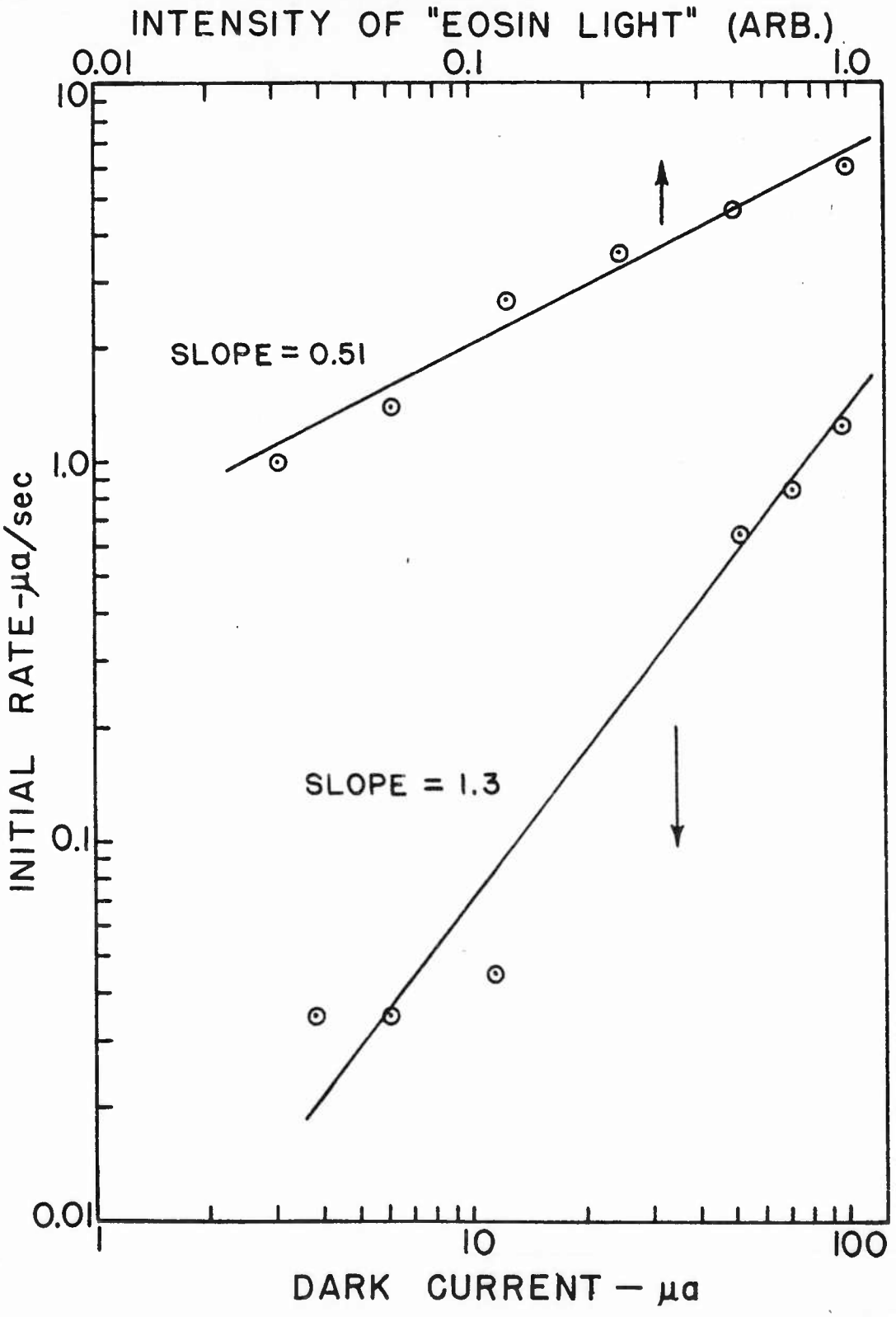

Figure 8. Dependence of initial build-up rate of sensitized photoeffect on dark current and eosin-light intensity.

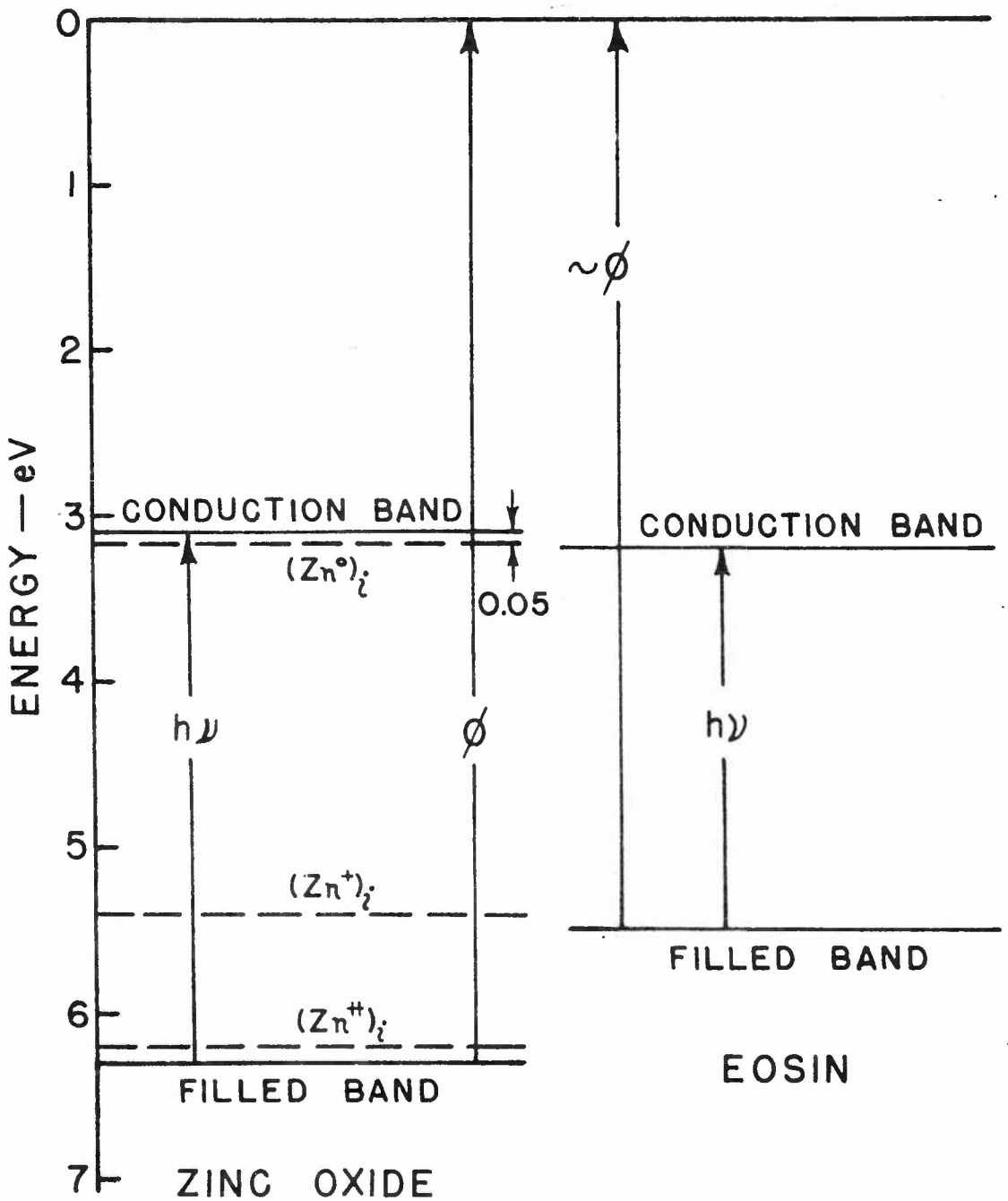

Figure 9. Approximate energy level diagram.

E4. FIELD ELECTRON EMISSION FROM SEMICONDUCTORS

W. R. Savage
Materials Research and Development Laboratory
Texas Instruments
Dallas, Texas

ABSTRACT

The phenomenon of high field electron emission consists of the tunneling of electrons through the deformed potential barrier at the surface. The thinned barrier results from the action of a high electrostatic field at a conductor-vacuum interface. For a semiconductor the field emission current originates from both the conduction band, j_c, and valence band, j_v. The relative magnitudes of j_c and j_v depend on the bulk properties and surface condition of the semiconductor. Stratton has recently revised the theory of field emission from semiconductors. The theory includes corrections for the difference between effective and free electron masses with detailed results obtained for spherical energy surfaces. The current arising from the conduction band is proportional to the probability for emission from the Fermi level for positive Fermi energies or the bottom of the conduction band for negative energies. Deviations from linearity in the Fowler-Nordheim graph, $\ln j_c$ versus $1/F$, arise from changes in surface potential as a function of external field. The current arising from the valence band is approximately proportional to the probability of emission from the top of the valence band and is essentially independent of temperature. Experimentally the emission parameters of Fermi energy, surface potential and electron affinity plus band gap energy may be varied by selection of cathode material, bulk doping levels and surface treatment. The essential features of the theory are qualitatively consistent with experimental results.

Introduction

When a high electrostatic field is applied to the surface of a metallic or semiconducting material, electrons are emitted through the potential barrier at the surface by the quantum mechanical tunneling effect. The experimental observation

of field electron emission has been known for almost as long as thermionic, photoelectric and secondary electron emission. Field emission certainly occurred in early physical electronic experiments and was described by Wood in 1897.[1] The experimental observations of field emission have been difficult and beginning with the application of Schottky's theory of field enhanced thermionic emission[2] the theory has generally been in advance of the measurements. The first successful explanation of the field emission phenomenon was given by Fowler and Nordheim[3] in 1928. The first major advance in experimental technique was the invention and development by Müller[4] of the field electron emission microscope in 1937. The subject of field emission has been reviewed by Good and Müller[5] and in an elementary way by Gomer[6]. Recently, the theory of field emission from semiconductors has been described by Stratton[7] and a number of experiments have been performed on semiconductors. Only three authors, Allen[8], Perry[9] and Fischer[10], report field emission from clean and smooth semiconductor cathodes.

Theory

Fowler and Nordheim use the electron gas model of the conduction electrons and the effective potential model of the metal. In addition the electrons inside the conductor remain essentially at equilibrium although a current is drawn from the material. When $N(E_x)dE_x$ is the number of electrons incident perpendicular to the surface with the x-part of their energy within dE_x per second per unit area and $D(E_x)$ is the probability of passage through the surface potential barrier, the product

$P(E_x)dE_x$ gives the number in the range dE_x which emerge per second per unit area from the conductor.

$$P(E_x)dE_x = D(E_x)\, N(E_x)dE_x \quad . \tag{1}$$

The electron current emitted per unit area is obtained from Eq. 1 as

$$j = e\int_{E_x} P(E_x)dE_x = e\int_{E_x} D(E_x)\, N(E_x)dE_x \quad , \tag{2}$$

where e is the unit electron charge. The function $N(E_x)$ has come to be called the supply function and $D(E_x)$ the transmission coefficient. The supply function is found from the equilibrium distribution function and following Good and Müller[5] is obtained by finding the number of electrons per second per unit area moving in the x-direction with x-momentum within dp_x. The result is

$$\int_{-\infty}^{\infty}\int_{-\infty}^{\infty} \frac{p_x}{m}\frac{2}{h^3}\,\frac{dp_x dp_y dp_z}{1+\exp\,(E-\zeta)/kT} \quad , \tag{3}$$

where m is the electron mass, h is Plank's constant, E is the total energy, ζ is the chemical potential, k is Boltzmann's constant and T is the absolute temperature. However, $p_x dp_x = m dE_x$ and

$$N(E_x)dE_x = \frac{2}{h^3}\,dE_x \int_{-\infty}^{\infty}\int_{-\infty}^{\infty} \frac{dp_y dp_z}{1+\exp\left(\frac{E_x-\zeta}{kT}+\frac{p_y^2+p_z^2}{2mkT}\right)} \tag{4}$$

The transmission coefficient is found from the solution to the time-independent Schrödinger equation for the motion of a single electron in the x-direction. Figure 1 gives the effective potential energy diagrams for a metal and a semiconductor. For the metal ζ is the Fermi energy, φ the thermionic work function -Wa the electron energy at the bottom of the conduction band. For the semiconductor ϕ is the electron affinity, E_g is the band gap energy, χ is the work function, $\phi + E_g$ is the photoelectric work function, E_a and E_d are the energy levels of acceptor and donor surface states. In Figure 1 the correction to the diagram for image potential is omitted.

In the WKB approximation the transmission coefficient is

$$D(E_x) = \exp\left[-\frac{4}{3} K \frac{(\varphi - E_x)^{3/2}}{F} v\left(\frac{e\nu F^{1/2}}{\varphi - E_x}\right)\right] , \qquad (5)$$

where $K^2 = 2m/\hbar^2$, F is the external electrostatic field, v is a tabulated function[11] arising from the image force correction, $\nu = (\epsilon - 1)/(\epsilon + 1)^{1/2}$, and ϵ is the dielectric constant. For a metal the field emission current is given by

$$j_m = \frac{e^3 F^2}{8\pi h t^2 \varphi} \exp\left[-\frac{4}{3} K \frac{\varphi^{3/2}}{F} v\left(\frac{eF^{1/2}}{\varphi}\right)\right] , \qquad (6)$$

where t is another tabulated function of the same argument as . (For details of the derivation, see Good and Müller[5].)

Following Stratton[7] the treatment of field electron emission will now be outlined. The requirement of the free electron mass model used in obtaining Eq. 6, can be removed by

replacing E_x with $E(p_x, p_y, p_z)-E_\perp$, where

$$E_\perp = (p_y^2 + p_z^2)/2m \tag{7}$$

and $E(p_x, p_y, p_z)$ gives the momentum dependence of electron kinetic energy for the semiconductor. For the conduction band the current is given by

$$j_c = e\frac{2}{h^3}\int_{px}^{\infty}\int_{-\infty}^{\infty}\int_{-\infty}^{\infty}\frac{D(E-E_\perp)}{1+\exp\left[(E-\zeta)/kT\right]}\frac{\partial E}{\partial p_x}\,dp_x dp_y dp_z \ , \tag{8}$$

where $\partial E/\partial p_x$ is the velocity of the field emitted electron perpendicular to the surface. For spherical energy surfaces, where E depends on the magnitude of the electron momentum, the integration can be performed. For non-spherical energy surfaces the maximum value of E_x depends on the orientation of the material with respect to the surface and the integral must be evaluated for a given orientation. Similarly to Eq. 8 the valence band current is given by

$$j_v = e\frac{2}{h^3}\int\frac{D_V(-\bar{E} + E_\perp)}{1+\exp\left[-(\bar{E} + E_q + \zeta)/kT\right]}\frac{\partial \bar{E}}{\partial \bar{p}_x}\,d\bar{p}_x d\bar{p}_y d\bar{p}_z \ , \tag{9}$$

where the bar indicates the measurement of the quantity with respect to the top of the valence band, and D_v is the penetration coefficient with the photoelectric work function substituted for φ. The detailed integration of Eqs. 8 and 9 is

discussed by Stratton[7] and only the principal results will be summarized here. The subscript O will denote the result of the analysis for the free electron mass. The results apply for a field sufficiently high to give appreciable emission and sufficiently low temperature to have no significant thermionic emission.

For positive Fermi energy the conduction band emission is given by

$$j_{co} = \frac{e4\pi m(kT)^2}{h^3} H_1 \exp\left[-\frac{4}{3} K \frac{3/2}{F} v\left(\frac{e F^{1/2}}{}\right)\right] , \qquad (10)$$

where H_1 is a slowly varying correction function tabulated by Stratton. For materials where the work function is independent of the external field, a plot of ln j_{co} vs (1/F) would be a straight line and deviations would result primarily from a field dependence of work function and not the slow variations of H_1 upon field. Fields of the order of 5×10^6 volts/cm are required for field emission. For slight negative Fermi energy the conduction band emission is given by

$$j_{co} = \frac{e4\pi m(kT)^2}{h^3} H_0 \exp\left[-\frac{4}{3} K \frac{\phi^{3/2}}{F} v\left(\frac{e\upsilon F^{1/2}}{\phi}\right) + \frac{\nu}{KT}\right] , \qquad (11)$$

where H_0 is another slowly varying function. H_0 varies even more slowly than H_1. If the first term of a series expansion of H_0 is retained and the relation between Fermi energy and electron density n,

$$\exp(\mathcal{J}/kT) = n\, h^{3/2}(2\pi mkT)^{3/2} \quad , \tag{12}$$

is used, the expression for j_{co} is

$$j_{co} = en(kT/2\pi m)^{1/2}\exp\left[-\frac{4}{3}\,K\,\frac{\phi^{3/2}}{F}\,v\left(\frac{e\nu F^{1/2}}{\phi}\right)\right], \tag{13}$$

The quantity $n(kT/2\pi m)^{1/2}$ electrons/cm^2 sec is the rate at which conduction electrons impinge upon the surface from the interior. In general, conduction band emission is temperature dependent by means of the influence of temperature on the pre-exponential factor in Eqs. 10, 11 and 13.

For field electron emission from the valence band the result is

$$j_v = \frac{e4\pi m}{h^3 C_v^2}\,(\gamma_p^{-1}-1)\exp\left[-\frac{4}{3}\,K\,\frac{(\phi+E_g)^{3/2}}{F}\,v\left(\frac{e\nu F^{1/2}}{\phi+E_g}\right)\right] \tag{14}$$

where $C_v = 2\sqrt{2}\, m^{1/2}t/hF$, $\gamma_p = 1-m_p/m$, where m_p is the effective mass of holes taken near the top of the valence band. The valence band emission is temperature independent. The main contributions to the valence band electron current come from near the top of the filled band if $m_p/m < 1$. Otherwise a detailed knowledge of the relation of electron energy on momentum would be required for the valence band if m_p/m is not less than unity. The corrections to field emission are detailed elsewhere[7] and will not be given in this brief account.

In Figure 1 the effect of surface parameters have been indicated by subscript s and the general effect of surface states by the bending of the electron bands at the surface. When an external field is applied to a semiconductor, the induced charge is located in an extended space charge region[12, 13] or it appears in the surface states. Depending on the bulk parameters and the particular surface states, the reduced Fermi energy at the surface, hence, the field emission current, will be a function of the external field. For low fields the surface states will hold the surface in its initial condition and a given field emission current will be observed. Then as the field increases the surface states will be filled and the bands become strongly bent down. The current should increase more strongly than exponentially in this transition region and a curvature would be observed on the ln j vs (1/F) plot. The range of field for which this curvature is observed will depend upon the material and surface treatment. Also, whether conduction band or valence band emission or a combination of both is observed depends upon the bulk parameters of a material.

Experimental

In order to obtain the high fields required for the electron emission process, the experimental apparatus consists of a fine pointed cathode and a suitable anode arranged in an ultra-high vacuum apparatus. Figure 2 is a drawing of a field

electron microscope tube as it is usually constructed of Pyrex glass. The cathode is chemically or electrochemically etched to about one micron radius and mounted in the tube with pressure clamps for semiconductors. The anode ring serves as a means for applying a high voltage to the space near the cathode. Usually, voltages of one to ten kV are necessary. The forward glass surface (which may be flat or hemispherical) is made conducting and is coated with a fluorescent material to permit observation of the electron emission from the various crystal faces of the cathode point. The usual ultra-high vacuum procedures are used to obtain the required operating pressures of less than 10^{-9} torr. The emission patterns are intense enough to be photographed. The physical data required are emitter shape, obtained by an independent observation of the cathode in a conventional electron microscope, and electrical measurements of emission current and applied voltage.

Results

Field electron emission has been observed for a number of elemental and compound semiconductors. Stratton[7] gives a list of references (which will not be repeated in this report) to experimental studies of field emission from CdS, CdSe, W_2C, Mo_2C, SiC, Al_2O_3, SiO_2, ZnS, Te, Si and Ge. Additional work has been reported on silicon (see Ref. 8, 9 and 10) and germanium (see Ref. 8). Also, recent work is reported for

compounds CdS[14], CdTe[15] and InSb[16]. Figure 3 is a reproduction of Allen's results for germanium field emission characteristics and Figure 4 for silicon. The experimental results on germanium and silicon by Allen, Perry and Fischer do not permit a clear interpretation on the role played by valence and conduction band emission. The best that may be said for the remaining experimental work is that the results are consistent with theory. Usually, a linear voltage-current result is obtained and usually either conduction or valence band emission will describe the transfer characteristics of the tube. In the case of the photoconductors CdS, CdSe and CdTe, the effect of enhanced emission under the influence of external illumination is established even for the contaminated cathode. Most attempts to measure temperature dependence have been crude but most investigators find no effect on emission current upon cooling to liquid nitrogen temperatures.

In the future detailed measurements of the temperature dependence of field electron emission should be a fruitful experiment. In this way the conduction and valence band emission may be separated. Since the usual voltage-current curve depends on an average over all the exposed crystal faces, the effects of crystal anisotropy and local work function could be obtained by collecting and measuring emission currents from just one crystal plane. One of the most complex experiments and, perhaps, most informative is the measurement of the energy distribution of the field emitted electrons. Preliminary

results have been published by Zhdan and Elinson[17] for the energy distribution of field emitted electrons. Now that methods are available for preparing reproducible field emission patterns, the major advance will result from experimental results directed toward establishing the range of application of the theory and the usefulness of the method as a materials research tool.

References

1. R. W. Wood, Phys. Rev. 5, 1 (1897).
2. W. Schottky, Z. Physik 14, 63 (1923).
3. R. H. Fowler and L. Nordheim, Proc. Roy. Soc. London, Ser. A, 119, 173 (1928).
4. E. W. Müller, Z. Physik 106, 541 (1937); 108, 668 (1938).
5. R. H. Good, Jr. and E. W. Müller, Encyclopedia of Physics, S. Flügge, ed., (Springer-Verlag, Berlin, 1956) Vol. XXI, p. 176.
6. R. Gomer, Field Emission and Field Ionization (Harvard University Press, Cambridge, 1961).
7. R. Stratton, Phys. Rev. 125, 67 (1962).
8. F. G. Allen, J. Phys. Chem. Solids 19, 87 (1961).
9. R. L. Perry, J. Appl. Phys. 33, 1875 (1962).
10. T. Fischer, Eighth Field Emission Symposium, Williams College, August 28-30, 1961.
11. R. E. Burgess, H. Kroemer, and J. M. Houston, Phys. Rev. 40, 515 (1953).
12. R. H. Kingston and S. F. Neustadter, J. Appl. Phys. 26, 718 (1955).
13. C. E. Young, J. Appl. Phys. 32, 324 (1961).
14. I. L. Sokol'skaya and G. P. Shcherbakav, Fiz. Tverd. Tela 4, 44 (1962); translation: Soviet Phys.-Solid State 4, 31 (1962).

15. W. R. Savage, J. Appl. Phys., to be published.

16. W. R. Savage, Ninth Field Emission Symposium, University of Notre Dame, June 13-15, 1962.

17. A. G. Zhdan and M. I. Elinson, Radiotekhn. i Elektron. 6, 671 (1961); translation: Radio Eng. and Electron. 6, 310 (1961)

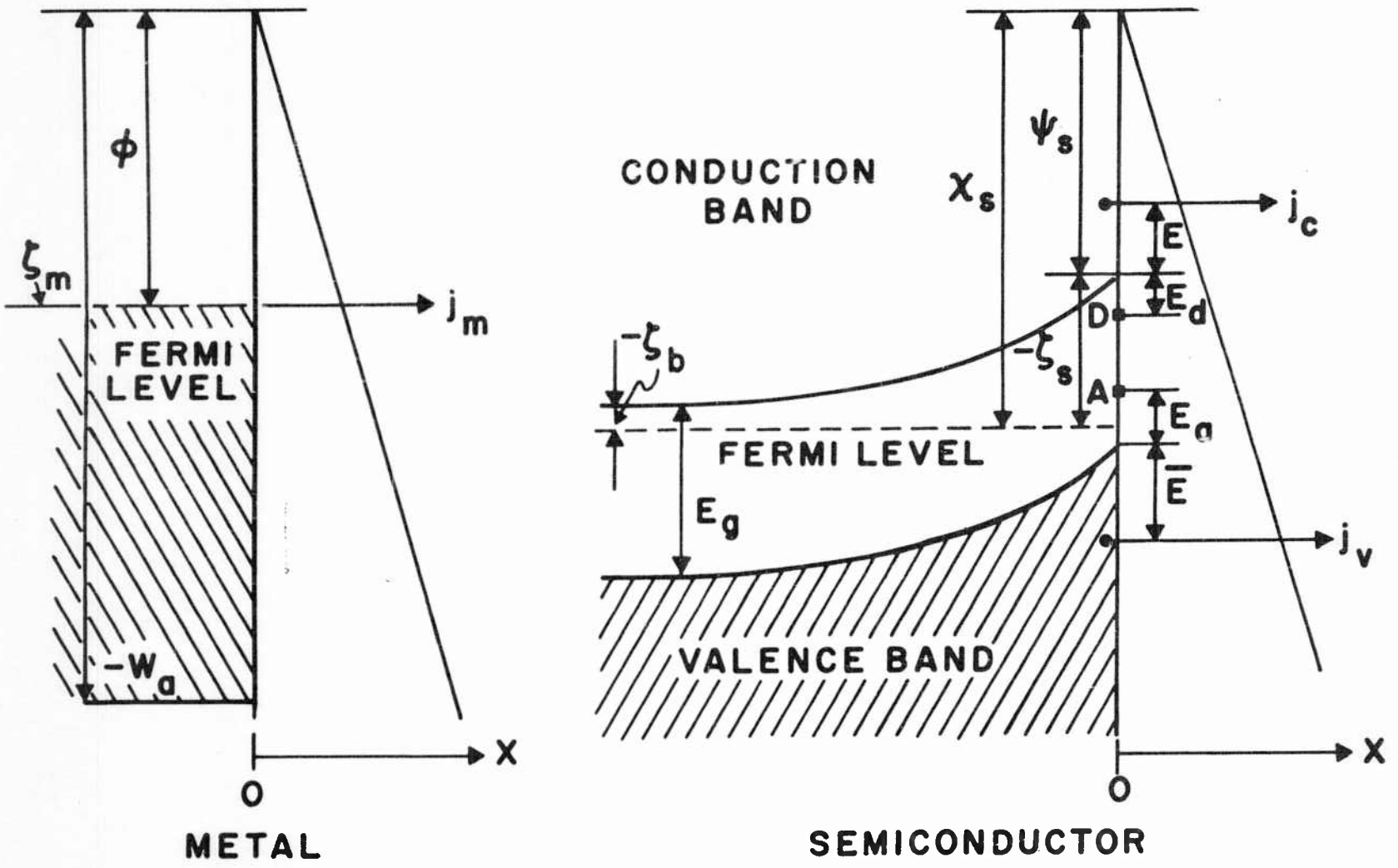

1. Electron potential energy diagram for a metal and a semiconductor. The image force correction is not shown for simplicity.

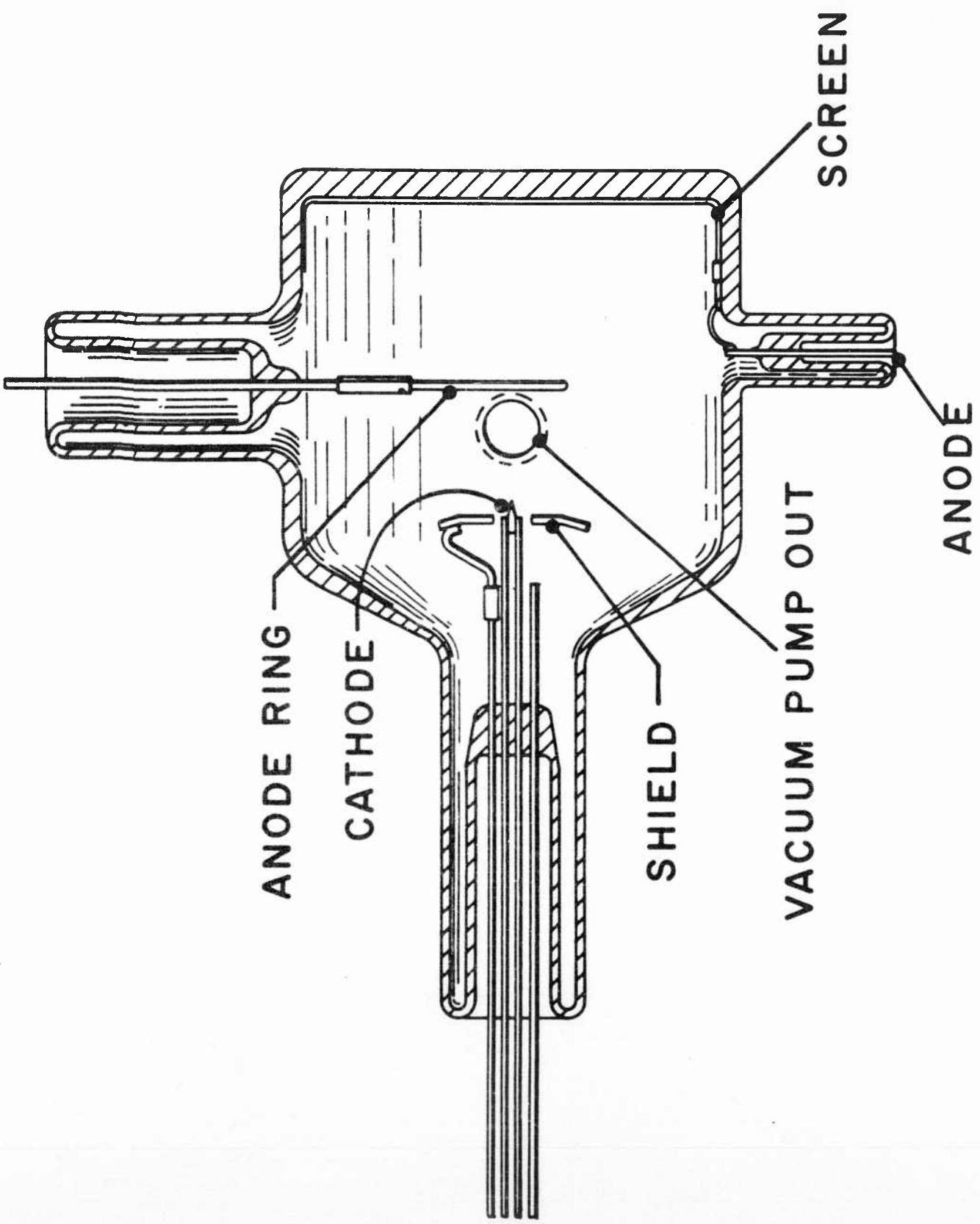

2. Field electron emission microscope tube.

Field emission current-voltage characteristics for germanium in field cleaned condition and in thermally annealed condition.

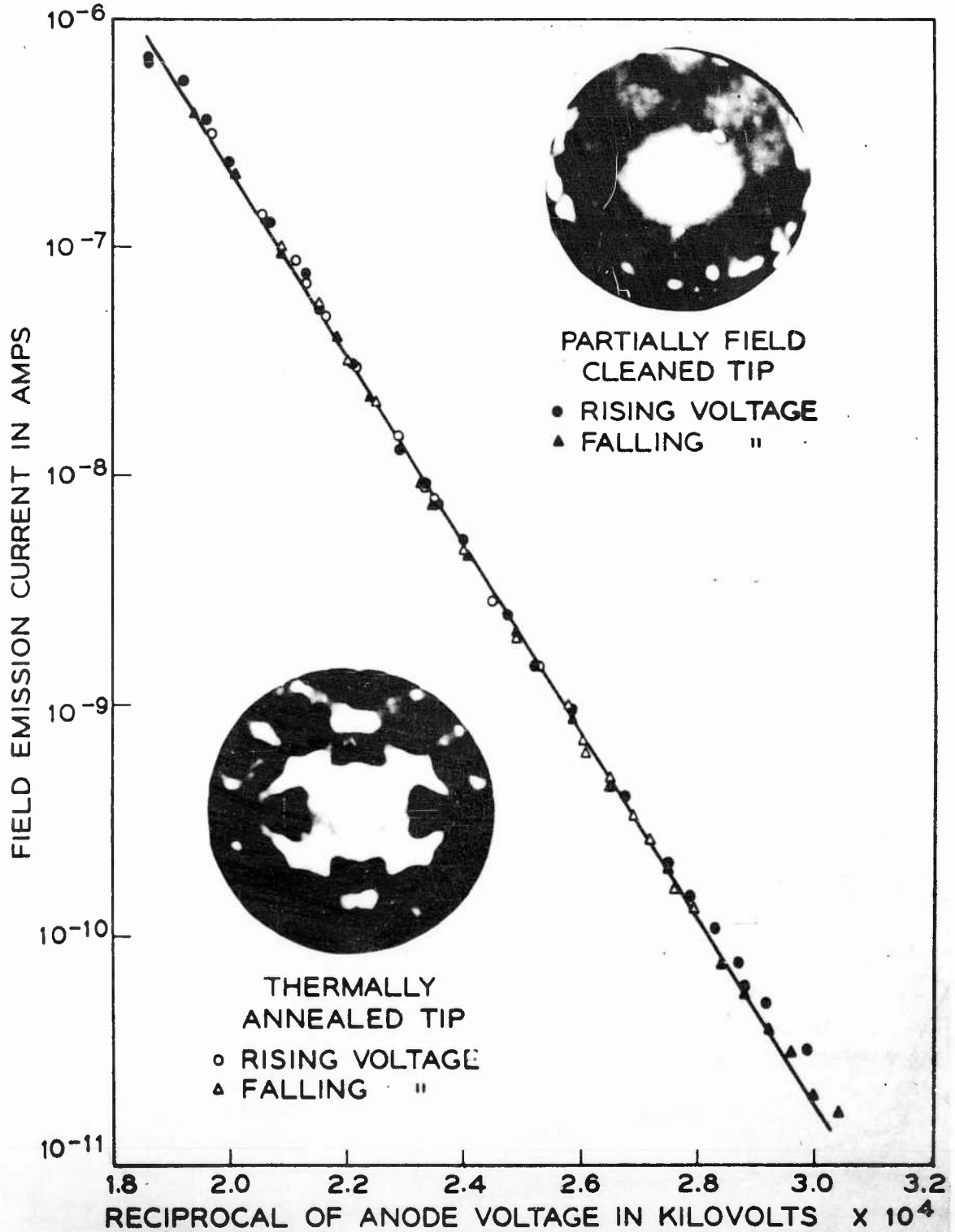

3. Current-voltage characteristic for germanium field electron emission. F. G. Allen, J. Phys. Chem. Solids 19, 87 (1961). (Courtesy of Dr. F. G. Allen.)

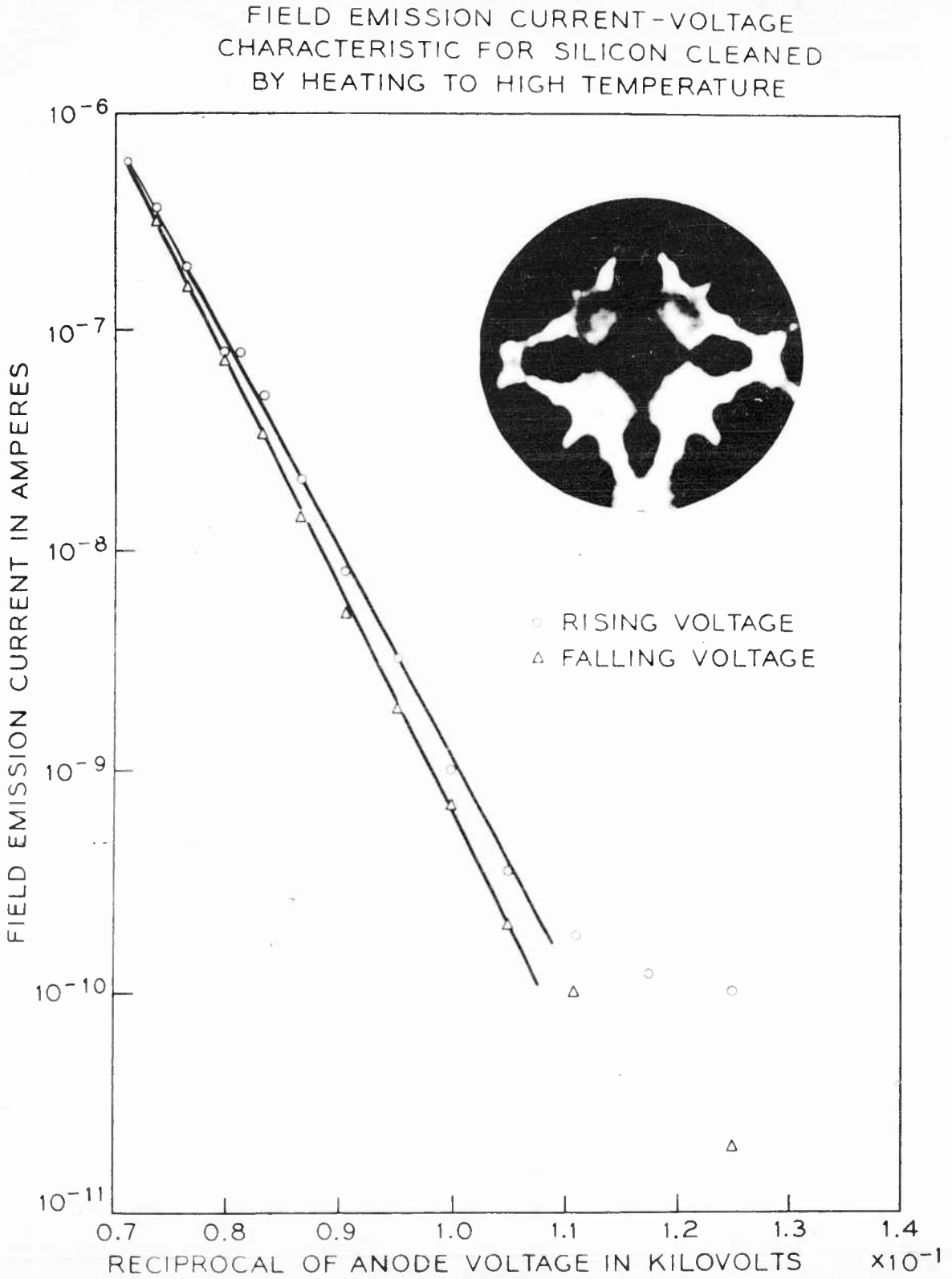

4. Current-voltage characteristic for silicon field electron emission. F. G. Allen, J. Phys. Chem. Solids 19, 87 (1961). (Courtesy of Dr. F. G. Allen).

F1. (Invited paper) PROPERTIES OF NONSTOICHIOMETRIC COMPOUND SEMICONDUCTORS

By

Wayne W. Scanlon
U. S. NAVAL ORDNANCE LABORATORY, WHITE OAK, MARYLAND

ABSTRACT

The composition, and hence the electrical properties, of a binary compound semiconductor crystal is a function of temperature and composition of coexisting gaseous or liquid phases. The types of composition changes which can occur in a given crystal and their dependence upon temperature and time are discussed. Illustrations of equilibrium values of composition and effects of composition change on various electrical properties of PbS and PbTe are given.

INTRODUCTION

One of the important requirements of semiconductor materials used in thermoelectric devices is stability of electrical properties while under thermal stress. The materials must be able to operate for long periods of time at high temperatures and large thermal gradients without deterioration of electrical characteristics. In the temperature range under consideration the electrical properties of the semiconductors are called extrinsic and are determined by the presence of various point defects in the pure crystal such as foreign atoms in normal lattice sites, lattice vacancies or interstitial atoms. These imperfections are the source of donor or acceptor energy

levels in the band structure of the semiconductor so that their kind and concentration control the electrical behavior of the semiconductor. In the case of thermoelectric materials fairly high concentrations of donors and acceptors are desired in order to optimize the thermoelectric efficiency. Carrier concentrations of about $10^{19}/cm^3$ are desired for this purpose.

In elementary semiconductors, extrinsic carrier concentrations are governed by the addition of suitable concentrations of foreign atoms to the crystal structure. These concentrations are generally found to be fairly insensitive to crystal temperature. In compound semiconductors there are two independent competing processes for adding carriers. One is by the addition of foreign atoms; the other by producing stoichiometric deviations in the composition of the crystal. The latter is a thermodynamical property of the crystal and is dependent upon the crystal temperature and the composition of liquid or vapor phases in contact with the crystal. Changes in temperature or ambient conditions result in internal changes in crystal composition and hence its electrical properties. The time rates of achieving equilibrium are governed by diffusion processes, which proceed more rapidly as the crystal temperature is increased. Hence at the elevated temperatures at which thermoelectric devices operate one may expect changes in the extrinsic carrier concentrations due to changes in the stoichiometric proportions of the elements in the crystal. The importance of these changes upon the electrical properties of the semiconductor

depends upon the nature of its phase diagram. If the solid phase exists over a wide range of composition, stoichiometric deviations could play an important role in the instability of the electrical properties. On the other hand, certain compounds have a very narrow range of nonstoichiometric composition and therefore might be expected to be stable under thermal stress.

The purpose of this paper is to discuss the underlying principles governing nonstoichiometry of composition in semiconductor compounds and to illustrate the principles with experimental studies of the phase relationships and electrical properties of a group of semiconducting compounds.

STOICHIOMETRY IN COMPOUND SEMICONDUCTORS

The bonding of atoms to form simple gaseous molecules is governed by fundamental principles of chemistry, such as the law of definite proportions. The resulting union can be expressed in terms of a unique and simple whole number of individual atoms. The atomic basis for this law is that the composition is governed by the number of covalent bonds that can be formed by the component atoms or by the valency of the ions.

When the compound condenses to form the solid phase, other considerations enter into the problem which may modify the exact composition predicted from electronic considerations alone. In the polar and valence crystal lattices the basic structural unit is the unit cell rather than the molecule. The composition of the unit cell is governed in addition to valence consideration by conditions of atomic packing and balance of charge. These

geometrical and electrical considerations result in a characteristic crystal structure associated with the compound.

In ionic compounds the basic feature in the construction of the unit cell is the purely geometrical disposition of a group of ions of characteristic radius and charge in a manner which has the greatest possible number of opposite charges around a given charge consistent with the conditions of electrical neutrality. In valence crystals the demands are more exacting because the bonds must satisfy certain orientation conditions as well.

The crystalline phase may incorporate certain lattice defects such as atoms or ions missing from normal sites or occupying interstitial positions. The resulting strain on the lattice is compensated by slight movement of neighboring atoms or ions and trapping of electrons or holes by the vacancy.

When these defects are predominantly of one atom or ion species, which is the usual case, then the composition will deviate from the ideal or stoichiometric proportions. Generally, the omission of more than a small proportion of one species from the lattice, much less than 1%, distorts and breaks up the crystal structure, so that stable compositions usually lie close to the ideal chemical formula.

DEFECTS IN CRYSTALS

In a binary compound having the formula AB, stoichiometric deviations may be incorporated in the lattice in three ways. For the case where there is an excess of B atoms in the crystal

the three types of nonstoichiometry are illustrated in Fig. (1), and are described as follows:

1. Substitutional: Extra B atoms replace A atoms on lattice sites normally occupied by A atoms.
2. Subtractive: B atoms occupy normal B sites, but some A sites are vacant.
3. Interstitial: Extra B atoms occupy interstitial positions.

In a real crystal it is possible to identify the important defect type on the basis of certain tests. In semiconductors with substitutional defects the conductivity is p-type when there is an excess of the cation or positive ion. The conductivity is n-type with an excess of the anion. On the other hand, with subtractive or interstitial defect solids the conductivity is opposite, being n-type for excess of the cation and p-type for excess of the anion.

A distinction between interstitial and subtractive defect solids can sometimes be made on the basis of careful X-ray and density measurements. An increase in density is observed for interstitial crystals, whereas a decrease is observed for subtractive crystals. Most nonstoichiometric crystals have subtractive or interstitial defects, and only a few incorporate the substitutional defects.

Substitutional crystals are likely to be intermetallic compounds in which ion repulsion is weak, Furthermore, a difference of atom valency of unity is desired. A well known

semiconductor of this type is Bi_2Te_3. Excess Te resides in normally Bi sites resulting in an n-type crystal, while excess Bi resides in normally Te sites making the crystal p-type. The Te atom has six valence electrons so that when it takes the place of a Bi atom which has a valence of five, the extra electron occupies a donor level. A similar argument applies to Bi in Te sites yielding acceptor levels.

Nonstoichiometric crystals of the subtractive type may be of three different types, illustrated in Fig. (2). Most of the semiconductors of interest fall into Group C with conductivity being n-type for excess cations and p-type for excess anions.

We shall consider next the magnitude of the deviations from stoichiometry and the dependence upon temperature and associated phase composition.

EQUILIBRIUM CONDITIONS FOR DEFECTS IN SOLIDS

The maximum permitted deviation from the stoichiometric proportions in crystals of binary compounds seldom exceeds 1%, however there are extreme cases that range as high as 20 to 40% in substances like TiO or Cu_2S down to almost imperceptible amounts in some of the intermetallic compounds like GaSb or InAs. Some substances, such as PbS or PbTe, tend to support larger departures from the ideal formula than covalent structure due to the less exacting demands regarding spatial orientation of bonds in ionic crystals. In principle, however, all crystals of compounds should show deviations in composition at temperatures above absolute zero.

In a given crystal, addition or removal of excess atoms or ions generally takes place with the gas or liquid phases surrounding the solid. The equilibrium concentration of the excess atoms in the solid depends upon the temperature and composition of the vapor phase or liquid phase contacting the solid. The principle of the phase relationships was established over 30 years ago by Wagner and Schottky[1] but only recently it has been used effectively to control the composition of binary compound semiconductors.

Let us consider the system composed of a crystal of PbS in equilibrium with its vapor, which might consist of atoms of Pb and S as well as of molecules of PbS and other molecular species of Pb and S. This system has two phases and two components so by Gibbs' phase rule it has two degrees of freedom. By fixing, for example, the temperature and pressure of one of the components the equilibrium system is perfectly defined. The composition of the solid and hence its electrical properties are also fixed.

In applying these principles to a given compound it is important first to establish the maximum limits of deviation from the stoichiometric composition. In the case of PbS these limits were found experimentally by Bloem and Kroger[2] by observing the onset of melting in a crystal held at a fixed temperature while the partial pressure of sulfur was increased. The composition of the crystal at the melting conditions was obtained by electrical measurements made on the crystal after being quenched rapidly to room temperature.

The maximum deviation in composition from the stoichiometric proportions for PbTe was obtained by a different technique by Brebrick and Allgaier[3]. In the equilibrium system composed of crystals of PbTe immersed in a Te rich or Pb rich liquid surrounded by the vapor phase, the crystals assume the maximum departure from stoichiometry corresponding to the temperature of the system. In this three phase-two component system there is only one degree of freedom. Thus the temperature alone fixes the system. A curve illustrating the limits of composition of PbTe is shown in Fig. (3). Here we note that the maximum solubility of excess Te is about .012% and for Pb it is .005%. While these amounts do not appear to be large departures from the stoichiometric formula, they result in about 10^{18} to 10^{19} electrons or holes in the conduction band and therefore play a large role in the electrical properties of these semiconductors. Similar limits apply to PbS and PbSe. The maximum melting point for PbTe occurs on the Te rich composition, hence the first material to crystalize from a near stoichiometric melt will possess this composition and be p-type. In the case of PbS the maximum melting point mixture lies in the excess Pb composition and is n-type. For PbSe the limits of the compound were established by Brebrick and Gubner[4] and the maximum melting temperature occurs for a p-type composition.

A continuous range of composition exists within the maximum limits of solubility of the excess atoms of these

compounds. The crystal composition is established through an equilibrium with the gaseous phase at various temperatures that can be expressed analytically. For the compound AB, the reaction equations involved have the form

$$A_g \rightleftharpoons A_s + V_B$$

or

$$B_g \leftrightharpoons B_s + V_A$$

where the suffix g refers to the atom in the gaseous state, s when it occupies a lattice site in the crystal, and V_A or V_B is the associated lattice vacancy created by the reaction.

The law of mass action defines a relationship between the concentrations C_{A_s} and C_{V_B}, of A atoms and B vacancies in the solid and the pressure P_{A_g}, of the vapor of A surrounding the solid.

$$C_{A_s} C_{V_B} / P_{A_g} = K.$$

Similarly the Schottky constant is

$$C_{V_A} C_{V_B} = k_s$$

The equilibrium constants are functions of E/RT, where E is an activation energy and T is the temperature.

In experiments on semiconductors, the concentrations measured are usually for electrons or holes obtained from values secured by the Hall coefficients. Assumptions must be made as to the number of such carriers associated with each defect and their ionization energy. Brebrick[4] worked out the analytical solution for the equilibrium system where each

vacancy contributes one electron or hole. He obtained the following expression containing the deviation from stoichiometry, δ:

$$- \ln(P_B/P_B^{\,i}) = \sinh^{-1}\left(\frac{\delta}{2\sqrt{k_s}}\right) + \sinh^{-1}\left(\frac{\delta}{2r_1}\right)$$

where P_B is the pressure of the B component of the vapor, $P_B^{\,i}$ is the pressure of the B component corresponding to the stoichiometric composition, δ is the concentration of free electrons minus the concentration of holes or (n-p), r_i is the intrinsic carrier concentrations and k_s is the Schottky constant.

Experimental studies of the vapor-solid equilibrium system of PbS have been made by Bloem[5] and Brebrick and Scanlon[6]. The combined data is summarized in Fig. (4). Lines of constant composition are indicated as well as the line for the stoichiometric composition.

The comparison of the experimental data on PbS with the theory shows that the partial pressure for the stoichiometric composition agrees with theory but the curves of non-stoichiometric composition are in disagreement[4].

Studies of the electrical properties of the PbS, PbSe, and PbTe crystals at high temperatures are complicated by the changing composition of the crystal unless special care is taken to adjust suitably the vapor composition at each temperature in order to maintain the fixed composition. The phase diagram also shows the equilibrium conditions required to produce any

desired crystal composition and hence any desired electrical properties within the limits of solubility of the compound.

PRECIPITATION EFFECTS IN CRYSTALS

An examination of the solidus curve for PbTe in Fig. (3) reveals regions of retrograde solubility in both the excess Pb and excess Te composition regions at temperatures below 700° - 800°C. Within the retrograde solubility region a crystal possessing the maximum excess concentration of cations or anions at a given temperature will become supersaturated upon cooling to a lower temperature. The excess ions may be disposed of by an internal precipitation process in which ions diffuse from normal sites to precipitation centers where they deposit out as neutral atoms. Dislocations in crystals act as centers for precipitation. The process is reversible.

Precipitation is therefore another mechanism which leads to lack of stability in the electrical properties in crystals since it results in thermal changes in the concentration of donor or acceptor levels in semiconductors. The rate of change in the concentration of these levels due to precipitation may be different from the rate of changes resulting from exchange of atoms through the surface to a surrounding liquid or gaseous state. The average distance to an internal precipitation center such as a dislocation is much shorter than the average distance to the surface. Hence equilibrium times for the internal process might be expected to be less than for the vapor diffusion process at the same temperature.

Recently I have made a study of precipitation rates in PbTe crystals[7]. P-type PbTe pulled crystals with an initial hole concentration corresponding to the maximum solubility of Te at 700°C were held at various lower fixed temperatures until the composition came to the equilibrium value appropriate for the temperature. Composition changes were monitored by observing the rate of change of thermoelectric power. This data was used to evaluate the rate of change in hole concentration and hence the precipitation rate. Similar experiments showed that excess Pb may also precipitate in the crystals but at a much lower rate than for Te.

A typical precipitation rate curve is shown in Fig. (5) for Te in PbTe. The unprecipitated fraction is W and the time is expressed in terms of a reduced time factor $\frac{Dt}{r_s^2}$ which normalizes for different diffusion constants D, and radii r_s of the trapping cylinder around a dislocation. The latter number is related to the density of dislocations, N, through $\pi r_s^2 = \frac{1}{N}$. Theoretical precipitation curves are drawn for comparison with the experimental points.

The equilibrium hole concentrations for PbTe at various temperatures are shown in Fig. (6) and the times to reach 95% of saturation concentration are shown in Fig. (7). From this data an activation energy for precipitation of Te in PbTe is found to be 0.88 ev assuming an exponential law governs the process. Also the rate of reaching equilibrium for internal precipitation is very fast at the higher temperatures; at 400°C

it is about an hour. By comparison, equilibrium times of the order of 1000 hours are required at this temperature for diffusion by the vapor process.

ELECTRON TRANSPORT PROPERTIES

We have seen how compound semiconductor crystals may change their internal composition through changes in their coexisting phases, as a result of temperature changes or by internal precipitation. We will now describe how these changes affect the transport properties of these materials.

An experiment was designed to demonstrate the influence of the gaseous phase of a PbS crystal upon its internal properties. An initially n-type crystal of PbS was held in a flow of helium in order to carry away the gaseous components and maintain a negligibly low partial pressure of these gas components near the crystal. Hall effect and resistivity curves were obtained from room temperature up to successively higher temperatures. The data shown in Fig. (8) indicate the magnitude of changes in electrical properties resulting from the heat treatments. The time required to obtain these curves was about 10 minutes per point. The ultimate composition that would be reached in these experiments corresponds to the atability limit for the crystal at the maximum temperature selected. In the experiments just described no attempt was made to obtain the equilibrium composition; nevertheless, order of magnitude changes in composition occurred during the course of a single Hall effect or resistivity run requiring but a few hours. Changes occur so

rapidly at the highest temperatures that it is difficult to make the measurements.

The effect of internal precipitation of Te on the thermoelectric power of p-type PbTe crystals is shown in Fig. (9). In this experiment relatively low temperature effects were studied. The crystal was held at various temperatures, ranging from 180°C to 380°C, for sufficient time for the crystal to come into equilibrium. These times ranged respectively from a month to two hours. The thermoelectric curves were then measured as quickly as possible. Extrinsic carrier concentrations, obtained from Hall effect measurements, show an order of magnitude change in these experiments.

In n-type PbTe crystals, internal composition changes resulting from the precipitation of Pb were also studied. Crystals were held for various times of the order of days at a given fixed temperature of 400°C. Equilibrium was not reached in these experiments. The initial conditions and changes in the Hall effect and resistivity of the crystal following anneal times of 15, 35, and 59 hours are shown in Fig. (10). Again large changes in crystal composition result from the internal precipitation mechanism.

CONCLUSIONS AND DISCUSSION

We have discussed two mechanisms by which the internal composition of non-stoichiometric compound semiconductors may be changed. One is through the thermodynamic relationships which exist between coexisting phases. The other is by internal

precipitation. Both of these effects may play a significant role in the stability of the electrical properties of compound semiconductors. Changes in electrical properties of an order of magnitude are observed in PbS or PbTe. The larger the range of stability of the compound, the more serious these effects become if stability is required in a given application of the material.

In some applications requiring very high carrier concentrations, it may be possible to dissolve foreign impurity atoms in sufficient quantity to provide donor or acceptor level concentrations greatly exceeding the ones established by phase considerations. In such cases the electrical properties of the crystals might be little influenced by the internal composition changes discussed in this paper.

REFERENCES

1. C. Wagner and W. Schottky, Z. Physik, Chem. (Leipzig) 11, 467 (1930).

2. J. Bloem and F. A. Kroger, Z. Physik, Chem. 7, 1-2, 1 (1956).

3. R. F. Brebrick and R. S. Allgaier, J. Chem. Phys. 32, 1826 (1960).

4. R. F. Brebrick, J. Phys. Chem. Solids 18, 116 (1961).

5. J. Bloem, Philips Res. Repts. 11, 273 (1956).

6. R. F. Brebrick and W. W. Scanlon, Phys. Rev. 96, 598 (1954).

7. W. W. Scanlon, Phys. Rev. 126, 509 (1962).

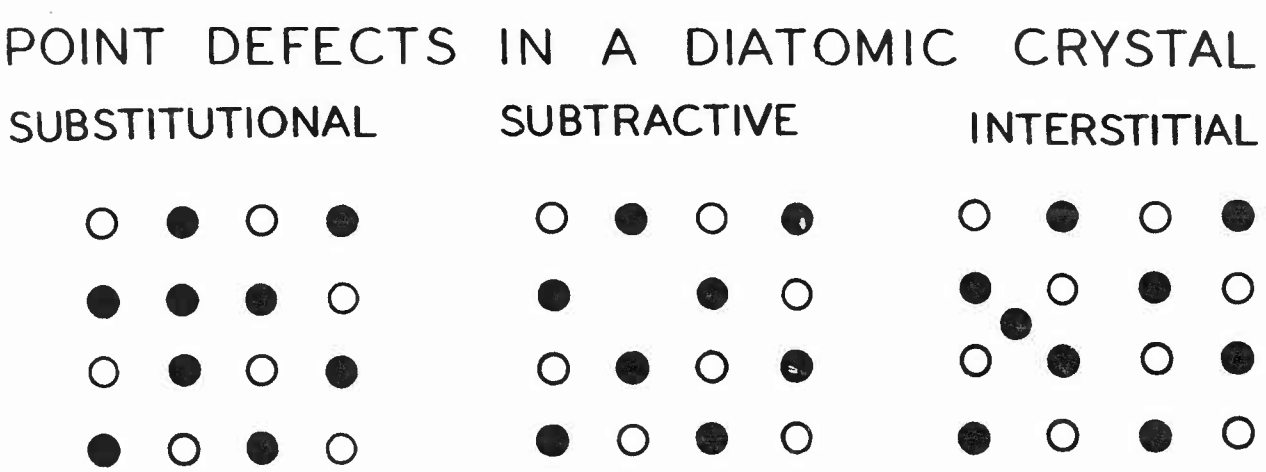

1. Types of point defects in a diatomic non-stoichiometric crystal.

TYPES OF SUBTRACTIVE CRYSTALS

	EXCESS IONS	CONDUCTIVITY	EXAMPLE
(a)	CATION	n-TYPE	NaCl with Cl vacancies (F centers)
(b)	ANION	p-TYPE	FeO, CuI
(c)	EITHER CATION OR ANION	n or p-TYPE RESPECTIVELY	PbS, TiO, etc.

2. Types of subtractive point defects in crystals.

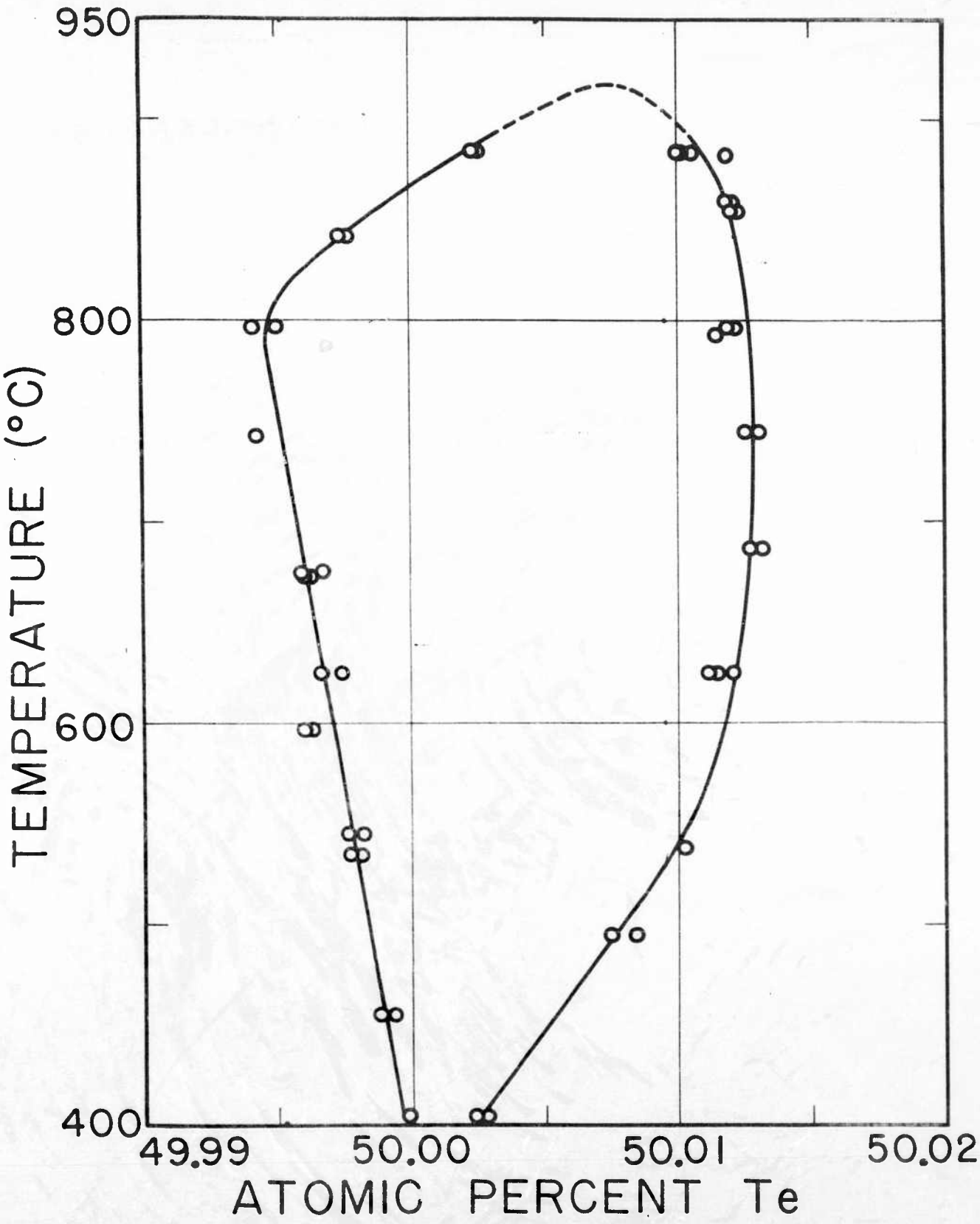

3. Composition stability limits for PbTe crystals, (R. F. Brebrick and R. S. Allgaier, J. Chem. Phys. 32, 1826 (1960)).

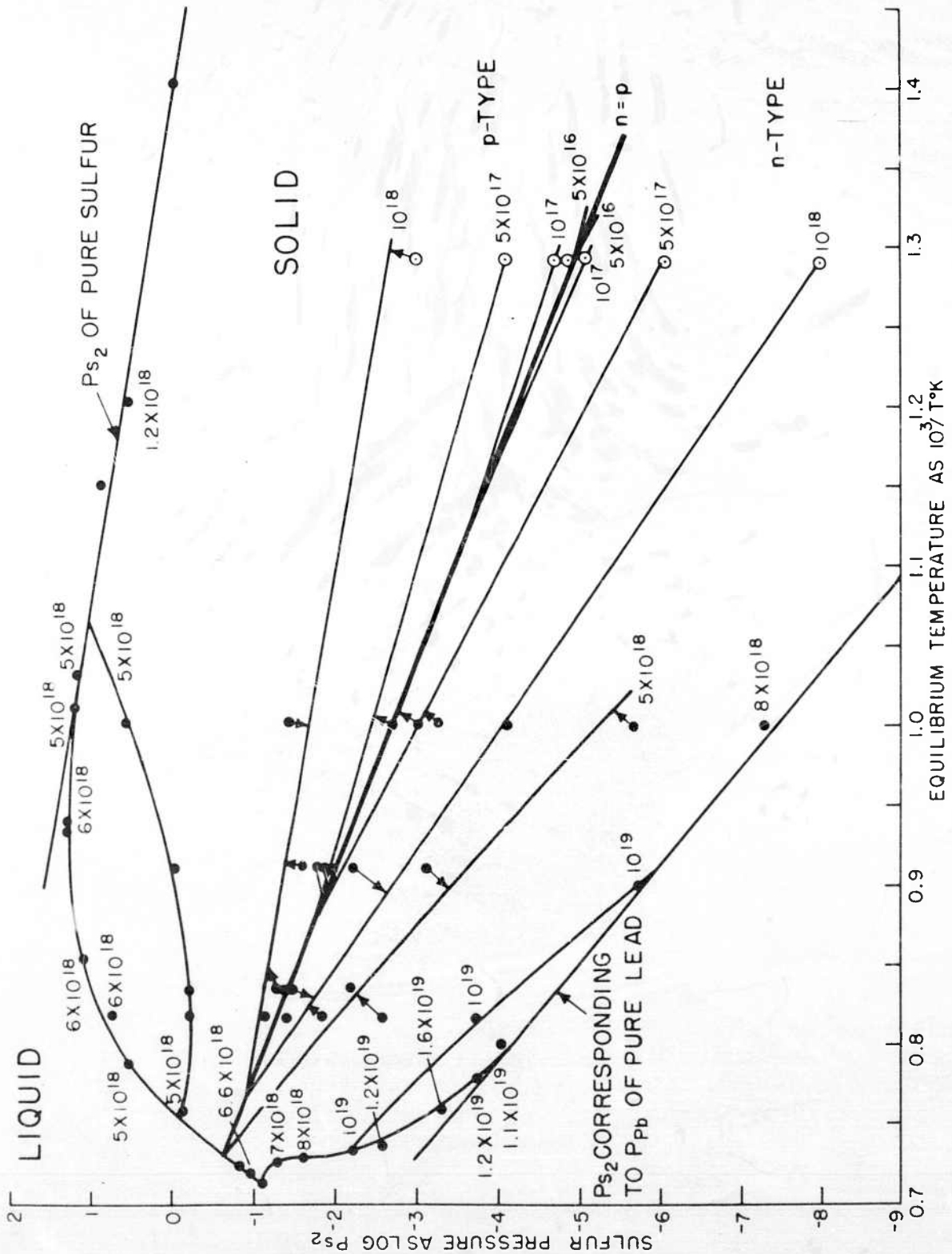

4. Phase diagram for PbS.

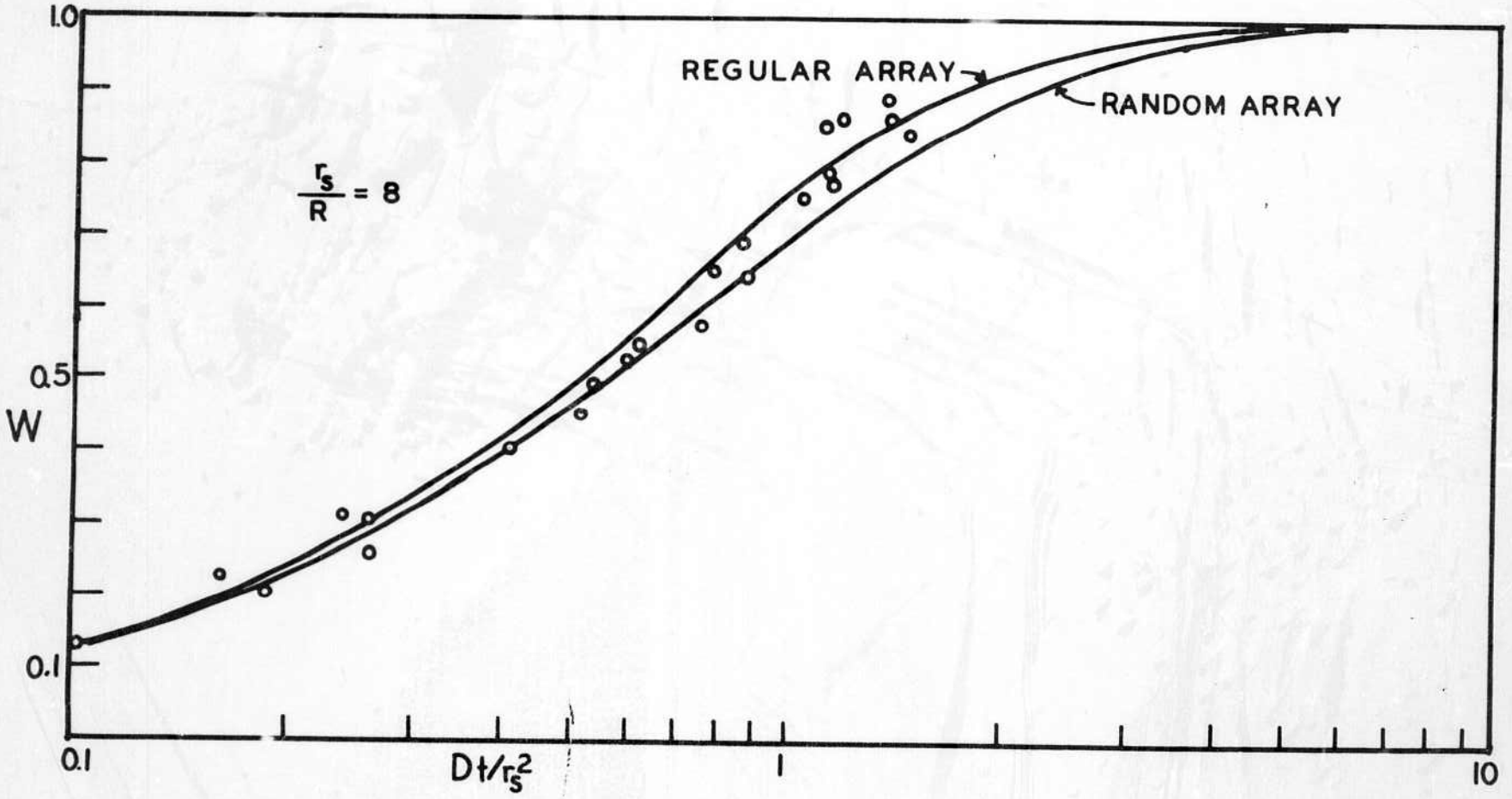

5. Precipitation rate of Te in PbTe crystal. (W = unprecipitated fractions, and $\frac{Dt}{r_s 2}$ = reduced time).

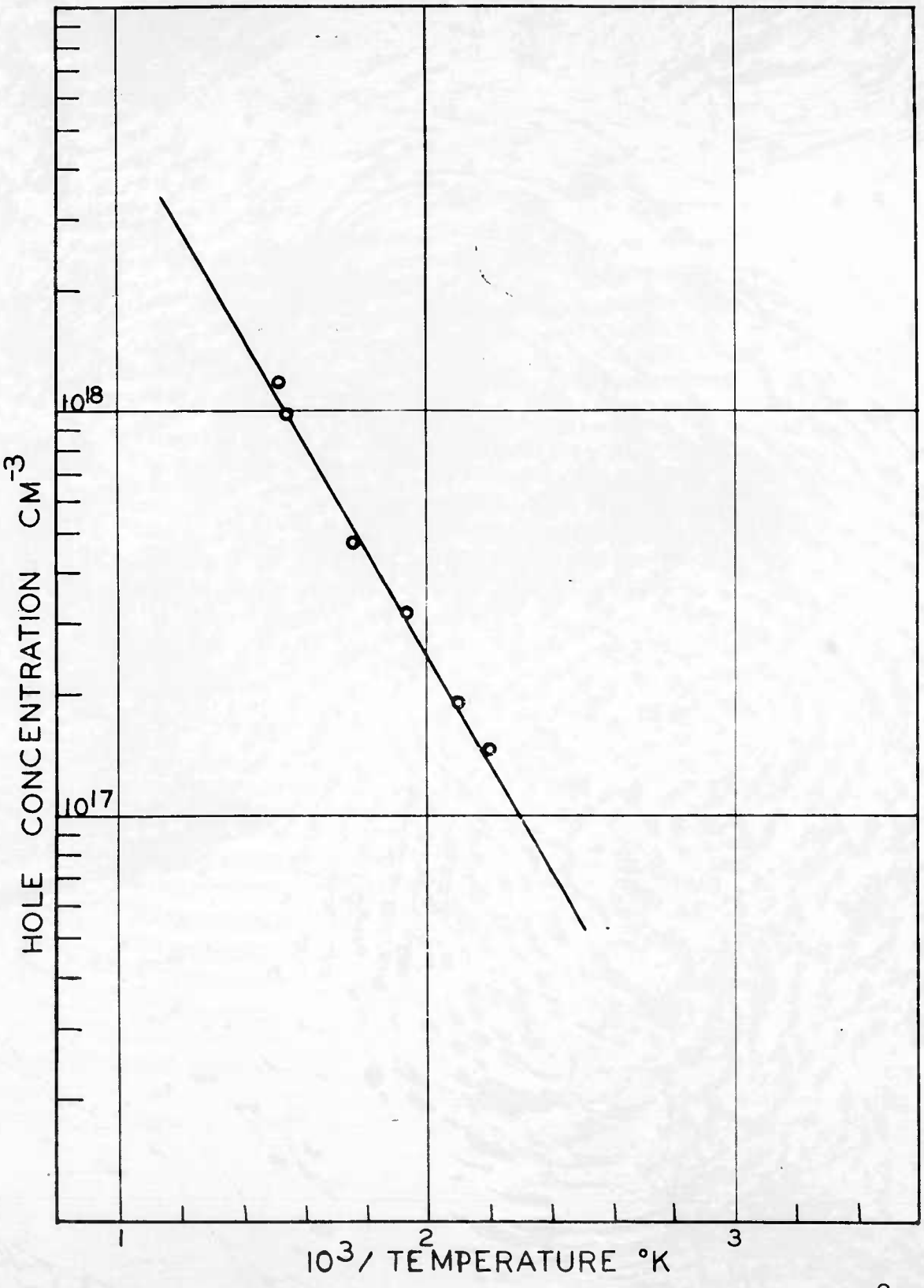

6. Saturation concentration of Te in PbTe crystal below 400°C.

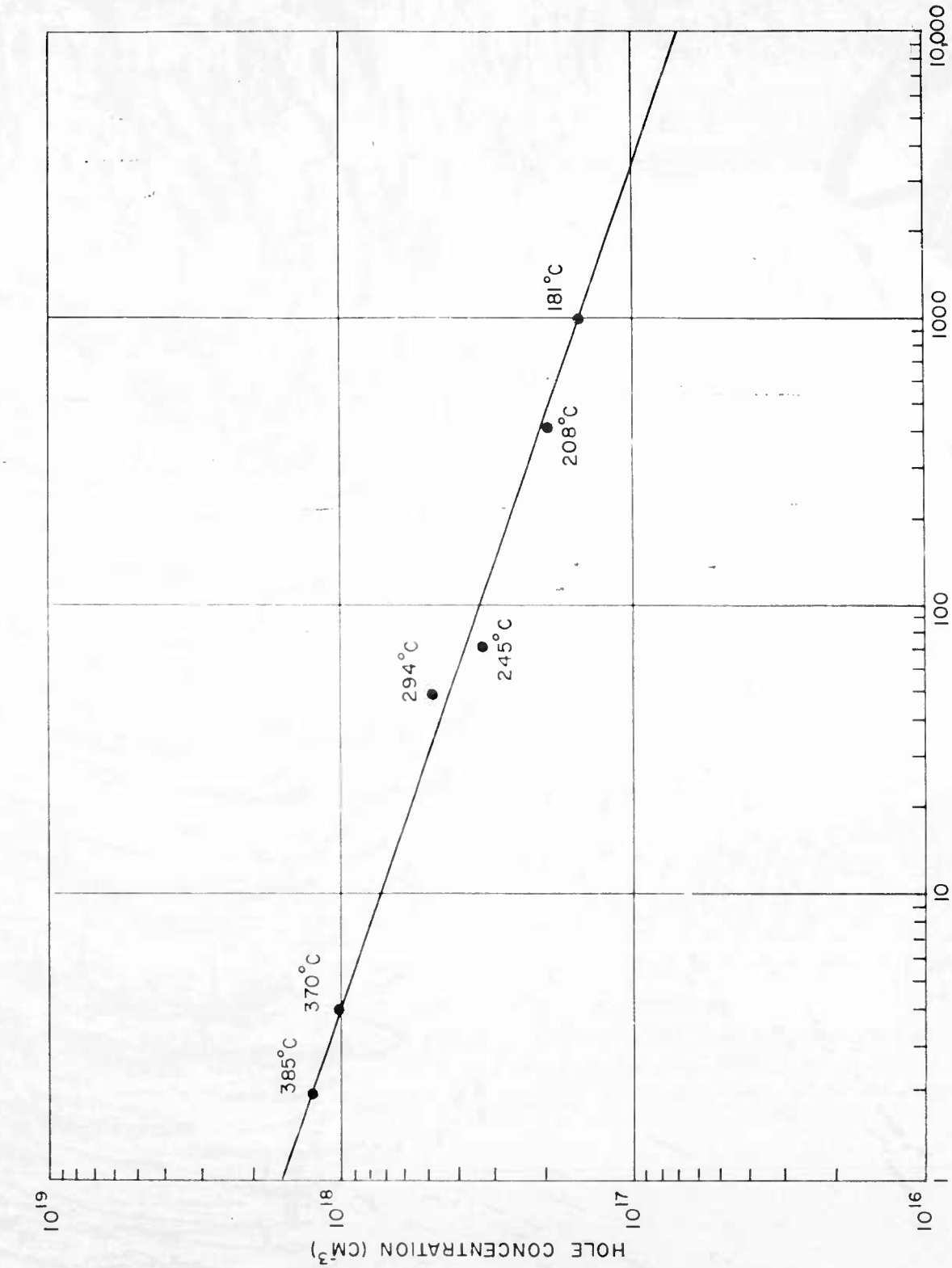

7. Precipitation equilibrium time, temperature and concentration of Te in PbTe crystals.

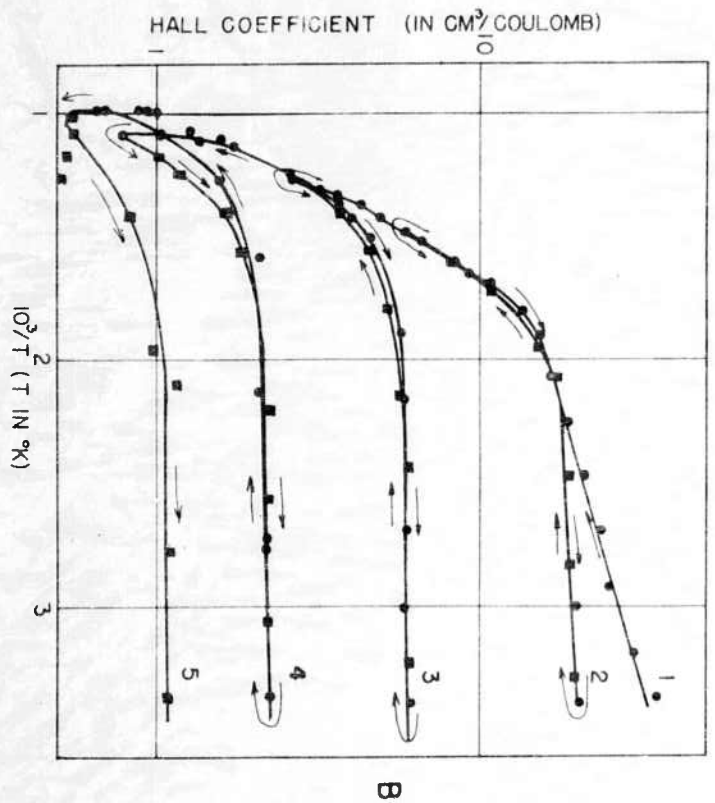

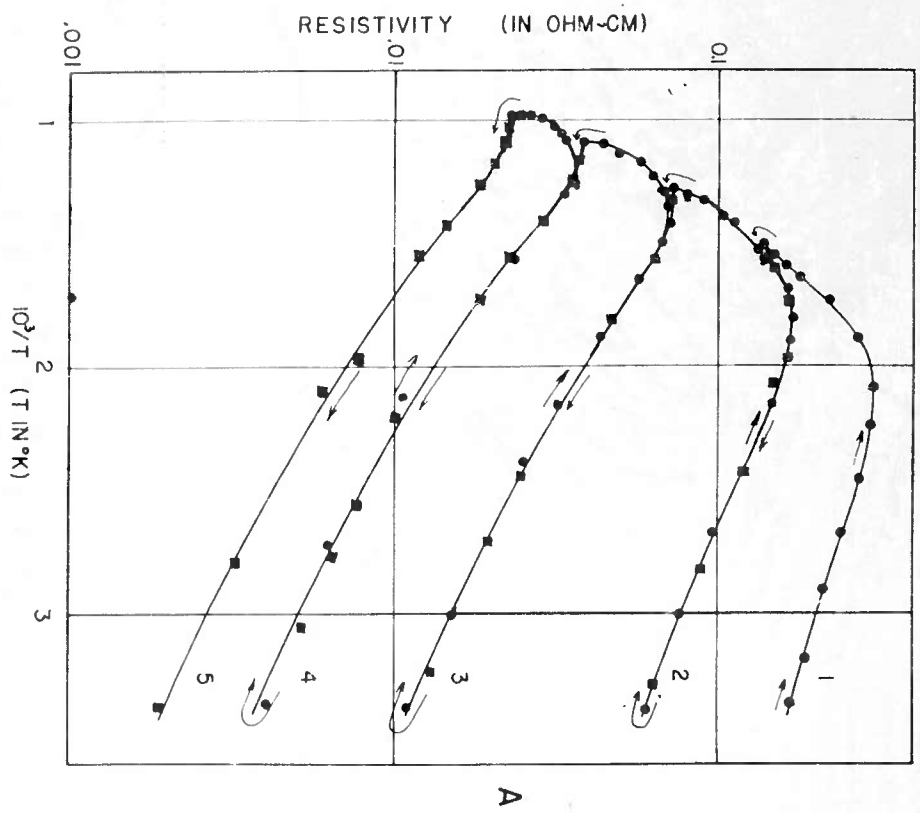

8. Resistivity and Hall effect in PbS crystal showing composition changes resulting from heating in an inert atmosphere to the following maximum temperatures: 1, 680°K; 2, 788°K; 3, 919°K; 4, 1023°K.

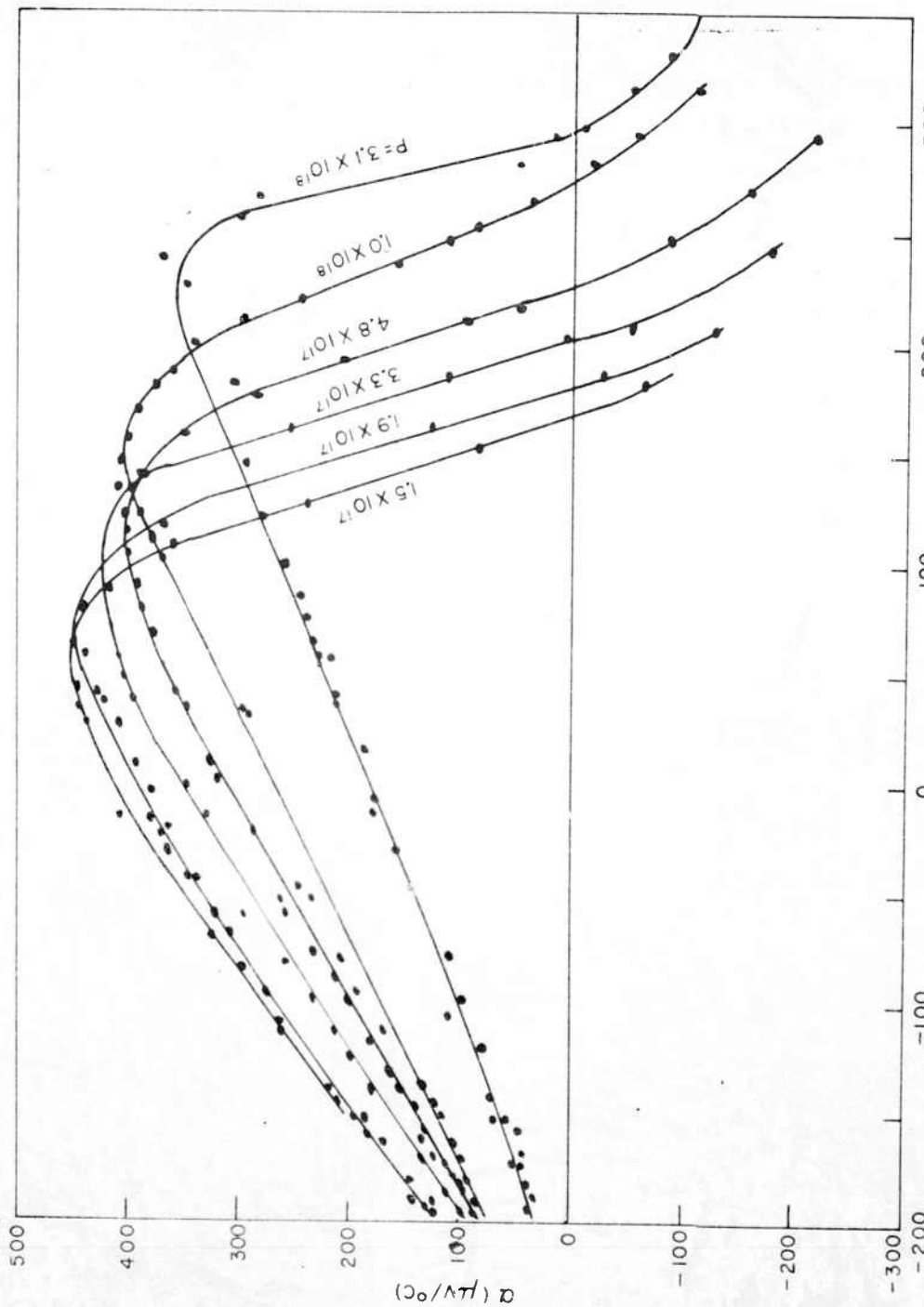

9. Thermoelectric power changes resulting from precipitation of Te in p-type PbTe.

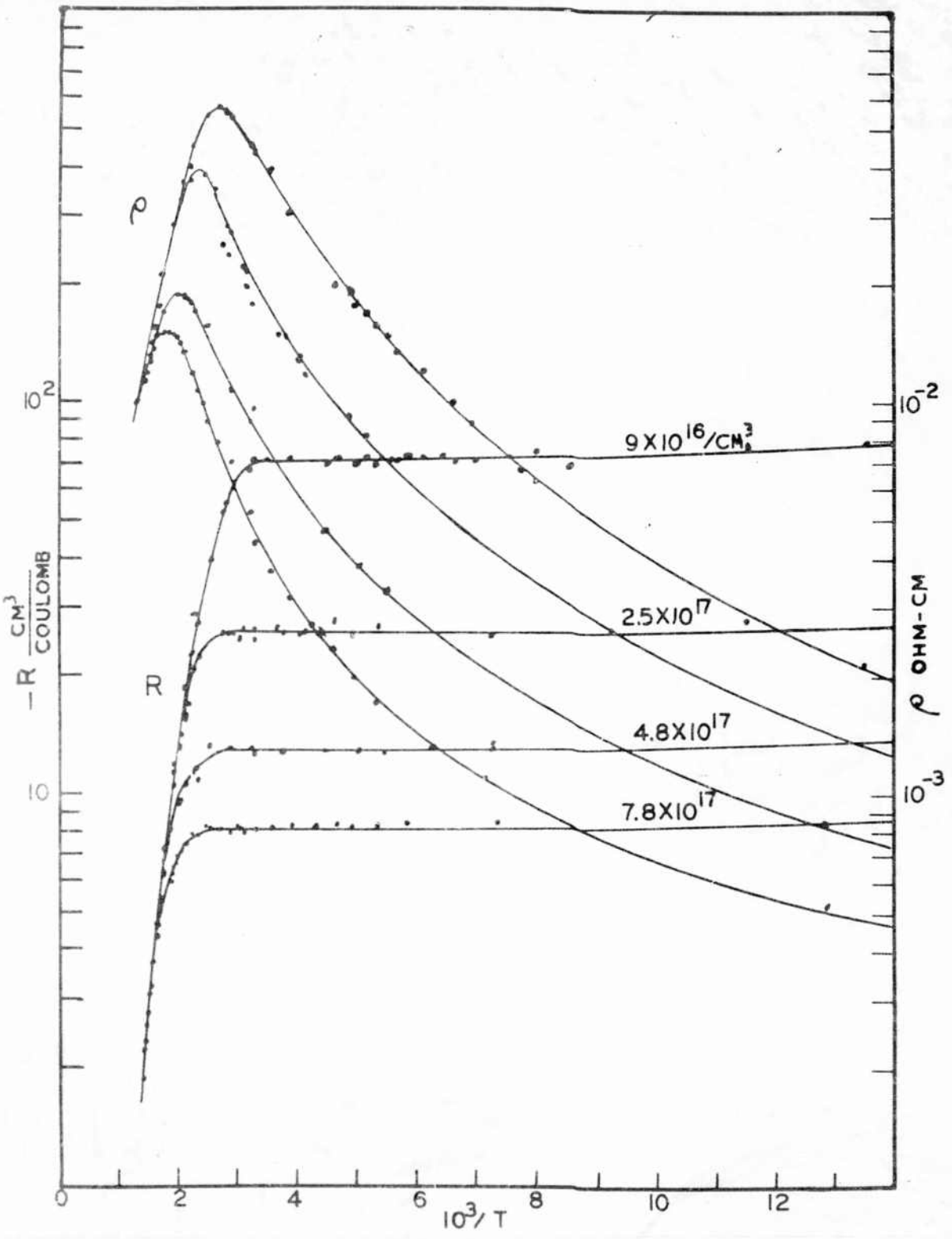

10. Changes in Hall effect and resistivity in n-type PbTe due to precipitation of Pb.